Emissions Predictions in Turbulent Reacting Industrial Gas Turbine Combustor Flows using RANS and LES methods

Sandeep Ebenezer Jella

A Thesis

In

The Department

Of

Mechanical and Industrial Engineering

Presented in Partial Fulfillment of the Requirements

For the Degree of Master of Applied Science (Mechanical Engineering) at

Concordia University

Montreal, Quebec, Canada

April 2008

Your file Votre référence
ISBN: 978-0-494-42521-3
Our file Notre référence
ISBN: 978-0-494-42521-3

ABSTRACT

Emissions Predictions in Turbulent Reacting Industrial Gas Turbine Combustor Flows using RANS and LES methods

Sandeep Jella

CFD predictions of emissions using conventional RANS methods have been shown to be inaccurate, sometimes by orders of magnitude. In recent years, deeper details of the chemistry-aerodynamics coupling in lean-premixed combustion regimes have been demanded from CFD predictions. Large Eddy Simulation (LES) of non-reacting flows provides high-fidelity predictions of flow field aerodynamics in gas turbine combustor chambers, critical for accurate emissions predictions. While LES has been validated for many simple lab combustors, there are few simulations that have used this method for practical industrial combustors at their baseload conditions. This thesis describes its application to an industrial gas turbine combustor at elevated pressures and temperatures. A well-validated commercial code, Fluent 6.3, has been used to obtain reacting and non-reacting flows that occur in this combustor geometry. The final emissions predictions were compared with rig test results.

ACKNOWLEDGEMENTS

On the University side of things, I thank my wonderfully patient supervisors to whom I owe far more than this simple acknowledgment: I thank Dr Marius Paraschivoiu, for being willing to take me on and support me – many times at his own expense. I am grateful for all the direction I received from him. I am grateful to Dr Pierre Gauthier, also the lead Combustion CFD specialist at Rolls-Royce Canada, whose excellent class on Combustion at Concordia in Fall '05 was primary motivation for me to delve into the subject. I am grateful for his taking pains to help me at a time I did not know which way to turn. It truly is a blessing for me to work under these gentlemen.

On the Industry side, it has been my pleasure and privilege to work with some of the best. I am indebted to Dr Gilles Bourque of Rolls-Royce Canada, for his leadership, support and methodical approach to the project as well as willingness to carefully answer my many questions. I also thank David Scott of Rolls-Royce Canada for his encouragement and willingness to share his seemingly absolute knowledge of the combustors he designs. I am grateful for the friendly welcome I always received from the staff I have had the chance to meet at Rolls-Royce Canada.

I also thank Joel Krajden, Senior Systems Analyst and cluster supervisor at Concordia, for his support and interest in my work and providing technical advice and supercomputing access on a scale that a person of my humble academic position very rarely finds.

I am thankful for the faculty (Thank you Dr Ghaly and thank you, Dr Vatistas! I have enjoyed my courses with you) and program advisers (Leslie and Charlene) at Concordia for all the help I have received from them.

I have no way of expressing my gratitude to my parents, Daniel and Usha, who constantly encouraged me to excel from my heart. Ma, I'll get back to the Violin, promise! I could say the same for my wisecracking sister Pavithra, who could see something funny even in a diverging CFD residual...I am in incalculable, divide-by-zero, debt to my beautiful wife, Sandhya, who not only agreed to marry me, but also bravely, carried through with it...I thank Saam Hessami my longsuffering colleague for putting up with my eccentricity and encouraging me despite his own anxieties – I truly owe you. My thanks to Raja Ramamurthy for his being available to chat and help me at some of the most difficult times. My thanks also to the great group of guys, Shahin, Kaveh, Jia and others of the CFD lab from whom I have learned much and have had many fruitful discussions with.

Finally, and most importantly, I thank God without whom none of this would be possible. My work isn't great, but what I have done; I could not have done without his grace.

DEDICATION

'Tis but an effort of a swirling cloud
Of dust that swept by on an autumn day,
Calmed by the dew of a morning's birth
And slept for a while, in a sunshine ray.
How temporal, in a spatial sense,
The time that space can never fill,
Much less, that time will cease to stretch,
In a temporal sense, it never will...
Dare I then, to fill this glass,
With the dust of my labour and the dew of my brow,
Mixed each day with the blood and sweat,
That must needs water the seeds of love;
And can this love for eternal glory,
Be carried in hands that will offer to lay,
It all down for the price of a cross,
That at the end is the burden of a better Way,
What price, O Soul, this forgettable work,
Can command you so to lie awake,
In anxious toil, yet fruitful work,
Oh do it all, for God's own sake!
And there, lies my hope, my dream, my tears,
That though this dust will soon dry,
In the wind that carries it swirling away,
While the shadows fall and the ethers die,
To the fragrant esters, I bid adieu,
To the lovers of [OH], I say [NO][1],
For the dust of this work will gently lie,
On God's green earth with a peaceful sigh.

I dedicate this simple work to Jesus Christ.

1. *Zhao et. al., 'Behaviour and effect on NOx formation of OH radical in methane-air diffusion flame with steam addition', Combustion and Flame 2002, vol. 130, n°4, pp. 352-360.*

TABLE OF CONTENTS

TABLES AND FIGURES **3**

ABBREVIATIONS **6**

1. INTRODUCTION **7**

Objectives and Method of the current work 18

2. TURBULENCE AND COMBUSTION MODELING **23**

2.1 Turbulence Modeling 23

2.1.1 RANS Turbulence Modeling and Governing Equations 25
2.1.2 Large Eddy Simulation and Governing Equations 33

2.2 Combustion Modeling 40

2.2.1 Species Transport Modeling 43
2.2.2 PDF methods 52
2.2.3 Emissions Modeling as a post-processing step 76

3. SOLUTION METHODOLOGY **95**

3.1 Description and brief survey of the Fluent Code. 95
3.2 Discretization Schemes 98
3.4 Mesh considerations 102

4. MODEL DESCRIPTION AND FLOW SPLITS **105**

4.1 Computational Domain 106
4.2 Operating Conditions and Gas Flow Path 110
4.3 Mesh 113

5. COLD FLOW RESULTS **116**

5.1 Mixing in the Primary Premixer 116
5.2 Mixing in the Primary Zone 122
5.3 Mixing in the Secondary Zone 132
5.4 Mixing in the Secondary Premixer 137

6. REACTING FLOW: PILOT STUDY OF A COAXIAL COMBUSTOR..... 140

6.1 RANS predictions. 144
6.2 Large Eddy Simulation 152
6.3 Combustion Model Evaluation 157

7. RB211-DLE REACTING FLOW SIMULATION 168

7.1 Setup of Sub models. 168
7.2 RESULTS 179
7.3 Some critical modeling considerations 188
7.4 Qualitative Comparisons 200

8. CONCLUSIONS 218

REFERENCES 224

APPENDIX: CONVERGENCE CHARTS 231

TABLES AND FIGURES

FIGURES

Fig 1.1 (a-e): Emission trends 10
Fig 1.2: Rolls-Royce RB211 DLE installation 12
Fig 1.3: DLE Engine - Rolls-Royce RB211 12
Fig 1.4: Schematic of Premixed Combustion 15
Fig 2.1.1.1: Review of RANS 26
Fig 2.2.1.1: Effect of mechanism 45
Fig 2.2.1.2: Eddy Dissipation Concept results 51
Fig 2.2.2.1: Logic Loop. 53
Fig 2.2.2.2: Borghi's 'Phase' Diagram 59
Fig 2.2.2.3: Effect of turbulence model and Sc number. 68
Fig 2.2.2.4: Effect of varying Schmidt number 69
Fig 3.1.1 – Fluent Speedup 96
Fig 3.3.1: Partitioning of the Grid 101
Fig 4.1: RB211 "long" combustor orientation in engine 105
Fig 4.1.1: RB211 "short" combustor fluid flow path. 106
Fig 4.1.2: The Secondary Premix Duct with fuel "arms" 107
Fig 4.2.1: Fluid flow path 110
Fig 4.3.1: Refined portion containing the centreline of the primary 113
Fig 4.3.2: Detail of the primary premixer 113
Fig 4.3.3: Detail of mesh on the secondary premix fuel arms. 114
Fig 4.3.4: RANS mesh 114
Fig 4.3.5: Cross section of the Hybrid mesh. 115
Fig 5.1.1: Jets in Cross Flow. 118
Fig 5.1.3: Fuel Injector Flows 119
Fig 5.1.4: DNS of JICF 119
Fig 5.1.5: Recirculation Zone vectors near Fuel Injector 120
Fig 5.1.6: Mixing in the swirl passages 120
Fig 5.2.5: Cold Flow LES Velocity Profiles. 130
Fig 5.2.6: Primary Outlet. 131
Fig 5.3.1: LES averaged temperature contours 134
Fig 5.3.3: Streamlines from secondary jets 136
Fig 5.4.1: Temperature contours 139
Fig 6.1: Mesh used for axisymmetric analysis. 142
Fig 6.1.3: Centerline Predictions with Sc=0.1 and varying turbulence model 146
Fig 6.1.4: Streamlines in symmetric duct. 148
Fig 6.1.5: Effect of turbulence model on temperature field 149

Fig 6.1.6: Effect of discretization scheme 151
Fig 6.2.1: Centerline Mixture Fraction. 152
Fig 6.2.2 (a-f): Instantaneous contours of the flamefront 155
Fig 6.2.3: Iso-surface of stoichiometric mixture fraction 156
Fig 6.3.1: Temperature Comparisons 158
Fig 6.3.2: CO mass fraction comparisons 160
Fig 6.3.3: Effect of including Scalar Dissipation rate (1/s) on CO and NO. 161
Fig 6.3.4: NO mass fraction comparisons 163
Fig 6.3.5: NO mass fraction from post processing 163
Fig 7.1.1: Flamelet library generated using the GRI3 mechanism. 169
Fig 7.1.2: Slice (Scalar Dissipation = 1/s) showing consumption of Oxygen. 170
Fig 7.1.3: Flamelet CO variation with scalar dissipation rate. 170
Fig 7.1.4: Flamelet NO Variation with Scalar Dissipation Rates. 171
Fig 7.1.5: NOx predictions with the infinitely fast assumption 173
Fig 7.1.6 NOx predictions using a global reaction curve fit by Steele 173
Fig 7.1.7: Modeling of the burning branch of the 'S-curve' 174
Fig 7.1.8: The 'S' Curve, as a solution of the flamelet equations 174
Fig 7.1.9: PDF table generation for non-adiabatic conditions. 176
Fig 7.1.10: Temperature predictions across equivalence ratios. 177
Fig 7.1.11: Laminar Flame Speed Polynomials calculated in Fluent. 178
Fig 7.2.1: Time Trace of LES over 9 ms (one flow through time) 180
Fig 7.2.2: Time Trace of Average Exit Temp over 9 ms 180
Fig 7.2.3: Temperature predictions along centerline 181
Fig 7.2.4: CO emission Results. 182
Fig 7.2.5: Unsteady Laminar Flamelet Probability Marker history. 184
Fig 7.2.6: NO predictions before and after running the post-processor 186
Fig 7.3.2: Effect of constant A 192
Fig 7.3.3: Default A=0.52 193
Fig 7.3.4: High Temperatures in the Premixer Ducts 196
Fig 7.3.5: Temperature Anomaly. 197
Fig 7.3.6: Compressibility Effects on pdf 199
Fig 7.4.1: CFD RANS of primary zone (Internal Data, 2004) 200
Fig: 7.4.2: FGM Model, Eggels 201
Fig 7.4.3: Current RANS Simulation of Primary 201
Fig 7.4.4: RANS simulation including torch swirl 201
Fig 7.4.5: RANS simulation of 'long' combustor. 202
Fig 7.4.6: Effect of central injection 203
Fig 7.4.7: Vortex Breakdown in the primary zone with torch swirl included. 205
Fig 7.4.8 (a-e in clockwise): LES Velocity Profiles (Reacting Flow). 208
Fig 7.4.9 (a-k): LES and RANS Temperature Contours 212

Fig 7.4.10: Temperature Contours on a slice between secondary windows..... 214
Fig 7.4.11: Slice through the secondary windows 215
Fig 7.4.12: Instantaneous snapshot of temperature contours – LES. 215
Fig 7.4.13: Vortical structures(Instantaneous LES)..... 216
Fig 7.4.14: Vortical structures near secondary entrance 217
Fig A1: Example of RANS Convergence 231
Fig A2: Example of LES Convergence (cold flow). 232
Fig A3: Example of LES Convergence (Reacting). 233

TABLES

Table 4.1: Boundary Conditions used for all the simulations. 112
Table 6.1: Boundary conditions for the pilot study..... 142

ABBREVIATIONS

DLE	Dry Low Emissions
GHG	Green House Gases
CD	Central Differencing
ISAT	In-Situ Adaptive Tabulation
QUICK	Quadratic Upwind Interpolation for Convective Kinetics
CFD	Computational Fluid Dynamics
TFC	Turbulent Flame Speed Closure
UFLA	Unsteady Flamelet Model
SFLA	Steady Flamelet Model
BCD	Bounded Central Differencing
RANS	Reynolds Averaged Navier Stokes
LES	Large Eddy Simulation
PDF	Probability Density Function
CRN	Chemical Reactor Network
GT	Gas Turbine
NOx	Nitrogen Oxide Emissions (Oxide, Di-oxide, Dinitrogen-tetroxides etc)

1. INTRODUCTION

The impact of toxic emissions on the environment from the combustion of fuels is well known. The introduction of such legislation as the US Clean Air Act, its many amendments (1963-1990) the signing of the Kyoto protocol (1987), the stringent emissions standards subsequently enforced through the Canadian Environmental Protection Act (CEPA, 1999) and several initiatives at international, federal and provincial levels, have motivated gas turbine designers to explore newer gas generation cycles, alternative fuels/fuel-flexibility and pursue ever stringent emissions standards particularly in the energy sector where industrial gas turbines using fuels such as natural gas are major producers of electricity. According to a recent report [1] from the National Climate Change Process Analysis and Modeling Group, Canada's participation in the Kyoto protocol indicates a goal to reduce emissions by 26% (Fig 1.1) during 2008-2012 from its projected 764 Mt (Mega tonnes), which would be the case at current trends. Several charts are reproduced in Fig 1.1 from this report detailing at a glance, the state of emissions in Canada and its projected trends.

Canada's Policy as Usual Emissions Projection and the Kyoto Protocol

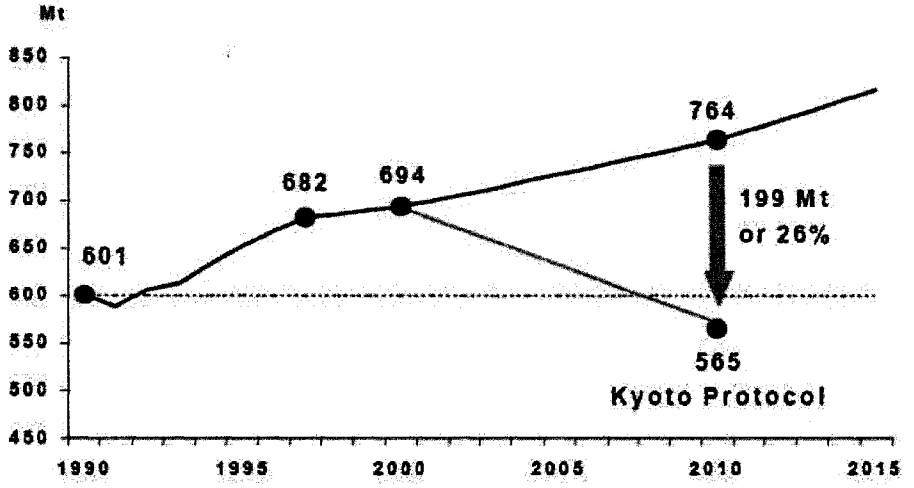

(a)

GHG Emissions By Gas

Mt of CO_2 Equivalent

	1990	1997	2000	2010	2020
Carbon Dioxide (CO_2)	461	520	537	596	662
Methane (CH_4)	75	90	90	92	97
Nitrous Oxide (N_2O)	57	64	57	62	65
Sulfur Hexafluoride (SF_6)	3	1	1	1	1
Perfluorocarbons (PFC)	6	6	6	6	6
Hydrofluorocarbons (HFC)	0	1	2	7	14
Total	601	682	694	764	845

Total may not add due to rounding.

(b)

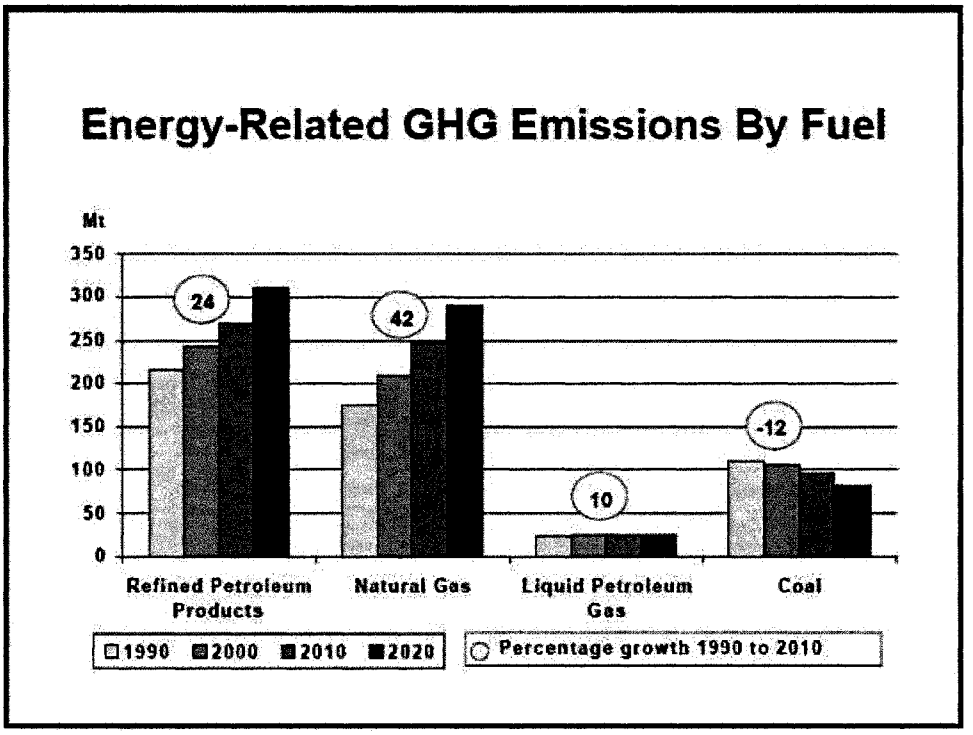
Energy-Related GHG Emissions By Fuel
Mt
350
300
250
200
150
100
50
0
24
42
10
-12
Refined Petroleum Products
Natural Gas
Liquid Petroleum Gas
Coal
1990
2000
2010
2020
Percentage growth 1990 to 2010

(c)

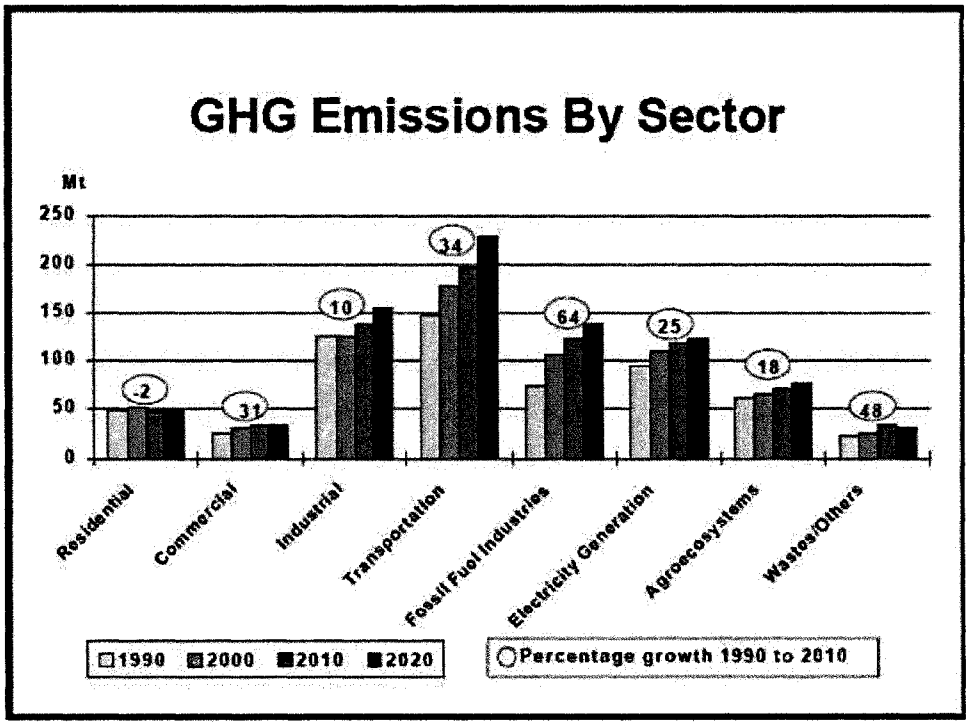
GHG Emissions By Sector
Mt
250
200
150
100
50
0
-2
31
10
34
64
25
18
48
Residential
Commercial
Industrial
Transportation
Fossil Fuel Industries
Electricity Generation
Agroecosystems
Wastes/Others
1990
2000
2010
2020
Percentage growth 1990 to 2010

(d)

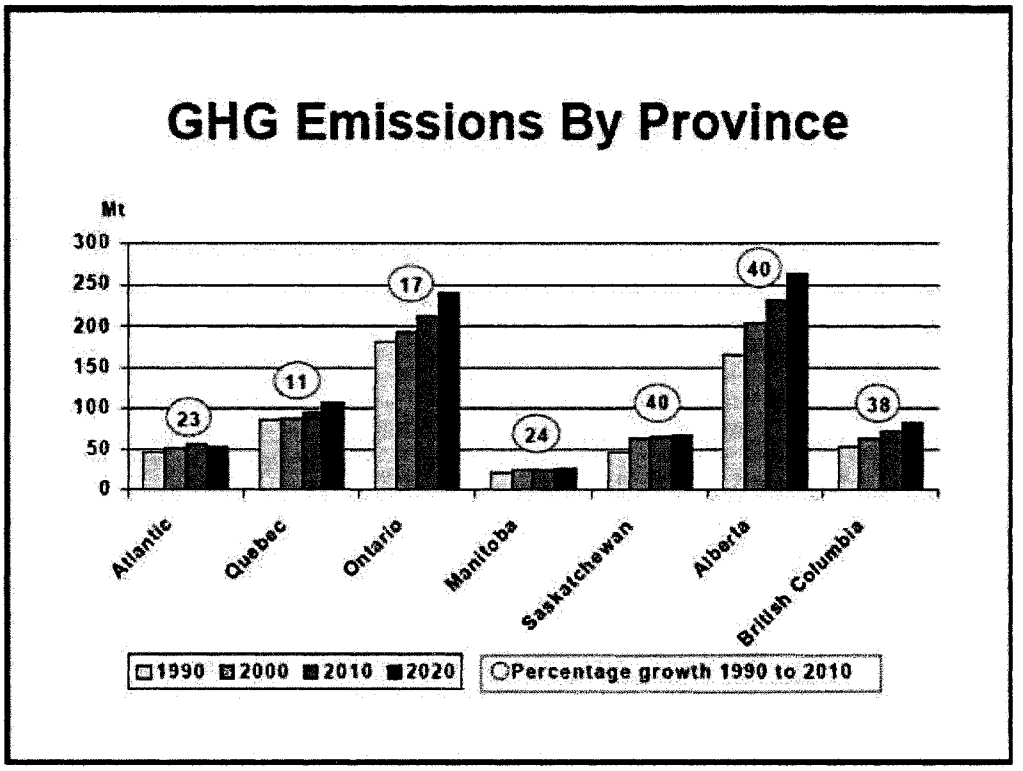

(e)

Fig 1.1 (a-e): Emission trends in various areas pertinent to Canadian industry [1].

It can be seen that the highest growth in GHG emissions comes from fossil fuel usage – motivation thus, to depend lesser on it and increasingly switch to alternative fuels, like syngas. The emissions due to electricity generation industry are predicted to grow by 25% by 2010. The majority of these emissions (over 84%) comes from using fossil fuels (coal) in the various combustion devices used in the process of generating electricity, while emissions due to the use of natural gas is at 9%. There is thus, the clear incentive to use natural gas as a fuel, best combusted through an industrial gas turbine engine. Unfortunately, the energy-

related emissions growth is highest for natural gas, which indicates the need for fundamentally different combustion methods in devices that aim to use natural gas although the greenhouse gases, from which these emissions are produced, are fairly consistent over the range of compositions that natural gas is available in. Dry Low Emissions technology promises to alleviate some of the concerns with using natural gas. The Kyoto protocol covers six greenhouse gases (GHGs) – carbon dioxide, methane, nitrous oxide, hydrofluorocarbons, perfluorocarbons and sulfur hexafluoride. Of these GHGs, it is NOx, CO and particulate (soot etc) emissions that are typical of Dry Low Emissions (DLE), single/dual fuel combustors. DLE combustors are typically land-based due to the large amount of auxiliary equipment required for emissions control. As the name indicates, DLE technology was developed to achieve the goal of very low NOx and CO emissions (less than 25 ppm for NOx and less than 10 ppm for CO if not eliminated altogether), which is unreachable by solely using steam or water injection. A typical installation is shown overleaf in Figs 1.2 and 1.3:

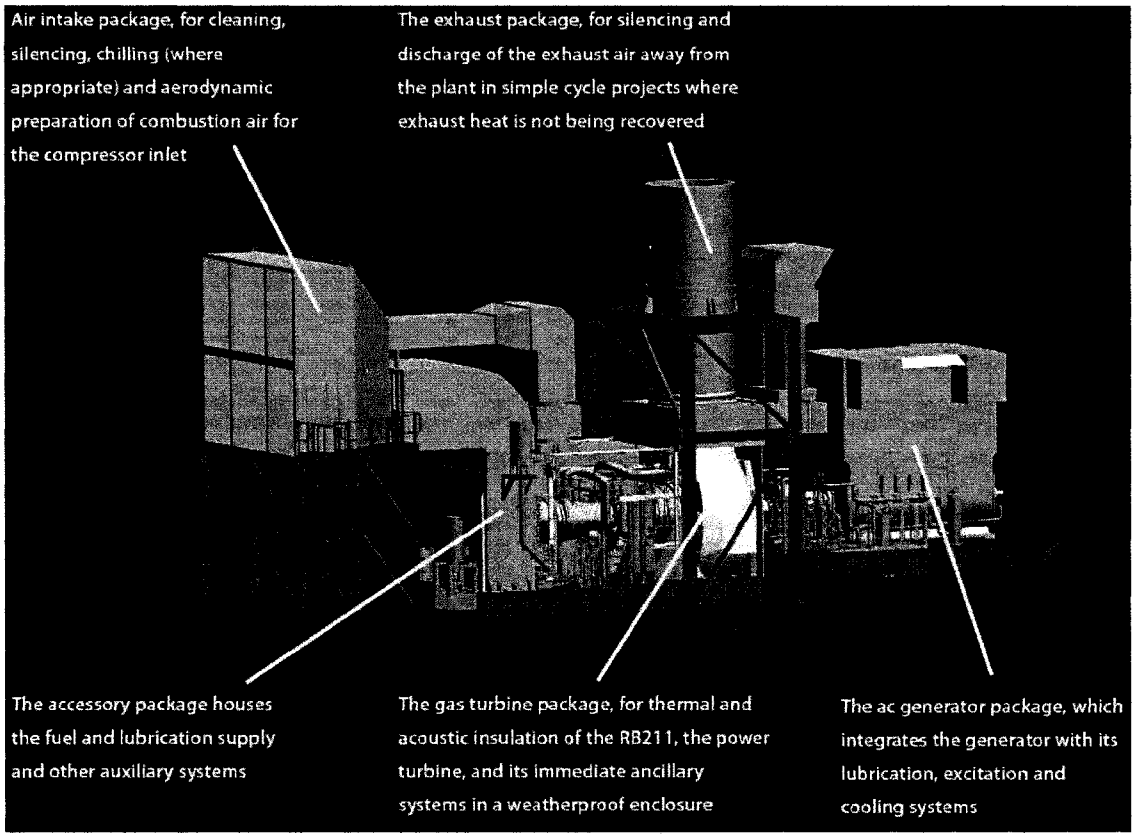

Fig 1.2: Rolls-Royce RB211 DLE installation (courtesy, Rolls-Royce Plc.)

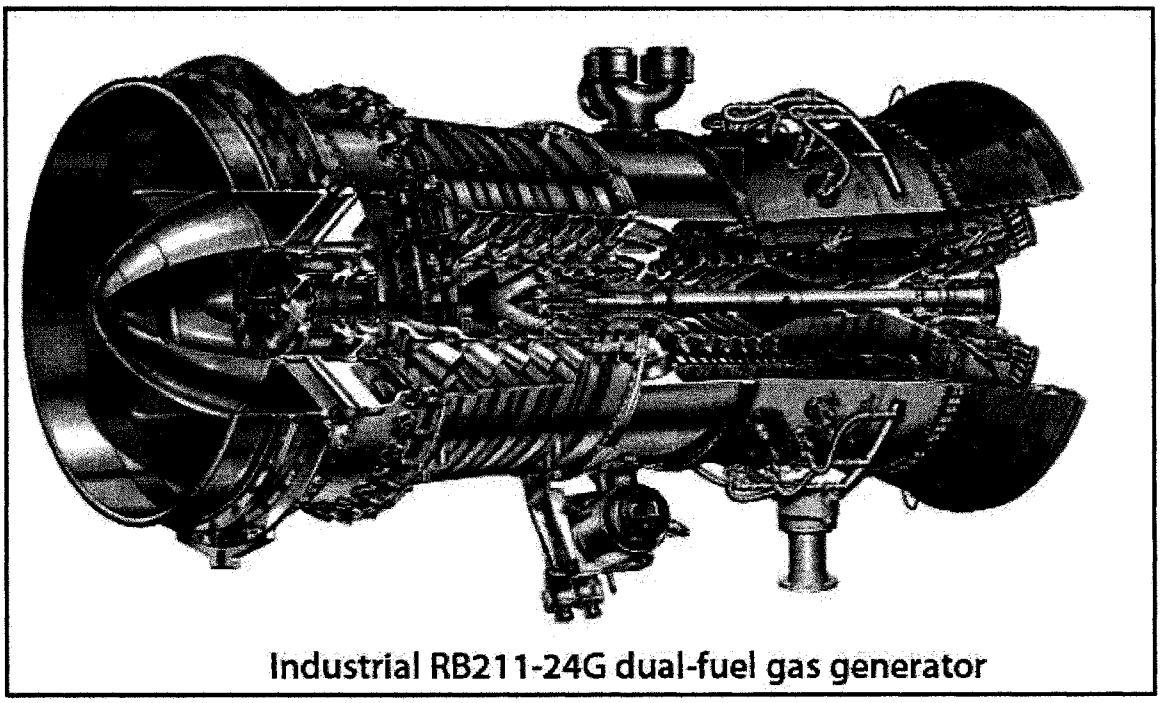

Fig 1.3: DLE Engine - Rolls-Royce RB211 (courtesy, Rolls-Royce Plc.).

With Natural Gas (NG) fuel compositions, several burners such as the Rolls-Royce RB211 (Fig 1.3), the Trent DLE, have proved to be commercially successful as well as environmentally friendly by retaining a consistent component life, while burning a lean mixture of premixed air and fuel and capable of burning both gaseous and liquid fuels. Fuel-flexibility in such combustors is most desirable as there is no consistent composition that natural gas exists in but varies from almost pure methane to compositions that contain significant quantities of ethane, propane, butane and even higher hydrocarbons. Fuel-flexibility studies indicate that a range of fuels can be used in these burners, which have run for tens of thousands of hours without combustion related problems. The amount of experimentation that must be done to finally arrive at a list of acceptable fuels is immense due to undesirable 'events' such as lean blowout, autoignition, flashback, thermo-acoustic instabilities – all primarily issues of inconsistent flame stabilization due to inconsistency in fuel composition. Full pressure rig testing at baseload, over the entire envelope of fuels still remains the only reliable method to gauge fuel acceptability. Typically, dozens of expensive rig tests are conducted for a broad range of fuel compositions. It can thus be seen that the problem faced by the combustor designer lends itself naturally to computational methods, parameterized by fuel composition. It is the aim of gas turbine research departments in the industry to

be able to come up with a method to eliminate the number of combustor design iterations or even cut down [3] on expensive rig tests using computational techniques. However the quality of modeling/simulation has been varied due to several well-known reasons: lack of computational power or time for advanced turbulence modeling, lack of rigorous combustion models, etc. CFD methods, for a long time, have been restricted to evaluating individual components with suitable 'boundary profiles' or obtaining 'first-pass' results or evaluating subtle changes in geometry or troubleshooting, rather than help accelerate major design changes. However, with the advent of the supercomputer, in recent years, it has become possible to use such computationally expensive turbulence models as LES on dense meshes for efficient and accurate predictions of turbulent, reacting flows to the extent of eliminating several tests that were otherwise conducted for lack of data. This report details the application of advanced turbulence models to the flow analysis of industrial lean-premixed combustors. Frequently, a cold-flow simulation yields insight into the highly complicated mixing processes that occur in a DLE gas turbine combustor and is critical to the prediction of combusting flows. Flow in a combustor is swirled in a premixer containing (usually) multiple fuel injection points. The 'complicated' nature of the final flow is due to the generation of large vortical structures due to the swirled nature of entry of premixed fuel and air into the combustion chamber.

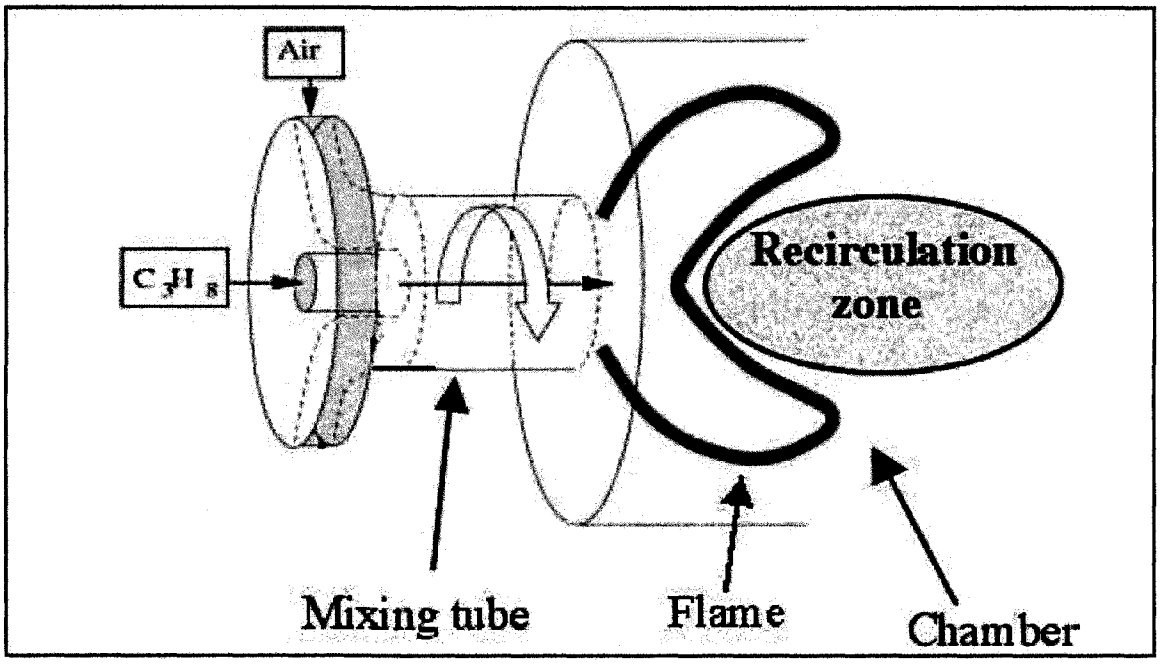

Fig 1.4: Schematic of Premixed Combustion, typical of DLE combustors [4].

Recirculation zones occur due to geometrical expansion as well as swirl induced vortex breakdowns. The central recirculation zone as seen in Fig 1.4 acts as an aerodynamic flame stabilizer, which precludes the need for a solid body flameholder usually used to prevent lean blowout. The mechanism of what exactly causes a vortex breakdown is complex and not understood clearly although it has been studied for decades [5]. A further complication is the effect of combustion on these recirculation zones. Experiments [6] show that the shape of the flame could drastically change depending on the swirl-number and/or degree of central injection of air or fuel. The current generation of combustors incorporate strongly swirled flows (strong enough to cause a 'vortex-breakdown'

which results in a 'bubble' type recirculation zone) to enhance the mixing of fuel and air in the primary zone of combustion. Due to the massively separated, high streamline curvature of the combustor aerodynamics, none of the RANS models can accurately capture the dynamics of the flow-field [7] e.g., size of the recirculation zones, to the degree that is necessary for both thermal and acoustic design of the combustor. With LES, the advantage lies in the fact that we do more simulation and less modeling. While reacting flows still remain challenging, it is recognized that even 'coarse' LES meshes can still attain a degree of accuracy that is greatly superior to that of RANS methods. Several works in the open literature indicate the suitability of LES to emissions predictions in complex, practical burners. A few examples are Mahesh et. al. [8], Schmitt et. al. [9], Selle et. al. [10], Wang et. al. [11], Roux et. al. [12], Sengissen et. al.[13] and Biagioli [7].

Combustion modeling is required to close the chemical source term that occurs in the transport equations for species or progress variables, depending on the quantity being transported. Combustion modeling has advanced to methods that can accurately predict species in clearly defined regimes of combustion, but are constrained by computational requirements. Typically, the partially premixed regime of combustion rather than the perfectly premixed or non-premixed approach is the most realistic situation encountered in practical combustors. The

industry continues to rely on fast chemistry, mixing-controlled approaches to predict mean heat release and while temperature fields are fairly well predicted by such species transport methods such as the EBU (eddy break-up) method by Magnussen and Hjertager [14] or the conserved scalar non-premixed pdf methods which incorporate effects of intermediate radical formations, the predictions of emissions of 'slow' or 'finite-rate' species like CO and NOx suffers and models must be tuned within a wide range to obtain realistic answers. Quantitative predictions of emissions are amongst the most difficult challenges to reactive CFD. Steady Flamelet methods, proposed by Peters [44] while incorporating the response of the flame to aerodynamic strain still assumes its instantaneous reaction and cannot predict such non-equilibrium phenomena as quenching, ignition and re-ignition. However an unsteady flamelet method presented by Barths et. al. [15], seems to produce very good predictions of CO in combination with LES. The works of Pitsch and Ihme [16] shows this to be the case. Most of the research has been concentrated on the simpler case of true non-premixed combustion and excellent results have been obtained through other models that seek to close the model in terms of conditional moments or means [17]. The model employed in the current study is suitable to partially premixed flames and employs a progress variable that separates the reaction zones into burnt and unburnt areas. Behind the flame front the mixture is assumed to be

mixing controlled and the non-premixed model is used. Ahead of it, the premixed model is used to calculate the temperature, density etc., of the unburnt mixture. This model is used in its non-adiabatic form as described by Biagioli [7]. It is attractive as it uses a pre-processed look-up table to calculate species mass fractions, which are linear functions of the run-time transported mixture fraction, the mixture fraction being a conserved scalar (thus eliminating a highly non-linear chemical source term) by virtue of the conservation of atomic elements in the multi-step chemical reactions that occur in the combustor.

Objectives and Method of the current work

It is proposed to use a well-validated commercial code, Fluent 6.3, using LES as a tool to obtain emissions predictions. The model is first tetrahedral meshed in GAMBIT and an LES of the cold flow is obtained for later comparisons. This mesh is converted into a polyhedral mesh in order to reduce cell count for purposes of reacting LES simulations. A RANS steady-flamelet simulation would first be carried out to obtain steady-state results. This will be used as an initial flow solution for the LES as well as another comparison with the reacting LES after averaging. When the statistics reach time periodicity, the flow will be sampled at regular intervals until the monitored emissions predictions and other

variables like temperature at a few points in the flow reach a steady, periodic value. At this point, the averaged flow field will be post-processed for NOx and CO emissions using a NOx post-processing method and the unsteady laminar flamelet method respectively. Thus the code is evaluated and validated with respect to its capability to simulate turbulent combustion in a real gas turbine combustor.

1. Lean premixed combustion, while consisting of initially non-premixed fuel and air, typically falls into the partially premixed regime of combustion. Predicting this regime is one of the most challenging tasks for computational methods [17]. Caracciolo et. al. [18] have done work in this area in the RANS context, and the present investigation extends this work to LES.
2. The combustor under investigation consists of two counter-rotating flows that greatly exacerbate the complexity of the flow-field. This work investigates how LES copes with this added feature.
3. The combustor under investigation is a two-stage device with secondary stage fuel and air being ignited by the flow of hot products from the primary reaction zone. It is thus an excellent test of the combustion model's effectiveness and provides valuable insight into an area of mixing

and combustion that is usually out of scope of experimental instrumentation.

4. A further investigation is made into assessing the effect of the turbulence model's effect on combustion predictions and whether it is sufficient or not for the combustion model's effectiveness.
5. The simulation is carried out at typical baseload conditions of high preheat of combustion air at high ambient pressures, conditions at which there are relatively few reports on. The effect of flame stretch, critical strain rate and turbulent flame speed is thus taken into account.

6. The boundary conditions are kept as far away as possible from the regions of interest in order to minimize their effect on the primary reaction zones. Thus the entire geometry is simulated and no boundary profiles are used. (Typically perfectly premixed boundary conditions). The effects of various features on emissions such as inhomogeneities in the primary premixer supply, the expedient of modeling cooling air using source terms and the influence of the turbulent flame speed on the emissions is investigated. Radiation however, has not been taken into account.

The nature of modeling in this work is complex and involves the use, selection and calibration of several sub-models ranging from sub-grid models for LES and several chemistry models. During the simulations, it was found that certain models were not applicable to the combustion regime. For example, while general methods simplify the problem by assuming boundary profiles from earlier calculations as input for the main calculations on a simplified domain, it was decided to model the full geometry in order to remove any constraints or questions faced by LES in determining boundary conditions to the main region of interest. In a similar fashion, premixed combustion problems often assume perfectly premixed boundary conditions, which leads to errors in emissions predictions since inhomogeneities (imperfect mixing) in the mixture fraction exist at the exit of the premixer passage. Thus to incorporate the real nature of the physics, the upstream geometry from almost the exit of the compressor has been modeled. In the same way, the secondary stage as well as the discharge nozzle just upstream of the turbine inlet guide vanes was included in the solution domain.

The succeeding chapters are laid out in the following fashion:

1. The description and nature of turbulence and combustion modeling.
2. The methods followed during post-processing for emissions predictions.
3. Cold flows analyses using RANS and LES.
4. Model setup for reacting flows, with justification behind the assumptions made and simplifications if any. An important part of this process is in analyzing the look-up tables produced during flamelet and pdf generation.
5. Reacting flow using RANS and LES with emissions predictions and comparisons with experimental data.
6. Analysis of the results.
7. Conclusions and future scope of work.

2. TURBULENCE AND COMBUSTION MODELING

2.1 Turbulence Modeling

A good way to understand the state of turbulence research in the past few decades is to consider the conclusions reached by Lumley and Yaglom in their excellent review [19] of turbulence research in the past century. To put the field in perspective, it is thought that after 100 years of experiments in turbulence, it is probable that this field of research has a very long duration since it is still in its infant stages, with very few breakthroughs and a non-linear structure to its growth (thanks to its first principles being visited and revisited and often revised!), which sets it apart from all other branches of physics. However, despite the empirical nature – uniqueness – of most experiments, the daunting task of modeling them is assuaged by the exponential increase in computing power, so that for everyday needs, atleast in industry, simplifying assumptions may be made – especially in the present age – without too much loss in the description of the flow physics.

Turbulence occurs when the inertia forces in the fluid become significant compared to viscous forces, and is characterized by a high Reynolds Number. The original Navier-Stokes (NS) Equations are exact for both laminar and turbulent flows. Direct simulation is preferable to modeling but the barriers are

insurmountable for complicated, dense meshes which are necessary in order to resolve the range of length and time scales that exist in a fully turbulent flow, with the added complexity of chemical reactions. The NS Equations are then used in their time-averaged or ensemble-averaged form, which gives rise to extra 'Reynolds stress' terms which require modeling in order to 'close' the set of equations that describe the turbulent flow field. To a first approximation, RANS turbulence models split the flow field into a 'mean' part and a 'fluctuating' part, and a statistical model is used in conjunction with the assumption of an isotropic turbulent eddy viscosity and thus closes the Reynolds stress terms in the Navier Stokes Equations. The k-epsilon model is an example. No attempt is made to account explicitly for the wide range of length scales that are present in real flows and thus this model suffers from over and under predictions of mixing. The LES method directly resolves the structure of 'larger' and highly anisotropic eddies in a turbulent flow, while using a simple eddy-viscosity isotropic, algebraic turbulence model to describe the nature of the smaller dissipative eddies. Analogous to the RANS method, it is possible to split the velocity field into a 'resolved' part and a 'filtered' part. The majority of the turbulent length scales are resolved directly, while the smaller, more isotropic eddies 'filtered-out' length scales are modeled using a simple algebraic turbulence model such as the Smagorinsky model, for example [26, 33].

2.1.1 RANS Turbulence Modeling and Governing Equations

For over three decades RANS models have been used as workhorses, especially in the industry, which is typically short on time for the analysis and design and production of new products. RANS turbulence models are accurate for simple flows and can give reasonably good predictions of the main flow characteristics such as pressure, temperature and velocity fields. However, the disadvantages of empiricism involved in the formulation of these models, the defects of the one-size-fits-all-simulations approach have become clearer and clearer as the level of resolution required increased due to the need for accuracy at very low levels, for example, chemical species predictions, turbulence intensities, scalar dissipation rates etc. A recent paper (2005) by Hanjalic [20] indicates that while it seems that the future of pure RANS methods may be in question (having failed to meet the original expectations), the large-scale use of CFD in the industry will continue to depend on conventional RANS models and possibly include some sort of hybridization with LES, popularly called 'Detached Eddy Simulation'. This is assuming Moore's law still holds. However any takeover of RANS territory by pure LES is still a matter of debate and unlikely in the near future, particularly in the matter of wall-bounded flows, such as aerodynamics of airfoils.

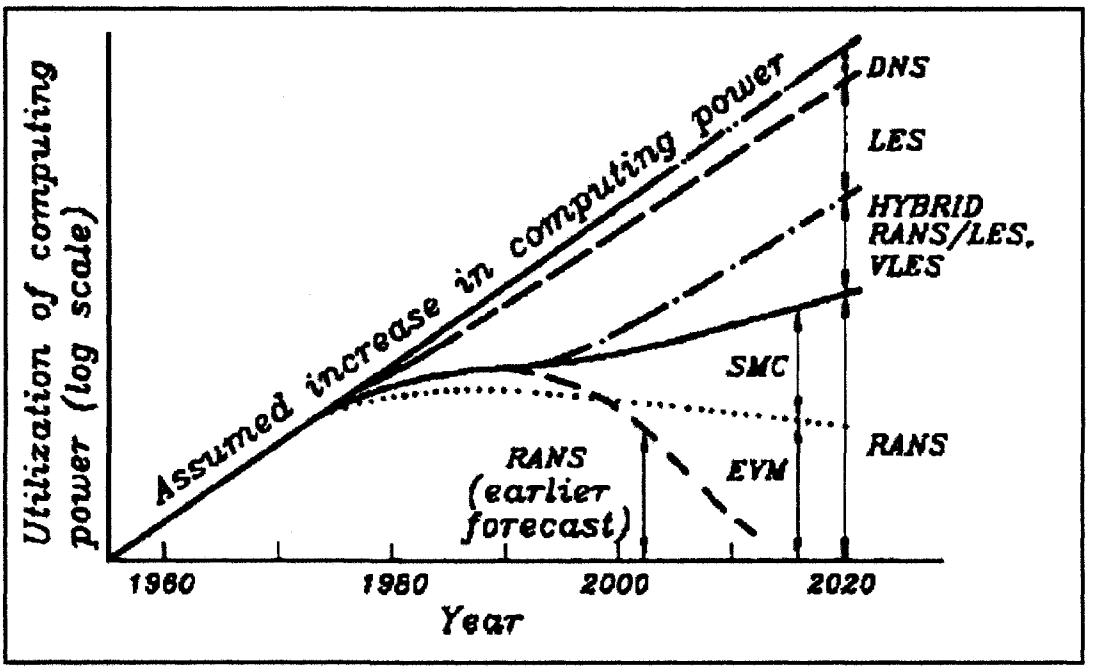

Fig 2.1.1.1: Review of RANS [19].

RANS turbulence models deal with the issue of closure of the stress terms in the NS equations by making simplifying assumptions such as the 'Boussinesq' hypothesis (used in several 'two-equation' models such as the k-epsilon, k-omega types) which attempts to relate the Reynolds stresses to the averaged velocity gradients by assuming the turbulent viscosity to be an isotropic scalar, which is not universally true. A brief description of a standard two-equation model is shown below as used in Fluent 6.3; along with the standard Reynolds averaged instantaneous equations for fluid flow, without reactions and body forces and gravitational effects.

The Continuity Equation

$$\frac{\partial \rho}{\partial t}+\frac{\partial}{\partial x_i}(\rho u_i)=S_m \tag{2.1.1.1}$$

The Navier Stokes Equations

$$\frac{\partial}{\partial t}(\rho u_i)+\frac{\partial}{\partial x_j}(\rho u_i u_j)=\frac{\partial}{\partial x_j}\left(\mu\frac{\partial \tau_{ij}}{\partial x_j}\right)-\frac{\partial p}{\partial x_i} \tag{2.1.1.2}$$

where the Boussinesq assumption is used to model the stress tensor, τ_{ij}.

$$\tau_{ij}\equiv\left[\mu\left(\frac{\partial u_i}{\partial x_j}+\frac{\partial u_j}{\partial x_i}\right)\right]-\frac{2}{3}\mu\frac{\partial u_l}{\partial x_l}I \tag{2.1.1.3}$$

Turbulence Model Equations

Turbulent Kinetic Energy

$$\frac{\partial}{\partial t}(\rho k)+\frac{\partial}{\partial x_i}(\rho k u_i)=\frac{\partial}{\partial x_j}\left(\left(\mu+\frac{\mu_t}{\sigma_k}\right)\frac{\partial k}{\partial x_j}\right)+G_k+G_b-Y_M+S_k \tag{2.1.1.4}$$

Eddy Dissipation Rate (the rate of turbulent kinetic energy dissipation)

$$\frac{\partial}{\partial t}(\rho\varepsilon)+\frac{\partial}{\partial x_i}(\rho\varepsilon u_i)=\frac{\partial}{\partial x_j}\left(\left(\mu+\frac{\mu_t}{\sigma_\varepsilon}\right)\frac{\partial\varepsilon}{\partial x_j}\right)+C_{1\varepsilon}\frac{\varepsilon}{k}(G_k+C_{3\varepsilon}G_b)-C_{2\varepsilon}\rho\frac{\varepsilon^2}{k}+S_\varepsilon \quad (2.1.1.5)$$

The Turbulent Viscosity, μ_t, is modeled as

$\mu_t=\rho C_\mu\frac{k^2}{\varepsilon}$, which assumes the 'linear' nature of the eddy viscosity. (2.1.1.6)

Several constants that are required for this model:

$C_{1\varepsilon}, C_{2\varepsilon}, C_{3\varepsilon}, C_\mu, \sigma_k, \sigma_\varepsilon$ take values of 1.44, 1.92, 0.09, 1.0, 1.3 respectively.

The standard model, has proved to be successful in simplifying the simulation of many industrial flows, but experience with it has shown that it performs poorly in the presence of recirculation due to solid obstacles in the flow (bluff body) or swirl-induced vortex breakdowns and other such highly unsteady phenomena that greatly increase the anisotropy of the system and in the case of combustion modeling, directly affecting the predictions of emissions/species mass fractions. One of the chief objections to using this turbulence model is its inherent tendency to overpredict turbulent diffusion, especially in the presence of heat release and

while very desirable for convergence, fails to accurately capture the flow physics. There are variants of this model, notably, the realizable k-epsilon model which is much more accurate in predicting flows with streamline curvature and recirculation by Shih et. al. [21] and the model developed from first principles using renormalization group theory, which can include swirl effects – the RNG k-epsilon developed by Yahkot and Orszag [22].

The realizable k-epsilon model is used in the RANS simulations used in this thesis due to its ability to resolves the 'round-jet anomaly' which indicates that the spreading rate of a round jet is poorly predicted by the standard k-epsilon model while that of planar jets were predicted better – a fact critical to the modeling of the dozens of round fuel jets that issue into the combustor premixers. The 'realization' of the turbulent kinetic energy in this model stems from the fact that the mean square velocity is always positive. By eliminating the case where unphysical (negative) values of the mean square velocity are obtained, by more rigorously incorporating the effects of strain, it is possible to obtain better flow-field predictions in rotating flows. The realizable model takes into account the Vorticity fluctuations and includes the effects of rotation into its turbulent viscosity formulation. The transport equation for the turbulent kinetic energy dissipation rate is reproduced below from [23].

$$\frac{\partial}{\partial t}(\rho\varepsilon)+\frac{\partial}{\partial x_j}(\rho\varepsilon u_j)=\frac{\partial}{\partial x_j}\left(\left(\mu+\frac{\mu_t}{\sigma_\varepsilon}\right)\frac{\partial\varepsilon}{\partial x_j}\right)+\rho C_1 S\varepsilon-\rho C_2\frac{\varepsilon^2}{k+\sqrt{\upsilon\varepsilon}}+C_{1\varepsilon}\frac{\varepsilon}{k}C_{3\varepsilon}G_b+S_\varepsilon$$

(2.1.1.7)

$$C_1=\max\left[0.43,\frac{\eta}{\eta+5}\right],\ \eta=S\frac{k}{\varepsilon},\text{ and }S=\sqrt{2S_{ij}S_{ij}}$$

The turbulent viscosity is calculated as

$$\mu_t=\rho C_\mu\frac{k^2}{\varepsilon}\qquad(2.1.1.8)$$

However, the C_μ term is now variable (unlike in the standard k-epsilon model, where it is constant at 0.09 from an empirical value taken from equilibrium boundary layers) and is a function of '*the mean strain and rotation rates, the angular velocity of the system rotation*', and the turbulence fields (k and epsilon) and is computed from

$$C_\mu = \frac{1}{A_0 + A_S \dfrac{kU^*}{\varepsilon}}$$

$$U^* \equiv \sqrt{S_{ij}S_{ij} + \tilde{\Omega}_{ij}\tilde{\Omega}_{ij}}$$

$$\tilde{\Omega}_{ij} = \Omega_{ij} - 2\varepsilon_{ijk}\omega_k \qquad \text{(2.1.1.9-12)}$$

$$\Omega_{ij} = \bar{\Omega}_{ij} - 2\varepsilon_{ijk}\omega_k$$

where, $\bar{\Omega}_{ij}$ is the mean rate-of-rotation tensor with angular velocity ω_k.

$A_0 = 4.04$ and $A_S = \sqrt{6}\cos\phi$

where

$$\phi = \frac{1}{3}\cos^{-1}\left(\sqrt{6}W\right) \quad \text{and} \quad \tilde{S} = \sqrt{S_{ij}S_{ij}}$$
$$W = \frac{S_{ij}S_{jk}S_{ki}}{\tilde{S}^3} \qquad S_{ij} = \frac{1}{2}\left(\frac{\partial u_j}{\partial x_i} + \frac{\partial u_i}{\partial x_j}\right)$$

This formulation undoubtedly incorporates some of the anisotropy of the vortex-dominated flows but still falls short since it cannot account for full closure of the Reynolds stresses. Such a thing can happen only if full second moment closure of the six independent Reynolds stresses is made. This does away with the

Boussinesq assumption, which poorly represents the effect of these stresses but involves the solution of five extra transport equations (one for each stress) and greatly increases the computational expense. It is beyond the scope of this thesis to discuss this greatly improved model, as it was not found feasible to use this model in the context of combustion flows where individual species each require a transport equation. While pdf methods (discussed later) are undoubtedly of help, LES has proved to be of greater accuracy for emissions predictions, which is what this exercise is all about. However, in a pilot study, this model was used in order to compare with the other models. This will be discussed in Chapter 6.

2.1.2 Large Eddy Simulation and Governing Equations

A review on the state-of-the-art Piomelli (1999) [24] indicates the onset of advanced subgrid-models and achievements made possible by the recent advances in supercomputing hardware and algorithms. Later reviews, directly dealing with the state of combustion LES by Pitsch (2006) [25] and Bilger et. al. (2005) [17], indicate that this is still an area of intense research and that the knowledge gained while immense, indicates that the *'necessary theory for combustion LES has yet to be developed...its full predictive potential has not yet been reached'*. [24]

Originally developed to model weather phenomena, large eddy simulation techniques have developed considerably in recent decades of advancements made in the general area of computational methods for fluid dynamics. Pope [29] indicates that the classic works in this field are by Smagorinsky (1963) [26], Lilly (1967) [27], Deardorff (1974) [28], Schumann (1974) [30]. The term 'Large Eddy Simulation', was used for the first time in the first successful LES simulation by Leonard (1974) [31]. Due to the lack of computing power at the time, LES has been used only to simulate very large vortical structures as are found in major weather phenomena such as ocean-mixed layers, cloud formations etc (Galperin

and Orszag, 1993) [32]. Thanks to increases in computing power as well as associated computer architecture, simulations containing larger ranges of length and time scales have been made possible to the current day scenario where LES may be adequately applied to complex geometries containing complex flow-fields. Indeed the only viable model best able to simulate turbulence with the least amount of modeling is the LES model. However, there are several *caveats* to this as outlined by Pope [29]. Indeed the views on the applicability of LES to various flow regimes is still a matter of discussion and debate and there exist many divergent theories, especially in the matter of the sub-grid model formulation.

The original Navier-Stokes Equations are fully complete and do not need closure. However they can only be used in discretized form and in the DNS context. The next level of simplification, indeed at a fraction of the cost of a DNS, is LES, where the large-scale eddies are explicitly resolved based on a 'cut-off' space filter, that leaves only the smaller, dissipative, 'sub-grid' eddies to be modeled. This cut off is what differentiates LES from DNS and reduces the computational cost by a factor of $Re_{\Delta}^{9/4}$, where Re is the subgrid Reynolds Number and Δ is the local grid spacing. A relatively uncomplicated algebraic model called a sub-grid model can be used at this resolution.

The filtered equations used for incompressible LES are similar to the RANS, but differ in their treatment of the stress tensor and the subsequent modeling of the subgrid turbulent viscosity. The overbar indicates the filtering operation. Several choices for a filter are reviewed by Piomelli [23].

The Filtering operation on a variable x of a test function $\overline{f}(x)$ is done in the following manner [23].

$$\overline{f}(x) = \int f(x')G(x,x';\overline{\Delta})dx' \qquad (2.1.2.1)$$

carried out over the entire domain. G is a filter function that accomplishes the actual filtering and can be gaussian, top hat or sharp Fourier cut-off functions. In the Fluent 6.3 formulation, the filtering operation is implicitly supplied by the finite-volume discretization and is defined as

$$G(x,x')\begin{cases} 1/V, & x' \in \nu \\ 0, & x' \text{ otherwise} \end{cases} \qquad (2.1.2.2)$$

The following equation set form the basis for the LES simulations in Fluent. They are presented in their incompressible form for simplicity. It is important to note

that all the combustion simulations used in this thesis use Favre-filtered governing equations, due to the large density changes.

The Continuity Equation

$$\frac{\partial \rho}{\partial t}+\frac{\partial}{\partial x_i}\left(\rho \bar{u}_i\right)=0 \qquad (2.1.2.3)$$

The Navier Stokes Equations:

$$\frac{\partial}{\partial t}\left(\rho \bar{u}_i\right)+\frac{\partial}{\partial x_j}\left(\rho \bar{u}_i \bar{u}_j\right)=\frac{\partial}{\partial x_j}\left(\mu \frac{\partial \sigma_{ij}}{\partial x_j}\right)-\frac{\partial p}{\partial x_i}-\frac{\partial \tau_{ij}}{\partial x_j} \qquad (2.1.2.4)$$

where σ_{ij}, the stress tensor due to molecular viscosity is defined as:

$$\sigma_{ij} \equiv \left[\mu\left(\frac{\partial \bar{u}_i}{\partial x_j}+\frac{\partial \bar{u}_j}{\partial x_i}\right)\right]-\frac{2}{3}\mu \frac{\partial \bar{u}_l}{\partial x_l}\delta_{ij} \qquad (2.1.2.5)$$

the same RANS assumption of isotropic eddy viscosity is made for the sub-grid stresses, and τ_{ij}, which in the LES context is the subgrid-scale stress defined as:

$$\tau_{ij} = \rho\overline{u_i u_j} - \rho \bar{u}_i \bar{u}_j \qquad (2.1.2.6)$$

The subgrid scale stresses must be modeled and they consist of three kinds: Leonard stresses, L_{ij}, (stresses entirely due to the unresolved subgrid scale eddy's contribution to the main kinetic energy of the flow), cross stresses, C_{ij}, (stress due to the course of interaction between the resolved large scale eddies and the small scale, filtered-out eddies) and subgrid Reynolds stresses, R_{ij}, defined in [24] as

$$\tau_{ij} = \rho\overline{u_i u_j} - \rho\overline{u}_i\overline{u}_j = L_{ij} + C_{ij} + R_{ij} \qquad (2.1.2.7)$$

where

$$\begin{aligned} L_{ij} &= \overline{\overline{u}_i\overline{u}_j} - \overline{u}_i\overline{u}_j \\ C_{ij} &= \overline{\overline{u}_i u_j'} + \overline{\overline{u}_j u_i'} \\ R_{ij} &= \overline{u_i' u_j'} \end{aligned} \qquad (2.1.2.8,9,10)$$

A key difficulty is in identifying how much to filter out, since the amount of resolved turbulent kinetic energy cannot be known apriori in order to make the best choice and further, is directly proportional to the local grid spacing, Δ, so that there cannot be true grid independence. Further, if too coarse filtering is done, energy could be transferred back up into the larger, explicitly resolved energy scales – a phenomenon similar to the aliasing that happens in electronic signal analysis when a signal is sampled at less than twice its bandwidth and causes high frequency signals to appear at low frequencies – also called 'backscatter' or aliasing errors, when sharp, Fourier cut-off filters are used. This

positive transfer of energy from eddies that are supposed to be dissipating, causes numerical instability and results in unphysical results. However, depending on the main flow features, a grid can be built based on the post-processing of the turbulent kinetic energy resolution from an initial arbitrary grid built from experience with the type of flow being simulated.

The sub-grid scale requires a sub-grid turbulence model in order to mitigate the effect of leaving a part of the energy unresolved due to the small length scales and deal with the subgrid-scale 'closure' problem of modeling the sub-grid scale stresses. In this thesis, the dynamic procedure of Germano et. al. [33] by using 'test-filters' to dynamically determine the model constants as the solution progresses, was used to compute the turbulent Prandtl and Schmidt numbers based on knowledge of the resolved flow field which provides the energy content of the smallest resolved scale [24]. (This is a key feature of LES and removes the 'constant' assumption, used in RANS models, which have been known to predict wildly different results when the constants were 'tuned' in order to match experimental data (c.f. Chapter 6), as well as compute the sub-grid model constants so that a 'constantless' model is obtained. A recent paper by L-Y Jiang [34] confirms this author's experience with a simple dump combustor non-premixed simulation, the results of which are presented in

section). The dynamic procedure does have its drawbacks as Piomelli [24] outlines the increasing complexity of the procedure, which consumes a significant portion of CPU resources. The dynamic sub-grid model used in the LES simulation in this thesis is called the 'dynamic Smagorinsky-Lilly model', which is the dynamic procedure of Germano et. al. [33] and subsequently Lilly [35], applied to the original Smagorinsky model.

The original Smagorinsky model is defined in Smagorinsky [26] and only the modeling of the turbulent viscosity is shown below

$$\mu_t = \rho L_s^2 \left|\overline{S}\right| \qquad (2.1.2.11)$$

where

L_s is the mixing length for subgrid scales determined as $\min\left(\kappa d, C_s V^{1/3}\right)$ where κ is the von Karman constant, d is the distance closest to the wall, $C_s = 0.17$ [35] is the Smagorinsky constant and V is the volume of the computational cell.

And $\left|\overline{S}\right| = \sqrt{2\overline{S}_{ij}\overline{S}_{ij}}$. (2.1.2.12)

The dynamic procedure updates the C_s value over space and time.

Wall boundary layer resolution requires DNS-like grids [24] and it is hard to do this without drastically increasing the overall grid density. While unstructured

meshes can help, LES suffers greatly when numerical diffusion is present. Central Differencing Methods are used to combat this. A bounded central differencing (BCD) scheme is provided by Fluent to alleviate the wiggles produced by pure CD.

2.2 Combustion Modeling

Two recent reviews provide an excellent commentary on the state of combustion modeling with implications of various paradigms in the past five decades, and more specifically, turbulent combustion in the LES context by Bilger et. al. [17] and Pitsch [25] respectively. This thesis seeks to contribute towards the assessment of LES for combustion predictions, the chief aim being the accurate predictions of highly mixing dependent, species concentrations. Combustion modeling is an area of intense research and after thirty years, much of the modeling seems to resemble that of turbulence research, with models proposed decades ago, still the standard workhorses of today's simulations. Similar to the turbulence closure problem for the Reynolds stresses, combustion modellers face a closure problem for the chemical source term in the species mass fraction transport equation, which accounts for the convection, diffusion, production and destruction of chemical species formed as a result of the reactions. In the case of a progress variable transport equation which tracks the location of the flame front

in premixed and partially premixed approaches to combustion modeling, a definition of the turbulent flame speed is required to close the model. A further complexity, is the introduction of widely varying chemical timescales due to species reaction rates ranging from very fast to very slow (pollutant formation etc.). Still aggravating, is the chemical process itself, which does not work through single step 'global' reactions, but must proceed through often hundreds of intermediate reaction steps, that involve typically hundreds of radicals. The reaction rate is directly influenced by the mixing processes and hence dependent on very accurate predictions of turbulence. The standard way of dealing with the chemistry effects, with the least amount of modeling, is to introduce a general scalar transport equation for each of the species and attempt to model the source term. This is clearly impossible due to the number of species involved and further modeling is necessary to bring down the 'dimensionality' of the problem with simplifying assumptions such as infinitely fast chemistry or the 'conserved-scalar' mixture fraction approach which reduces the transported quantities to a single scalar which describes the local equivalence ratio. In this section, a brief note is made of the modelling process, where assumptions need to be made, the effect of such assumptions. Some of the more established combustion models are described and finally discuss the reason why a particular model is chosen for the practical problem in question. Combustion modeling has seen approaches that

seek to focus on perfectly premixed combustion, non-premixed combustion as well as models applicable to the more challenging situation of partially-premixed combustion. To go into detail on each, is beyond the scope of this thesis as the data on each is exhaustive and the reader is encouraged to consult the reviews mentioned above to get a fuller understanding of where we are. Suffice to say, that there are models now, which permit higher accuracy and pack in more physics, and computationally less expensive than the simple models routinely used. It is also most important to note that in the models used, the quality of species predictions directly depend on the quality of the turbulent quantities predictions or rather, the main flow field mixing predictions. Often a good combustion model performs very poorly due to incorrect modeling of the main mixing regions, a fact that will be discussed in one of the author's simulations in Chapter 6. The solution is to keep boundary conditions far away from the region of interest, as well as have a well-validated cold flow prediction prior to a reacting flow simulation. While this may not always be possible due to lack of experimental data, the aerodynamics of the combustion chambers are self-evident in most cases. A Large Eddy Simulation carried out also proves that excellent mixing predictions are not enough for accurate species predictions since the combustion models routinely reveal their flaws due to over-simplification of the physics of chemical kinetic effects on the main flow. Present day commercial

CFD codes, as noted in a (non-reactive) comparative analysis (of CFX, Fluent and StarCD) at the Center for Turbulence Research, Stanford University, (Iaccarino, 2001) [36], present the CFD user with a bewildering array of choices for turbulence and combustion sub-models and choosing this and not that, is in itself a challenge, particularly so, to a user who wishes to (ill-advisedly) operate the code as a black box.

2.2.1 Species Transport Modeling

It is well known that it is not possible with current (or foreseeable) computational resources, to transport every specie that takes part in the chemical process of combustion flows. As a first simplification, the multi-step chemical kinetic equations can be reduced to a few 'global' equations that are significantly more dominant (by virtue of the stability and effect on the main temperature field by the chemical species involved). These 'reduced' mechanisms contain fewer species and eliminate most intermediate product formations, the association/dissociation radical reactions etc. Well known mechanisms for methane, that are tractable for computational use in the transported species method are the 6 species, 2-step methane-air mechanism of Westbrook and Dryer [37], Peter's 4-step mechanism [38], Nicol's 5-step mechanism [39] etc. For emissions predictions, the above lack NOx species and thus implies the need for

8-9 step mechanisms such as Novosselov's [40], which include these species, at the very least. The performance of these mechanisms can show deviations from experimental data depending on factors such as high pressures, equivalence ratios etc. In this context, care must be taken to consider the envelope of pressures and equivalence ratios over which these mechanisms are validated. Care must also be taken in avoiding over-simplification of the chemistry model. A paper by Pope and Cao examines the influence of skeletal as well as comprehensive chemical mechanisms on transported pdf simulations in Ref 60. The physics of the combustion device must also be considered, for example, whether the purpose of the investigation is to merely obtain a qualitative overview or simulate specific 'events' like autoignition (in which case, many more species (hundreds) are required!) or extinction and quenching or reignition etc. Usually, however, the main interest is in the steady-state combustion regime and studies [10, 12] indicate good results from explicitly transporting species, with as less as 2-steps in the mechanism when used in conjunction with LES. A comparison was done between two and four step mechanisms in the LES context by (Bissieres et. al., CERFACS, 2005) and it was found that the four-step mechanism predicted flame-stabilization much better at a higher fuel-air ratio (FAR) than the 2-step mechanism. It must be mentioned that the studies above worked on similar – if not the same – combustor.

A figure reproduced from Bissieres [41] (left) highlights this, while the figure on the right, reproduced from Bell et. al. [42] indicates the effect of the chemical mechanisms on ignition delay at very high pressures.

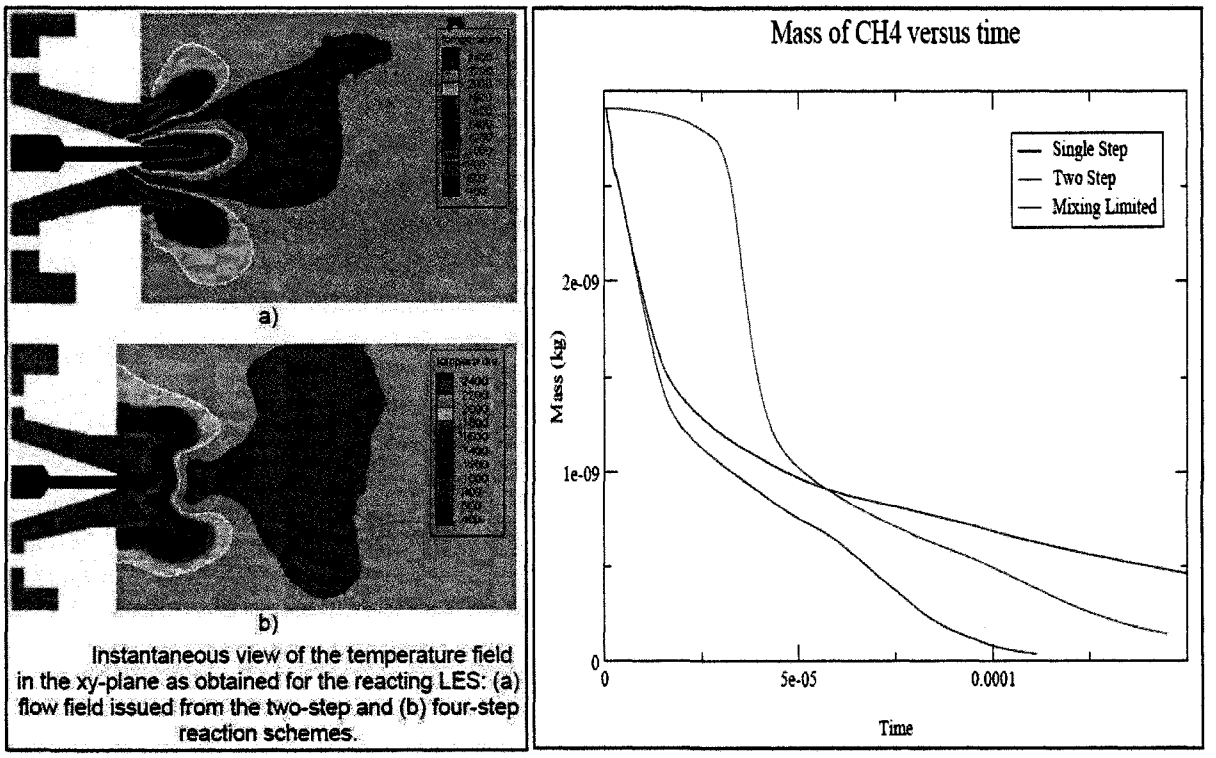

Fig 2.2.1.1: *(left)* Effect of mechanism on flame-stabilization [41] and *(right)* ignition delay in the context of species transport [42].

Fluent uses the following transport equation to transport i-th species Y_i

$$\frac{\partial}{\partial t}(\rho Y_i)+\nabla\bullet(\rho\vec{v}Y_i)=-\nabla\bullet\vec{J}_i+R_i+S_i \qquad (2.2.1.1)$$

where R_i is the net rate of production of species i by chemical reaction and is given by the equations:

For Irreversible reactions

$$\hat{R}_{i,r} = \Gamma\left(\nu''_{i,r} - \nu'_{i,r}\right)\left(k_{f,r}\prod_{j=1}^{N}\left[C_{j,r}\right]^{\left(\eta'_{j,r}+\eta''_{j,r}\right)}\right) \tag{2.2.1.2}$$

where

Γ is the net effect of third bodies involved [23]

$\nu'_{i,r}$ is the reactant species stoichiometric coefficient

$\nu''_{i,r}$ is the product species stoichiometric coefficient

$C_{j,r}$ is the molar concentration of species j in reaction r

$\eta'_{j,r}$ is the rate exponent for reactant species j in reaction r

$\eta''_{j,r}$ is the rate exponent for the product species j in reaction r

For Reversible reactions

$$\hat{R}_{i,r} = \Gamma\left(\nu''_{i,r} - \nu'_{i,r}\right)\left(k_{f,r}\prod_{j=1}^{N}\left[C_{j,r}\right]^{\left(\eta'_{j,r}\right)} - k_{b,r}\prod_{j=1}^{N}\left[C_{j,r}\right]^{\left(\nu''_{j,r}\right)}\right) \tag{2.2.1.3}$$

The forward rate constant $k_{f,r}$ is given by the Arrhenius expression

$$k_{f,r} = A_r T^{\beta_r} e^{-E_r/RT} \tag{2.2.1.4}$$

where

A_r is the pre-exponential factor

β_r is the temperature exponent

E_r is the activation energy for the reaction (J/kgmol)

R is the universal gas constant (J/kgmol-K)

$\vec{J}_i$ is the diffusion flux of species i, and in turbulent flows, is modeled as

$\vec{J}_i = -\left(\rho D_{i,m} + \frac{\mu_t}{\mathrm{Sc}_t}\right)\nabla Y_i$ where $\mathrm{Sc}_t = \frac{\mu_t}{\rho D_t}$ is the turbulent Schmidt number and though considered generally to be a constant near 1.0, a number of authors have questioned the Reynolds' analogy on which this assumption is based and have found that this 'constant' needed to be tuned between 0.1 and 1.0 in order to tally with experimental data. Some discussion and results of this is presented in the next section.

The Species transport method can be implemented in three ways for fully turbulent flows, in ascending order of computational complexity:

1. *Considering chemistry to be infinitely fast* – suitable for non-premixed combustion and assumes mixed is burned. This approach assumes that the fuel consumption is a function of the local turbulence level of the flow, and releases heat energy wherever turbulence is present. However, this approach (originally due to Spalding, 1971 [43]) causes premixed fuel-air mixtures to burn immediately upon entering the domain and thus causes

numerical autoignition in mixing ducts prior to the main chamber. This model is called the eddy-break up model by Spalding.

2. *Considering chemistry to be mixing controlled* – suitable for non-premixed, perfectly premixed and partially premixed combustion, but limited to two or four step chemical kinetic mechanisms where the effects of Arrhenius reaction rates are neglected behind the flame-front and the calculation proceeds according to approach 1. The Fluent implementation is based on the work of Magnussen and Hjertager [14], which modifies the original approach to use the Arrhenius rate as a 'switch' to separate combustion zones from non-combustion (premixer ducts for example) zones. The switch acts by considering the minimum of the timescales of the Arrhenius rate of reaction and the eddy-dissipation rate. These two rates are defined in the rate of production of species as below, reproduced from [23] .

$$R_{i,r} = \nu'_{i,r} M_{w,i} A \rho \frac{\varepsilon}{k} \min_{\Re} \left(\frac{Y_{\Re}}{\nu'_{\Re,r} M_{w,\Re}} \right) \qquad (2.2.1.5)$$

and

$$R_{i,r} = \nu'_{i,r} M_{w,i} AB \rho \frac{\varepsilon}{k} \left(\frac{\sum_P Y_P}{\sum_j^N \nu''_{j,r} M_{w,j}} \right) \qquad (2.2.1.6)$$

where

Y_P is the mass fraction of any product species, P

$Y_{\mathfrak{R}}$ is the mass fraction of a particular reactant, $\mathfrak{R}$

A and B are empirical constants equalling 4, 0.5 respectively.

These 'constants', A and B are generally 'tuned' within a very wide range in order to match experimental results and is considered a serious flaw of this model. For some discussion on this, the reader is encouraged to consult Novosselov [40], Peters [44]. An additional disadvantage is the inability of this model to predict radical species forming due to its limited capability for simulating with multi-step chemical kinetic mechanisms. Despite the flaws, however, this method has been the workhorse of the industry for decades and has proved to be a reasonable trade-off between the first and the third approaches.

3. *Considering the full effect of Arrhenius chemical finite-rate kinetics as well as turbulence effects.* – This approach overcomes most of the deficiencies of the above two, but is also computationally most demanding as the full equation set of the chemical kinetic mechanisms are considered and Arrhenius rates differ so non-linearly that the equation set is considered

very stiff and requires considerable treatment and conditioning. The nature of the model is to simulate combustion at fine scales, assuming each cell as a constant pressure reactor, with initial conditions taken to be the cell's current species and temperature and cell volume. The Arrhenius rate of reaction over the residence time (characteristic timescale) governs the formation of products and intermediate products. Since the calculations involve stiff matrices, an ISAT technique [45] (In-Situ Adaptive Tabulation) is used to build trees of linear interpolations of initially directly integrated solutions so that subsequent operations involve 'adds' and 'retrieves' through querying the dynamically growing tree table rather than full integration. The theory of this method is beyond the scope of this thesis and the reader is encouraged to consult for further information. It is sufficient to state that this method is not tractable for very large chemical mechanisms, which contain dozens of steps, especially in the case of higher hydrocarbons. Results, atleast in the RANS context, in complex geometries however bring out this defect very clearly as seen in the Fig 2.2.1.2 overleaf, reproduced from [46]:

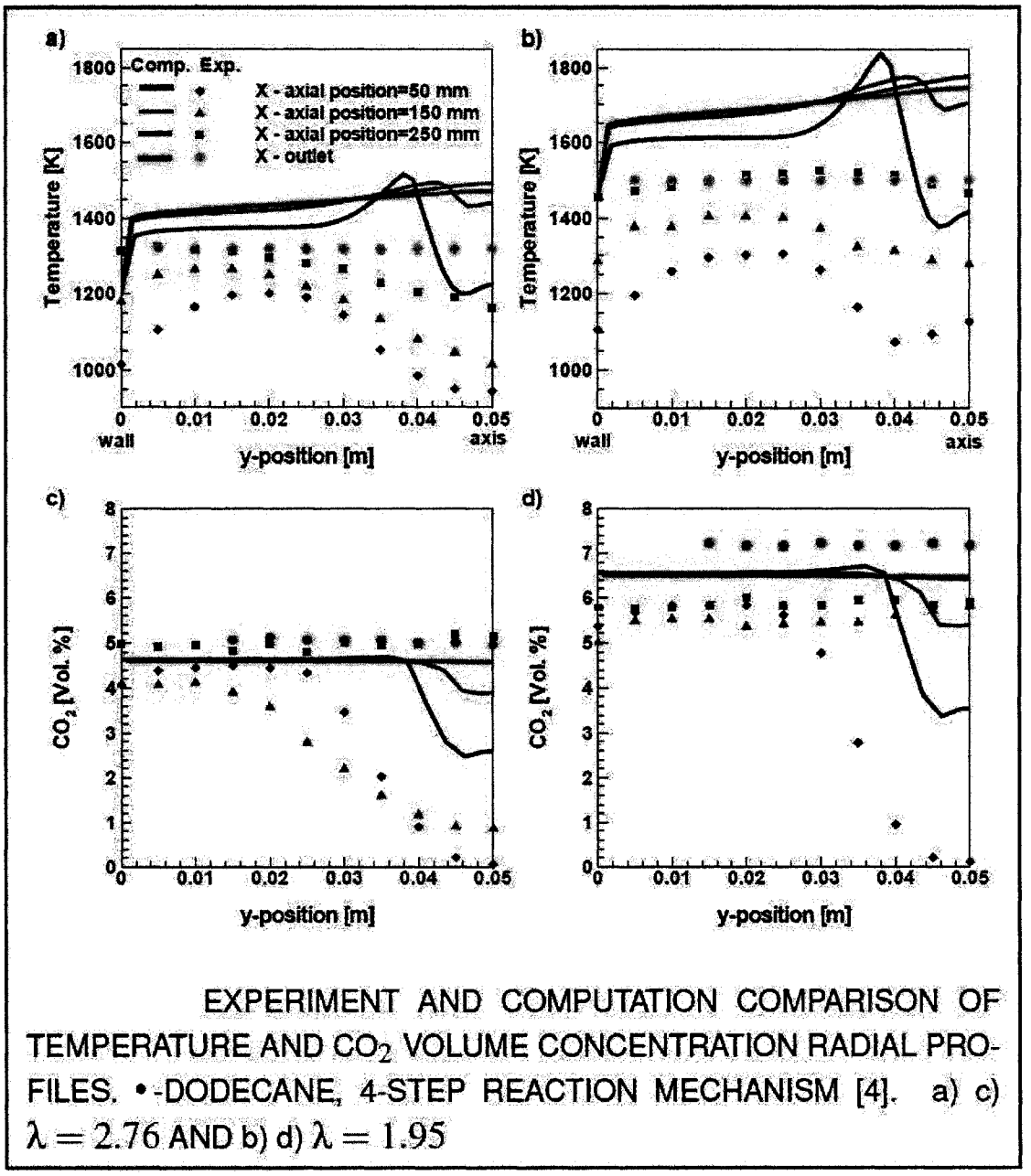

EXPERIMENT AND COMPUTATION COMPARISON OF TEMPERATURE AND CO_2 VOLUME CONCENTRATION RADIAL PROFILES. •-DODECANE, 4-STEP REACTION MECHANISM [4]. a) c) $\lambda = 2.76$ AND b) d) $\lambda = 1.95$

Fig 2.2.1.2: Eddy Dissipation Concept results [46].

Considering all these approaches, it was decided that the finite-rate effects of chemical mechanisms *must* be included in some way if proper predictions of emissions can be made and the best way forward seems to be a statistical method that can reduce the complexity of the problem – the assumed shape probability

density function (PDF) method, indicates better predictions, in many cases with lesser computation. This is the subject of the next section.

2.2.2 PDF methods

It is possible to account for the effects of intermediates and radical species on the main temperature field, by considering their *instantaneous* fractions to be linear functions of a conserved scalar, called the mixture fraction, which simply, is a measure of the local equivalence ratio. The diffusion of all species is assumed to be equal, implying a Lewis number of unity[1]. In such a case, only the mean and variance of this scalar, f, needs to be calculated. The *mean* mass fraction of the species in question is found by weighting the integral with the probability of f occurring with a specific value during a specific period of time, the probability defined by an assumed-shape probability density function of the samples (fluctuations) taken, over all the possible values of the mixture fraction. The great savings in computational effort is achieved, due to the nature of obtaining these mass fractions by creating a look-up table of these values, *prior* to the solution run-time. At run time, the mean species mass fractions are calculated by looking-up this table and interpolating accordingly as values of the mean, variance of f are obtained from their transport equations. If there are heat losses/gains to the

[1] This however may be dangerous numerically, to assume, if significant quantities of fuels like Hydrogen are present in the fuel composition. The equations must then be reformulated to include the Lewis number effect.

system, the mass fraction of the species is a function of the enthalpy also. In which case a transport equation for the enthalpy, rather than the usual energy equation is solved, resulting in a three-dimensional look-up table.

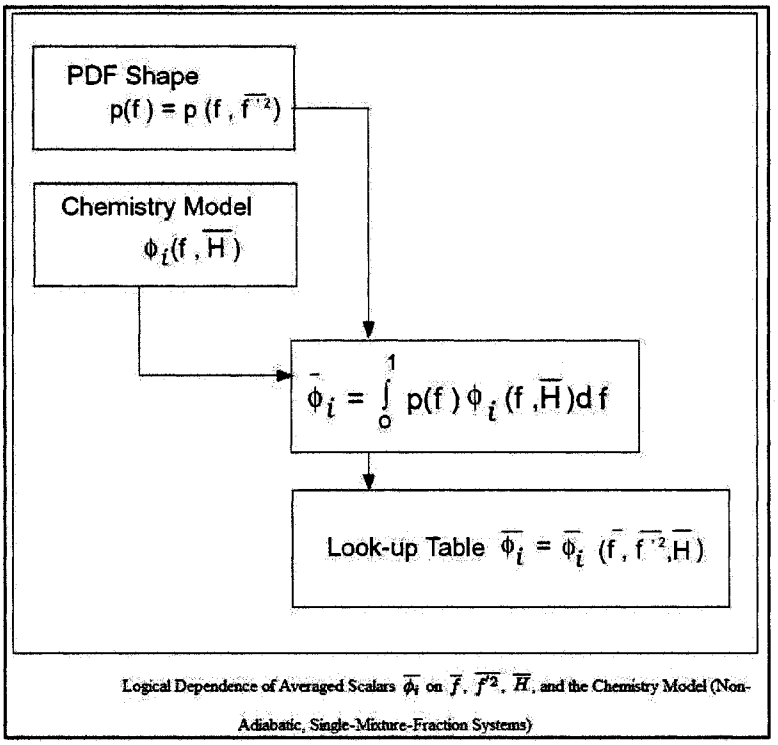

Fig 2.2.2.1: The loop used to calculate the mass fraction of specie *i* as a function of mean, variance and enthalpy, reproduced from [23].

The Mixture Fraction can be defined in various ways [47], however the Fluent implementation states it to be the *'elemental mass fraction that originated from the fuel stream'*.

$$f = \frac{Z_i - Z_{i,ox}}{Z_{i,fuel} - Z_{i,ox}} \qquad (2.2.2.1)$$

The mixture fraction is directly related to the local equivalence ratio, ϕ, as

$f = \frac{\phi}{\phi + r}$ and $\phi = \frac{FAR}{FAR_{stoich}}$ where FAR stands for Fuel-Air Ratio and r is the number of moles of oxidizer required for stoichiometric burning of the fuel.

In a turbulent flow, the diffusion due to turbulence is assumed to overwhelm the diffusion due to material (molecular) diffusivity. This enables one to use the simplifying assumption of equal diffusivities for all species and thus reduce the species equations to a single equation for the mixture fraction.

The equations that describes the transport of the mixture fraction and its variance are defined as

$$\frac{\partial}{\partial t}\left(\rho \bar{f}\right) + \nabla \bullet \left(\rho \vec{v} \bar{f}\right) = \nabla \bullet \left(\frac{\mu_t}{\sigma_t} \nabla \bar{f}\right) \qquad (2.2.2.2)$$

and

$$\frac{\partial}{\partial t}\left(\rho \overline{f^2}\right) + \nabla \bullet \left(\rho \vec{v} \overline{f^2}\right) = \nabla \bullet \left(\frac{\mu_t}{\sigma_t} \nabla \overline{f^2}\right) + C_g \left(\nabla \bar{f}\right) - C_d{}^2 \rho \frac{\varepsilon}{k} \overline{f^2} \qquad (2.2.2.3)$$

respectively. σ_t, C_g and C_d are constants that take default values of 0.85, 2.86 and 2.0 respectively. σ_t, is the turbulent Schmidt number and is computed dynamically when the dynamic Smagorinsky Model is used

In the case of LES, a transport equation is not necessary for the mixture fraction variance since it resolve the large scale values and the effect of fluctuations from the subgrid scale is taken into recovered through the following definition for it

$\overline{f^2} = C_{\text{var}} L_s^2 \left| \nabla \overline{f^2} \right|$ where C_{var} is dynamically computed when the dynamic Smagorinsky model is used and L_s is the subgrid length scale as defined in equation 2.1.2.11.

The probability density function that describes the fluctuations of the mixture fraction is defined in non-adiabatic equation for density-weighted species mass fraction, $\overline{\phi_i}$

$$\overline{\phi_i} = \int_0^1 p(f) \phi_i \left(f, \overline{H} \right) df \qquad (2.2.2.4)$$

where $p(f) = \dfrac{f^{\alpha-1}(1-f)^{\beta-1}}{\int f^{\alpha-1}(1-f)^{\beta-1} df}$, assuming a Beta function for its shape

and $\alpha = \overline{f}\left[\dfrac{\overline{f}(1-\overline{f})}{\overline{f}^2} - 1 \right]$, $\beta = (1-\overline{f})\left[\dfrac{\overline{f}(1-\overline{f})}{\overline{f}^2} - 1 \right]$

The transport equation of mean enthalpy is given by

$$\frac{\partial}{\partial t}\left(\rho\bar{H}\right)+\nabla\bullet\left(\rho\bar{v}\bar{H}\right)=\nabla\bullet\left(\frac{k_t}{c_p}\nabla\bar{H}\right)+S_h \qquad (2.2.2.5)$$

Again, as in the case of species transport, the modeling can range from simple to extremely complex. There are further choices of implementation accordingly as the problem is deemed to be non-premixed, perfectly premixed or the most general (and challenging) case: partially premixed. In the descriptions below, more emphasis is laid on the premixed/partially-premixed regime of combustion as that is the case the simulations in this thesis were performed assuming. The case of premixed combustion is covered under 'Partially premixed combustion' as the model employs both non-premixed and premixed combustion theories in order to suit the real situation in a practical combustor. The following points serve to include the order of complexity and physics that can be included into the model. The physics include perspectives of both chemistry as well as combustion aerodynamics.

1. *Equilibrium assumption:* the assumption of infinitely chemistry, as in the eddy dissipation model, assumes the mixed-is-burned approach. Basically, the combustion process is assumed to be mixing controlled and if the assumptions of fast chemistry hold, significant accuracy over that of

species transport can be achieved, due to the better-resolved temperature field. An immediate observation that can be made is that this approach does not model complex effects like quenching/extinction or partial premixing such as is found at the base of a lifted flame, for example. Furthermore, the flame response to strain rates, stretch, etc is not incorporated and most non-equilibrium phenomena that have a direct bearing on the emissions cannot be modeled. Fluent attempts to take into consideration, non-equilibrium due to rich zones and avoids the kinetic calculations in such areas by imposing a rich flammability limit (RFL) to the equivalence ratio, so that mixtures in these zones are considered to be mixed but unburnt. The non-premixed equilibrium assumption fails to account for any premixing and cannot be used for premixed/partially-premixed combustion. Turbulent diffusion flames can be modeled, however, lifted flames cannot be accurately predicted as the simulations show anchoring at walls, sharp surfaces, corners, etc which is not physical at the physical strain rates found there. An illustration is provided in the results section. Fluent provides a partially premixed combustion model that can be used with the equilibrium assumption.

2. *Flamelet theory:* non-equilibrium phenomena due to aerodynamic strain can be incorporated into the pdf model by assuming combustion to take place in thin one-dimensional and time-dependent layers called 'flamelets' by Peters [44] which make up the turbulent brush. A non-dimensional number, Da, the Damköhler exists to relate the timescales of diffusion and chemical kinetics as a ratio. Peters [44] used asymptotic methods to expand the Da of the rate determining reaction (of the multi-step kinetics) and proved that this assumption is valid. An additional variable, the mixture fraction scalar dissipation rate is introduced to represent the effect of flame stretch on the local flow-field. Accordingly, over a range of scalar dissipation rates, the flame is considered to burn and at high dissipation rates, to extinguish, thus emulating the physical observation of the phenomena that occurs in flames strained in opposed flow configurations, that are gradually increased in velocity until strain increases to the point where it is impossible for the flow to sustain a flame. Flamelets are used differently in non-premixed and premixed conditions due to their different strengths of interaction with the main flow field. For premixed combustion, the interaction is described by Peters to be considerable more due to the flame-fronts ability to propagate normal to itself. Different regimes are established depending on the degree to which the flame is

stretched by the local turbulent intensities. These are shown in the figure below, reproduced from Peters.

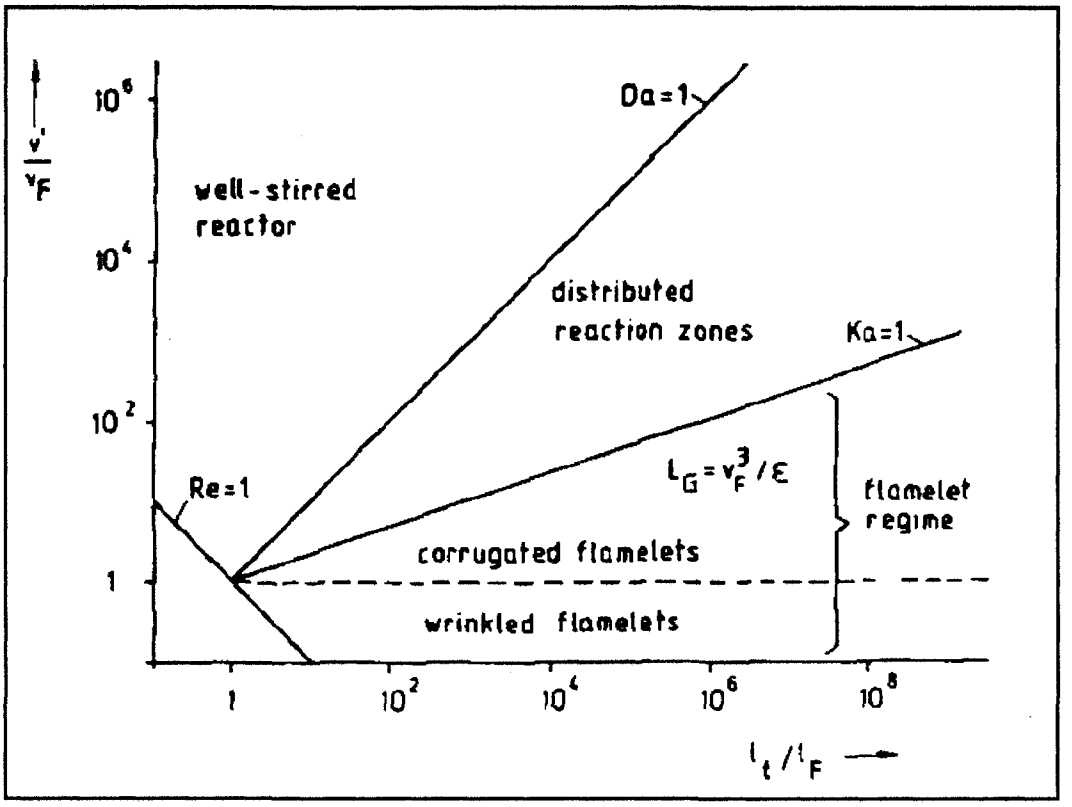

Fig 2.2.2.2: Borghi's 'Phase' Diagram depicting different flamelet states [44].

When Re, Da <1, the phase corresponds to laminar and perfectly premixed flames (well stirred reactor), respectively.

'Wrinkled' and/or 'corrugated' flames make up the typical flames responding to varying stretch, caused by turbulent flows, at the Kolmogorov microscale where the flamelet theory is valid – i.e., the flame thickness is on the order of the Kolmogorov microscale. They are

characterized by turbulence and fast chemistry with weak flame stretch. These phenomena are quantified by the introduction of a turbulent 'Karlovitz' number for flame stretch (ratio of laminar flame thickness to the laminar flame speed, divided by the Kolmogorov characteristic timescale) apart from the Reynolds number (turbulence) and the Damköhler number (chemistry time scale). The three numbers are related as $Re = Da^2 Ka^2$. These phases are separated from the 'distributed reaction zones' (the boundary given by the 'Klimov-Williams' criterion where flame thickness is equal to the Kolmogorov scale) where the stretch is considered to be very strong and small eddies can enter the flame structure and 'thicken' the flame. This method assumes the chemistry in such a situation to be again, fast so that predictions of slow species is again suspect. This assumes that the flame responds instantaneously to strain imposed by the local flow-field turbulence. The complete theory describing the inner structure of flamelets and their behaviour in premixed mixtures, as well as the mathematical justification for dividing the flamelet regime into wrinkled and corrugated flamelets is given in [44].

To model the effect of aerodynamic strain, the situation of a counter-flow diffusion flame is considered and a flamelet library (in case of multiple flamelets) is built by varying the scalar dissipation rate from some arbitrary initial value until an extinguishing value, considering a particular chemical kinetic mechanism. The ensemble of laminar flamelets is considered to make up a turbulent flame brush. How exactly this is 'made up' is by defining a probability density function of the instantaneous mixture fraction and its scalar dissipation rate. Thus modifying the original pdf of equation 2.2.2.4, we get the equation for the density-weighted mean mass fraction of a particular chemical species as

$$\bar{\phi} = \iint \phi\left(f, \chi_{xt}, \bar{H}\right) p\left(f, \chi_{xt}\right) df \; d\chi_{xt} \qquad (2.2.2.6)$$

where

$$\chi_{xt} = \frac{a_s \exp\left(-2\left[erfc^{-1}\left(2f_{st}\right)\right]^2\right)}{\pi} \qquad (2.2.2.7)$$

$$\chi = 2D\left|\nabla f\right|^2 \qquad (2.2.2.8)$$

A joint pdf of f, χ_{st} can be computationally demanding and would require a transport equation for the variance of the scalar dissipation rate, so a simplifying assumption of statistical independence between the mixture fraction and the scalar dissipation rate is made, thus ignoring the fluctuations in χ_{st} and using a delta function for its assumed shape pdf. In the LES context, the mean scalar dissipation rate is modeled as

$$\chi_{st} = C_\chi \frac{\mu_t + \mu}{\rho \sigma_t} \left| \nabla \tilde{f}'^2 \right| \text{ and } C_\chi = 2 \qquad (2.2.2.9)$$

The double integral for the mean mass fraction above, is pre-processed and a lookup table is built to avoid solution time evaluation.

A steady flamelets library is generated according to the following equations in mixture fraction space (f is the independent variable), following [44],

$$\rho \frac{\partial Y_i}{\partial t} = \frac{1}{2} \rho \chi \frac{\partial^2 Y_i}{\partial f^2} + S_i \text{ for each species } i. \qquad (2.2.2.10)$$

$$\rho\frac{\partial T}{\partial t}=\frac{1}{2}\rho\chi\frac{\partial^2 T}{\partial f^2}-\frac{1}{2c_p}\rho\chi\left[\frac{\partial c_p}{\partial f}+\sum_i c_{p,i}\frac{\partial Y_i}{\partial f}\right]\frac{\partial T}{\partial f} \qquad (2.2.2.11)$$

$$\chi(f)=\frac{a_s}{4\pi}\frac{3\left(\sqrt{\rho_\infty/\rho}+1\right)^2}{2\sqrt{\rho_\infty/\rho}+1}\exp\left(-2\left[erfc^{-1}(2f)\right]\right) \text{ [48]} \qquad (2.2.2.12)$$

With these definitions, flamelets are generated accounting for the varying scalar dissipation/strain rates as

$$\chi_i=\begin{cases}10\chi_{i-1} & \text{for } \chi_{i-1}<1/s\\ \chi_{i-1}+\Delta\chi & \text{for } \chi_{i-1}\geq 1/s\end{cases} \qquad (2.2.2.13)$$

Until extinguishing, at which point, the extinguished flamelet is excluded from the flamelet library.

3. *Partially premixed combustion:* Practical combustors, especially, lean-premixed ones, operate in semi-*stratified* combustion regimes, where the objective is to burn stratified mixtures so that stoichiometric spots of fuel-air mixtures does not happen, thus lessening the amounts of emissions produced. However, due to instabilities of such systems (lean blow-out, quenching etc), various devices are employed (pilot fuel), which causes non-premixed and premixed regimes to co-exist. The modeling becomes considerably challenging and is the focus of current research [17]. There is no combustion model that can be said to be perfect for this type of simulation but notable success has been achieved in blending models for both non-premixed and partially premixed combustion to take into account partial premixing. Lean premixed combustors mix the air and fuel prior to the main combustion zone and any combustion model hoping to model this unburnt mixture as well as the post mixing burned mixtures should be able to reproduce these regimes consistently. Such a thing is possible by using a progress variable of reaction to track the location of the flamefront. As a simple approximation, the model in Fluent, first proposed for adiabatic homogeneous combustion of perfectly premixed reactants by Zimont, and later extended to non-adiabatic, heterogeneous mixtures by Colkjat, Polifke [49] and Biagioli [50], solves a transport

equation for the progress variable and considers the flow ahead of the flame to be mixed but unburnt and post flame, uses the equilibrium or steady flamelet pdf model to simulate the heat release. The key to modeling this type of regime is the turbulent burning velocity defined to be the velocity a turbulent flame front propagates normal to itself [44]. Many expressions for the turbulent burning velocity have been considered in the context of premixed combustion. The physics governing the combustion process and flame location is the turbulence of the main flow-field. If the local flow velocity is larger than the turbulent velocity the model quenches the flame. Physics in the partially premixed combustion are complex and are subjects of current research. It is clear however, for lean-premixed combustors, the lean fuel situation indicates the stratified[2] premixed type [17]. A discussion of the main equations that can help model this complex regime, with reasonable accuracy is given in the next section. This is the model that was used for all the simulations in this thesis.

[2] Stratified mixtures are 'frozen' mixtures that result from intense premixing. Such mixtures still fall short of perfect premixing but are close to uniformity and are very desirable for combustor design.

The Turbulence Flame Speed Closure Model

It is helpful to discuss a few key points in premixed combustion modeling at this point.

Premixed combustion regimes, mentioned already, divide the reaction zone into burnt and unburnt regions. The flame-front accomplishes this. In order to track the flame-front propagation, a progress variable of some product specie or other indicator of reaction location (entropy [52]), etc is transported through the domain. The transport equation for the mean progress variable c, is defined as

$$\frac{\partial}{\partial t}(\rho c)+\nabla\bullet(\rho\vec{v}c)=\nabla\bullet\left(\frac{\mu_t}{\mathrm{Sc}_t}\nabla c\right)+\rho S_c \qquad (2.2.2.14)$$

A note on the Schmidt Number Sc_t

The Schmidt number plays an important role in relating turbulent diffusivity to mass diffusivity and assuming it constant seems to be debatable, as it seems to require tuning, in order to match experiments for many simulations. The generally accepted value of 0.85 seems to consistently underpredict the mixing when used with the RANS

turbulence models. This fact is borne out by the author's pdf simulations and will be discussed in the pilot study in Chapter 6. Jiang and Campbell [34] indicate that the turbulent scalar transfer depends on the 'Reynolds Analogy' concept and that better approaches should be used in order to quantitatively predict the velocity and temperature fields, which are the basis for species/emissions predictions. The Reynolds analogy was postulated first, a century ago by Reynolds who carried out experiments in steam boilers and postulated that heat-flux is analogous to momentum flux and suggests the dimensionless Schmidt and Prandtl numbers should be constant and near 1.0 for gases. While this works well for wall-bounded flows such as those found in heat-exchanger pipes, the analogy seems to deteriorate with massively separated flows, such as found in combustion chambers. The following figures bear this fact out.

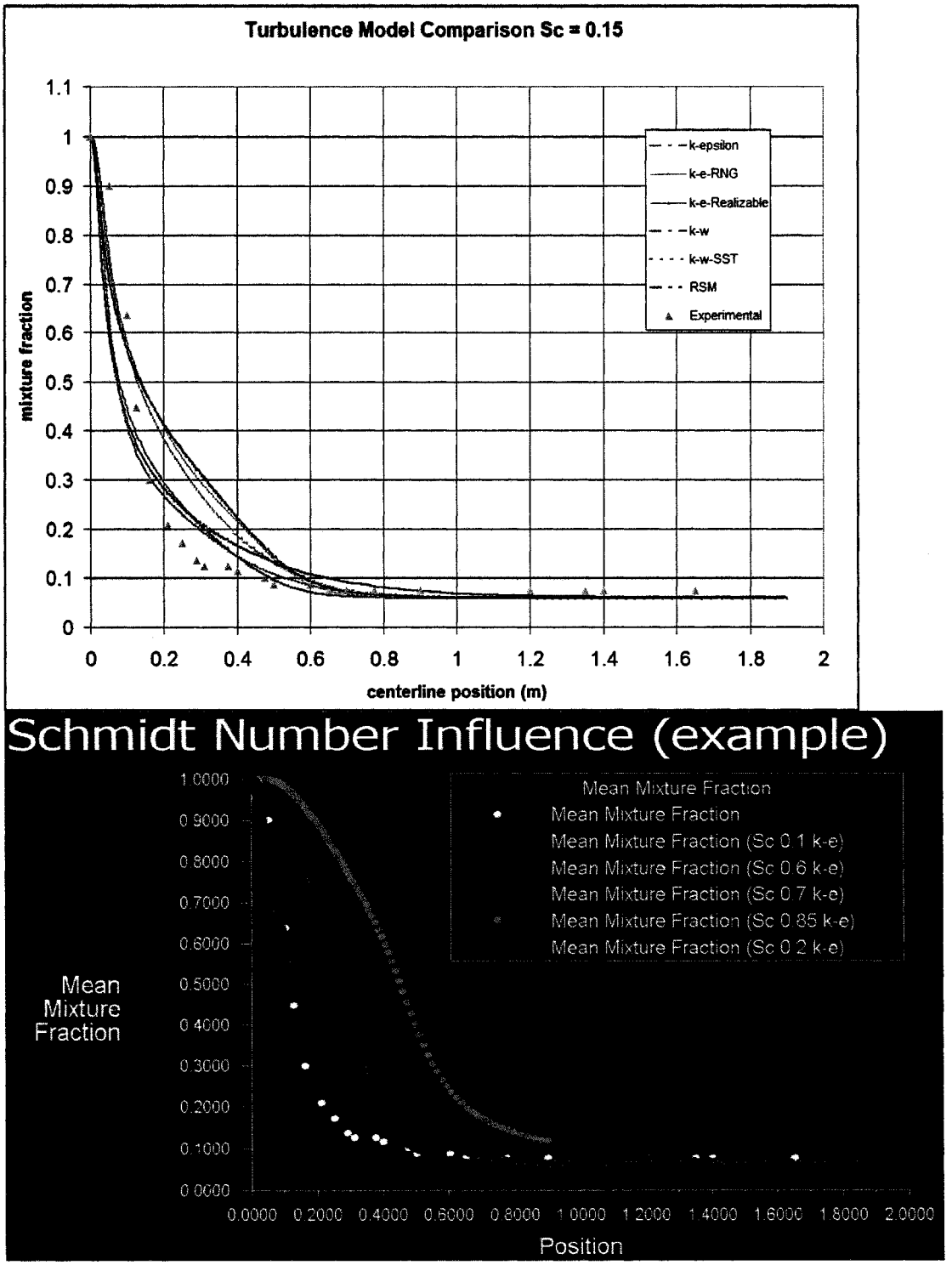

Fig 2.2.2.3: The figures above indicate that the turbulence model has little effect on the centreline decay of the mixture fraction *(top)*, while the turbulent Schmidt number has significant effects *(bottom)*.

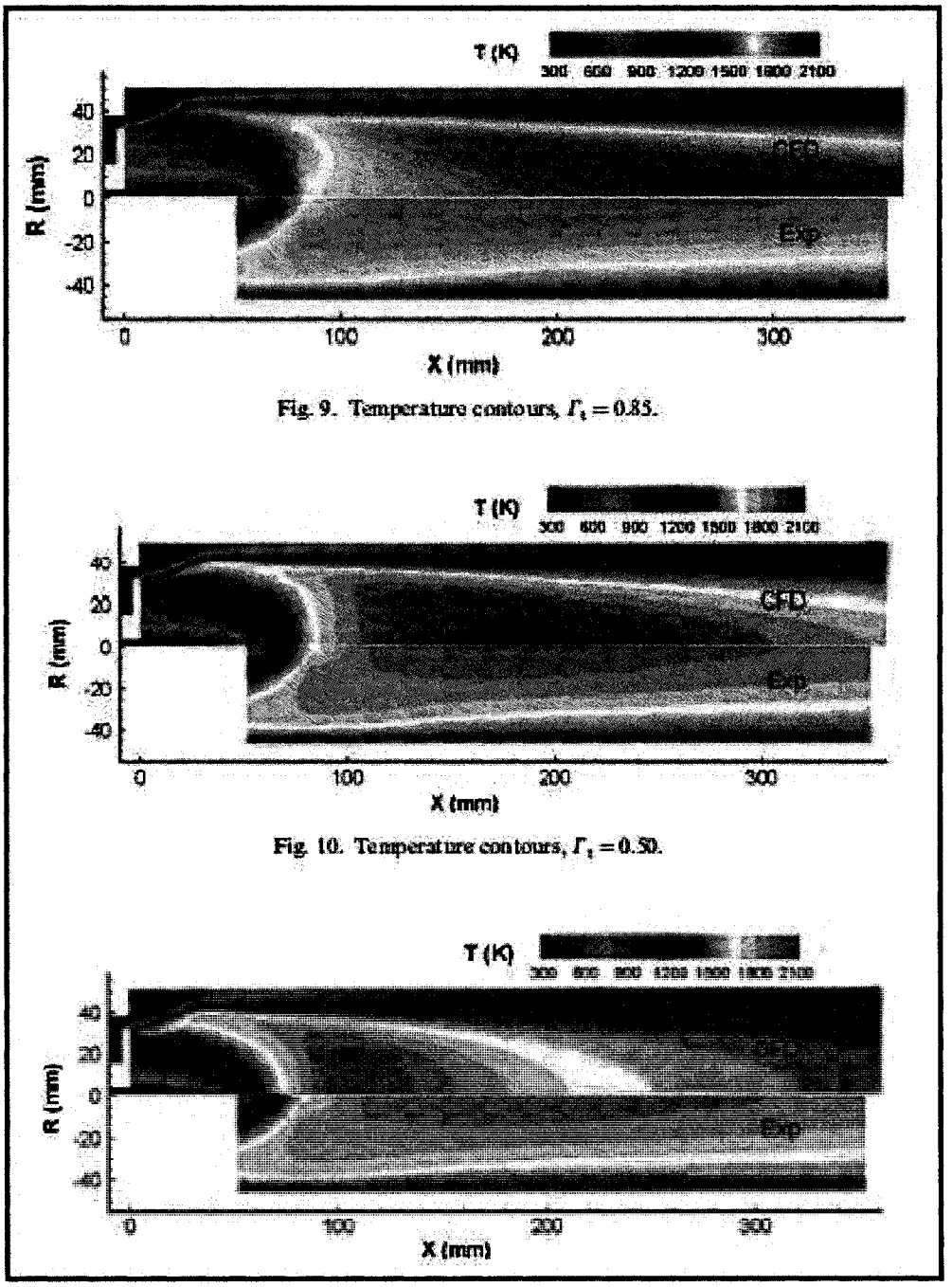

Fig. 9. Temperature contours, $\Gamma_t = 0.85$.

Fig. 10. Temperature contours, $\Gamma_t = 0.50$.

Fig 2.2.2.4[3]: Effect of varying Schmidt number on the main temperature field, reproduced from [34] also c.f. pilot study in Chapter 6.

The cases above are for RANS. No such 'tuning' seemed necessary for LES of the same case, however the current simulations indicate that the

[3] Exp – experiment.

dynamic procedure for the Schmidt number lowered it to 0.25. In the RANS context, authors such as Riesmeier et. al. [52], have found it necessary to decrease the value of the Schmidt number, in context of gas turbine combustion.

The Progress Variable *c*

$$c = \frac{\sum_{i=1}^{n} Y_i}{\sum_{i=1}^{n} Y_{i,eq}} \quad \text{where } n \text{ is the number of products.} \qquad (2.2.2.15)$$

In the Fluent code, the progress variable is chosen to be a *'normalized sum of the product species'*. The normalization is done by the sum of the mass fraction of the product species at equilibrium. Thus it can be seen that in completely burnt regions, the progress variable c, takes a value of unity and 0 in the unburnt regions. Intermediate values of the progress variable appear in averaged simulations and indicate periodic combustion. There is however some debate on the value of this progress variable in post flame regions as indicated by Wood [53] as well as Polifke et al [49]. Biagioli [54] also recommends the value of 1 (burnt) for flows entering the

primary zone of combustion excepting the main flow from the premixer. Such a flow in the RB211 is through the torch igniter. There is more discussion on this, in Chapter 6. For an extended discussion on the advantages and disadvantages of using a progress variable including the choice of it, the reader is encouraged to consult Bray et. al.,[56].

The source term S_c in equation 2.2.2.14 tracks the reaction progress and requires closure. This is key to the premixed modeling since it introduces the concept of the turbulent flame speed and its effect.

$$\rho S_c = \rho_u U_t |\nabla c| \qquad (2.2.2.16)$$

where ρ_u is the unburnt mixture density and U_t is the turbulent flame speed which needs to be modeled and is done as follows by Zimont using dimensional analysis

$$U_t = AG(u')^{3/4} U_l^{1/2} \alpha^{-1/4} l_t^{1/4} \qquad (2.2.2.17)$$

where A is a model constant at a default of 0.52 (sometimes 'tuned' between 0.52 to 3) in order to guess the correct turbulent flame speed. It is

surmised by Biagioli [7] that the original value was empirically defined in situations of atmospheric pressure, idealistic mixtures etc.

u' is the RMS velocity

U_l is the laminar flame speed

$\alpha = \frac{k}{\rho c_p}$ is the thermal diffusivity

l_t is the turbulence length scale.

and

$$G = \frac{1}{2}\operatorname{erfc}\left\{-\sqrt{\frac{1}{2\sigma}}\left(\ln\left(\frac{\varepsilon_{cr}}{\varepsilon}\right)+\frac{\sigma}{2}\right)\right\} \qquad (2.2.2.18)$$

is a log-normal distribution of the turbulence dissipation rate ε_{cr}. It is a stretch factor which is <= 1 that is used to *'represent the probability that stretching will not quench the flame'* [23]. It can be seen that an infinite value

of the critical strain rate - g_{cr} - will cause the value of G to become 1, i.e., no quenching.

where

$$\sigma = \mu_{str} \ln\left(\frac{L}{\eta}\right) \text{ and } \varepsilon_{cr} = 15\upsilon g_{cr}^2 \qquad (2.2.2.19,20)$$

This model is generally valid where flamelet models are valid i.e., when equilibrium is assumed in the small-scale turbulence as found in the thin reaction zone combustion regime, outlined in the flamelet theory above. The model is valid specifically for the 'Intermediate Steady Propagation' regime in gas turbine combustors where the turbulent flame-brush increases with time.

The laminar flame speed curve mentioned above is calculated from using chemical mechanisms (particular to a fuel), which must be chosen carefully after considering the physics (especially pressures) of the problem to be modeled. Although Fluent provides a curve fit for pure fuels, in general, the situation may be radically different when fuel-flexibility is used. The calculation imposes a lean and rich limit on the

burning and if exceeded, quenches the flame with a 'zero' progress variable. Fortunately, curves for practical industrial combustors are available, for example the work of Bourque et. al. [58]. Other data include Gottgens et. al. [58], which is what Fluent uses by default. The modeling of the laminar flame speed is discussed in the model set up in Chapter 6.

4. *Composition PDF Transport*: The PDF transport method by Pope [59] consists of deriving a transport equation for the single-point, joint probability density function of velocity and composition, from the original N-S equations. This formulation removes the simplification of an assumed shape and instead determines the temperature, reaction rate etc., directly from the transport equation. Even more importantly, the method takes into account the molecular diffusion process that is fundamental to the combustion process. Needless to say, all this comes at a high cost. The dimensionality of the pdf is N+1 where N is the number of the species and cannot be solved directly. Hence a statistical method is employed. The chief difficulty arises in seeking to model mixing in pdf methods, a consequence of the close coupling between turbulence and chemistry. Chemical reactions occur at the smallest scales due to molecular mixing. Since such a resolution is beyond any foreseeable computational

resources, a mixing model for these small scales must be employed. A large number of particles are released into each cell to simulate molecular mixing and heat release. The number of particles required is very large (necessary for statistical steadiness) and is the chief source of modeling error. The model that has proved to be the best is the EMST (Euclidean Minimum Spanning Tree) model, which mixes particles that are close to each other in composition space, the assumption being that they would be close to each other physically. The ISAT algorithm is used to solve the equations that arise. The theory of this highly complex method is beyond this discussion and indeed the inability of current codes to track tens of millions of particles simultaneously dissuades one from using this method for highly dense meshes as are required for practical combustor geometries. The method however has been used with excellent predictions for CO and NOx in simulating the Sandia Flames (see Pope et. al. [60, 61]) and has proved to correctly simulate highly non-equilibrium phenomena such as ignition, extinction etc. However, the application is restricted to fairly simple geometries with relatively coarse meshes. In Fluent, the author has noted the size of the data file to grow to 100GB for a 1 million cell simulation of a 22.5 degree pie slice of the RB211 primary zone at 20 particles per cell.

2.2.3 Emissions Modeling as a post-processing step

Steady RANS simulations routinely predict with inaccuracy predictions of CO and NOx since both species cannot be considered in equilibrium instantaneously as the reactions proceed. For this reason, special post-processing of the flow field is done to include the history of mixing and time-dependent methods are used to arrive at more accurate predictions. While lean-premixed combustion regimes are more amenable to CO predictions assuming fast chemistry, rich mixtures cannot be simulated thus and these rich pockets occur in these combustors do to imperfect premixing which cause inhomogeneities in the mixture entering the main reaction zone. NOx emissions are very slow species compared to the others and can never be considered using fast chemistry approaches. Instead, reaction rates taken from experimental correlations are used to model the source terms of the NOx transport equations, accordingly as thermal, prompt and fuel NOx is considered. N2O is modeled as this path to NOx production becomes important in oxygen surplus environments. For this work, both methods have been employed and the results are discussed in Chapter 6. In this section a little background will be provided with some brief comments on the use of these methods.

The Unsteady Laminar Flamelet Method

Temperature changes do not follow instantaneously the changes in scalar dissipation rates i.e., strain rates in real life. But to simplify the modeling, this is one of the premises of the steady laminar flamelet theory. While good predictions can be obtained for fast species such as the OH or O radicals following this assumption, finite rate species that depend on the residence time, history of mixing etc., depend on the unsteady characteristics of the flow. In the steady flamelet equations, the scalar dissipation is modeled as a function of the mixture fraction according to Equation 2.2.1.14. This is no longer the case with the unsteady flamelet method, where the scalar dissipation and the mixture fraction are treated as independent variables. The flamelet library computed for the steady flamelet analysis is considered in the context of trying to find a particular flamelet at a particular point in space and instant in time by solving a transport equation for a so-called probability marker for particles that represent the flamelets. The initial positions are determined based on their deviation towards the rich side from the stoichiometric mixture fraction. This generally places the initial positions of the particles in the vicinity of the fuel injectors. As these particles processed through the domain, the characteristics of the flamelets that they represent can be obtained as function of the local flow properties that

have been obtained already through the steady-flamelet method. These are used to update the species mass fractions and temperature. This probability marker and the unsteady flamelet equations are time marched until the particles have left the domain. The transient species mass fractions and temperatures are calculated and averaged over time thus leading to different means of these parameters than the steady flamelet predictions. The equations that describe this process are detailed below [23]. It must be mentioned that the progress variable is not coupled with the unsteady flamelet method as followed in the work of Pitsch and Ihme [16] but considered as part of the instantaneous flamelet boundary conditions.

Transport equation for the Probability Marker:

$$\frac{\partial I}{\partial t}(\rho I)+\nabla\bullet(\rho\vec{v}I)=\nabla\bullet\left(\frac{\mu_t}{\sigma_t}\nabla I\right) \qquad (2.2.3.1)$$

$$\text{where } I=\begin{cases}1 & \text{for}\,\overline{f}\geq f_{init}\\ 0 & \text{for}\,\overline{f}\leq f_{init}\end{cases} \qquad (2.2.3.2)$$

Scalar Dissipation is expressed as a volume weighted function of the local stoichiometry calculated from the steady flamelet method prior.

$$\chi_{st}(t)=\frac{\int_V I(\vec{x},t)\rho(\vec{x})\overline{\chi}_{st}^{3/2}(\vec{x})dV}{\int_V I(\vec{x},t)\rho(\vec{x})\overline{\chi}_{st}^{1/2}(\vec{x})dV} \qquad (2.2.3.3)$$

The Temperature is calculated at each instant as a function of the local mixture fraction obtained from the solution of the steady flamelet method.

$$T(f,t)=T^{adiabatic}(f,t)\xi(f,t) \qquad (2.2.3.4)$$

where

$$\xi(f,t)=\frac{\int_V I\rho T(\vec{x}|f)\Big/ T^{adiabatic}(f,t)dV}{\int_V I\rho dV} \text{ for non-adiabatic cases.} \qquad (2.2.3.5)$$

The unsteady flamelet mean species mass fraction are obtained as

$$\overline{Y}_k^{ufla}=\frac{\int_0^1 I\rho\left[\int_0^1 Y_k(f,t)P(f)df\right]dt}{\int_0^1 I\rho dt} \qquad (2.2.3.6)$$

A typical example of monitoring the particles progress through the domain is shown below, reproduced from the LES/steady flamelet simulation done in this

thesis. The exit of the domain was monitored. The time-step was adaptive and the equations were solved in a coupled implicit manner. The total time taken was approximate to the fluid residence time of the combustor.

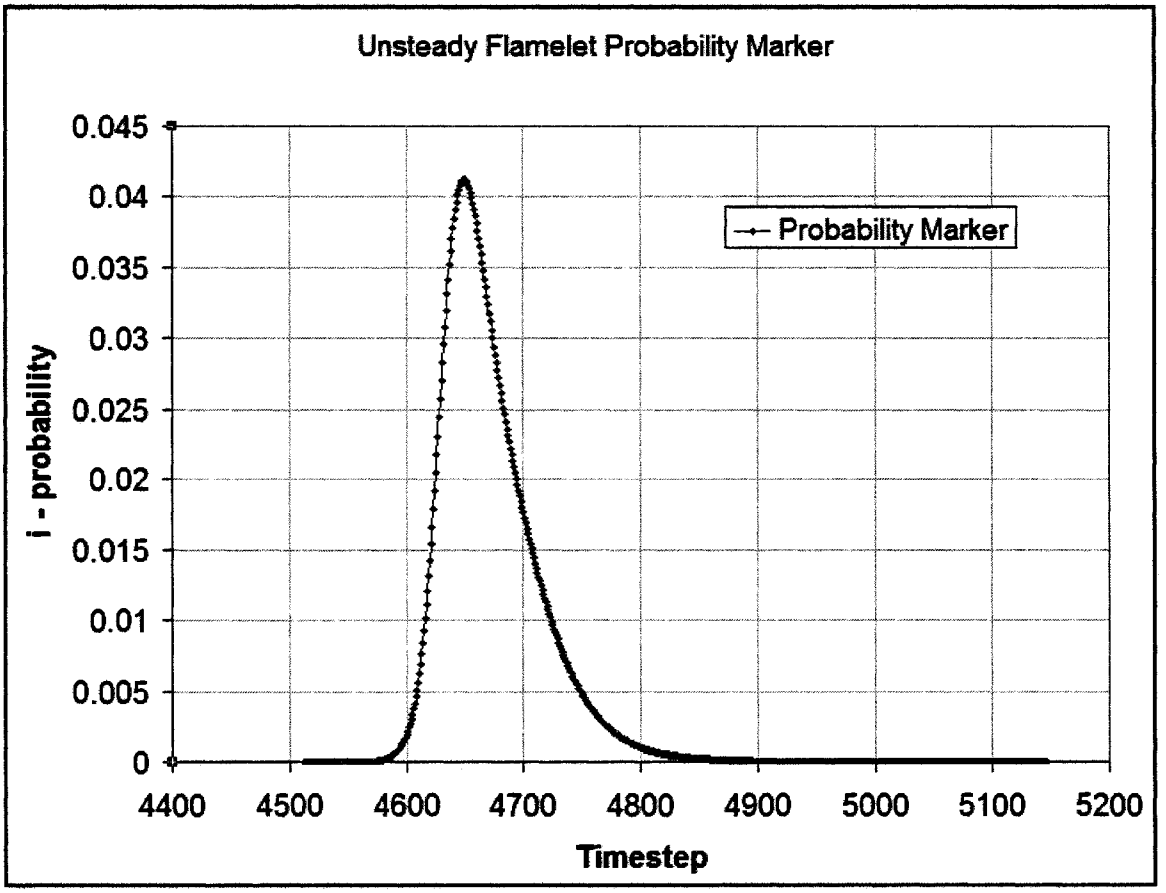

Fig 2.2.3.1: Progress of particles representing flamelets through the domain.

Post-processing for NOx.

The dominant contributions to the production/destruction of Nitrogen Oxides in combustors are well known. NOx forms either due to nitrogen fixing in the fuel, rich mixtures, high temperatures, intermediate radical formations, re-burn by reduction of NO by CHx radicals to produce hydrogen cyanides. Pollution control strategy [17] favours the use of stratified combustion such as partially premixed combustion regimes, in which the mixture of air and fuel is thoroughly premixed and 'stratified' prior to combustion. This has the advantage of eliminating stoichiometric pockets (ideally) and lower the heat of combustion to levels which preclude the formation of thermal NOx (again, ideally). Lean-premixed combustion further implies, an oxygen surplus, which gives rise to the effect of intermediate N2O radical formations that could account for as much as 30% of the NOx production from molecular N2 in gas turbine combustors. The simulations in this thesis indicate a very significant contribution of the N2O pathways to NOx production. Thermal NOx is of lesser significance since the average temperatures of combustion is below 1900K. However, transient temperatures have been observed over 2000K and these events contribute to the overall NOx. Prompt NOx - also called Fenimore NOx – contributes to NOx formation in richer mixtures at low temperatures such as found in the partially

premixed, close to reaction areas such as at the exits of the premixers. Prompt NOx is also proportional to the number of carbon atoms present per unit volume. Fuel NOx is of concern when the fuels considered contain nitrogen and typically solid and liquid fuels are examples of this. The intermediates formed (HCN, NH3, N, CN, NH etc.,) during the pathways leading to NOx production are important and their transport effects need to be considered – this leads to additional complications in modeling, especially since the reaction rates required to model the source terms of the production of these radicals is still not well understood.

In this thesis, a natural gas composition of over 96% methane was used and consequently, fuel NOx was excluded from the analysis though about 1% of the fuel contained N2. However gas turbine specialists consider fuels with 30% Nitrogen and this may soon become a requirement to include. Reburn was considered and the turbulence chemistry interaction was modeled, using a presumed pdf approach which will be detailed in the following description of the equations used. The post-processing step starts by obtaining a converged flow field. Transport equations are solved for NO and the individual contributions of thermal, prompt, and N2O intermediates are taken into account through the NO source term. Re-burn was considered by taking into account the

reduction of NOx to HCN by considering the predictions of CH, CH2 and CH3 radicals obtained from the converged solution.

The pathways of NOx production considered in the calculations in this thesis are detailed below along with the source term details. There are several approaches to calculate the source terms which involve the use of predicted mass fractions of O2, O, CH, CH2, CH3 etc; however only the ones with the greatest possible accuracy were used – which in the context of the simulations undertaken in this thesis took advantage of the accurate predictions of fast radicals from the instantaneous solutions, rather than use the partial-equilibrium or equilibrium approaches.

Transport Equations [23]

NO

$$\frac{\partial I}{\partial t}(\rho Y_{NO}) + \nabla \bullet (\rho \vec{v} Y_{NO}) = \nabla \bullet (\rho D Y_{NO}) + S_{NO} \qquad (2.2.3.7)$$

N2O

$$\frac{\partial I}{\partial t}(\rho Y_{N_2O}) + \nabla \bullet (\rho \vec{v} Y_{N_2O}) = \nabla \bullet (\rho D Y_{N_2O}) + S_{N_2O} \qquad (2.2.3.8)$$

If Fuel NOx is considered, similar equations are used to track HCN and NH3.

The source terms in equations 2.2.3.33 and 2.2.3.34 are evaluated separately for different NOx mechanisms.

A brief description of each of the mechanisms used for the simulations in this thesis will be detailed below and the section concludes with the details of how these chemical mechanisms are convoluted with the fluctuations in temperature and species due to turbulence-chemistry interaction – accounted for by a probability density function methods similar to the one used for mixture fraction calculations in the non-premixed approach.

Thermal NOx Formation

The original Z'eldovich mechanism (equations 2.2.3.9,10) is augmented by equation 2.2.3.37, which is significant at near-stoichiometric conditions and in fuel-rich mixtures:

$$\begin{aligned} O + N_2 &\rightleftharpoons N + NO \\ N + O_2 &\rightleftharpoons O + NO \\ N + OH &\rightleftharpoons H + NO \end{aligned} \qquad (2.2.3.9\text{-}11)$$

While the detailed NOx formation includes the formation of many intermediate radicals, the number growing with the carbon number of the fuel, the coupling of these mechanisms with turbulence is difficult. For example a sub-model used for NOx in unsteady flamelet calculations, by Barths et. al. [15] contains 14 chemical species and 106 reactions. The Leeds NOx mechanism [62] includes 43 species. However, a trade-off is achieved by considering only the dominant (global) species and explicitly calculating their species mass fractions.

The net rate of formation of NO through this mechanism is given by:

$$\frac{d[NO]}{dt} = k_{f,1}[O][N_2] + k_{f,2}[N][O_2] + k_{f,3}[N][OH] - k_{r,1}[NO][N] - k_{r,2}[NO][O] - k_{r,3}[NO][H] \qquad (2.2.3.12)$$

From this, the source term is expressed as:

$$S_{thermal,NO} = M_{w,NO} \frac{d[NO]}{dt} \qquad (2.2.3.13)$$

f and b denote forward and backward rate constants for each of the reactions. Experimental data is used to determine this constants (Hanson and Salimian).

The concentrations of O, N2, N, OH, and H are retrieved from the steady flamelet calculations which used the GRI3 mechanism. Since the underlying assumption of fast response to scalar dissipation changes is valid for these species, the accuracy in their predictions is high and can so be used without resorting to equilibrium or quasi-steady methods, which would otherwise have to be used. Of special importance is the O radical 's concentration changes due to its third body reactions which lead to higher concentrations at equilibrium.

Prompt/Fenimore NOx Formation

Usually the contribution of Prompt NOx formation to the overall NO concentration is small when compared to thermal NOx, especially since the over mixture is lean and premixed. However rich pockets, which are conducive to prompt NOx formation can exist in staged combustors [23, 65]. The simulation of a multi-stage combustor such as the one in this simulation increases the significance of this route to NO formation. The route to NO formation is expressed as a set of global reactions (since too many intermediates, which are not economical to compute, will otherwise have to be considered):

$$\begin{aligned} CH + N_2 &\rightleftharpoons HCN + N \\ N + O_2 &\rightleftharpoons NO + O \\ HCN + OH &\rightleftharpoons CN + H_2O \\ CN + O_2 &\rightleftharpoons NO + CO \end{aligned} \qquad \text{(2.2.3.14-17)}$$

Of these, equation 2.2.3.14 is shown [Ref 320, 23] to be the most dominant reaction near the flamefront and is subsequently modeled as a global rate reaction controlling the formation of the overall prompt NOx. However due to uncertainties in the reaction rate constant for this equation, a global rate constant was derived by De Soete [64] by considering the rate of production of NO from

prompt NOx is equal to the prompt NOx rate of reaction that remains after the overall N2 formation is removed. This is justifiable since the superequilibrium O radical under rich conditions prefers to oxidize Nitrogen to NO rather than allow N2 to form.

Thus the reaction rate is expressed as:

$$\frac{d[NO]}{dt} = k_{pr}[O_2]^a[N_2][FUEL]e^{-E_a/RT} \qquad (2.2.3.18)$$

The model has been observed to exhibit inaccuracy for high pressures and higher hydrocarbons when tested against experimental data by Backmier et. al. In order to reduce this inaccuracy, the Fluent implementation includes a correction term which takes into account the overall equivalence ratio and the number of carbon atoms per volume since prompt NO formation is directly proportional to these factors rather than to the hydrocarbon fuel composition. The modified De Soete model is detailed below, incorporating the correction factor and a pressure dependent rate constant.

$$\frac{d[NO]}{dt} = k'_{pr}[O_2]^a[N_2][FUEL]e^{-E'_a/RT} \qquad (2.2.3.19)$$

where the modified rate constant $k_{pr}^{'}$ is expressed as

$$k_{pr}^{'} = 6.4\times10^{6}\left(RT/p\right)^{a+1} \tag{2.2.3.20}$$

and the Activation Energy $E_a^{'} = 303474.125\,J/gmol$

The correction factor is expressed as a curve fit, valid for equivalence ratios between 0.6 and 1.6 for alkane hydrocarbons:

$$f = 4.75 + 0.0819n - 23.2\phi + 32\phi^2 - 12.2\phi^3 \tag{2.2.3.21}$$

The oxygen reaction order, a is expressed as the following ranges according to De Soete [64]:

$$a = \begin{cases} 1.0 & X_{O_2} \le 4.1\times10^{-3} \\ -3.95 - 0.9\ln X_{O_2} & 4.1\times10^{-3} \le X_{O_2} \le 1.11\times10^{-2} \\ -0.35 - 0.1\ln X_{O_2} & 1.11\times10^{-2} < X_{O_2} < 0.03 \\ 0 & X_{O_2} \ge 0.03 \end{cases} \tag{2.2.3.22}$$

The concentration of O2 is directly calculated from the steady flamelet solution.

The prompt NO source term is expressed as:

$$S_{prompt,NO} = M_{w,NO}\frac{d[NO]}{dt} \tag{2.2.3.23}$$

Intermediate N2O pathways to NOx formation

NOx formation due to recombination reactions between nitrogen and oxygen and subsequent oxidation of nitrous oxide to NO is important has been found to be a significant contributor to the overall NO formation in the current simulations. Melte and Pratt first proposed this mechanism, deemed important in the presence of high ambient pressures and oxygen surplus. While the contribution can be as much as 90% to the total NOx, typical contributions in a lean premixed gas turbine combustor can reach upto 45% [39]. This is mostly due to the lower and lower temperatures of combustion where the significance of thermal NOx decreases and hitherto less dominant routes become of importance and must be considered for emissions reduction strategies.

Two reactions are considered as its global pathway:

$$N_2 + O + M \rightleftharpoons N_2O + M$$
$$N_2O + O \rightleftharpoons 2NO \qquad (2.2.3.24,25)$$

M is a third body, chemically inert species that becomes significant at high pressures and temperatures, increasing the collision frequency of various atoms.

Here it facilitates the recombination of N2 and O. O further, makes the reactions favourable be being a highly reactive species and in abundance due to the oxygen rich environment in lean premixed combustion regimes. Taken together, the production of NOx from subsequent oxidation of N2O becomes highly probable.

The rate of reaction is expressed as:

$$\frac{d[NO]}{dt} = 2\left(k_{f,2}[N_2O][O] - k_{r,2}[NO]^2\right) \qquad (2.2.3.26)$$

The concentration of N20 is obtained by considering its rate of reaction as quasi-steady and consequently accounting only for its transport without production when solved for with a transport equation. The concentration can be obtained as follows:

$$[N_2O] = \frac{k_{f,1}[N_2][O][M] + k_{r,2}[NO]^2}{k_{r,1}[M] + k_{f,2}[O]} \qquad (2.2.3.27)$$

NO reduction through Reburn

NOx can deplete due to its reduction by CHx radicals to hydrogen cyanides. However these reactions occur within a narrow band of temperature and Fluent considers the following mechanism to be valid between 1600K and 2100K. Since this temperature range is found in the current simulations, it was decided to model NO depletion in order to avoid NO overprediction.

$$\begin{aligned} CH + NO &\xrightarrow{k_1} HCN + O \\ CH_2 + NO &\xrightarrow{k_1} HCN + OH \\ CH_3 + NO &\xrightarrow{k_1} HCN + H_2O \end{aligned} \qquad (2.2.3.28)$$

Where temperatures are outside this range, NO depletion due to reburn is not calculated [23].

The NO destruction rate is calculated as a sink term to the overall NO transport equation:

$$-\frac{d[NO]}{dt} = k_1[CH][NO] + k_2[CH_2][NO] + k_3[CH_3][NO] \qquad (2.2.3.29)$$

$$S_{reburn,NO} = -M_{w,NO}\frac{d[NO]}{dt} \qquad (2.2.3.30)$$

The concentrations of the CHx radicals are taken directly from the computed values from the steady flamelet method.

NO chemistry – Turbulence Interaction

Since all the foregoing rate of reaction formulations, chemical mechanisms and curve-fits were in the context of experimental datasets from analysis of laminar flame speeds and shock tube studies, the equations cannot be directly used in the context of turbulent flames. In order to account for the significant effects of fluctuations in temperature and species mass fractions due to turbulence, a pdf method is used to obtain the mean turbulent reaction rate in terms of the instantaneous reaction rate and a joint probability distribution function of temperature and species, which in these simulations has been taken to be the oxygen radical. Thus the following procedure is used to obtain the mean source term of NO in turbulent flows:

$$\overline{S}_{NO} = \iint S_{NO}(T,[O])P(T)P([O])dTd([O]) \qquad (2.2.3.31)$$

assuming statistical independence of T and [O].

The presumed shape (beta-pdf) is used and while no special treatment is required for species mass fraction of O (since it lies between 0 and 1), the temperature is normalized so that its mean lies between these limits and thus valid for use within a beta function. The calculation of variance does not follow from a transport equation but instead is approximated to:

$$\sigma^2 = \frac{\mu_t}{\rho}\frac{k}{\varepsilon}\frac{C_g}{C_d}\left(\nabla \bar{m}\right)^2 \text{ [23]} \qquad (2.2.3.32)$$

In the case of LES, the k/epsilon term is the dissipation rate and is taken directly from the variance computed as part of the mixture fraction calculations.

3. SOLUTION METHODOLOGY

3.1 Description and brief survey of the Fluent Code.

Fluent 6.3 by Fluent Inc., New Hampshire, is a well-validated commercial CFD code used for simulations that involve the solution of non-linear partial differential governing equations of the type discussed in the previous sections. Both pressure (segregated equations solving) and density (coupled equations solving) based solvers are available and is suitable for incompressible and compressible flows. The finite volume method is used for discretization of the PDE's and both algebraic and geometric multigrid solvers are available for use. Fluent is an unstructured code and is designed for general-purpose applications and thus suffers in speed for some applications (notably particle tracking and multiphase). Of recent past, Fluent has made combustion simulation a top priority [66] and has included several models that testify to this [23]. To extend its capabilities for user-defined sub-grid turbulence models or user-defined combustion models a C programming functionality is built into Fluent that makes it highly customizable. Studies were undertaken using 4 to 32 processors on the recently acquired on the 'Cirrus' HP XC cluster at Concordia University to determine optimal usage. Memory usage was a conservative 1 GB per processor. A speedup curve can be seen below.

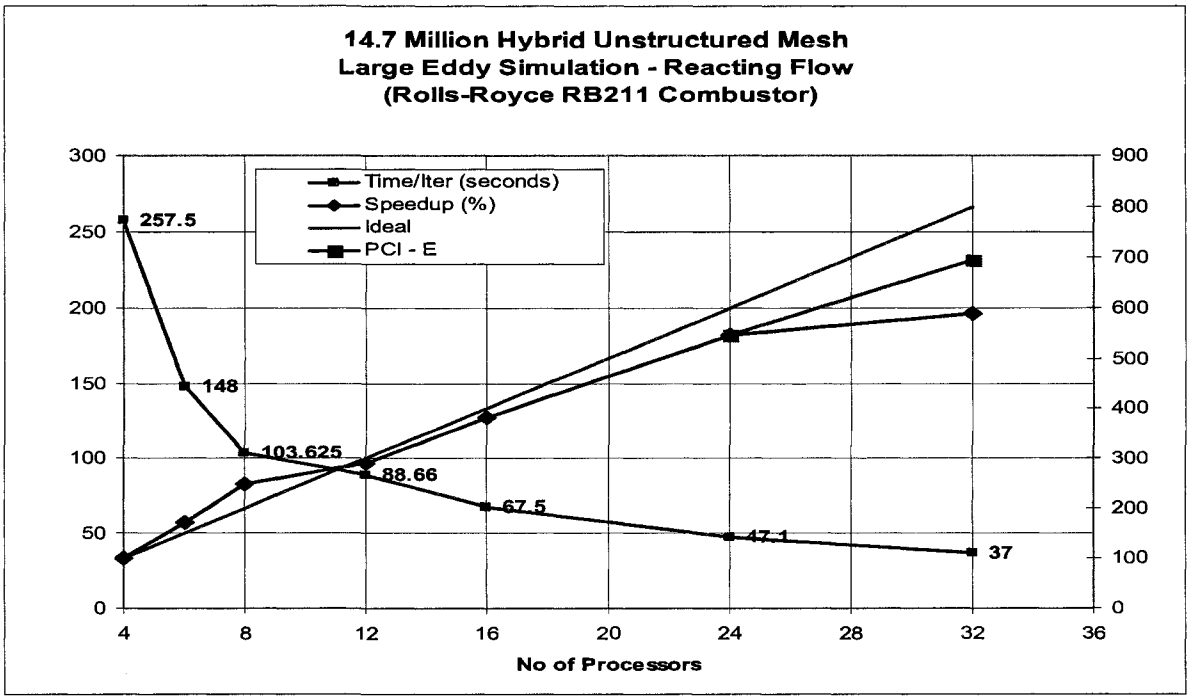

Fig 3.1.1 - Fluent Speedup ((left) seconds (right) % speedup)

The Fluent code has been used in the literature and the results are quite encouraging. In the context of the codes validation in regards to combustion, Riesmeir et. al. [52], used an unsteady flamelet method of Peters [44] to predict pollutant formation in a BMW Rolls-Royce combustor. Caracciolo and Rubini [18] applied the code's applicability to partially premixed combustion. Price et. al. [67] , used the code's steady flamelet method to predict NOx emissions in the GE LM1600 combustor at partload. Samuelsen et. al. [69], used Fluent to gauge the role of unmixedness and aerodynamic effects on premixed natural gas combustors. Biagioli et. al. [50], used the TFC model through Fluent's UDF functionality to predict NOx and CO emissions for a DLE industry combustor. Biagioli further compared the RANS simulation to LES in predicting a highly

unsteady phenomenon of intermittent flame anchoring using the partially premixed approach, in the Alstom EV burner. Polifke et. al. [49], modeled the effect of inhomogeneities in premixed combustion by extending the TFC model, on the BERL combustor as well as the Alstom EV burner and compared species transport with the pdf method. Polifke et. al. [69] also used the code to predict the effect fuel nozzle shapes on combustion stability and thermo-acoustics. Gordon et. al. [70], used the PDF transport method in Fluent, to simulate methane autoignition in a vitiated co-flow burner. Lysenko and Solomatnikov [81] used Fluent to predict heat exchange in combustion chambers with detailed benchmarking.

3.2 Discretization Schemes.

The Partial Differential Equations in Chapter 2 need to be discretized and assembled into a set of algebraic equations, which are then solved using the GMRES multigrid solver Fluent provides. This discretization is done using several schemes. RANS simulations were second order accurate, except in the case of combustion, where second order accuracy could not be reached to the default convergence criteria of 1e-6 on enthalpy.

RANS:

The cell-centred, Second Order Upwinding scheme of Barth and Jesperson [71], which uses a Taylor series expansion of the solution stored at the cell centroid, was used for all equations. Thus, the solution reconstruction at the face is done as follows:

$\phi_{face,SOU} = \phi + \nabla\phi \bullet \vec{r}$ where $\nabla\phi$ is the gradient of cell-centred value ϕ in an upstream cell and $\vec{r}$ is the displacement vector from the upstream cell centroid to the face centroid. ϕ_{face} is computed using the weighted Green-Gauss node-based gradient evaluation given by

$\phi_{face} = \frac{1}{N_{nodes}} \sum_{n=1}^{n=N_{nodes}} \phi_{node}$ where N_{nodes} is topology dependent and cannot be used for polyhedral meshes and is the number of nodes on the face. For polyhedral meshes, the least squares method, which evaluates the gradient by assuming the solution to vary linearly between the neighbouring cell centres. This method is more accurate for polyhedral meshes and is the one used for all polyhedral grid simulations in this thesis. For more details in the procedure used in the weighting process of the least-squares method, the reader is referred to [23].

LES:

LES suffers when numerical diffusion is high. Current codes still favour structured grids, aligned with the flow. But complex geometries necessitate the use of arbitrary topology, introducing the need for highly accurate, low-diffusion schemes. Pure central differencing is preferred whenever Peclet number constraints are not excessive. However, the environment in a typical gas turbine combustor consists of compressible jets in cross flow, high velocities of the burnt gas, etc which often give rise to unbounded solutions, particularly when a less than high quality grid is employed. Fluent provides a Bounded Central

Differencing (BCD) based on a normalized variable diagram which can be used with a 'convection-boundedness' constraint in order to prevent unphysical results caused often by a pure central differencing method's tendency to 'wiggle'. The BCD scheme prevents this by blending central differencing with a second order Upwinding scheme and a first order Upwinding scheme that is used only when the boundedness criterion is violated.

Central Differencing is implemented in the following manner

$$\phi_{face,CD} = \frac{1}{2}(\phi_0 + \phi_1) + \frac{1}{2}(\nabla\phi_0 \bullet \vec{r}_o + \nabla\phi_1 \bullet \vec{r}_1)$$

$$\phi_{face} = \phi_{face,UP} + (\phi_{face,CD} - \phi_{face,UP})$$

where 0 and 1 refer to cells that share the face. The second term in Eq.. consists of the cell gradients for cells 0 and 1 respectively. The vector *r* denotes the direction vectors from cell centroid towards face centroid for cells 0 and 1 respectively.

The nominally third order QUICK scheme of Leonard and Mokhtari [72] was used for all scalars.

3.3 Grid Partitioning

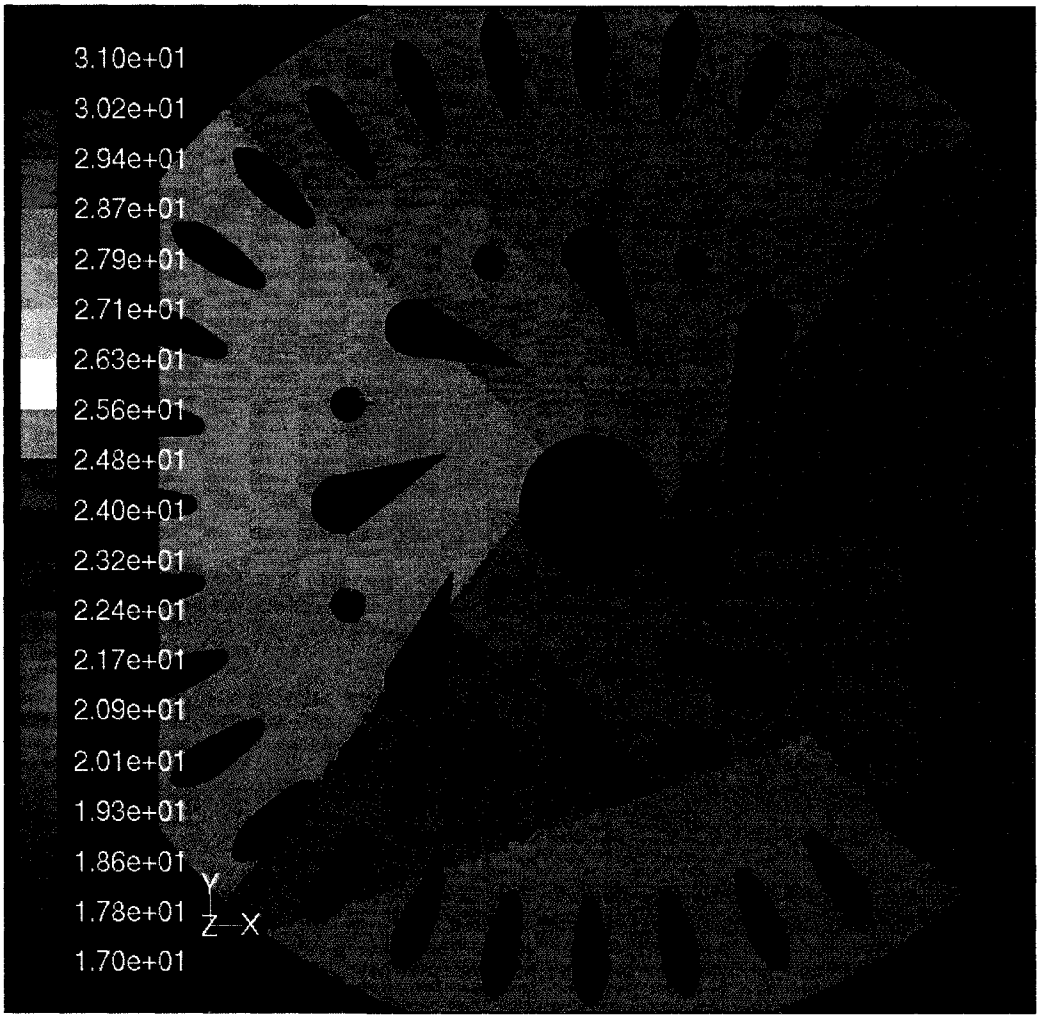

Fig 3.3.1: Partitioning of the Grid - Primary premix detail (13 out of 32 domains shown).

The Grid was partitioned into 32 domains using a principal axis scheme that eliminates orphan clusters. The minimum number of neighbours to each partition was two and the maximum was 15. The load was evenly balanced with maximum and minimum cells in each partition at 511762 and 511763. The load was kept equal, as the compute nodes were identical.

3.4 Mesh considerations

A considerably fine mesh is required due to LES constraints. Two issues that can immediately be identified are near-wall resolution and sub-grid model effectiveness. It is well known that near-wall layers require extremely fine meshes for proper resolution. Infact, the cell sizes required to resolve wall layers are so fine that they approach DNS type density [24]. The focus of the current project is not the resolution of wall boundary layers since the region of interest is the central flame zone. The situation is more optimistic, though still of some aggravation, when the cells in other zones are considered. Due to the isotropy of flow at smaller length scales (smaller cells), a simple, algebraic turbulence model is usually sufficient. However, as cell size increases, the assumption of isotropy does not hold and increasingly degrades sub-grid model performance: the worst scenario being, the case where energy containing, flow-coupled, highly anisotropic, large vortical structures are modeled by the sub-grid model, rather than resolved by the filtered Navier-Stokes equations.

With these considerations in mind, and based on preliminary testing of different geometries (ranging from an axially symmetric combustor to a sector of the RB211 primary), and in keeping with the 'advanced' nature of this project, four

meshes have been generated with cell counts ranging from 3.5 to 20 million cells. It must be mentioned that the high density of cells does not imply better resolution of reacting species in time and space, since chemically reacting processes occur at molecular level. However numerical diffusion is kept to a minimum, coherent structures that directly affect the flow are resolved with a degree of fidelity unavailable with any RANS model and turbulence-chemistry interaction is better accounted for (in the context of reacting flows).

Domain Decomposition is still necessary, but due to the flexibility offered by the unstructured approach, it is kept to a minimum. Current turn-around time for the grid generation of an entire RB211 combustor is between 3-5 days with the current methodology. All grids have been generated on computers with enough RAM to generate grids without use of hard-drive swap-space or page file.

1. An unstructured, all-hex, non-conformal mesh. (> 20 million cells)
2. An all-tetrahedral/prism mesh. (~ 16 million cells)
3. A hex-dominant mesh. (~20 million cells)
4. A polyhedral mesh. (~3.5 million cells)

Mesh 1 is suitable for parametric simulations where meshing time is scarce and a component needs to be modified without having to regenerate the entire mesh. This mesh was not used in the simulations due to the very high computational requirement.

Mesh 2 is the "workhorse" mesh that offers a good trade-off between accuracy and computational demand.

Mesh 3, is the one used for all high fidelity RANS simulations.

Mesh 4 is essentially Mesh 2 converted to polyhedra and has a cell count of ~ 3.5 million (due to the agglomeration of tetrahedral elements resulting in a cell count drop by a factor of 3.8-5, while retaining the same order of node count, e+7). This mesh was used for all the LES simulations. Despite its low cell count, literature indicates such coarse meshes may be used for LES simulations when 'engineering' solutions are required. Good examples are the GE LM6000 [73] and the Alstom EV [7] combustors meshed with only 700,000 and 400,000 cells respectively.

4. MODEL DESCRIPTION AND FLOW SPLITS

Descriptions and details of the flow-splits of air and fuel are shown in this chapter. The multi-staged nature of this combustor can be seen below in Fig 4.1. Top right in the picture is a cut-view of the combustor itself. The combustor is a reverse flow combustor situated perpendicular to the main flow path of the compressor air to the turbine (right in the picture, indicated by long arrow). At the apex, the torch igniter assembly can seen which provides the initial 'spark' of hot gas to bring the main mixture to ignition.

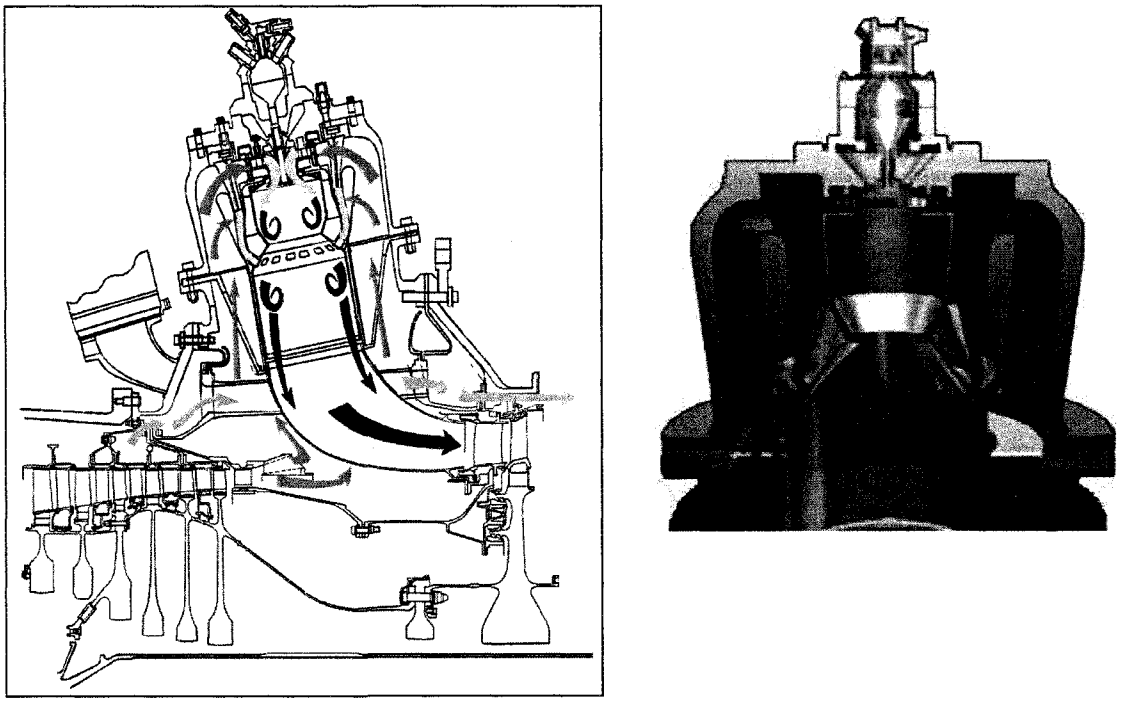

Fig 4.1: RB211 "long" combustor orientation in engine, with flow paths [74]. (*right - courtesy of Rolls Royce Plc*).

4.1 Computational Domain

The solid model prior to meshing is shown below. The geometry is symmetric until the end of the primary zone after which, to accelerate the air such that it comes out with a high tangential velocity to spin the turbine, the geometry is tapered in a highly asymmetric fashion. The bottom picture indicates the secondary premixer assembly, which ducts the secondary mixture to the second stage of combustion.

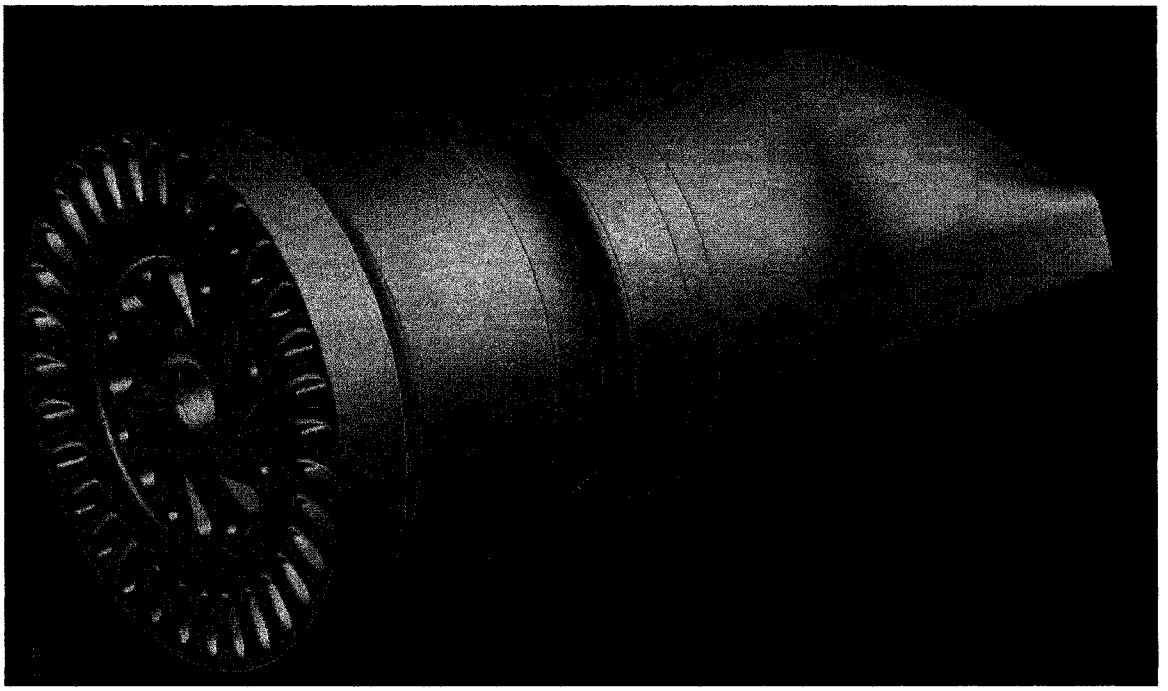

Fig 4.1.1: RB211 "short" combustor fluid flow path with main inlet removed.

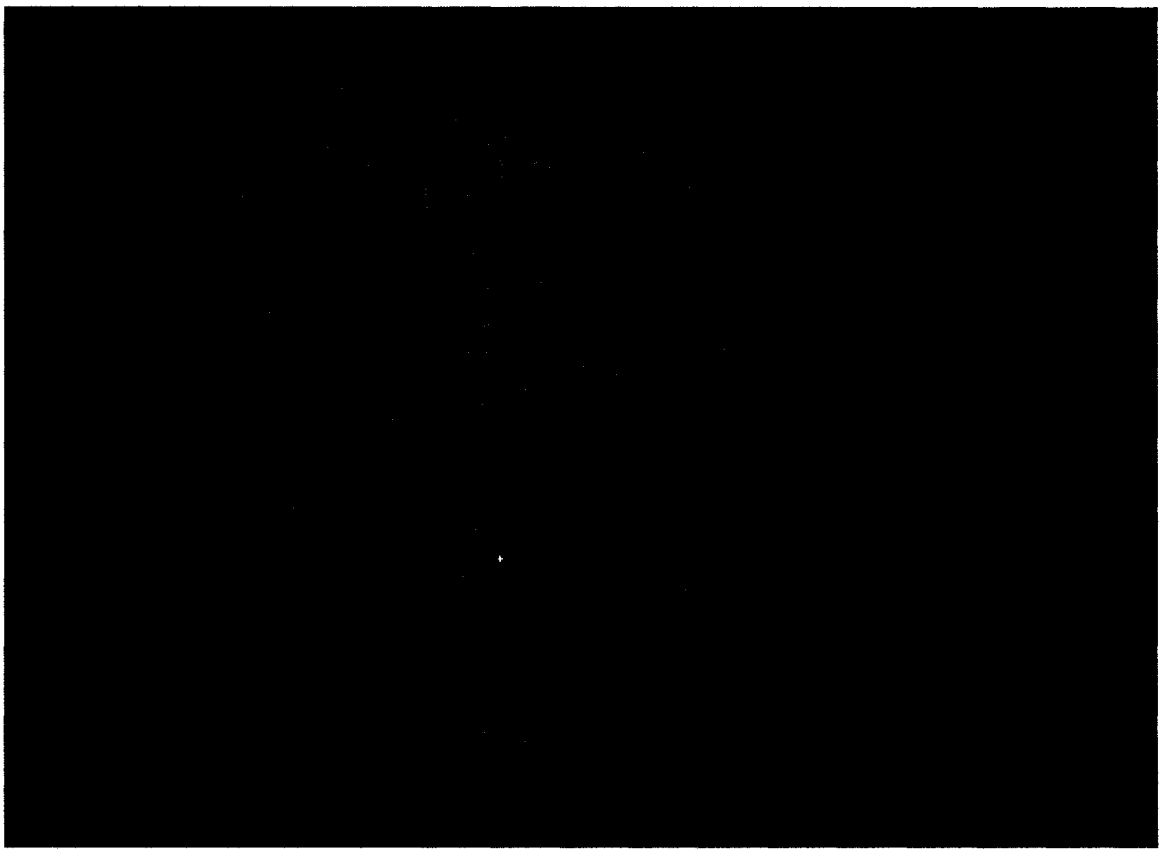

Fig 4.1.2: The Secondary Premix Duct with fuel "arms".

The computational domain consists of the following features:

1. A Plenum chamber that supplies preheated air from the compressor, to the primary and secondary premix chambers through a common inlet.

2. A Primary Premix zone that consists of two concentric swirl passages with a common exit into the primary combustion zone.

a. 80 Fuel injection points connected to "fuel-bars" to inject fuel in a "jet-in-crossflow" type configuration.

b. Swirl is imparted to the flow by swirl vanes and the end result is two swirl passages conducting counter-rotating flows, which exit into the primary zone, with a net swirl of zero at exit point.

3. A Secondary Premix zone that consists of 32 premix ducts that conduct air for premixing with fuel injected from 192 injection points coupled to "fuel-arm" structures that provide necessary structures for the passage of fuel lines to injection points (Fig. 4.1.2).

a. The Secondary Premix Zone is concentric with the primary zone and is inline with the Primary premixer.

b. Fuel is injected into the crossflow and mixes thoroughly in the passage downstream of the fuel-arms.

4. The Primary Zone is the first stage of combustion and is connected through a converging-diverging area of cross section, to the secondary zone.

5. The Secondary Zone is the second stage of combustion and receives material from both the primary zone as well as premixed gas from the secondary premixer that exits into the secondary zone through 16 inlet "windows"

6. The Secondary Zone connects with the discharge nozzle and the geometry blends from a circular cross section to a rectangular outlet just upstream of the turbine IGVs).

4.2 Operating Conditions and Gas Flow Path

The gas flow path described in the previous section is shown visually in picture 4.2.1. This is also a slice of the polyhedral mesh used in the LES simulations in Chapter 6.

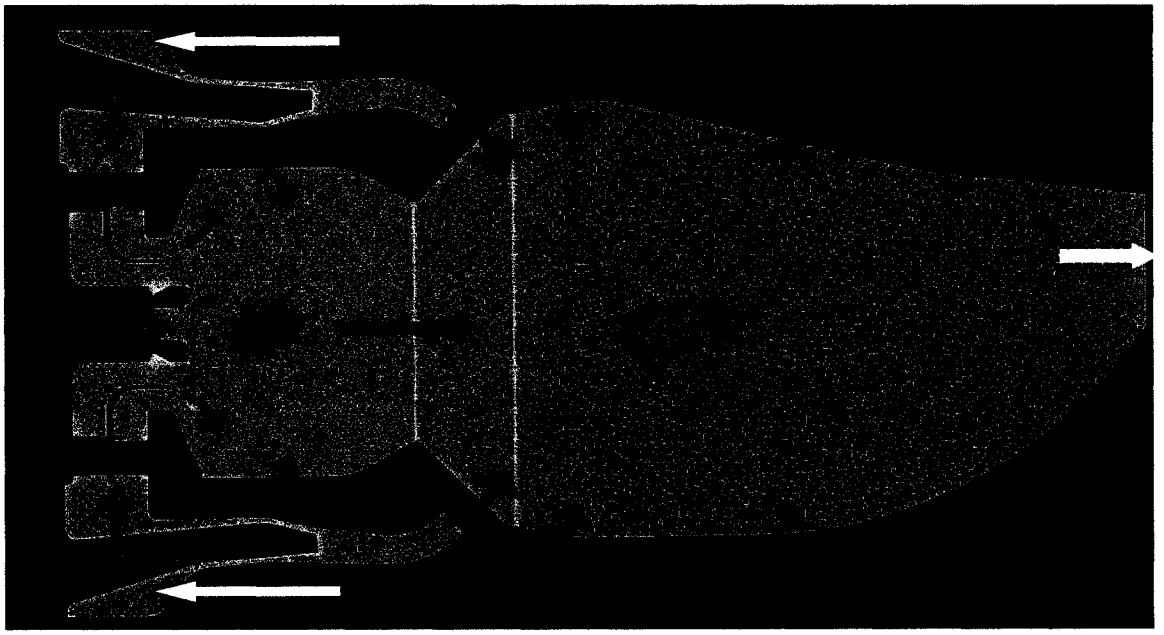

Fig 4.2.1: Fluid flow path, detached blanked regions indicate wall structures, not represented in this slice (swirl vanes, fuel arms, wedges etc).

White Arrows	–	preheated air from the compressor.
Pink Arrows	–	flow split to primary and secondary premixers.
Orange Arrow	–	torch air for ignition.
Green Stars	–	fuel injection points.
Red Arrows	–	premixed gas from primary premixer.
Green Arrows	–	premixed gas from secondary premixer.
Blue Arrows	–	cooling air to primary, secondary and discharge nozzle zones.
Yellow Arrows	–	burnt products at outlet.

- Flow flows out of the domain in the negative Z direction.
- Diffusion Inlets are not used at Baseload
- Cooling Flows were modeled using energy and mass source terms for wall boundary cells.

Boundary Conditions

The Boundary Conditions were used from a scaled rig test conducted at Rolls-Royce Canada.

Operating Pressure	5 bar
Air Temperature	702K
Wall Temperatures	adiabatic
Turbulent Intensity	10% for all except cooling flows which are at 3%
Turbulent Viscosity Ratio	10 for all
Overall Equivalence Ratio	0.416

Mass Flow Splits:

Name	Type	Material	Qty	% of Intake air
Primary Premix	Mass Flow Inlet	Air	1	35
Secondary Premix	Mass Flow Inlet	Air	1	40
Torch (Pilot)	Mass Flow Inlet	Air	1	2
Primary Cooling*	Mass Flow Inlet	Air	1	9
Secondary Cooling*	Mass Flow Inlet	Air	1	4
Discharge Nozzle Cooling*	Mass Flow Inlet	Air	1	8
Primary Fuel	Mass Flow Inlets	CH4	80	1
Secondary Fuel	Mass Flow Inlets	CH4	192	1
Outlet	Pressure Outlet	Products	1	-

Table 4.1: Boundary Conditions used for all the simulations.

Fuel is natural gas - typical base fuel without any blends > 96% CH4.

4.3 Mesh

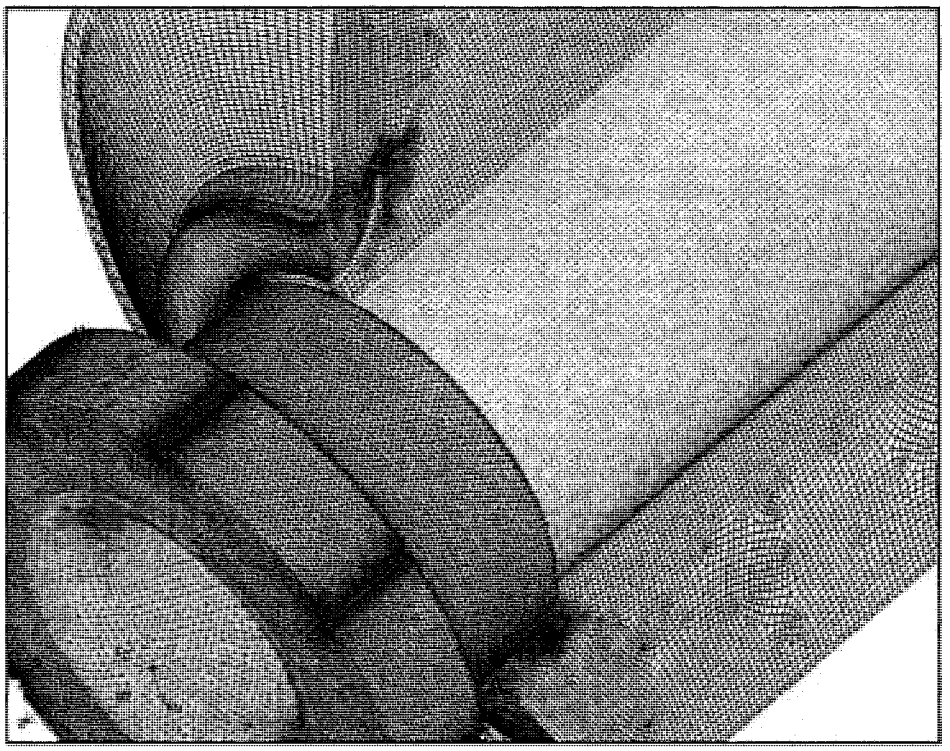

Fig 4.3.1: Refined portion containing the centreline of the primary.

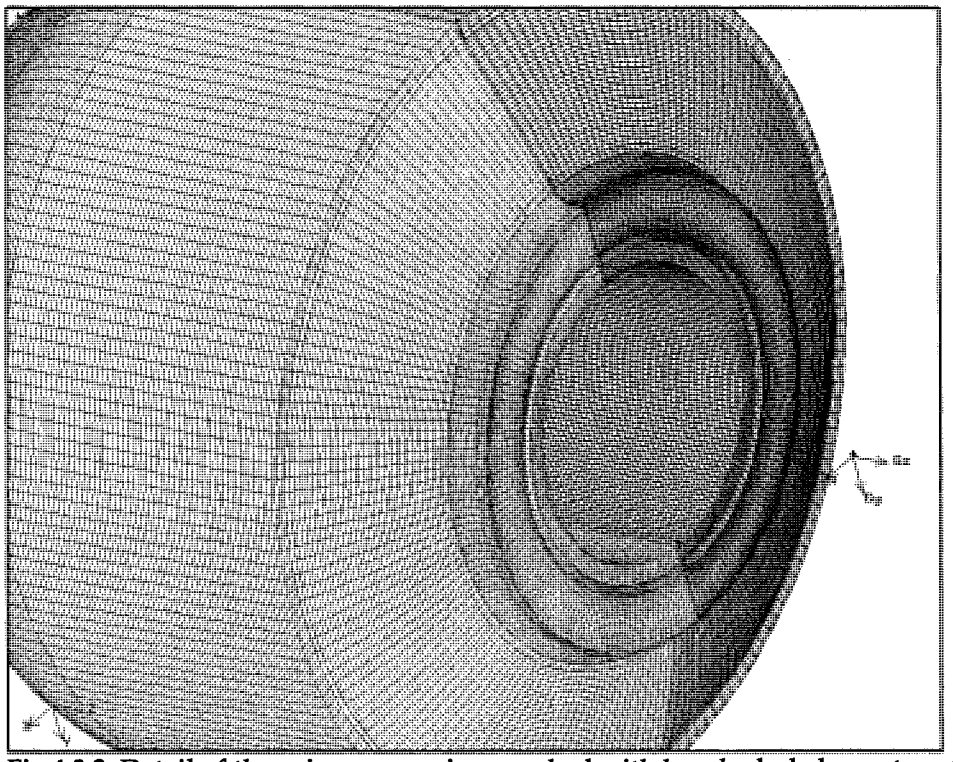

Fig 4.3.2: Detail of the primary premixer meshed with hexahedral elements entirely.

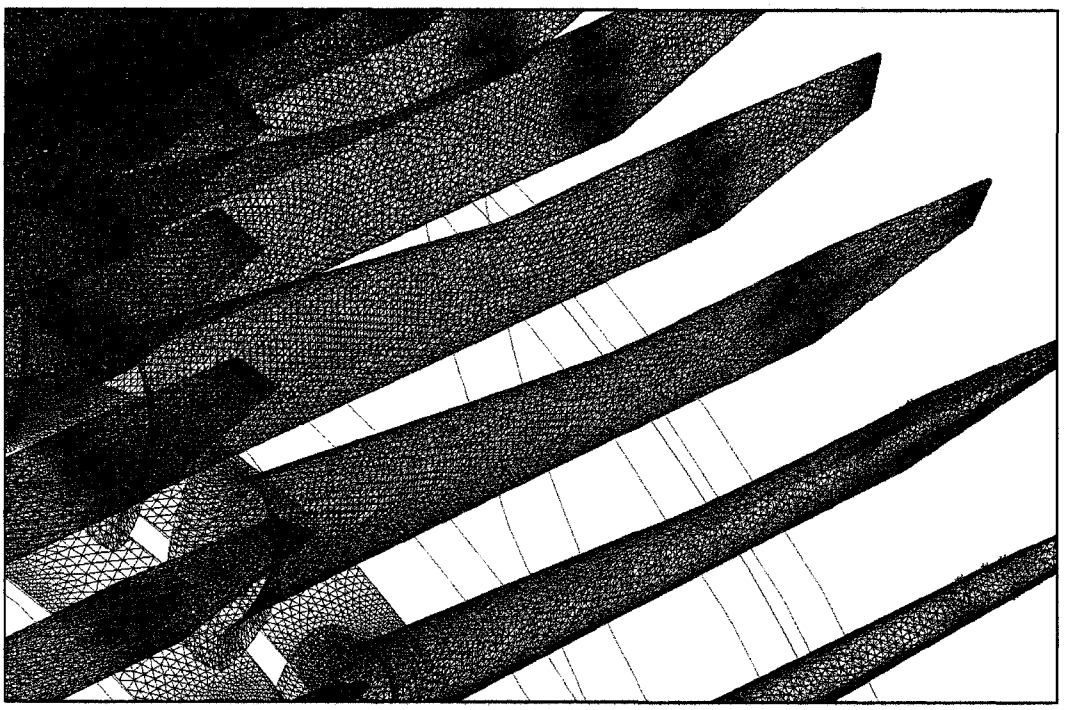

Fig 4.3.3: Detail of mesh on the secondary premix fuel arms.

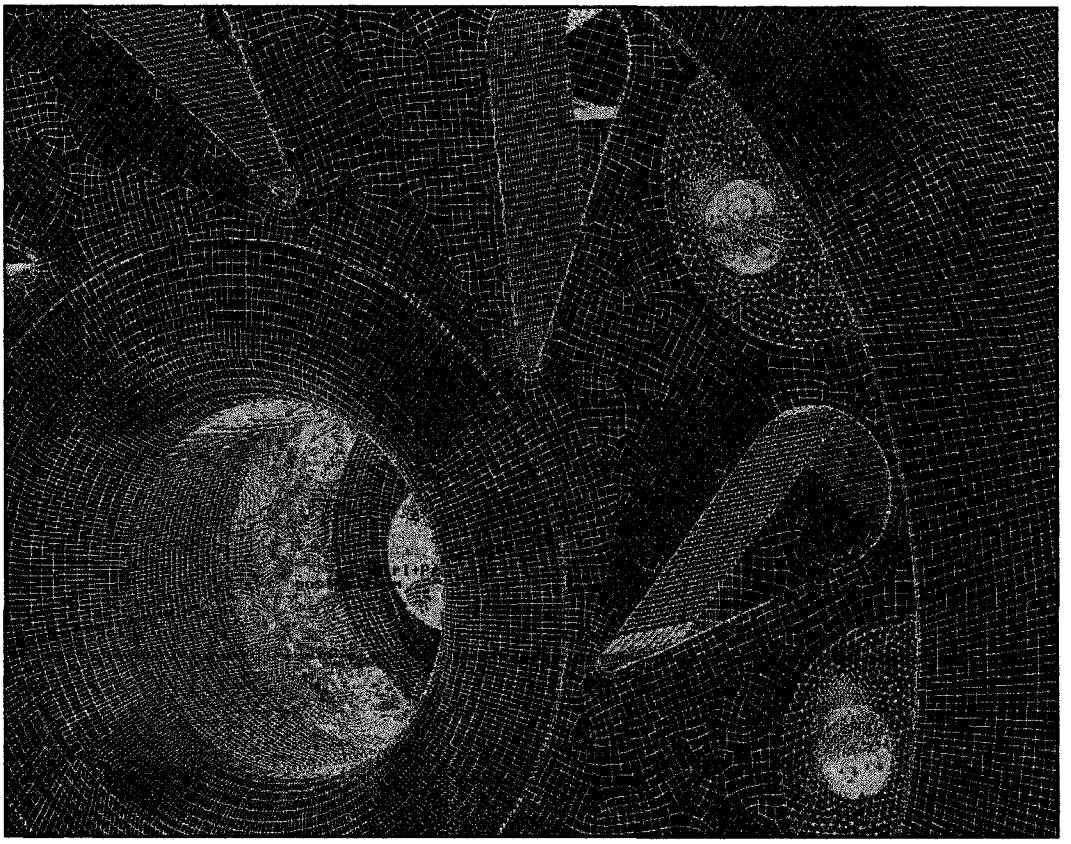

Fig 4.3.4: RANS mesh: Hex premixer, primary and secondary, tetrahedral elements have been used only for the injector zones and secondary premix.

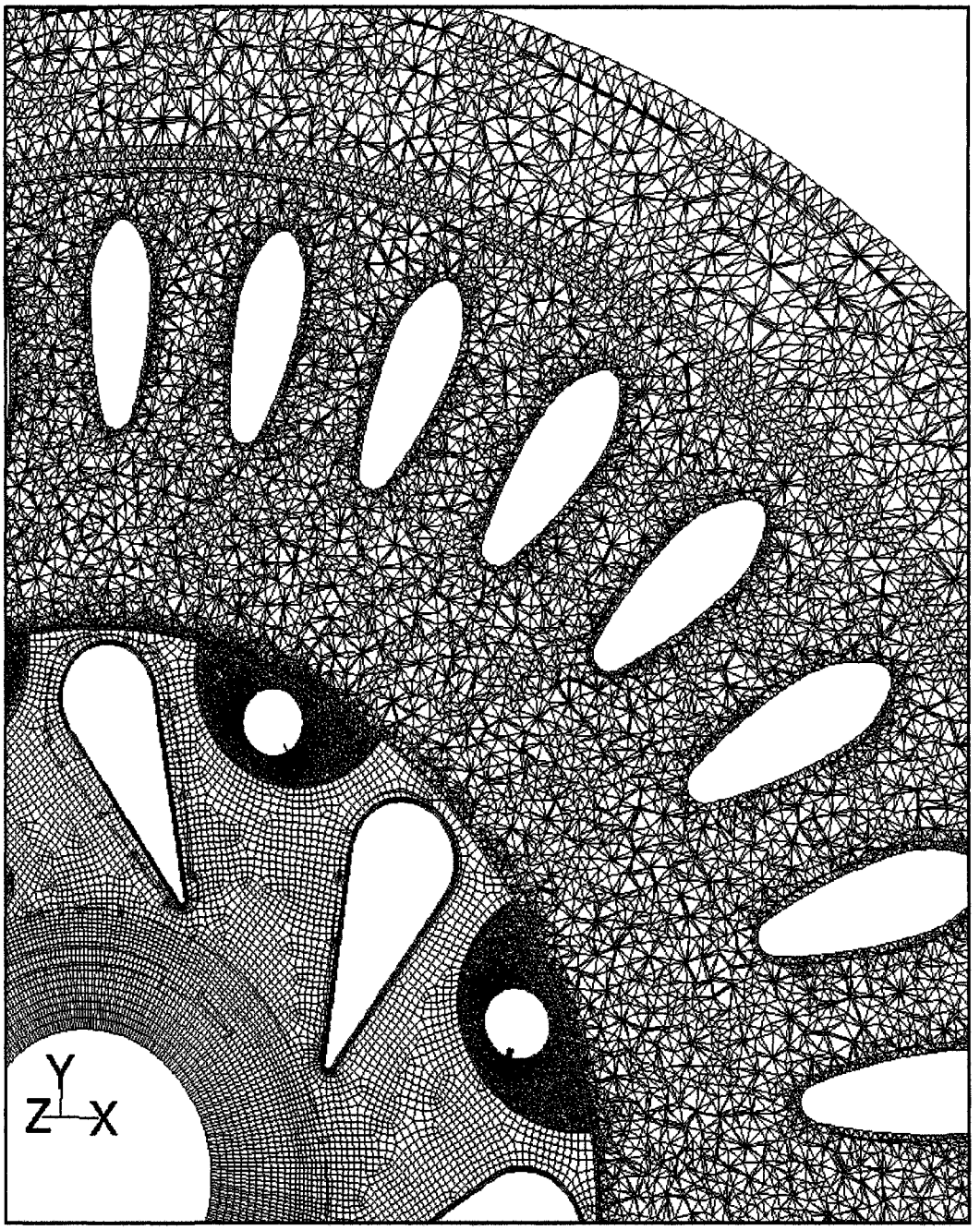

Fig 4.3.5: Cross section of the Hybrid mesh.

Refinements were done based on experience with simulations using different meshes. However, the main regions of interest were the primary and secondary zones as can be seen in Fig 4.2.1. In Fig 4.3.5, refined meshes were built near the fuel injectors which inject fuel at very high velocities.

5. COLD FLOW RESULTS

Analysis of mixing processes in the various flow zones.

5.1 Mixing in the Primary Premixer

Fuel premixing is necessary for low emissions [75]. The premix chamber exists to prepare a uniform mixture of fuel and air into the primary zone of combustion. Fuel is added in a non-premixed fashion into a cross flow of air from a plenum chamber. This flow of air from the plenum enters the premixer radially and guided into the central exit passage that connects to the primary flame zone through angled vanes, which impart swirl to the mixture. Two such swirl chambers exist to provide counter-rotating swirls. These rotating mixtures are kept apart through concentric passages until the point of entry into the primary zone where they meet. Great care must be taken in order to avoid recirculation zones that increase the fuel residence time in the premixer. This is because the air is preheated and brought close to ignition temperature. This can form a combustible mixture that is susceptible to flashback or auto-ignition and would cause catastrophic damage should the event occur. All lean-burn combustors face this problem and incorporate a variety of devices to combat it. In the RB211 combustor, fuel is added downstream of an aerodynamic pressure loss – i.e. at a place where velocity is low, such as in the wake of a fuel bar (cylinder shape).

Premix residence times are two orders of magnitude lower than the autoignition time of the fuel mixture. The mean velocity of the flow is also several orders of magnitude higher than the turbulent flame speed of the combustible mixture. This ensures that a flame cannot be stabilized in the premixer. Experiments [76] have proved that when a flame is introduced into the premix (spark), it is quickly quenched and does not cause the premix to ignite. However, the angle of the fuel jets into the cross flow is critical and when modeled, care must be taken to ensure adequate resolution of its shape (round nozzle). Inadequate resolution of the shape, leads to fictitious recirculation zones that cause the combustion model currently used to light up numerically. Another issue that needs to be taken into consideration is the issue of cold fuel mixing with hot air. The fuel jet exit configuration plays a great role in this regard. Some combustors have free fuel jets and others are injected along the wall. The latter are susceptible to autoignition due to the slowing down inside the viscous boundary layer. Fuel jets exit with a velocity of O(2) from their nozzles and along a wall, viscous effects can retard the flow and cause a net heat flux *into* the fuel from the heated walls and delay their propagation long enough to cause autoignition. DNS studies indicate that 'fast turbulence' (small-scale eddies) such as found in the near wall region, facilitate autoignition. Jets in cross flow (JICF) have been identified as a research topic by the MOLECULES project in 2001 [77] of very

practical interest to the industry. Several authors have investigated JICF and some of the results obtained in the current cold flow analyses visualize and compare with them. The issue of cold fuel mixing with preheated air is shown in Figs 5.1.2 and 5.1.5 as the fuel jets entrain by virtue of counter-rotating vortex pairs (CVPs). Fig 5.1.1 shows a slice through them. It has been possible to capture this in the current simulations, with highly refined grids in the vicinity of the fuel

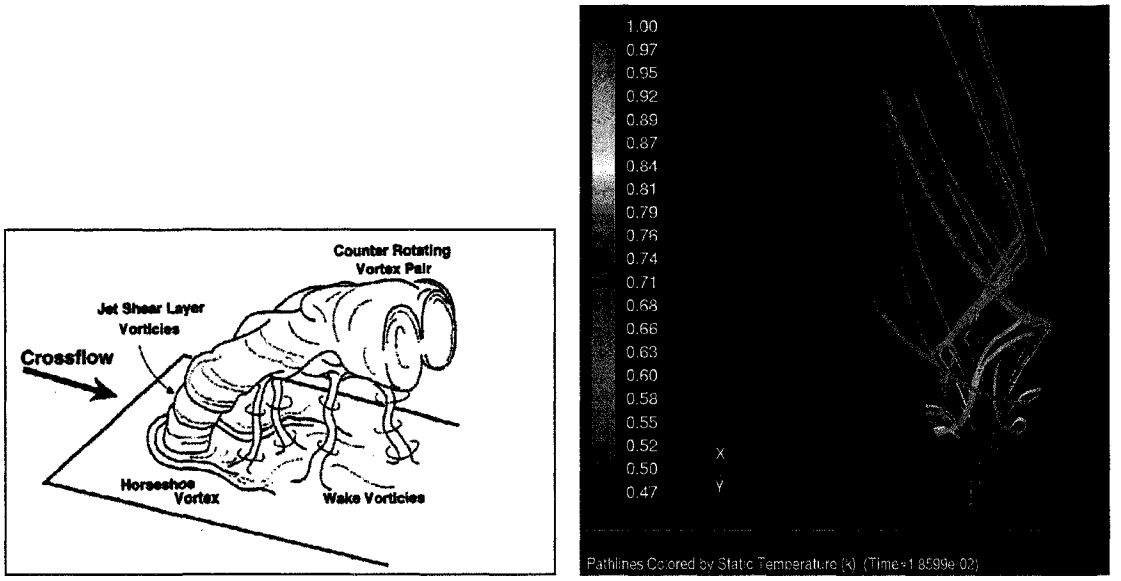

Fig 5.1.1: *(left)* Counter-rotating vortex pair contributes to the entrainment of jet (78) *(right)* LES result depicting the CVP from a single injector.

injectors. A sketch of these vortex pairs is reprinted from [78] in Fig 5.1.1 Schulter and Schoenfeld [78] validate an LES method for a Siemens fuel injection system, by simulating several experiments conducted for the purpose of researching JICFs. They explain that the CVPs merge downstream due to the Coanda effect that occurs in a parallel jet configuration. These zones create areas

of unmixedness. In present calculations, each fuel bar has three or two injectors and that means at least two pairs of CVPs which bend towards each other, trying to entrain each other and thus end up merging. LES visualizations of the mixedness have important implications for fuel injector design, as it is now possible to view the instantaneous state of 'mixedness' immediately downstream of the fuel injectors. Time-averaged profiles of the LES cold flow show very different results as is evident from Figs 5.2.

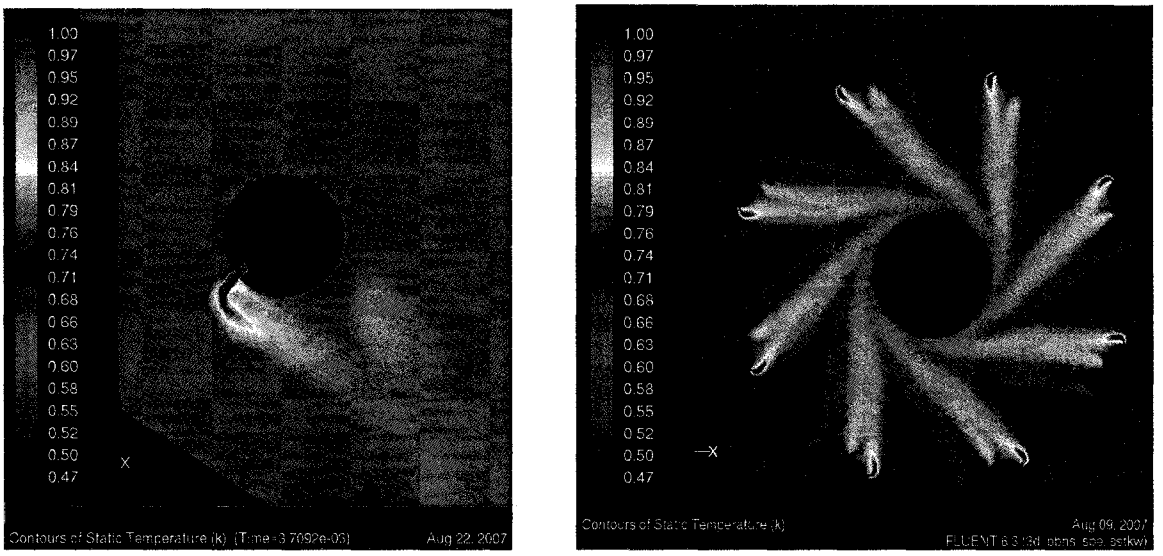

Fig 5.1.3: Fuel Injector Flows(*left*) averaged LES *(right)* RANS-SST *(zoomed out).*

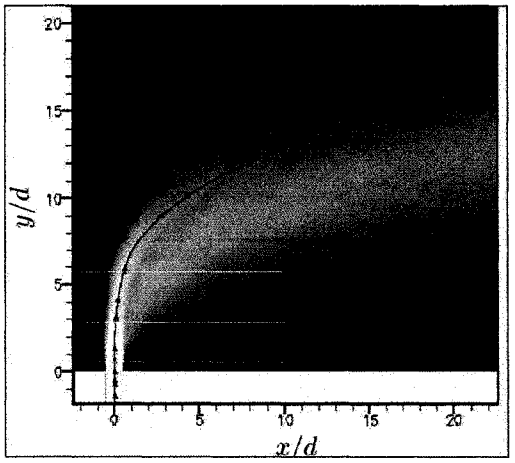

Fig 5.1.4: DNS of JICF (from [79])

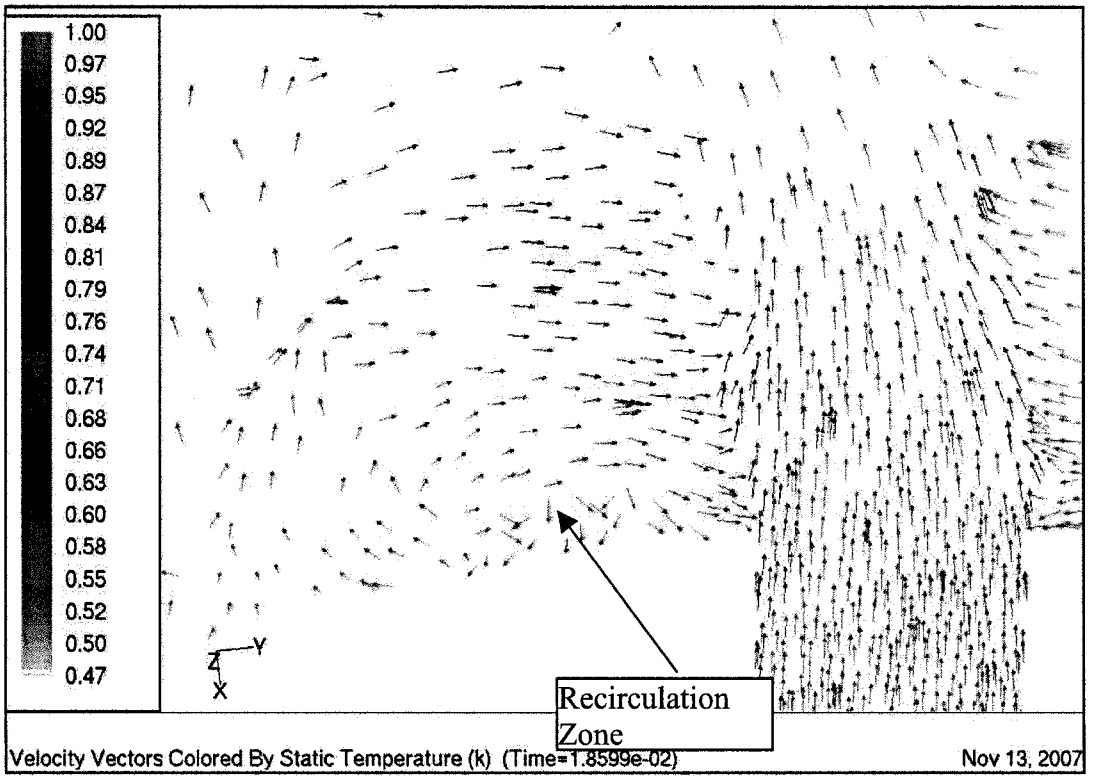

Fig 5.1.5: Recirculation Zone vectors near Fuel Injector

The pictures below show a time averaged LES description of the flow and indicate a significant difference from the RANS picture above (see Fig 5.1.3)

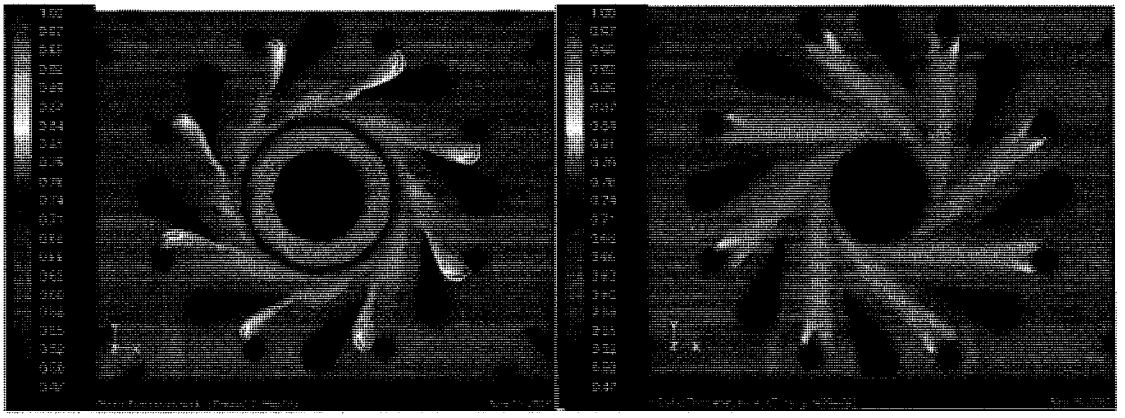

Fig 5.1.6: Mixing in the swirl passages: *(left)* Swirl Injector, *(right)* Swirl combustor

In the picture Fig 5.1.6 (right) the central annulus is a section of the passage connecting the swirl injector to the primary zone. The swirl combustor passage is coaxial with this passage. Flow is *into* the page.

The temperature non-uniformity of the flow entering the combustor is evident from this picture. Mixing is fairly uniform although the swirl combustor does indicate that the chamber itself may be further from perfect premixing than the swirl injector chamber. The degree of temperature non-uniformity is higher as can be seen above. This has implications for simplified simulations, as the flow issuing into the primary from these swirl passages is definitely not perfectly premixed. The effect of different passage lengths from the swirl chambers to the primary zone also on the uniformity of the mixture at the exit of the swirl chambers is also a detail worthy of investigation from a design point of view since the swirl combustor passage has very less time to mix the fuel and air before the mixture is dumped into the main chamber. Considering the fact that the vortex formed in this chamber is also the outer vortex, the probability is greater that unburned fuel will enter the secondary. Running a particle tracking simulation can test this hypothesis. However due to time constraints this was not done.

5.2 Mixing in the Primary Zone

The concentric, contra-rotating streams of premixed fuel-air mixture enters the primary zone and by virtue of its helical motion and strong swirl, causes a vortex breakdown, reverses a major part of the flow (swirl-reversal) and generates a 'bubble' type recirculation zone downstream which grows in time and size as downstream flow enters it and moves it upstream where it forms two stagnation points on the axis and oscillates about each point with a dominant frequency. This has implications for noise and other acoustic instabilities as well as the thermal stress that could happen when an antinode of a standing wave coincides with a point of heat release resulting in an artificial hotspot (Willis, [76]). The main design requirement is to use these recirculation zones to thoroughly (turbulently) mix the fuel-air mixture as it combusts and ensure a stable flame that grows round the edge of the recirculation zones (RZs). RZs have been studied extensively in the literature and their interaction and superposition are amongst the most complex flows to simulate numerically. These are very large vortices (comparable to the domain size), influence most of the mixing and thus best defined by LES methods. The incoming fresh mixture from the premixer confronts a fully formed on-axis RZ and is obliged to flow around it as if it were a bluff body. Indeed, the RZ stabilizes the flame and acts as an aerodynamic

flameholder. Inside the RZ fresh mixtures as well as burned products enter and leave. The RZ is a fairly homogeneous zone and is often considered as a perfectly stirred reactor in chemical reactor network analyses [40]. Ignition primarily occurs in the RZ as flow inside the RZ circulates for a time greater than the ignition delay time. Thus the design and position of these zones is a critical aspect of combustor design. From a modeling stand-point, turbulence models which can account rigorously for streamline curvature effects are the only models that should be used when accuracy is desired. Since the flame front is dependent on the outer streamlines of the RZ where the mass exchange takes place, the hot shear layers must be calculated accurately in order to predict the flame brush, which widens away from the zone. Extensive numerical and experimental cold flow analyses of these zones are available in the literature. Several authors have commented that RANS models (barring the Reynolds Stress 2^{nd} moment closure models) are unable to determine accurately the size and shape of these recirculation zones. It must be mentioned; that the k-epsilon model derived from the Renormalization Group theory [22] overcomes some of the limitations of the k-e model in its response to curvature in strongly swirled flows by incorporating a swirl number modification. Neither the ke-RNG model nor the Reynolds Stress Model were investigated either since its computational cost was comparable to DES due to the large grid size in the latter case and the

former due to time constraints. Recirculation Zones may be observed in the LES and RANS contexts in the pictures below (Figs 5.2.1, 5.2.3, 5.2.5).

Due to lack of experimental data for cold flow scenarios (long and short RB211) the results were compared with internal studies. The results were found to match qualitatively although it must be argued that the LES methodology used in the current context might provide better insight into the mixing process.

Key features of the flow:

1. Strong vortices form in the primary due to vortex-breakdown and the on-axis flow-reversal enhances the turbulent mixing (Fig 5.2.4). An animation of this is available and shows the mass transfers between various parts of the domain, particularly between the central and corner recirculation zones.
2. Shear Layers are present at the interface between the torch-flow and central recirculation zone, and between the corner recirculation zones and the main flow (Fig 5.2.1). It is in these areas that combustion is expected.
3. Flow entering through the torch almost immediately gets caught up into the recirculation zone due to the strong flow reversal (5.2.3). Any unburnt

fuel propagating with the products will be completely burned due to the fresh influx of oxidizer.

4. Flow also shears from the tip of the swirl combustor and injector dividing wall, creating the potential for a hot spot at some design condition (Fig 5.2.1). However the velocity is high enough at this point, so that the flame is probably quickly quenched. Experiments indicate that this happens, though.
5. Stagnation points form on the axis as well as at the 'eyes' of the recirculation zones and these are observed to oscillate with time (Fig 5.2.1). Again, only an animation is able to depict this.
6. The usual way to isolate turbulent structures is by iso-values of Vorticity, and this is shown in Fig however, other methods that are more rigorous (and perhaps with better physical insight) can be applied such as those derived from velocity gradient tensor matrix invariants (see Chapter 6).
7. Stagnation points were predicted by previous CFD analyses to lie outside the primary zone or near the exit. This study suggests it lies almost at the exit with a slight amount of recirculation happening at the centreline on the primary outlet.

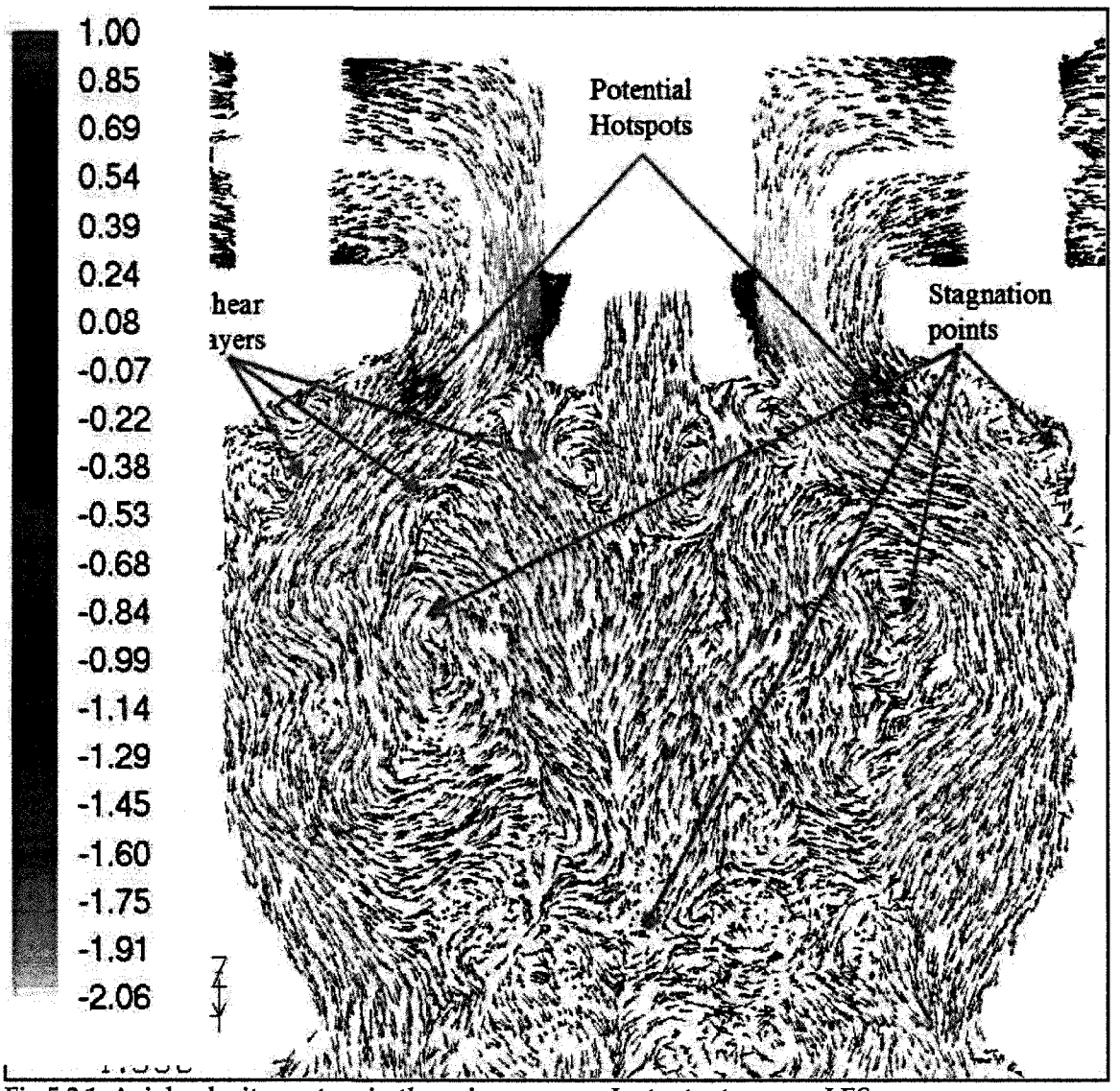

Fig 5.2.1: Axial velocity vectors in the primary zone. Instantantaneous, LES.

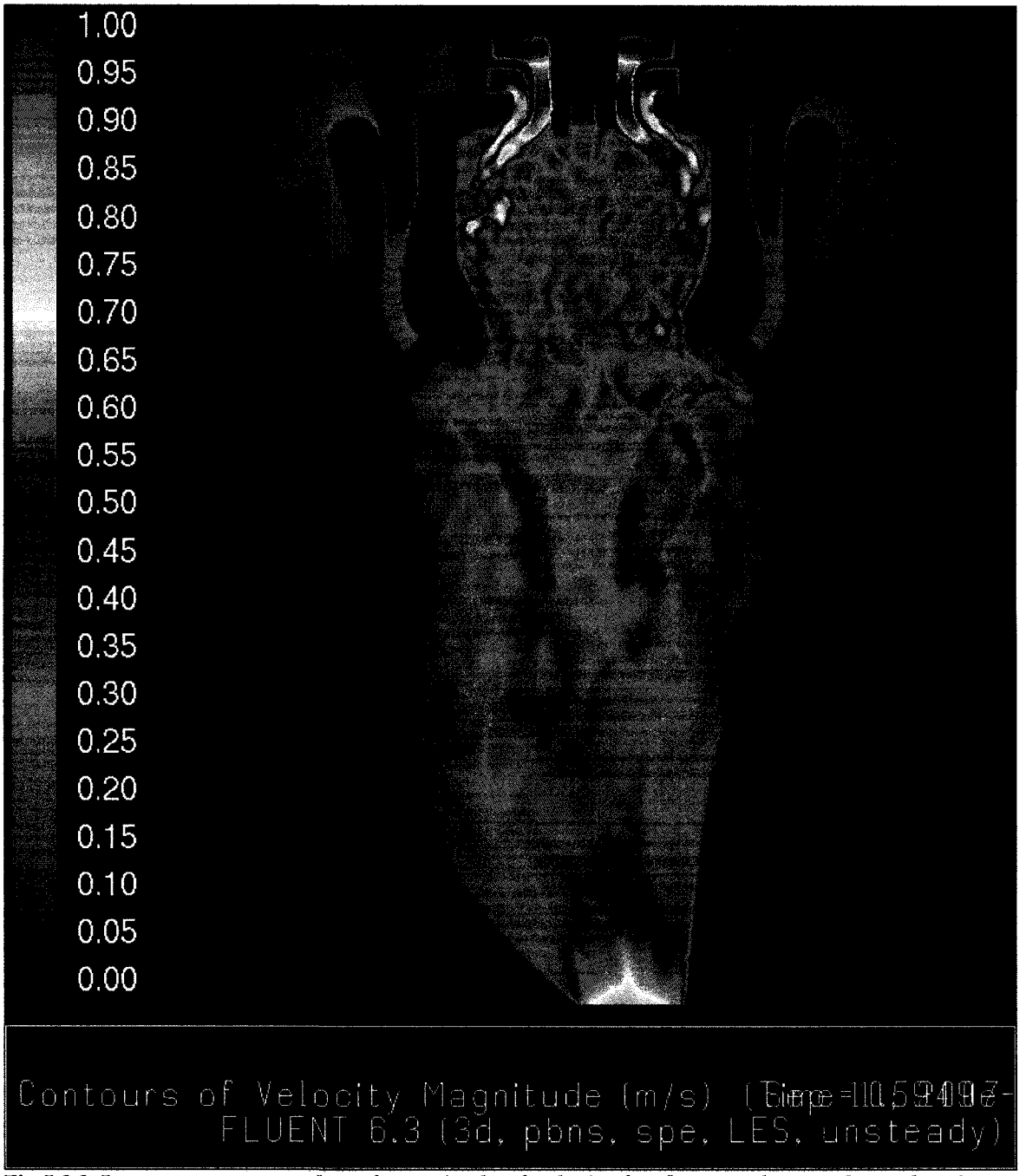

Fig 5.2.2: Instantaneous snapshot of magnitude of velocity for short combustor. Secondary jets can be seen to meet in the middle.

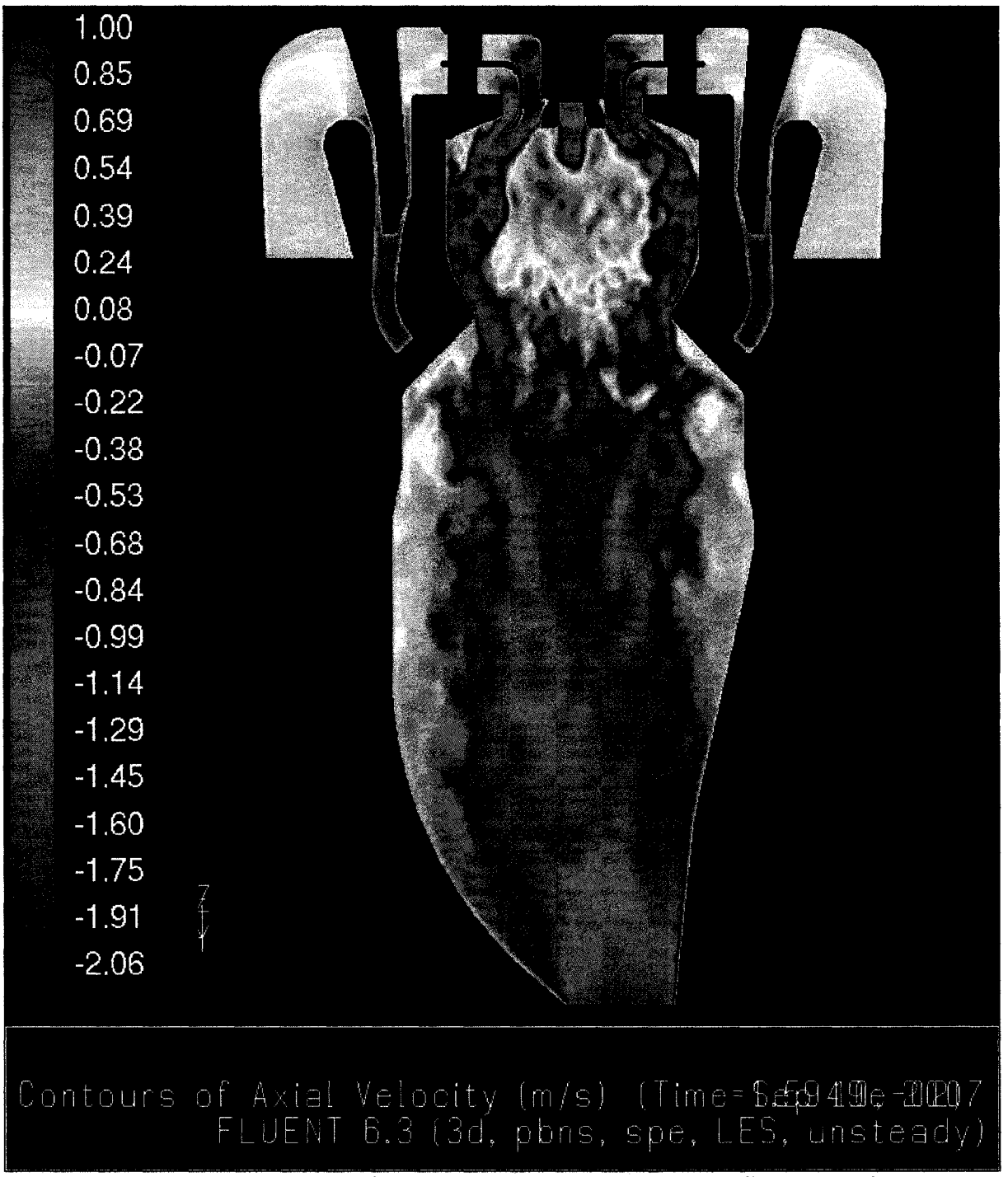

Fig 5.2.3: Instantaneous snapshot of Axial-velocity contours. LES. The flow reversal can be clearly seen in the primary premixer (red). Secondary recirculation zones due to the contour of the chamber's body are observed along the walls (yellow-green).

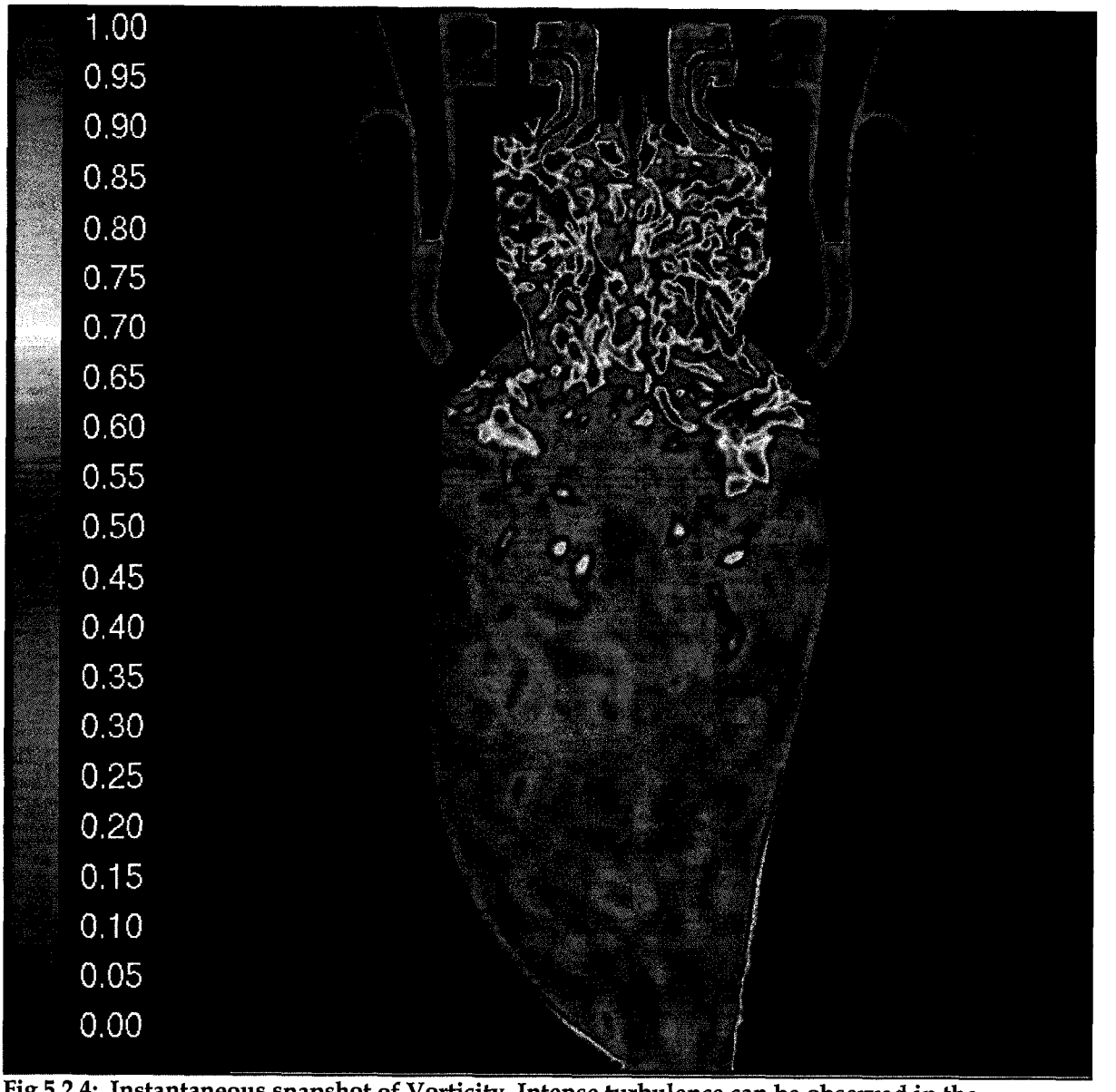

Fig 5.2.4: Instantaneous snapshot of Vorticity. Intense turbulence can be observed in the primary and the secondary zone. QinetiQ's report [80] on the reacting flow confirms large degree of structure extending from primary into the secondary interface between primary and secondary zones, fading out as the chamber widens.

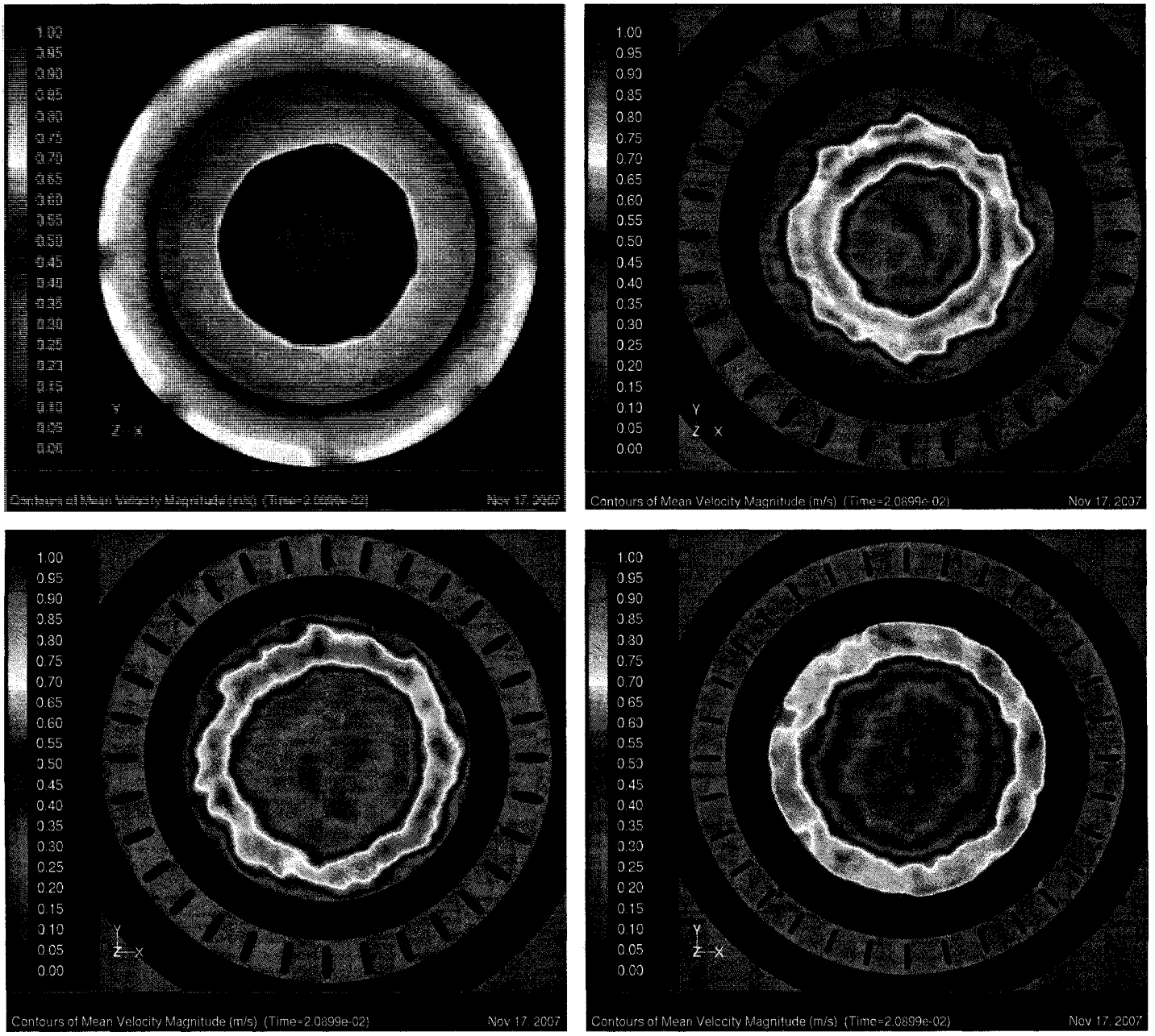

Fig 5.2.5: Evolution of initially separated counter swirling flows through the combustion chamber. Slices were taken at z= 42.7, 61.4, 73.5, 111.1 mm. Picture sequence is from left to right and top to bottom. A slice through the concentric secondary premixer is also shown. The 'smoke-ring' is observed to spread outward before being constrained by the wall boundary. However, the taper at the end of the primary, increases the velocity. Compare with the same pictures under combustion conditions in Chapter 6 – Fig 6.2.20 where a polyhedral mesh is used.

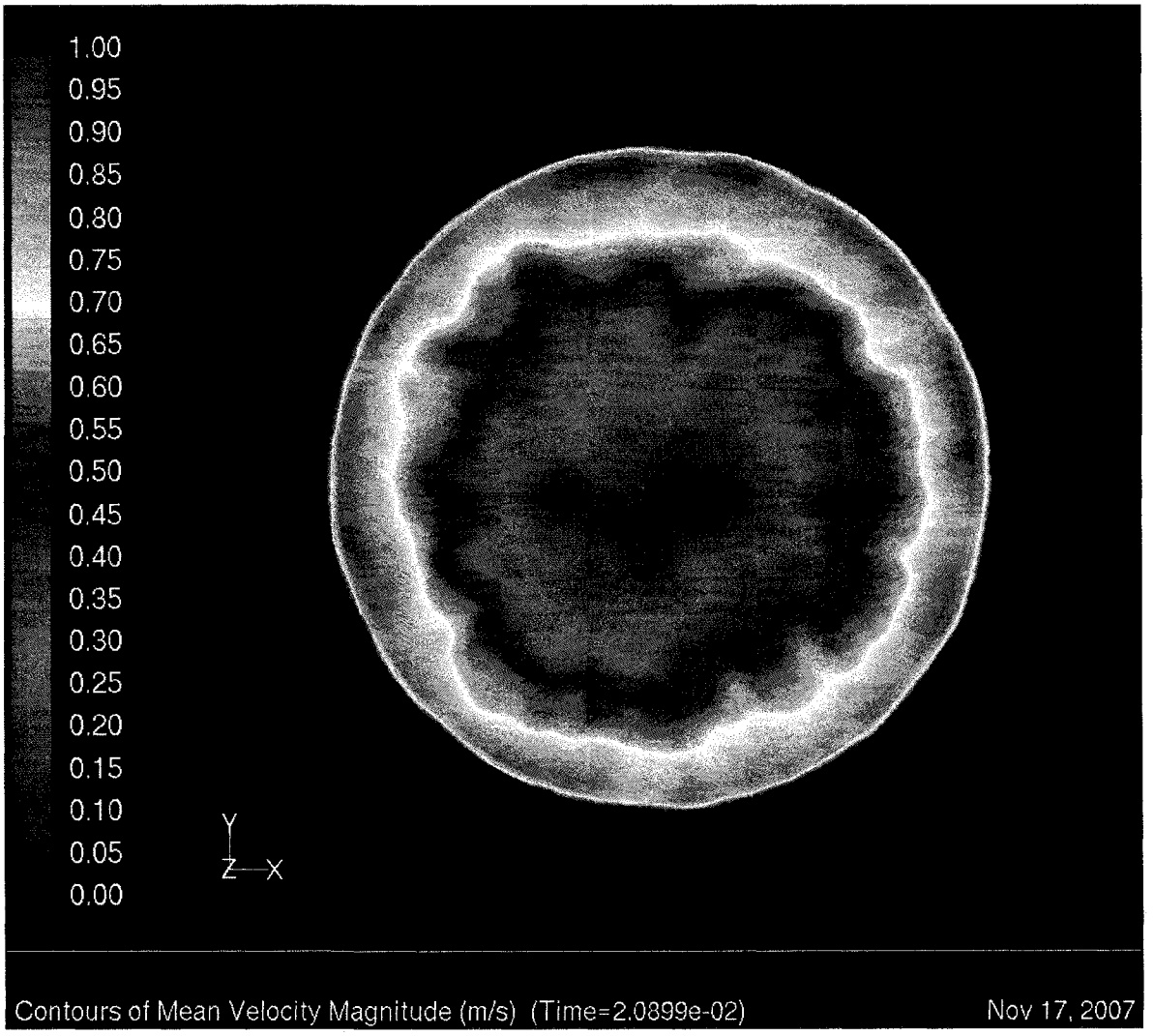

Fig 5.2.6: Primary Outlet. The smoke ring is observed to thicken and the reversed flow can be seen clearly in the center. In a reacting context, this reversed flow may disappear and the stagnation point moves upstream towards the torch.

5.3 Mixing in the Secondary Zone

The principle of staged combustion stands behind the need for a secondary zone. The secondary zone exists to reduce the high NOx produced in the primary zone as well as provide a secondary chamber to burn fuel at lesser temperatures in order to induce CO burnout. With multi-stage combustion, CO emissions were virtually eliminated and NOx emissions as low as 17 ppm were obtained. Premixed fuel and air enter from the secondary premixer through 16 jets angled so that the mixture is injected directly into a stream of hot products from the primary zone. The slice in Fig 3.2.2 shows two such jets.

Key Features:

1. Due to the high crossflow velocity from the primary outlet, these jets do not meet immediately at the center but someway into the secondary chamber. (Fig 5.3.1, 5.3.2)
2. The velocities are higher in the case of the shortened combustor due to reduction of the diffuser part. A central vortex core forms perhaps due to the high swirl imparted to the core flow by the secondary jets.

3. Recirculation Zones form along the sides of chamber due to the contour and possibly entrains some cooling air.
4. Adverse operating conditions could cause cooling air to be entrained resulting in over-hot walls, potentially. While this problem is more of a modeling aggravation than real-life event, it poses serious problems when the recirculation zones become stronger due to larger mass flux of air. Ideally, the normal component of the air velocity should be set to zero in the mass source term described below.
5. Modeling of cooling air becomes critical due to LES results showing that effusion air is directly entrained into the main flow if injected perpendicular. For the reacting case, the cooling air will be introduced as a mass source term in the cells adjacent to the wall.
6. RANS models cannot cope with the extreme degree of non-uniformity of flow-field found in this region. This has implications for RANS combustion modeling where there are pockets of unburned fuel and air mixtures indicated by the QinetiQ report. Experience indicates that RANS methods cannot predict these unburned pockets.
7. Averaged LES pictures are shown below. However, a longer period of averaging may be necessary to resolve. While the temperature profiles are well averaged (little differences), velocity profiles may require more time.

Three flow-through times were used currently, but much longer periods have been suggested by Fluent. Computational restrictions may indicate the need for a smaller mesh. It may not be too much of a problem as several reports indicate excellent resolution of turbulent kinetic energy with quite coarse grids.

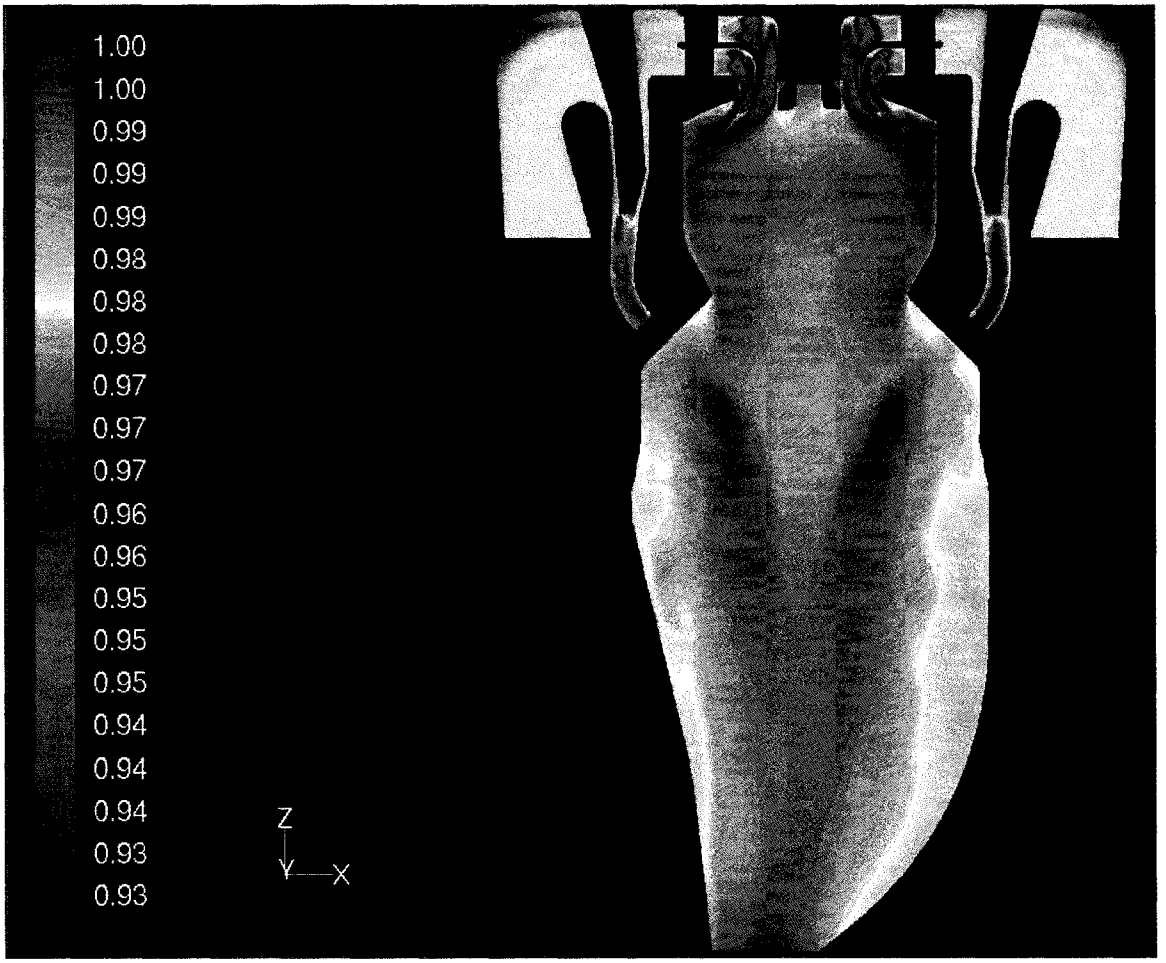

Fig 5.3.1: LES averaged temperature contours (cold fuel hot air).

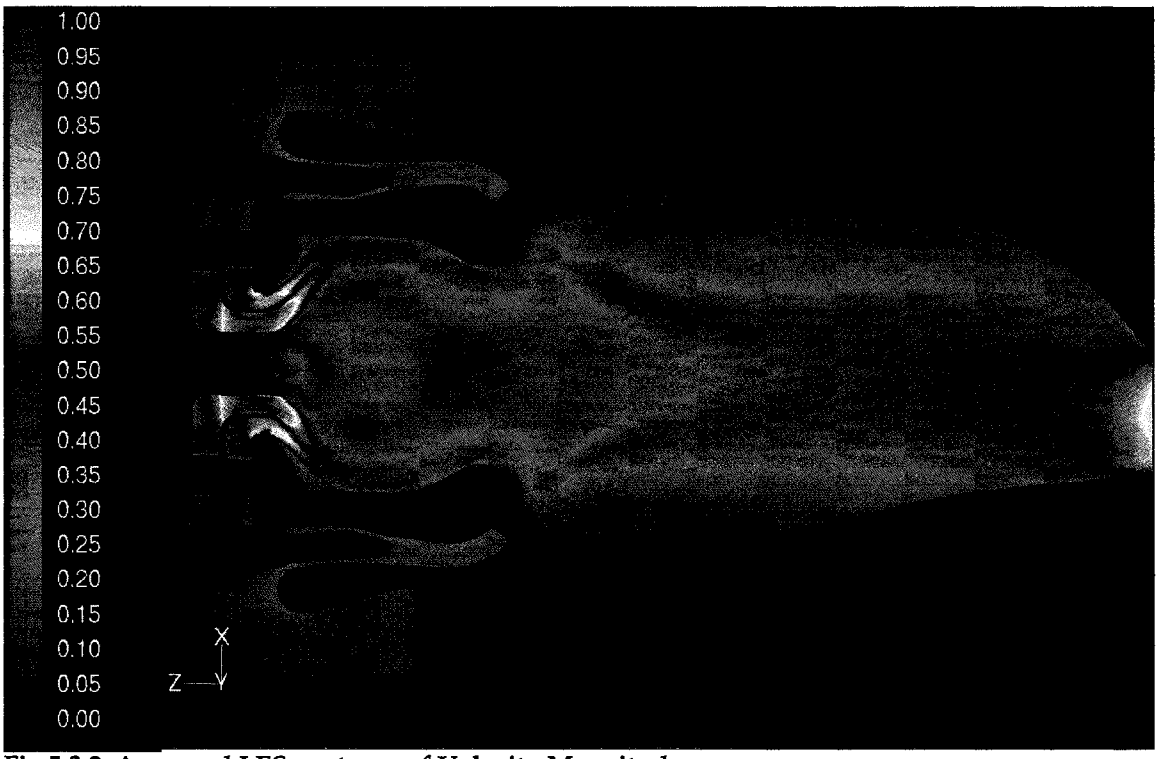

Fig 5.3.2: Averaged LES contours of Velocity Magnitude.

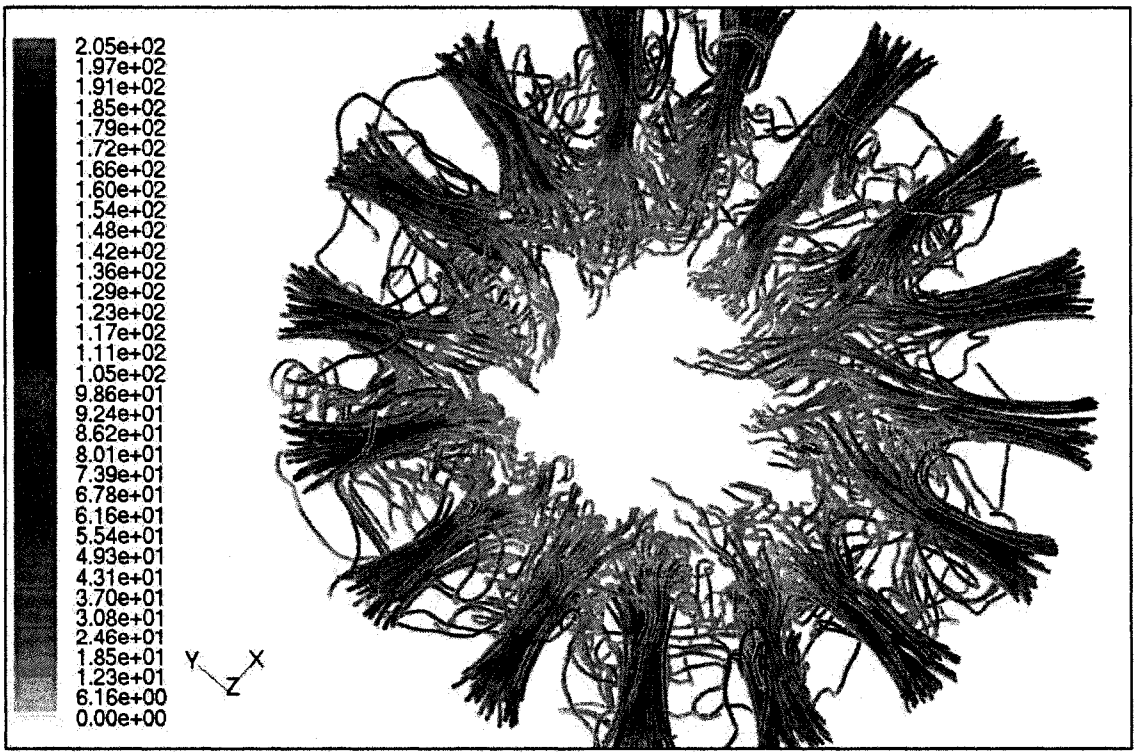

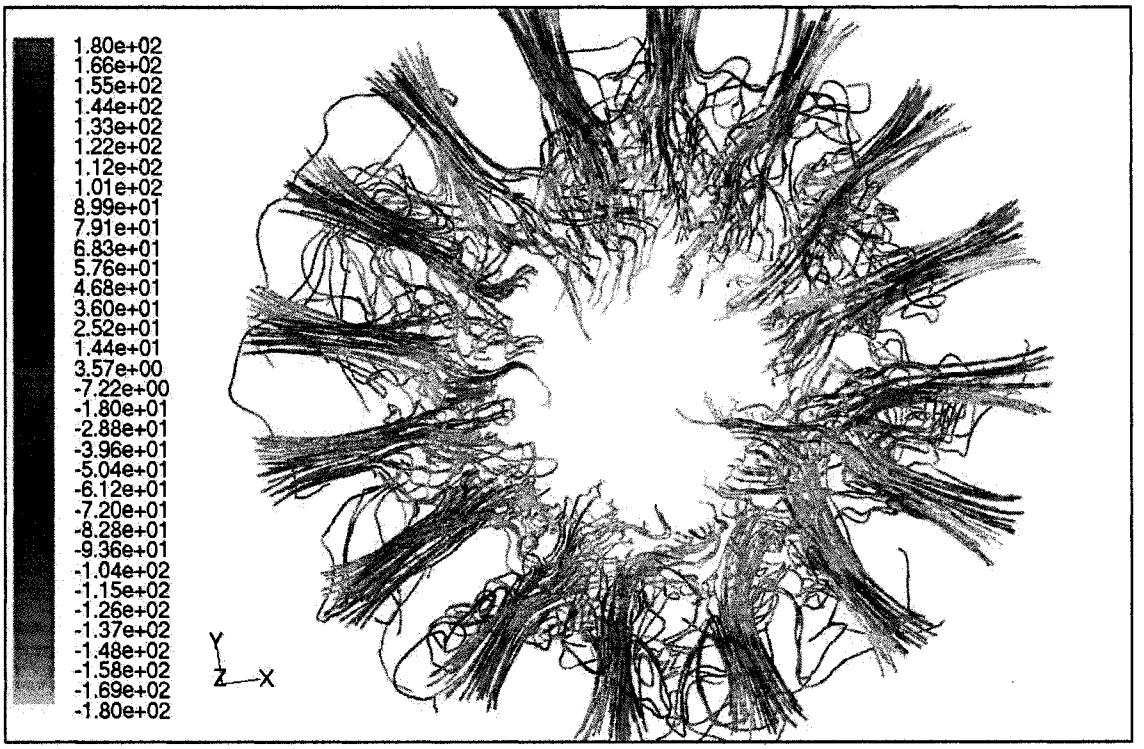

Fig 5.3.3: *(Top)*: Streamlines indicating premix jet penetration into secondary, colored by velocity magnitude. *(Bottom):* Colored by relative velocity angle, to show entrainment of jets into small recirculation zones between each jet due to sudden expansion of secondary premix flow into the main chamber. Averaged LES.

5.4 Mixing in the Secondary Premixer

It was not possible to verify mean values of velocity with the LIF experimental data, as the boundary conditions were not provided. Very little experimental data is available. However the vane configuration contribution to mixing has been studied taking the secondary 'fuel-arm' vanes separately. The present analysis compares qualitatively with this data and indicates good agreement. This data cannot be depicted for confidentiality reasons.

Key findings:

1. The averaged LES data indicates that the final temperature of mixing is fairly uniform, but could be sensitive to wall boundary conditions, due to the large number of wall boundaries in confined channel.
2. A very large number of grid points are necessary to resolve flow features in the secondary premix duct. Due to the near wall flows, there is lesser confidence in LES in this zone, due to sub-grid issues. However, a DES simulation with the k-w SST model may provide better results.
3. Flow turns through an angle and exits the secondary premix duct as shown in Fig 5.3.3, which indicates that flow from the duct openings, is

not uniform. A later report will detail the distribution of the mixture fraction given this non-uniformity.

4. It is therefore shown that flat boundary profiles assumed for secondary duct windows will not provide the best initial conditions for a simplified simulation in which the duct is removed.
5. The complexity of the duct indicates numerous secondary flows due to incomplete blockage of the duct by the fuel vanes.
6. As in the experimental findings, the simulation does not indicate fuel injection flows to impinge on the opposite walls due to its high velocity in the cross-flow. Another simulation with a different configuration of vanes may result in this. However the focus was to obtain a reasonably good profile at the exit of the secondary windows.
7. Non-uniformities can be observed at the separating wedges. However this could be due to the assumed wall temperature boundary conditions. The heat transfer is significant. It is necessary to include correct boundary conditions in the secondary-premix to avoid excessive loss of preheat for example. The wedge walls boundary condition in this case was kept at 702.1K to err on the side of caution.

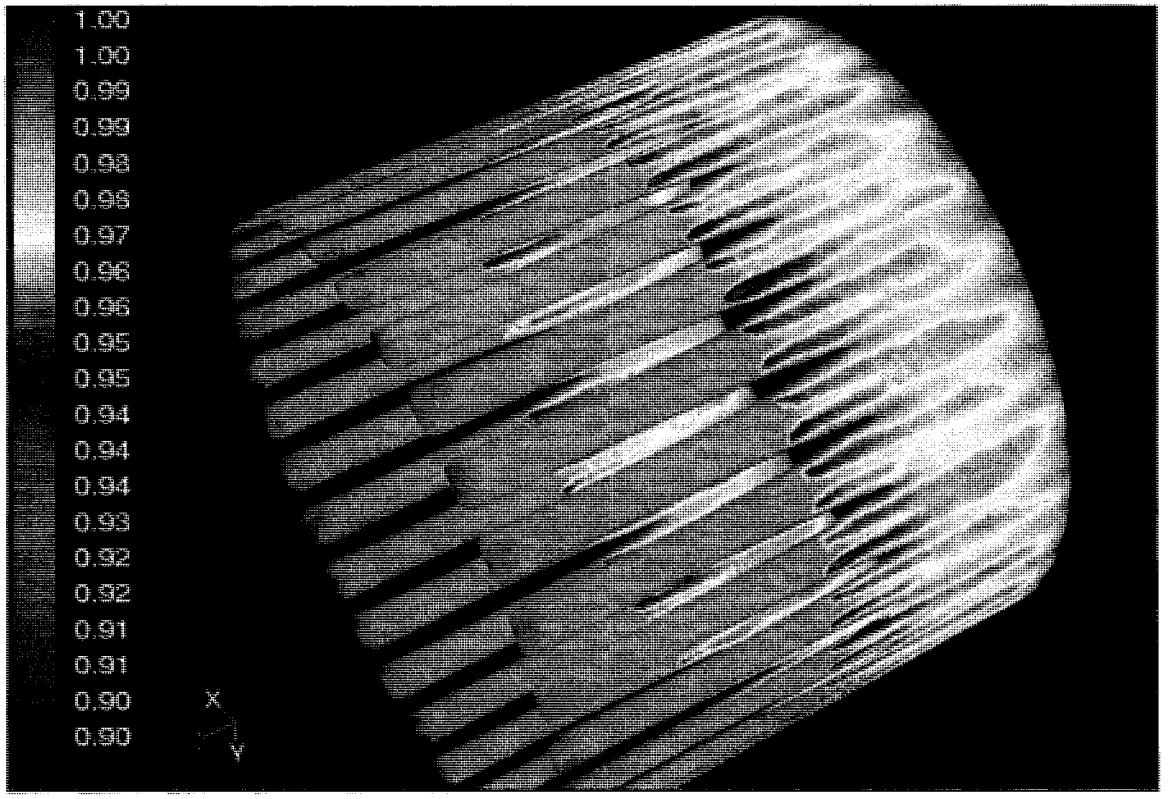

Fig 5.4.1: Temperature contours (cold fuel at 350K with hot air at 750K). Flow is from left to right on a slice through the secondary premix channel at an iso-radius.

Comparisons with the RANS results are done in Chapter 7. The main emphasis in this thesis was on the reacting flow and the foregoing is simply a matter of interest to compare with the effects of combustion on the flow field. Due to the lack of experimental data, the design engineers verified these results with internal studies, but this data cannot be presented here for confidentiality reasons.

6. REACTING FLOW: PILOT STUDY OF A COAXIAL COMBUSTOR.

It is generally accepted practice to model combustion problems on well-defined geometries and boundary conditions as a precursor to complicated geometry simulations as well as to evaluate complex chemical mechanisms. The literature contains many simulations and experiments conducted on coaxial jet type combustors for this reason. The best-known examples are Pierce and Moin's [83] LES simulation on Spadaccini et. al.'s burner [82], the simulations of the experiments of Bilger (Sydney Burner) [86, 85, 97], Simulations of the Sandia Flame series (C, D, E, F in increasing order of extinction probability [88, 95]). Other examples are Vanka (1985) [90], Kim and Chung (1989) [91] both done on the Lockwood burner [89], the latter using the Finite-Element method, Lin (1987), Lockwood et. al. (1974) [89].

A simple pilot study (both RANS and LES) on diffusion flames in a coaxial-jet combustor used by Lockwood et. al. [89] was undertaken to validate the various sub-models that are offered by Fluent. The geometry is a simple dump combustor but nevertheless consists of the basic flow regimes observed in a complex geometry combustor. First, the original experimental conditions were applied and the models were validated with published experimental data. Then the conditions were switched to the gas turbine typical conditions, with the same

air-fuel ratio and the inlet velocity ratios adjusted so that a primary recirculation zone is formed followed by a plug-flow zone. This ensured that most of the mixing happens in the primary zone, a short distance from the injector. The overall residence time is approximately the same for both combustors. This method is not intended as a 'simplifying' assumption on which predictions on the real combustor can be based, but only as an initial guide to evaluate the models and gauge emissions predictions rather than actual velocity profiles. At the very least, it is consistent with the way in which 1-D Chemical Reactor Networks are designed to 'mimic' practical combustors.

The geometry consists of an inlet by which fuel is fed into the combustor. A coaxial flow of air enters the combustor through an annulus. The central pipe measured 0.0195m in diameter and the annulus consisted of 0.0445 inner diameter and 0.0781m outer diameter. The overall diameter of the combustor was 0.210m, with a length of 1.9m. The fuel used, was town gas of the following composition:

CH4 27%, CO2 8%, N2 4%, H2 55%, CO 4%, C2H6 2% by Volume. The standard k-epsilon model was used for turbulence and the non-premixed combustion model was used for reacting flow predictions.

Details of the mesh (Fig 6.1) and boundary conditions (Table 6.1) follow:

Zone	Material	Type	Temperature	Pdf	Turbulence, Hydraulic Diameter
Central Injector	Fuel	21.57 m/s Velocity	300K	f=1 fvar=0	10%, Dh
Annulus	Air	13.47 m/s Velocity	300K	f=0 fvar=0	10%, Dh
Outlet	-	Pressure Outlet	-	-	10%, Dh
Walls	-	Adiabatic	-	-	-

Table 6.1: Boundary conditions for the pilot study.

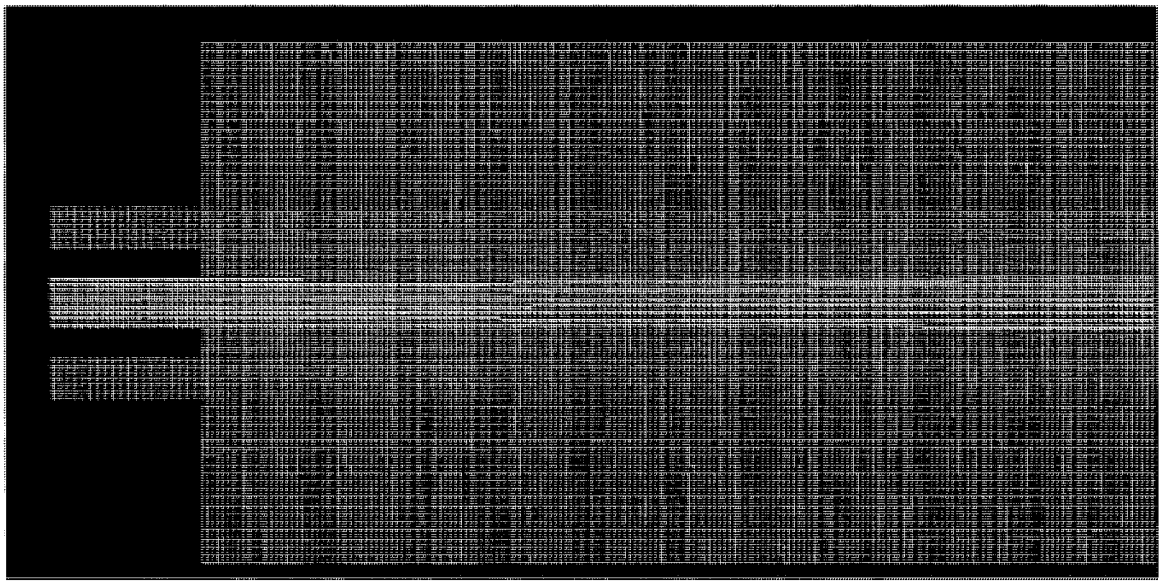

Fig 6.1: Mesh used for axisymmetric analysis of the pilot study combustor.

A 2D axisymmetric mesh of 14400 cells was used for a RANS study. After experimenting with several grids, this density was found to be enough for main temperature predictions. A basic laptop computer was more than adequate to obtain results within a few hours. Some questions regarding mixing were later resolved by running an LES simulation with a mesh with approximately 2.9 million cells.

Results and Discussion for the pilot study.

The pilot study was undertaken to validate the methodology to be followed for the main calculations involving the full combustor. Since several equally valid avenues of approach lie towards combustion modeling as well as turbulence modeling, it was decided to evaluate to a first order what the effects of each may be. As will be noted in the succeeding discussion, these effects can be very significant. Emissions predictions are especially sensitive to turbulence and combustion modeling. The objective of this study is to gauge that sensitivity for a very simple combustor, which will highlight the effects of a particular choice of model. The separate effects of turbulence model, combustion model, the discretization scheme as well as steady analysis versus unsteady analysis were studied keeping the complexity of the geometry low.

6.1 RANS predictions.

Running the simulation 'out-of-the-box' caused over and under predictions of the mixture fraction, though the main temperature field was predicted with reasonable accuracy. This is consistent with earlier simulations conducted on this model by Kim and Chung [91] and Vanka [90]. Velocity profiles were not checked due to lack of experimental data, but the literature shows overwhelmingly that most velocity predictions are very well predicted when the turbulence model is tuned properly. The emphasis in this analysis lies on the mixture fraction predictions. Experimental data is available for mixture fraction profiles at centreline and at various radial stations. After the model was validated at its experimental conditions, the specific predictions of CO and NOx were studied with the post-processors (unsteady flamelet and NO transport). Very significant changes were observed corresponding to the level of simplification built into each combustion model. The trend observed was that, despite model complexity and computational expense, the increased physics taken into account justified the cost. In particular, NOx and CO emissions were greatly influenced by including partial premixing and non-equilibrium. As expected the steady flamelet method did not provide much advantage in predicting NOx emissions, but greatly impacted CO emissions. Similar trends, though not to such great discrepancies, were observed amongst the turbulence

models. The k-w model indicated a flame that cooled down more rapidly than the others.

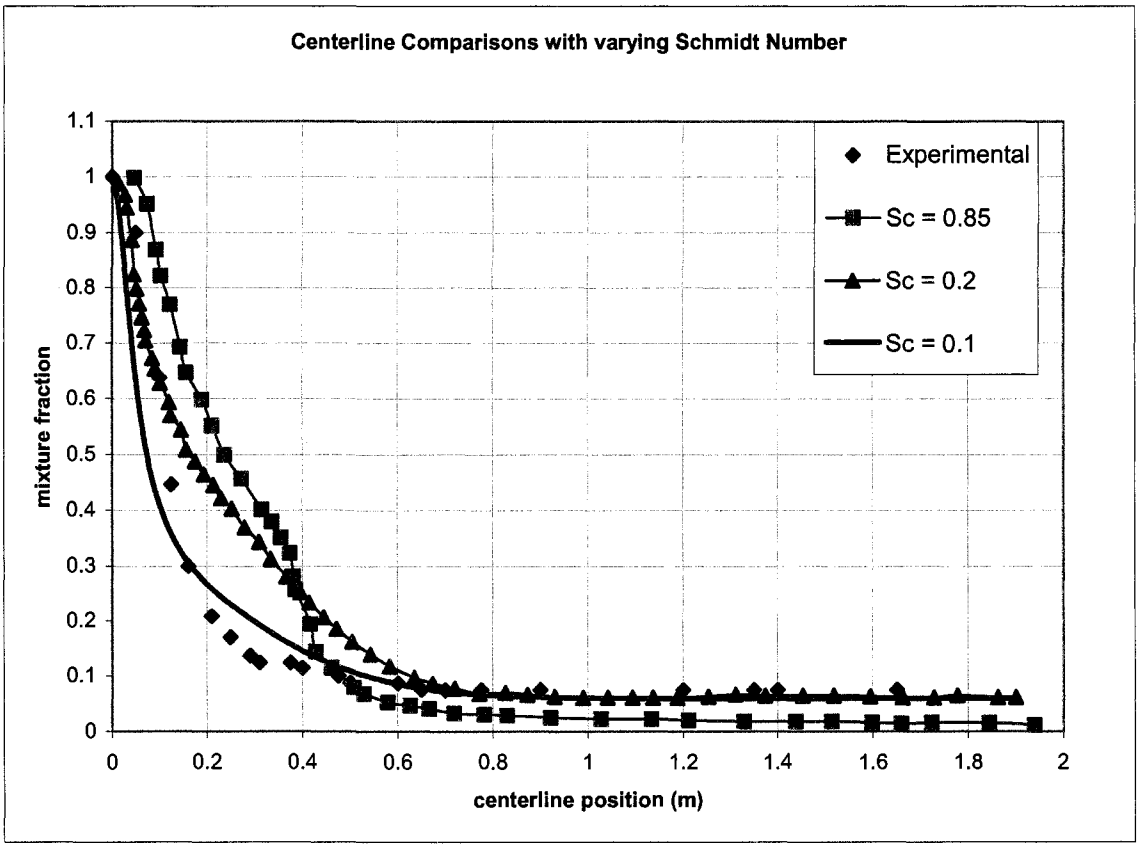

Fig 6.1.2: Centerline mixture fraction prediction.

The centreline predictions (Fig 6.1.2) show that the model is able to predict reasonably well the decay of the mixture fraction providing the Schmidt number undergoes some adjustment. Some over and under prediction of the decay can be seen even with a Schmidt number of 0.1, in the rich zones and this is shown in the figure below to be independent of the turbulence model. Decreasing the Schmidt number to match the mixing is consistent with the findings in the literature, Jiang et. al. [34], for example is a comprehensive study undertaken at

the RANS level. These results lead to the physical reasoning that with the default Schmidt number, mixing at small scales is under-predicted when using RANS turbulence models. To resolve this question, an LES of the same geometry was carried out, with a dense mesh, since it is capable of accounting explicitly for mixing at much smaller scales than RANS. These results will be shown following the results obtained below (Fig 6.3) for varying the turbulence model.

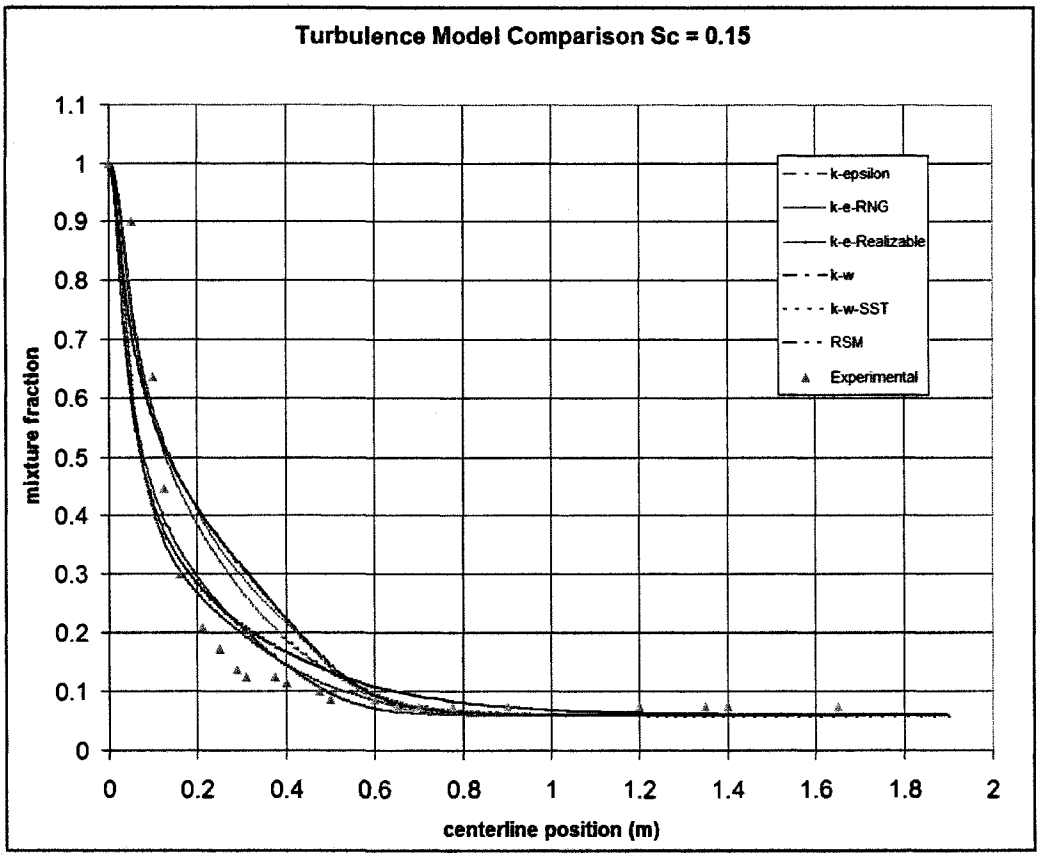

Fig 6.1.3: Centerline Predictions with Sc=0.1 and varying turbulence model.

Other turbulence models such as the k-e, k-w, k-w SST, the ke-realizable, the ke-RNG models, RSM were used without any tuning of constants to predict the

variation of the mixture fraction. All models consistently under predicted the rate of mixture fraction fall off at the default constants. It is not surprising, given the fact that a recirculation zone stabilizes the burning and eddy viscosity models are known to be at best approximate, in predicting turbulent mixing in the shear layers between the Recirculation Zone (RZ) and the "plug flow". The RZ length was well predicted and agrees with [91] finite element predictions of its length being 1.4D. Efforts were made to investigate impact on turbulence-chemistry predictions by the eddy viscosity models and to isolate this effect, the discretization scheme, grid density and unsteadiness were studied. The discretization scheme was varied from 1st order upwind to 3rd order MUSCL scheme for spatial accuracy and the number of cells was varied from 14000 to 50000 on a 2D slice. The predictions of turbulence varied slightly as grid independence was achieved in the RANS context at very low cell counts due to the relatively simple physics modeled (no swirl, axisymmetric, moderate Reynolds number, large domain for settled flow, etc). Streamlines in a 3-D model reported below (Fig 6.1.3), show that the flow consists of rather large corner recirculation zones whose shear layers with the main flow zone, act as flame stabilizers.

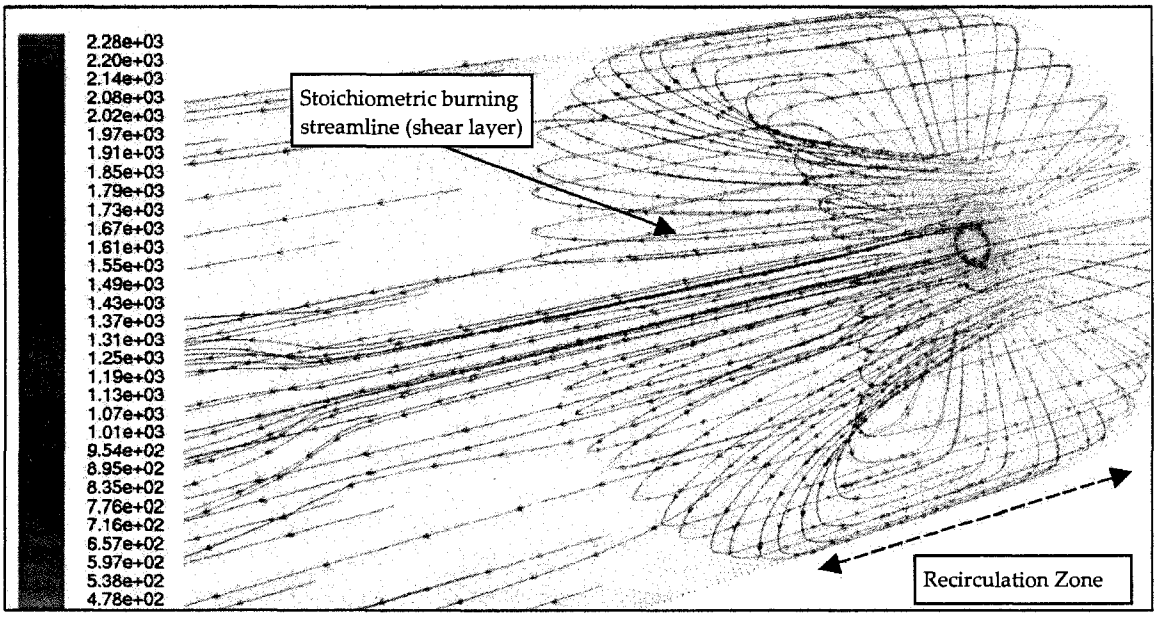

Fig 6.1.4: Flow enters from left and streamlines colored by temperature show the corner recirculation zone that forms near the entrance.

The RSM and k-w-SST predict the point of stoichiometric mixing on the centreline accurately enough. The Experimental value was given to be around 700 mm. The predictions of various turbulence models were:

RSM - 663 mm

k-w-SST - 656 mm

k-e-RNG - 625 mm

k-e-REAL - 617 mm

k-w - 606 mm

k-e - 546 mm

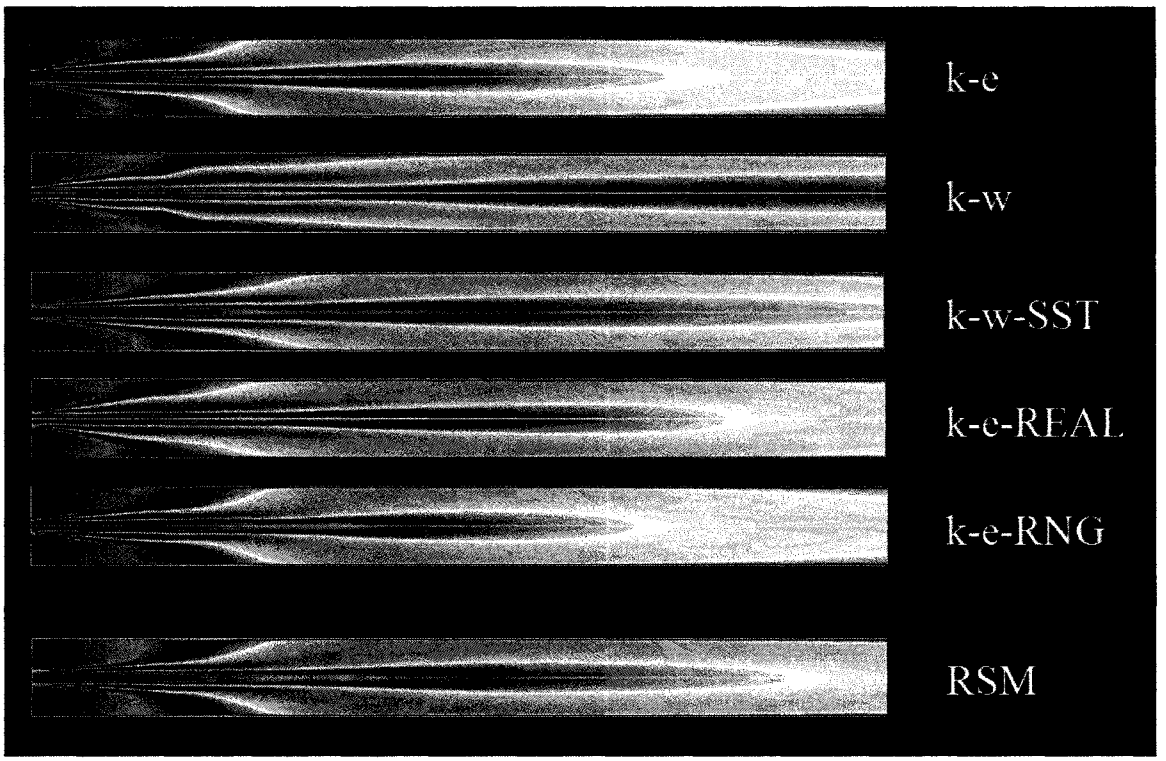

Fig 6.1.5: Temperature fields obtained by varying turbulence model. Flow is from left to right.

Fig 6.1.5 shows significant changes in the predicted temperature fields when the turbulence model is varied, while keeping all other factors constant. Centerline decay differences are immediately noticeable. All the models predict an attached flame to the lip of the injector exit. The effect of varying sizes of recirculation zones can also be seen near the injector exit. The standard k-omega model indicates poor mixing in the separated regions (which is consistent, since it is a model designed for near wall, attached flows). Also evident is the fact that the k-epsilon models show a more uniform post-combustion zone, while the uniformity is delayed in the case of the k-w models.

Radial profiles at different stations throughout the model offer agreement with experimental data ranging from fair to very good. 3rd order MUSCL predictions on the coarse grid gave reasonable agreements with the radial profiles away from the fuel-rich zones, with increasing success towards the exit. This implies that a finer mesh is required for better species predictions. The following pictures indicate that good agreement is obtained with the higher order discretization scheme. Fig 6.6 *(top)* shows the agreement in a rich-zone and here it is more than possible that the poor prediction of the of the 2nd order scheme is not merely due to the discretization scheme but also the inability of the combustion model to model rich mixtures. Further investigation is warranted in this case. This reasoning is justified by Fig 6.1.6 *(bottom)*, which shows the agreement in a lean zone where both schemes show good agreement. Other profiles taken in the rich and lean zones show similar trends. It must be mentioned that merely obtaining correct mixture fraction results is not enough since the species mass fraction predictions are only as good as the mixture fraction prediction in a conserved scalar approach used in the pdf methods. Transporting the species can lead to different results. This fact however has not been researched due to the time constraints.

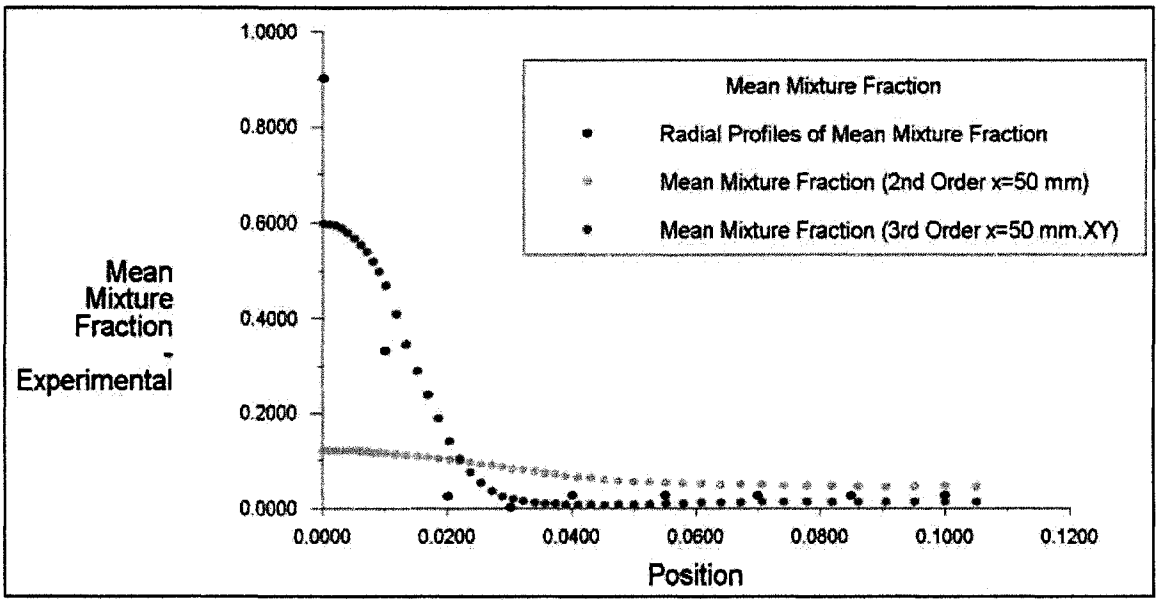

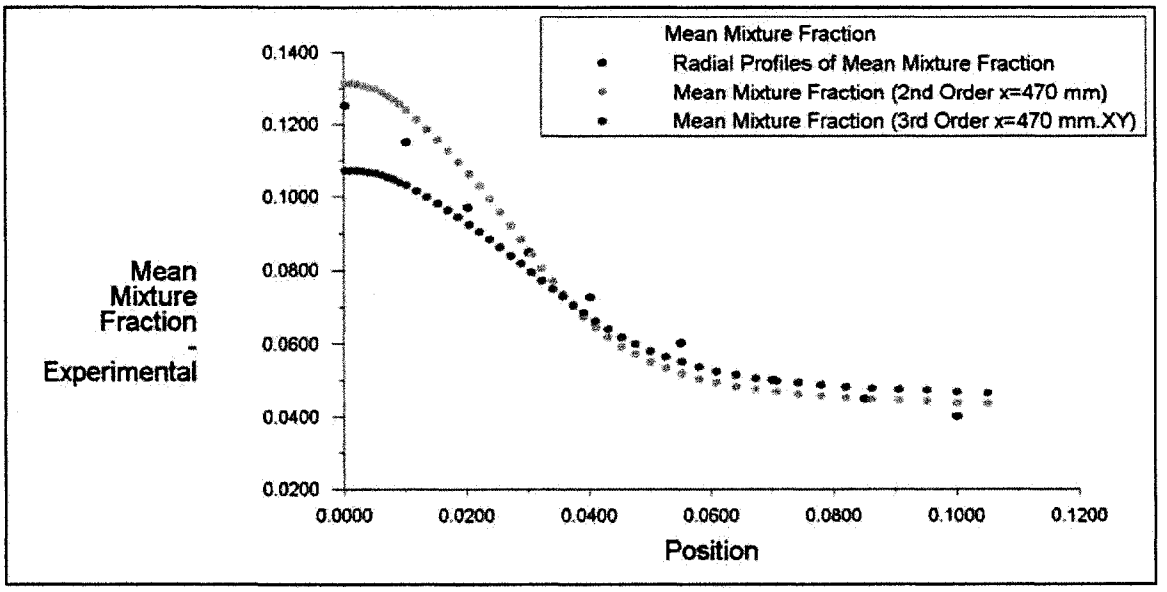

Fig 6.1.6: Effect of discretization scheme *(top)* x=50mm *(bottom)* x=470mm. (black dots = expt.)

6.2 Large Eddy Simulation

An LES was carried out on the geometry without the dynamic procedure on the Schmidt number to provide some insight into the Schmidt number question.

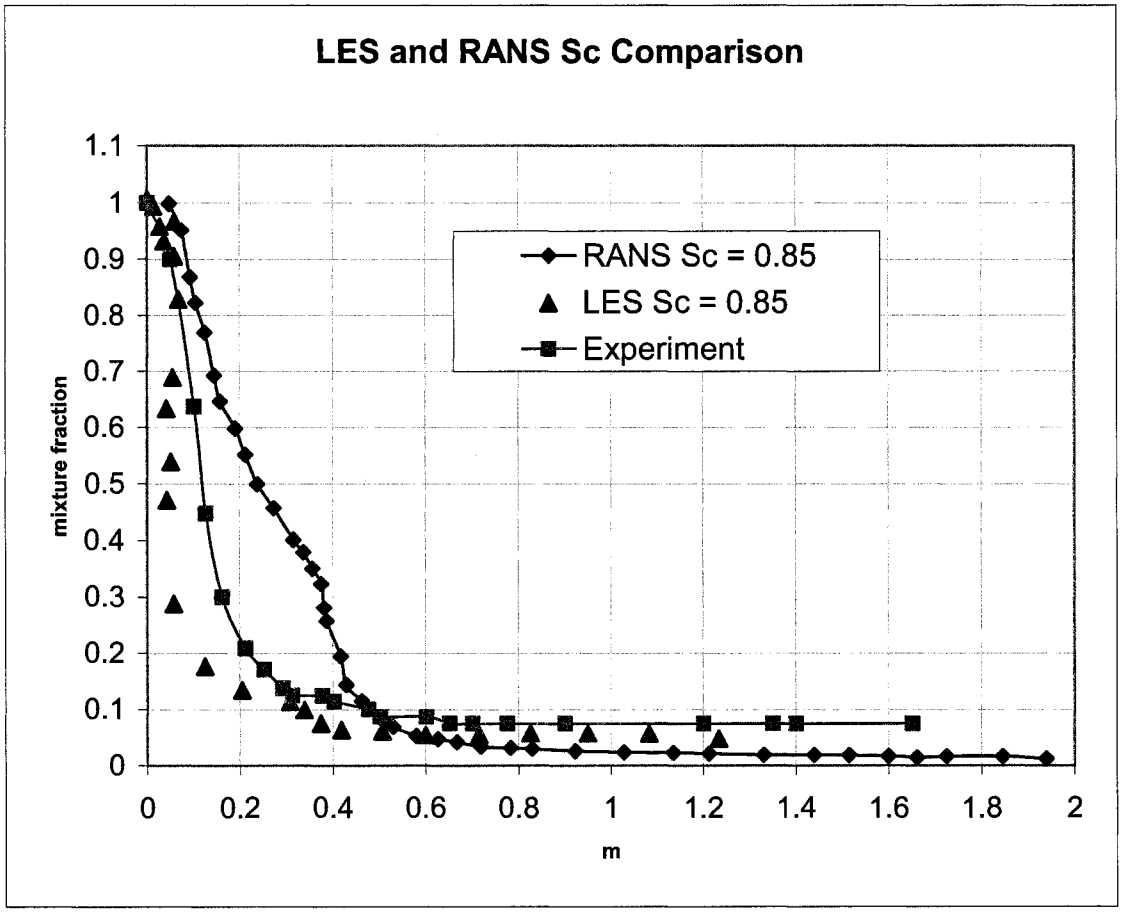

Fig 6.2.1: Centerline Mixture Fraction Predictions: Effect of Sc number.

This figure clearly shows that tuning the Sc number was not necessary in LES which lends credence to the hypothesis that explicit computation of mixing at smaller scales, atleast, alleviates the uncertainty in using the constant Sc number

assumption. However this may be regime dependent since accounting for mixing in a swirling flow is a much more complex issue. Indeed, in the complex geometry combustor, the subgrid Sc number obtained through the dynamic procedure showed it to be reduced to 0.25, which interestingly, is quite close to the RANS result. This indicates that isotropic eddy viscosity models whether used as RANS for the main flow predictions or used as a simple algebraic model for sub-grid modeling, result in mixing that is under-predicted – atleast in the models that were used in this thesis. More work needs to be done in generalizing this hypothesis to other regimes, even though the flows simulated in this thesis ranged from simple to very complicated. It also raises the question of LES filter size/grid density since it is mixing decreases with the increase in isotropy of the flow-field and hence to take it to its infinite limit should cease at the wall. This implies that the effect of the Schmidt number could diminish with finer and finer grids as more and more mixing is explicitly accounted for by the LES. Again, due to the time constraints, LES simulations parameterized by grid density were not done. The following set of time-accurate pictures (Fig 6.2.2 a-f) shows the development of the flamefront at different time-steps. A time-step of 1e-6 seconds was used with the bounded central differencing scheme applied to the momentum equation

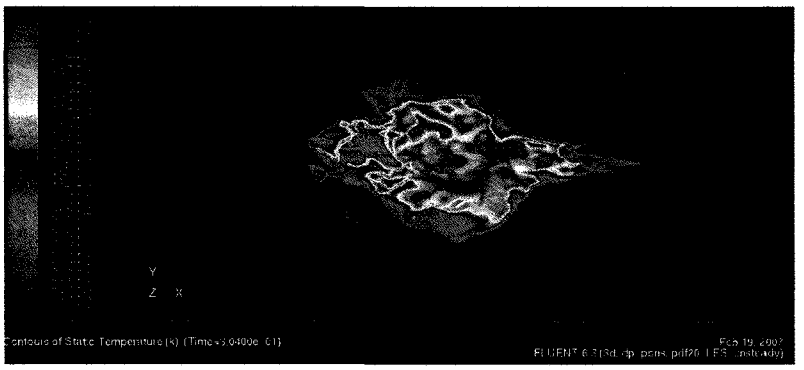

(a) t = 0.304 seconds

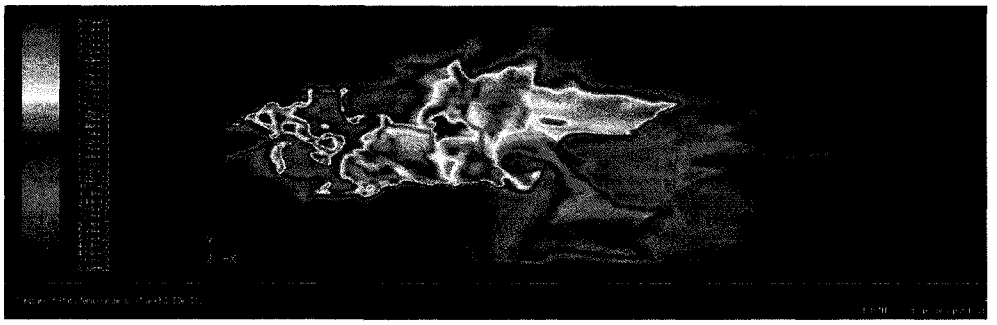

(b) t = 0.321 seconds

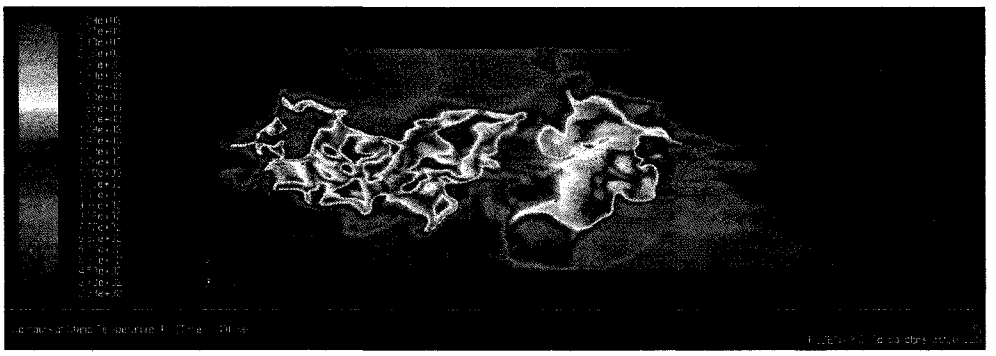

(c) t = 0.349 seconds

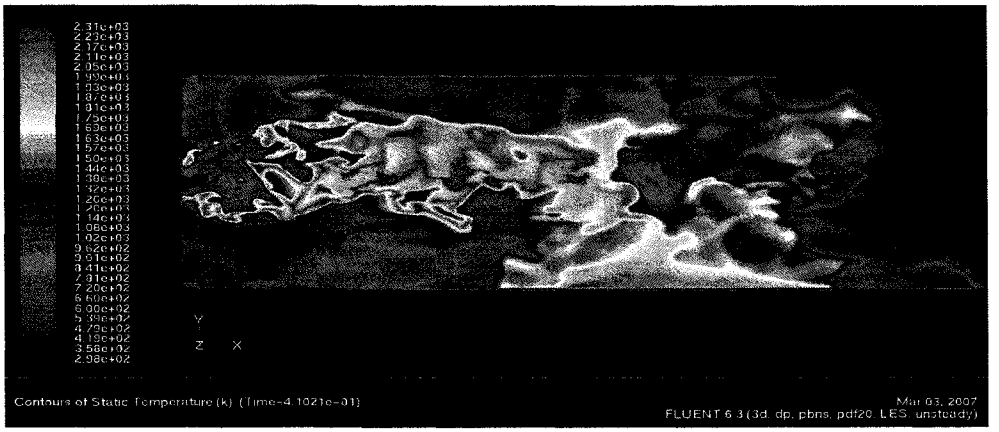

(d) t = 0.410 seconds

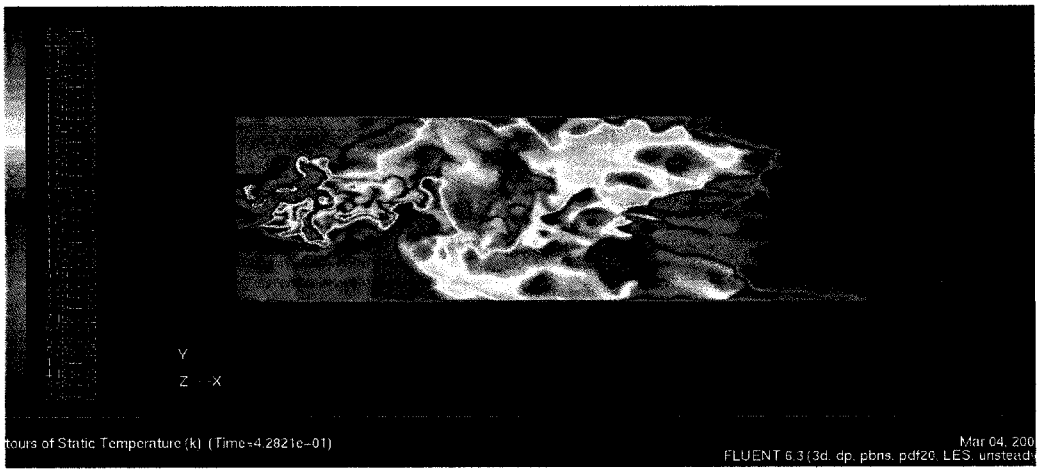

(e) t = 0.428 seconds (zoomed out)

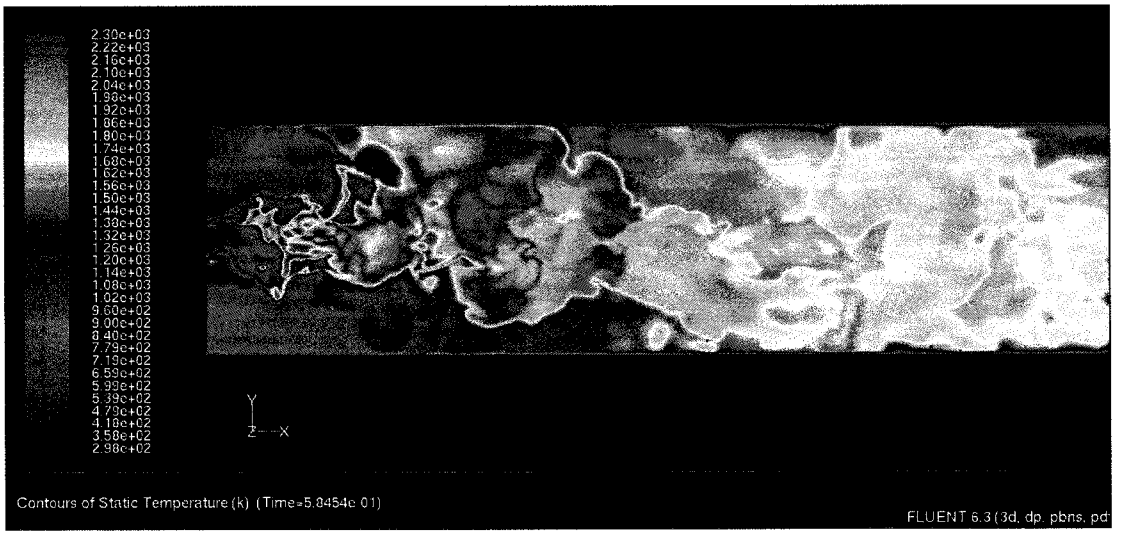

(f) t = 0.584 seconds.

Fig 6.2.2 (a-f): Instantaneous contours of the flamefront, colored by temperature.

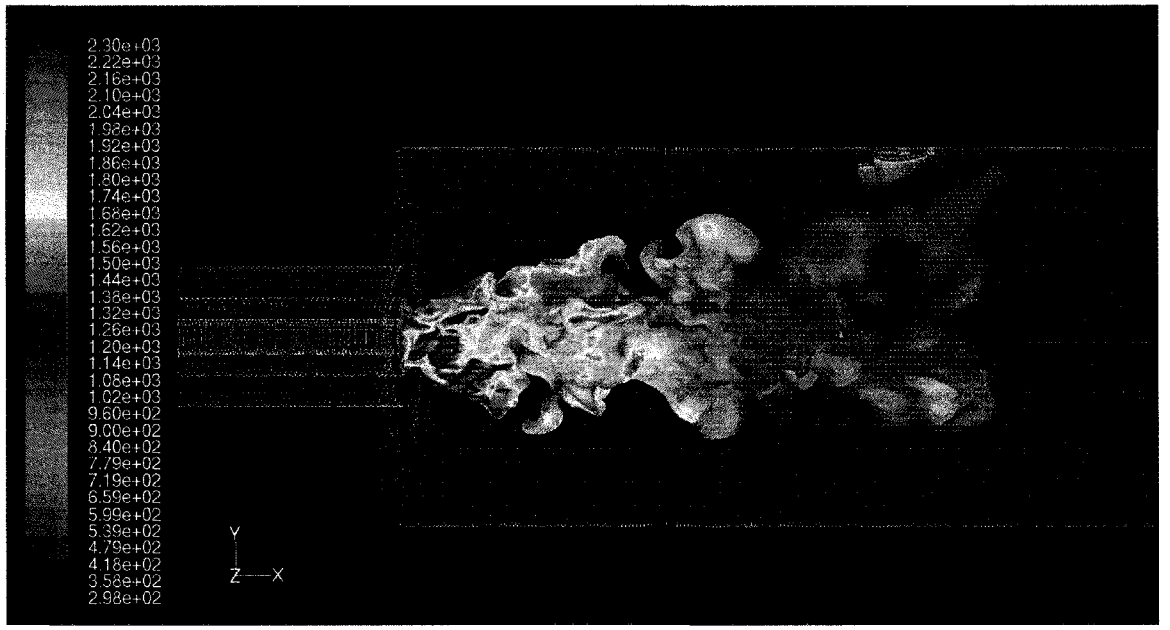

Fig 6.2.3: Iso-surface of stoichiometric mixture fraction coloured by Temperature.

The flame was observed to attach and detach from the lip of the burner in a very unsteady fashion. This phenomenon is consistent with the findings of Pierce [51]. The Rich Flammability Limit option in the non-premixed combustion model accounts for some degree of partial premixing, in the sense that it considers any mixtures less than 0.1 to be unburnt, but mixed. This is clearly seen in Fig 6.2.3, where the stoichiometric mixture fraction contours do not all burn at the flame temperature. The richest regions are near the central injector and stoichiometric mixing happens some way downstream, which is consistent with the experimental results. However, the RANS turbulence models all predict an attached flame as seen in Fig 6.1.5 when used with the non-premixed model. This was later seen to be a feature of the combustion model when the jet velocity was

increased so that an attached flame could no longer exist. The non-premixed combustion model predicted an attached flame, but when the effect of premixing was explicitly included with a transported progress variable, a lifted flame was observed. This will be discussed more in the main calculations done on the industrial combustor in Chapter 7.

6.3 Combustion Model Evaluation

All the pdf combustion models (except transport-pdf) in Fluent were investigated in the pilot study in the RANS context. The formulation of these models as described in Chapter 3, provided much insight into effect of various simplifying assumptions that were necessarily to be made due to the complexity of the phenomena. For this purpose, the boundary conditions were changed to typical gas turbine conditions in order to gauge the effect of change of ambient conditions. The velocity ratio of the central fuel to the annular air jets was also changed in order to move the main mixing zone from the corners to an on-axis recirculation zone, followed by a plug flow zone, which is roughly the case in the gas turbine combustor where a primary zone is almost entirely a recirculation zone, followed by a second stage combustion zone, where the fuel and air mixture is dumped into the exhaust of the primary zone products. The velocity

of the jets was also increased so that there was no possibility of an attached flame. The results of these adjustments are shown overleaf. The velocity ratio was increased to 39 and the ambient temperature and pressure were 702K and 5 bar.

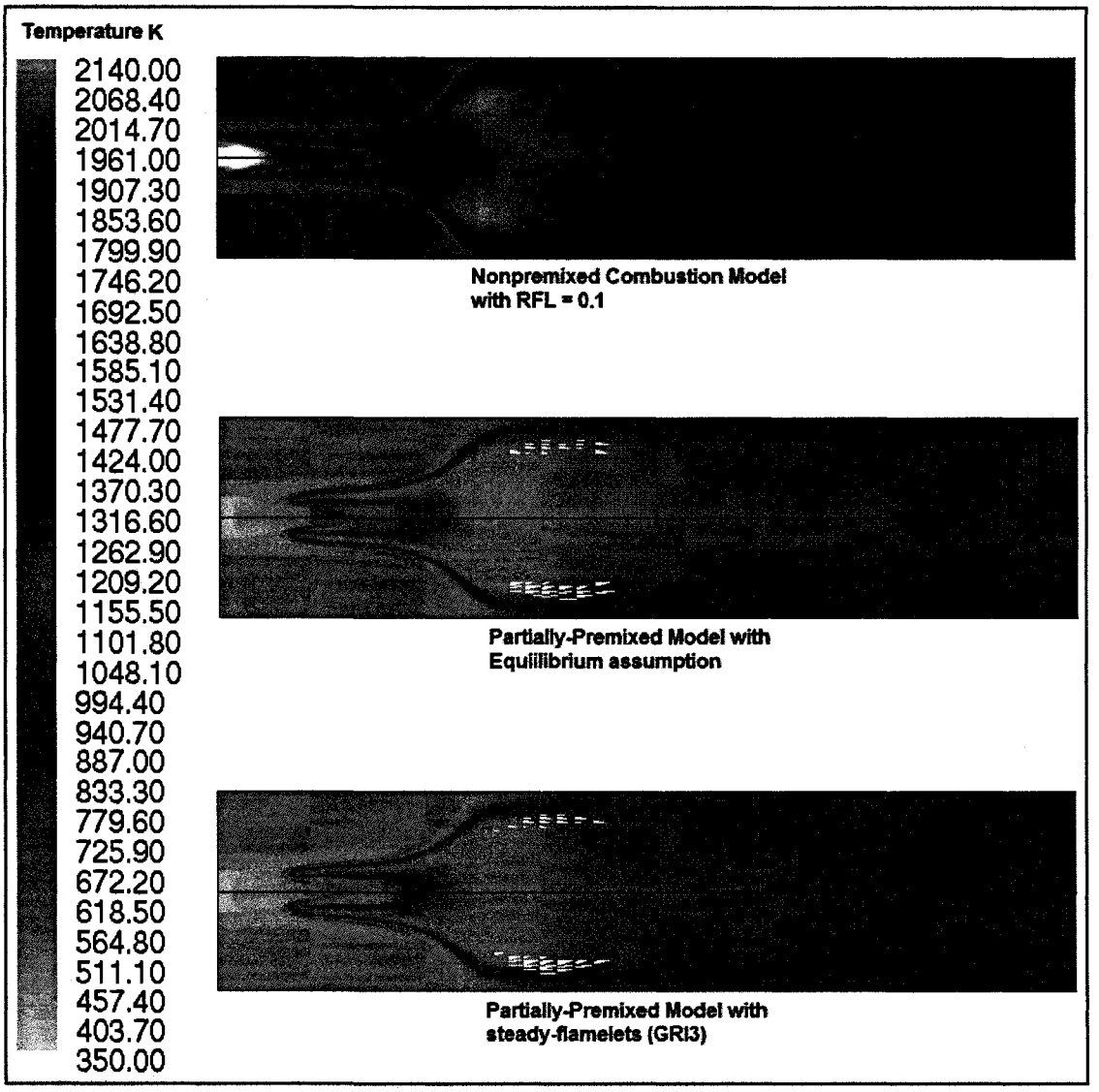

Fig 6.3.1: Temperature Comparisons

It is clear from Fig 6.3.2, that the non-premixed model is not capable of predicting a lifted flame, where as the partially premixed model does so. The partial premixing can be seen immediately downstream of the fuel injector. There isn't much of a difference in the main temperature predictions between the partially premixed flamelet and equilibrium model except in the post-combustion zone, where the flamelet model predicts a slightly lower temperature. However, the real differences are shown in the emissions predictions in the figures overleaf.

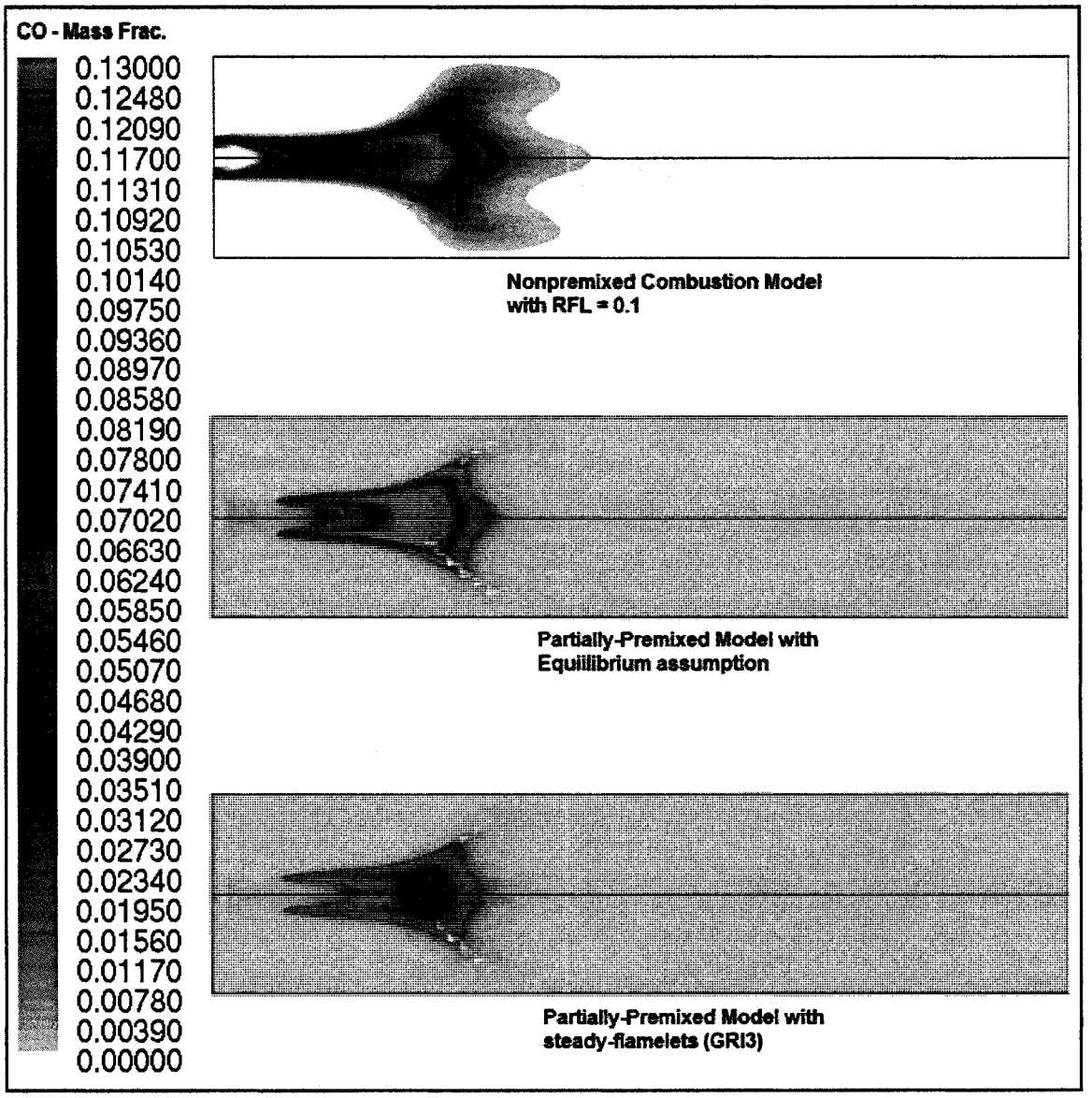

Fig 6.3.2: CO mass fraction comparisons

The flamelet model predicts much lower CO emissions than the other models showing the effect of including non-equilibrium through the scalar dissipation rate. The peak predictions of CO falls to less than half than that indicated by the equilibrium model. This is consistent with the figure below (Fig 6.12), which shows the differences in the expected species mass fraction with and without the

scalar dissipation rate. This issue is dealt with more fully in the next section, which deals with the flamelet library generation and its impact on the pdf model.

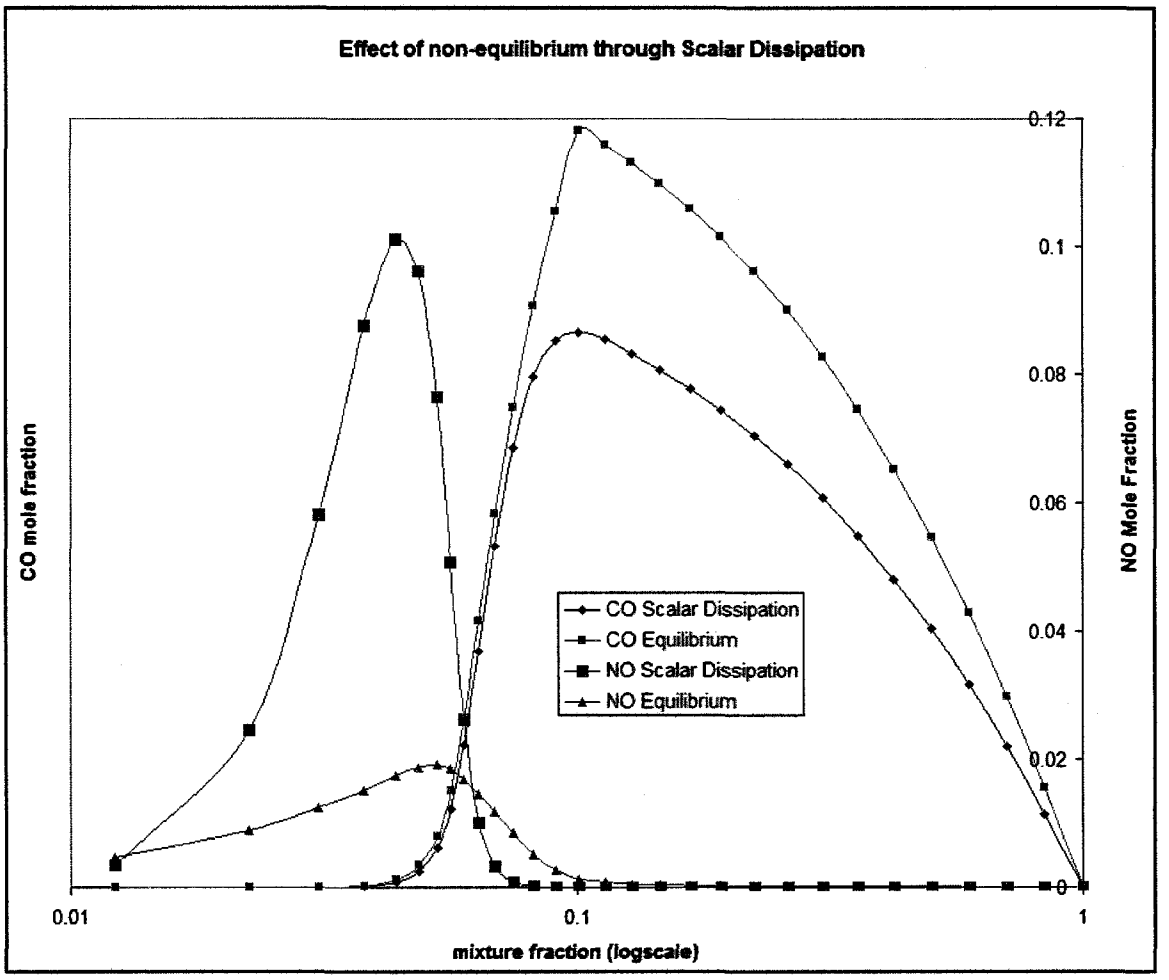

Fig 6.3.3: Effect of including Scalar Dissipation rate (1/s) on CO and NO.

The effect is clear. Including a realistic non-equilibrium parameter such as the scalar dissipation rate, greatly affects the predictions of species mass fractions. In particular the NO mass fraction is shown to be an order of magnitude lower (Fig 6.3.5) in the steady flamelet model than when compared to equilibrium

predictions (Fig 6.3.4). However the finite-rate effects still dominate, as the emissions predictions in the main calculation did not match even with the inclusion of Scalar dissipation rates. Post-processing with an unsteady flamelet method is still required in order to capture residence time effects. In this case, post-processing was done using a NOx post-processor, which Fluent provides. It is here that a major difference in NO species predictions can be observed. The predictions using the NOx post-processor proved to indicate much lower levels of NOx and are of the same limits as the experimental curve fit shown in Fig 7.6.

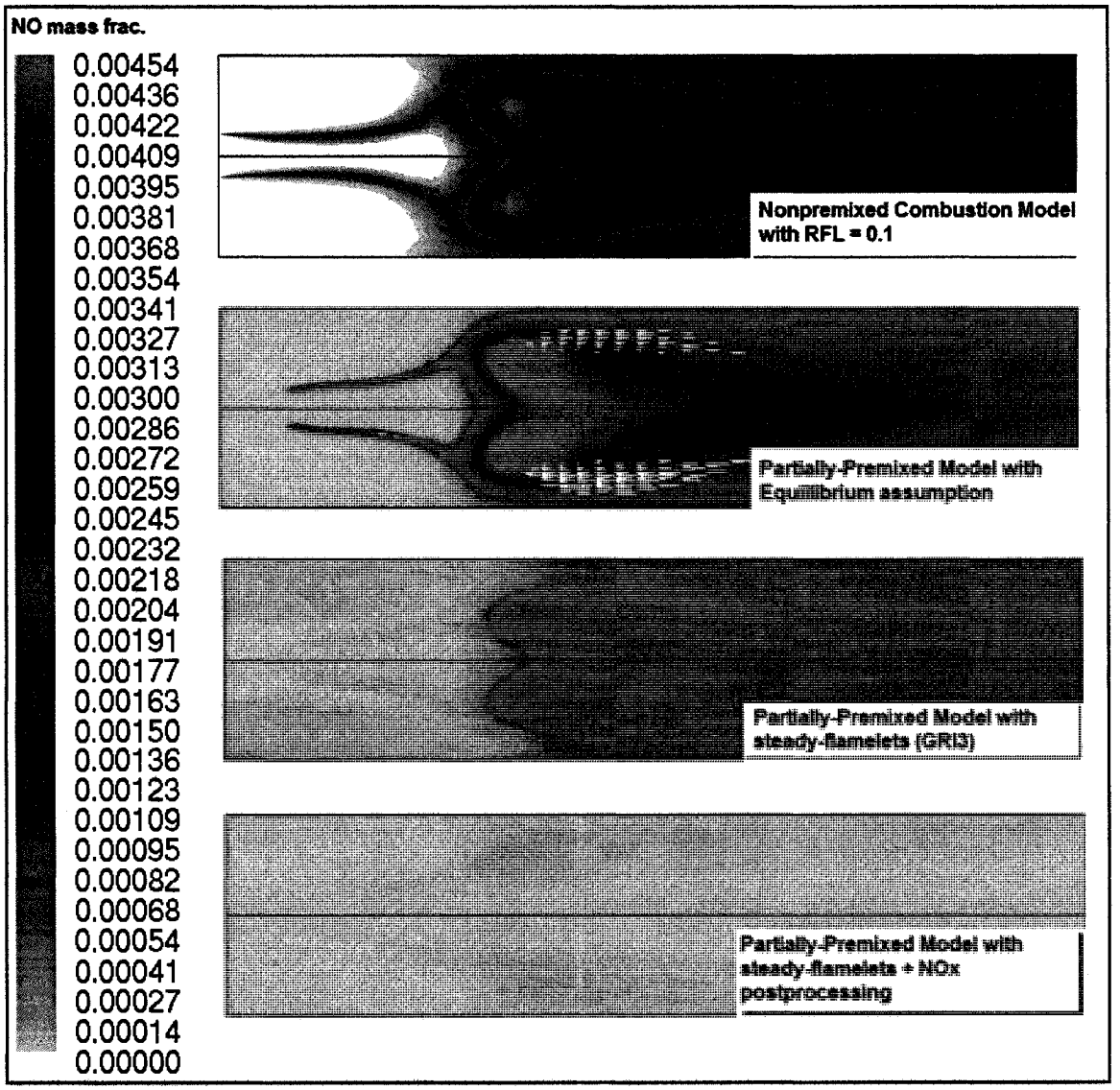

Fig 6.3.4: NO mass fraction comparisons (the bottom picture is clarified below).

Fig 6.3.5: NO mass fraction from post processing (Max (blue regions): 0.0004127, Min 0).

The main conclusions of the pilot study were:

1. K-e realizable and K-w SST models gave the best predictions while the RSM model more correctly determined the point of stoichiometric combustion on the centreline than the other models.

2. RANS Turbulence models differed significantly in predicting combustion aerodynamics such as size and shape of recirculation zones but failed consistently to predict correct mixture fraction profiles. The agreement was qualitative at best.

3. The RANS RSM model proved – unsurprisingly – to be the best model to depict the recirculation zone characteristics due to the anisotropy built into the model.

4. Velocity profiles were not available but a cold flow analysis of another coaxial dump combustor (Habib and Whitelaw) showed that the turbulence models based on the isotropic eddy viscosity hypothesis routinely overpredict or underpredict the velocity profiles due to their incorrect modeling of diffusion away from the walls. This directly affects

the coupling between the mixture fraction transport equation and the momentum equations.

5. Schmidt number tuning was found necessary and proved to be the only factor decisive in bringing RANS predictions in line with experimental data. At an appropriate Schmidt number, *all* turbulence models gave very similar results, thus raising the issue of the eddy viscosity hypothesis that these models are built on.

6. The discretization scheme indicated that a higher order scheme is necessary when the grid is coarse for good species predictions. While gross features like the mean temperature field were well predicted, it showed that small-scale features require denser grids and more rigorous treatment for numerical diffusion even with hexahedral grids.

7. LES proved to eliminate this consideration atleast in the models studied in this thesis but the accuracy and generality is at a high computational expense. Further, the LES Schmidt number was reduced in the dynamic procedure for evaluating model constants, in the main calculations of the complex geometry combustor.

8. The non-premixed model efficiently predicted the turbulence-chemistry interaction but fails to account for partial premixing, which is known to happen in real situations. However, LES does give a better picture of the unsteady phenomena that accompany sudden expansions of jet streams into confined spaces. Most noteworthy is the turbulence model's interaction with the presumed shape mixture fraction pdf approach used in the non-premixed model, to predict intermittent flame lift off and localized extinctions

9. Since only a global 1-step chemical reaction was used and the chemistry was assumed to be infinitely fast, the quality of the engineering solution was judged to be acceptable enough to introduce its methodology into the next phase where additional geometrical complexities would be introduced.

10. Effects of non-equilibrium significantly affect the species predictions but do not affect the mean temperature field to the same effect. In particular the laminar flamelet generated values for NO and CO show the same

trends in the turbulent predictions indicating the need to carefully generate the pdf.

11. The 'simplified' model provides emissions predictions very close to observed experimental values for the complex geometry combustor due to similar residence times. While this is not any justification for validation purposes, the point is well made: the predictions of NO are largely dependent on the temperature field and the residence time. Equilibrium models cannot predict correct results even in laminar flames.

Emissions predictions were not available in the experimental database. Furthermore, the issues raised in the discussion above were treated only superficially to get an idea of what needs to be considered with care when a complex simulation is attempted. The aim was to merely highlight the crucial areas of modeling. These issues were more fully explored in the main calculations of the complex geometry combustor, which included further complications like premixing, swirl and secondary air and cooling flows.

7. RB211-DLE REACTING FLOW SIMULATION

7.1 Setup of Sub models.

The mesh used in the cold-flow analysis in Chapter 5, was converted into a polyhedral mesh as shown in Fig 4.3.6 in order to bring down the cell count since experience with the cold flow LES of the 16 million cell mesh in Chapter 5 indicates that the additional complexity of the combustion model would cause simulation times that are not feasible in the current studies. It was also of interest to validate the topology change, as there are very few Combustion LES calculations on polyhedral meshes in the literature. The potential cut down in simulation time is very attractive and was an issue worthy of further exploration. The mesh shown in Fig 4.3.5 was used for all the main RANS calculations. The case set up is described in this section and the steady-flamelet model, with a flamelet library was used for all calculations.

Flamelet Library:

The flamelet library was generated using both mechanisms. Flamelets were generated for Scalar Dissipation rates ranging from 1/s upto extinction rates in steps of 10/s – this resulted in 36 flamelets generated, with the extinction scalar

dissipation rate predicted to be 181/s for the GRI3 mechanism and about 200 /s for the Smooke mechanism. The result for the GRI3 mechanism is shown below:

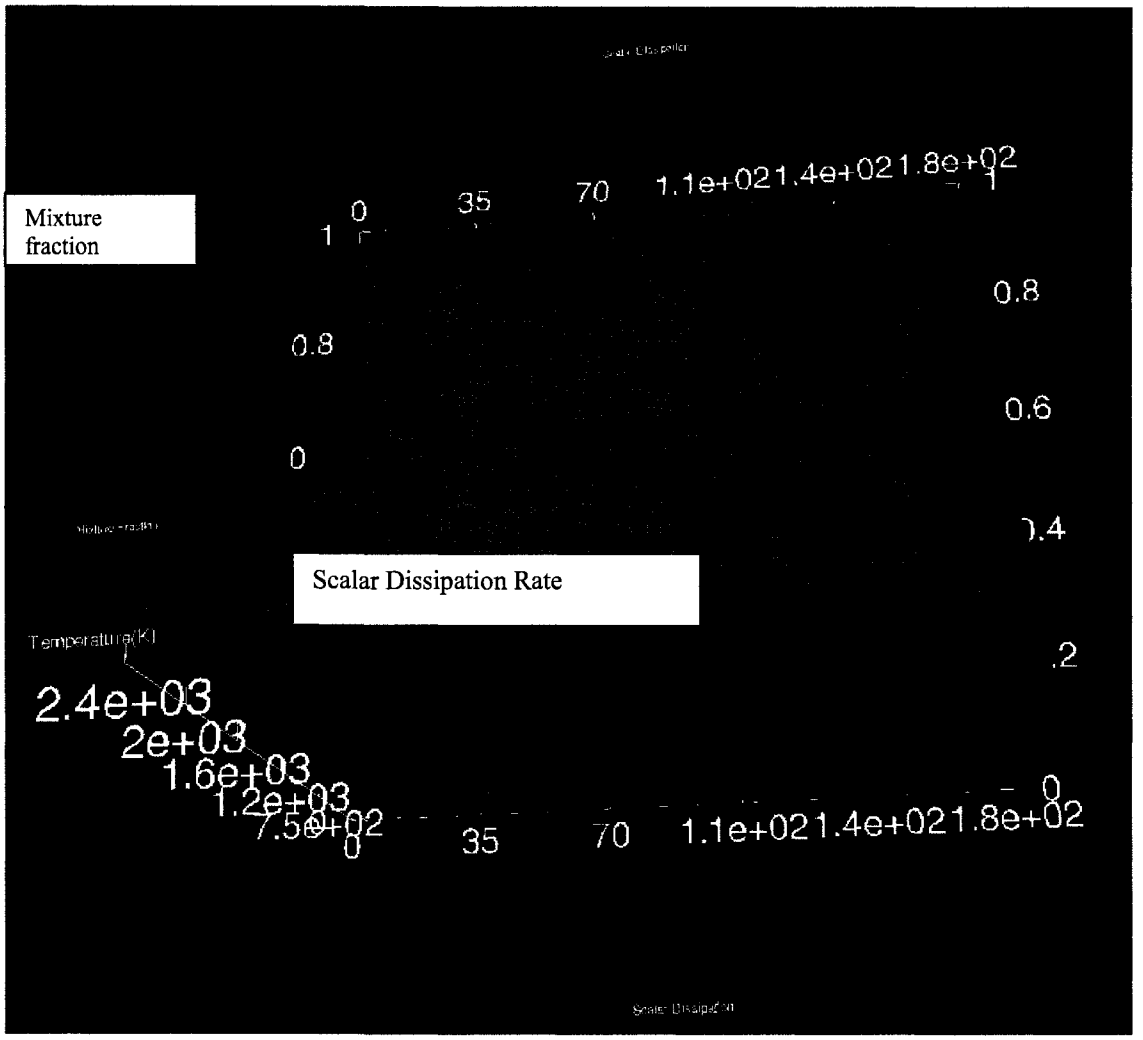

Fig 7.1.1: Flamelet library generated using the GRI3 mechanism.

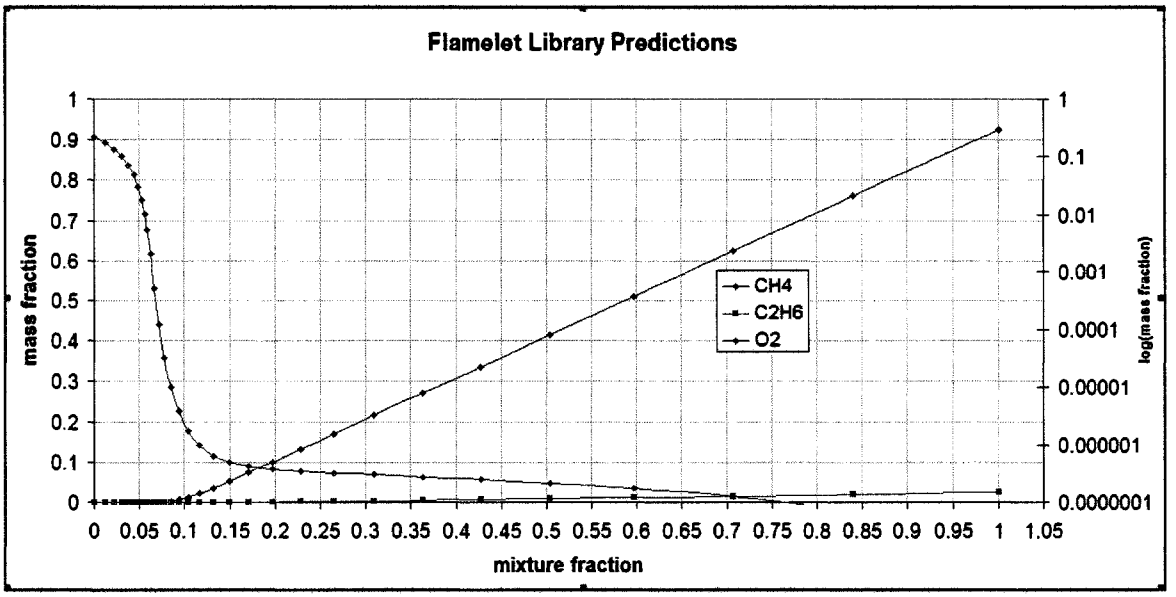

Fig 7.1.2: Slice (Scalar Dissipation = 1/s) showing consumption of Oxygen.

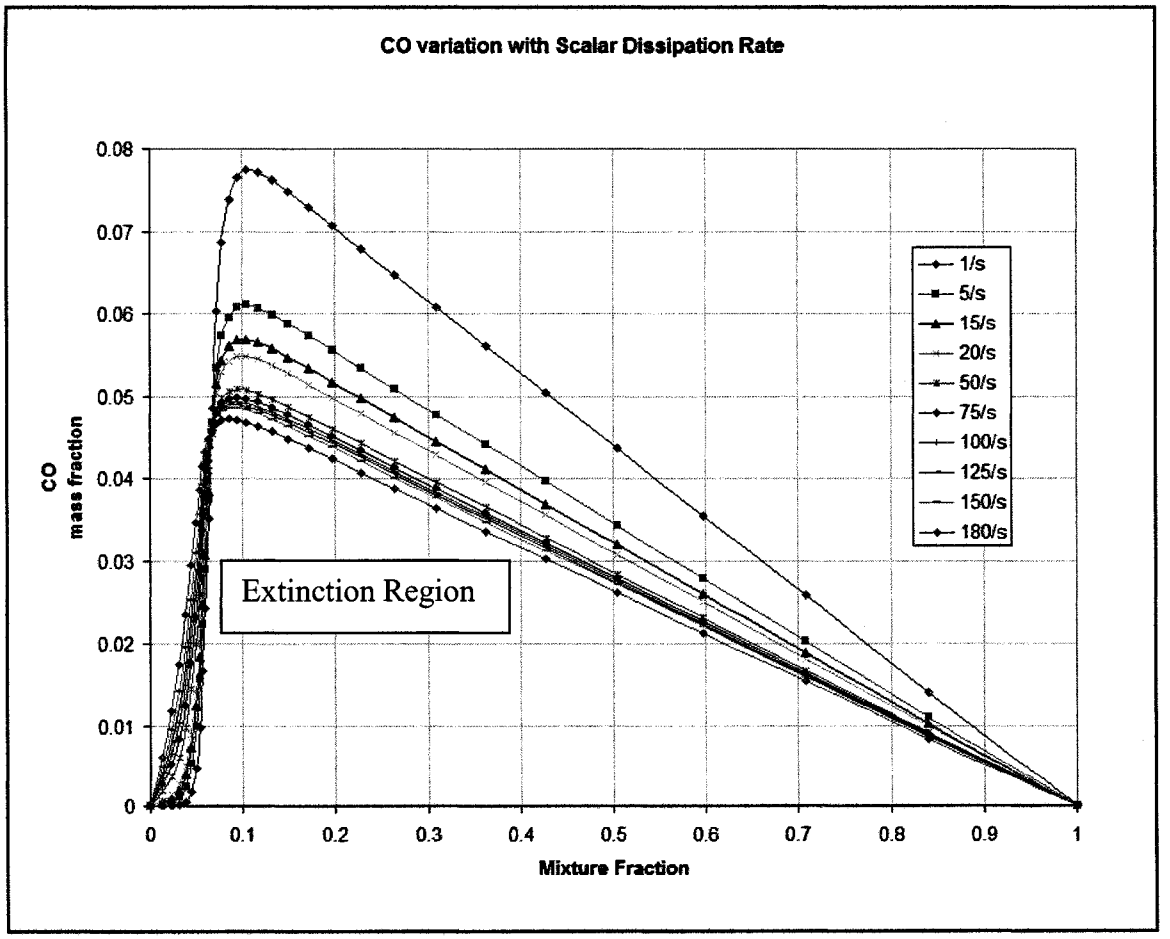

Fig 7.1.3: Flamelet CO variation with scalar dissipation rate.

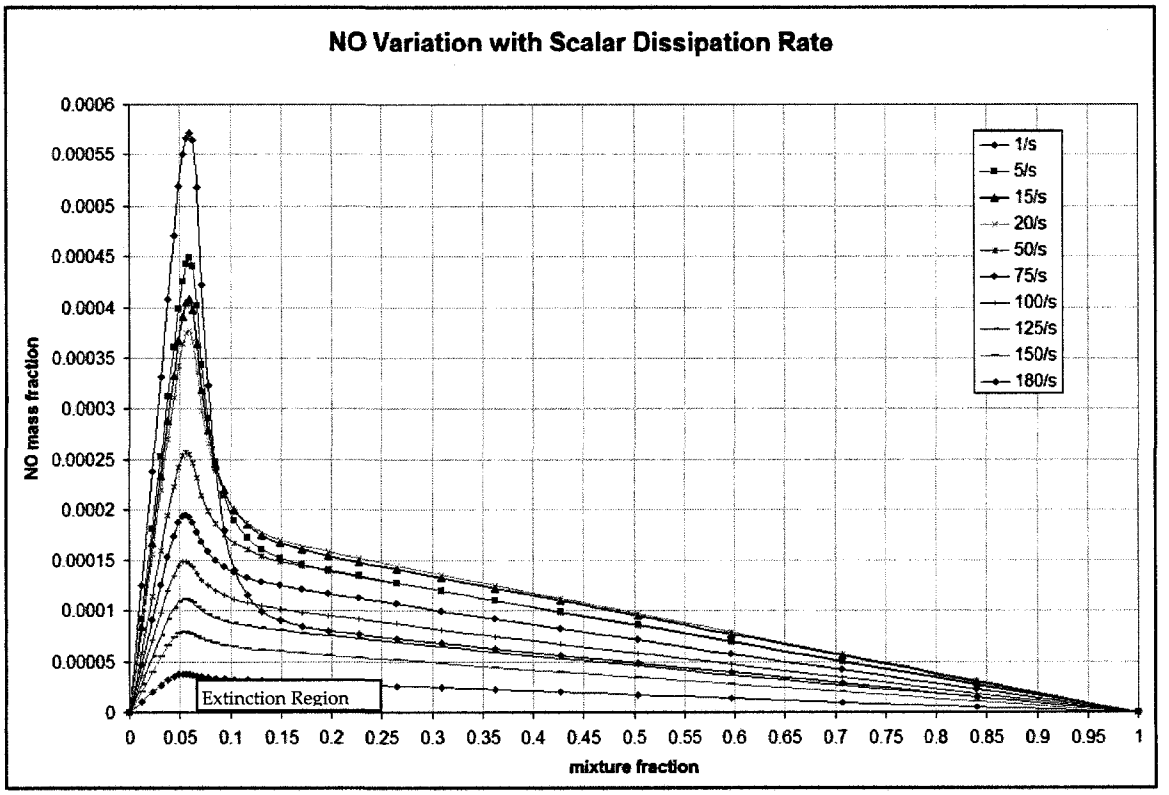

Fig 7.1.4: Flamelet NO Variation with Scalar Dissipation Rates.

Some 2-D slices are shown in Figs 7.1.2-7.1.4 to highlight the effect of varying strain rate through incorporating the scalar dissipation rate, on the emissions. It can be seen that the concentration decreases as the strain rate increases, which can be attributed to the extinction that happens physically as a flame sheet is stretched to the point where it cannot sustain itself. However, it must be kept in mind that the flamelet generation is based on methods for laminar flames. The modeling of the scalar dissipation rate is not as straightforward for turbulent flames. Quenching strain rates are subject to fluctuations in local scalar dissipation rates that may cause flames to exist at $\chi > \chi_{quench}$ and flames to

quench at $\chi < \chi_{quench}$ which is a paradox in the laminar flames context. This has been observed experimentally as well as numerically (Pitsch, [25]) in the context of turbulent flames. This is a direct consequence of ignoring the scalar dissipation fluctuations, which makes clear the weakness of the steady flamelet combustion model to adequately describe local extinction. It is evident that scalar dissipation rate limits to 0 for towards equilibrium, which while physical, can lead to an issue with prediction of NOx and CO at such conditions since the finite-rate effects of these species, especially NOx causes severely overpredicted results. This happens when flamelets are generated at very low scalar dissipation rates. The equilibrium flamelet solution is not included during the pdf convolutions with the flamelet library in the current simulation and the pdf calculations incorporate only those flamelets, which are generated at 1/s and above. The justification for this is that the finite rate species do not respond instantaneously to strain effects. If such an assumption is made then it is equivalent to assuming infinitely fast chemistry at zero aerodynamic strain, which leads to the well-known over-predictions in NOx. This can be seen in the inaccurate (by two orders of magnitude) predictions of NOx species in Fig 7.1.5 when compared with the curve fit provided by Steele [92] in Fig 7.6, which incorporates the finite-rate effects.

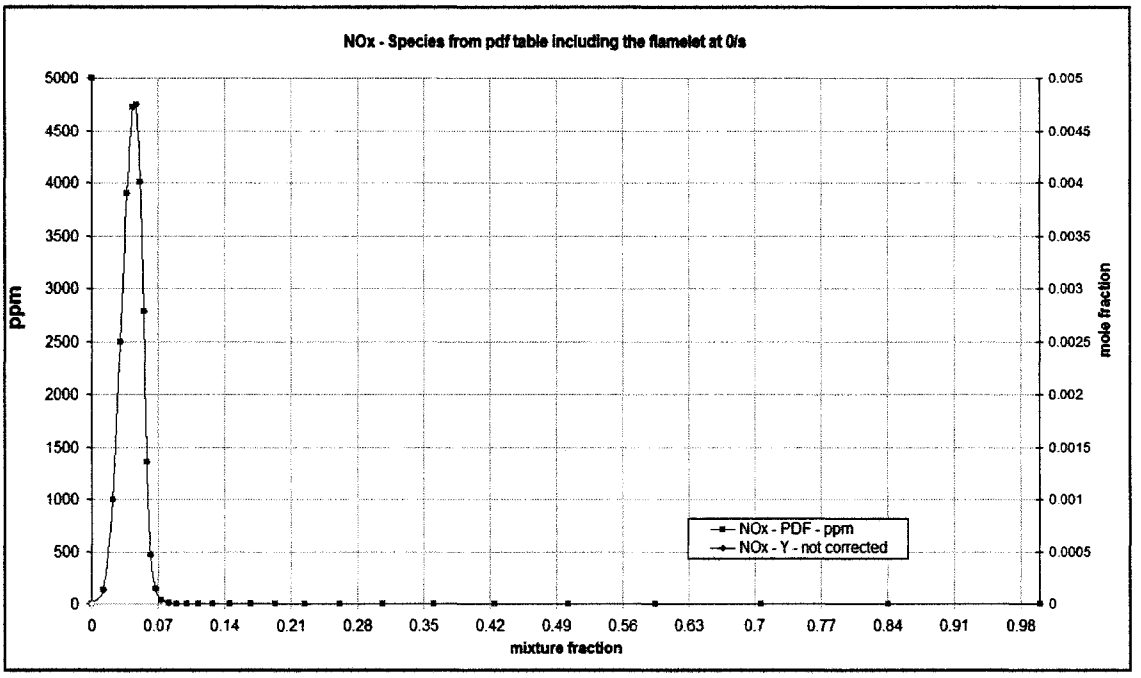

Fig 7.1.5: NOx predictions with the infinitely fast assumption in laminar flames.

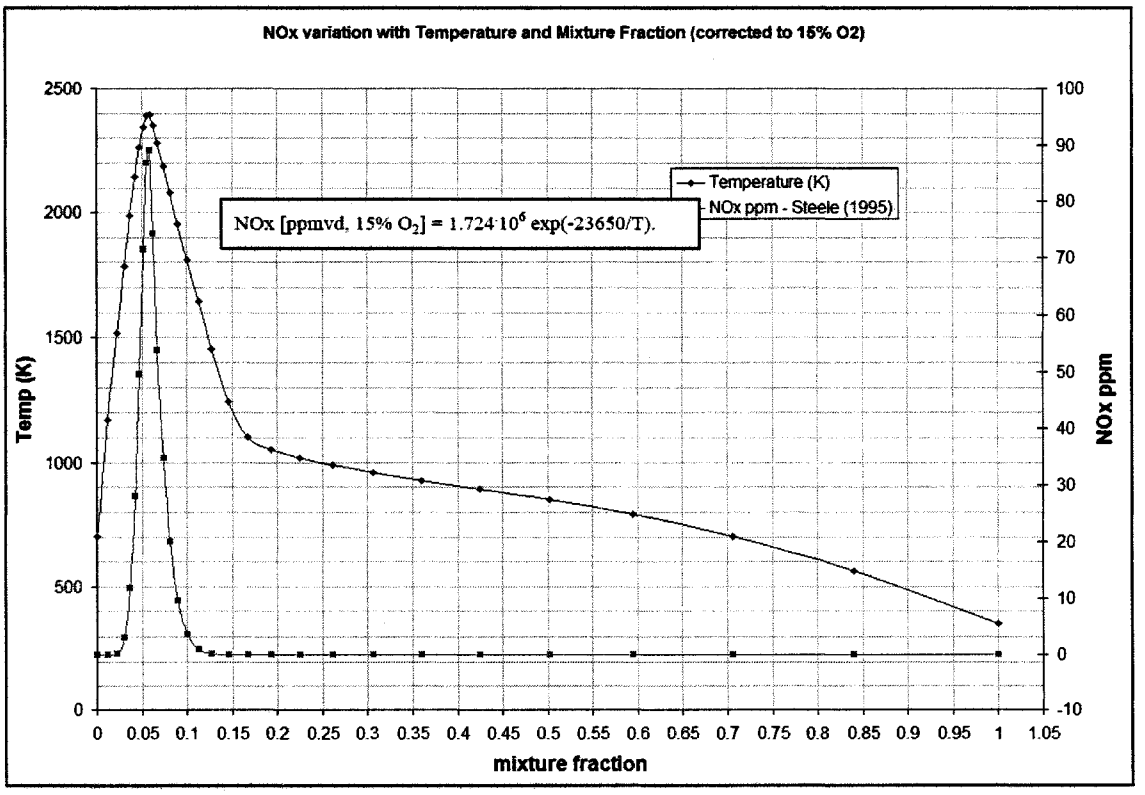

Fig 7.1.6 NOx predictions using a global reaction curve fit by Steele [92].

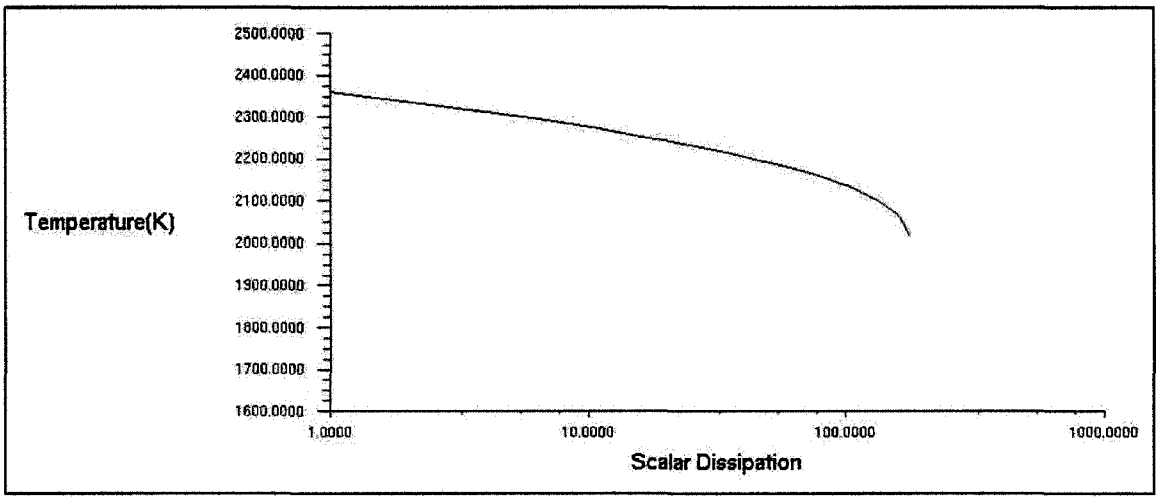

Fig 7.1.7: Modeling of the burning branch of the 'S-curve' in the current simulations.

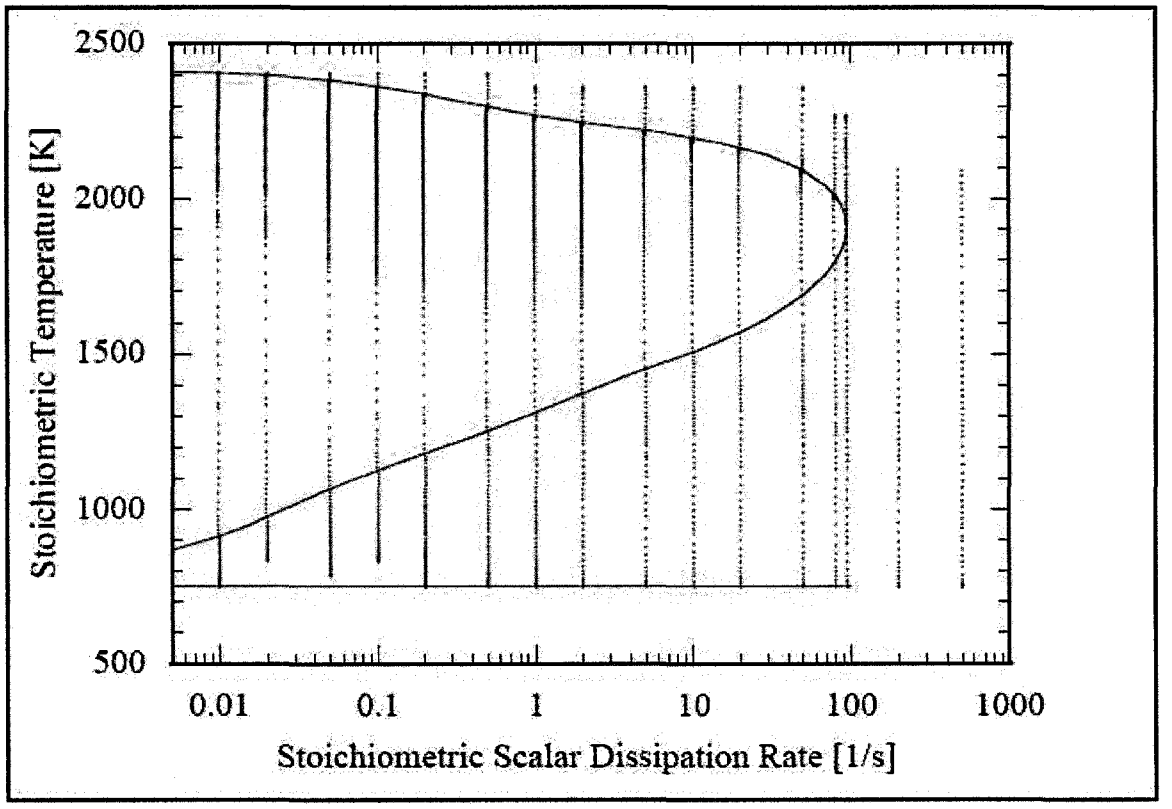

Fig 7.1.8: The 'S' Curve, as a solution of the flamelet equations, from Pitsch and Ihme [16]

The resulting flamelet library can encompass a range of scalar dissipation rates over which for each value of scalar dissipation, there can exist two values (Fig 7.1.8) corresponding to the two branches described by Pitsch and Ihme [16]. In the current simulations, the lower branch non-burning flamelets are not calculated (Fig 7.1.7).

PDF table generation

The flamelet library obtained in the previous step, was convoluted with the pdf of the mixture fraction, and as discussed in the previous section, excluding the equilibrium flamelet. The 3D lookup table is shown below (Fig 7.9) at constant value of scaled heat loss/gain (enthalpy). Similar tables are generated for different points of enthalpy.

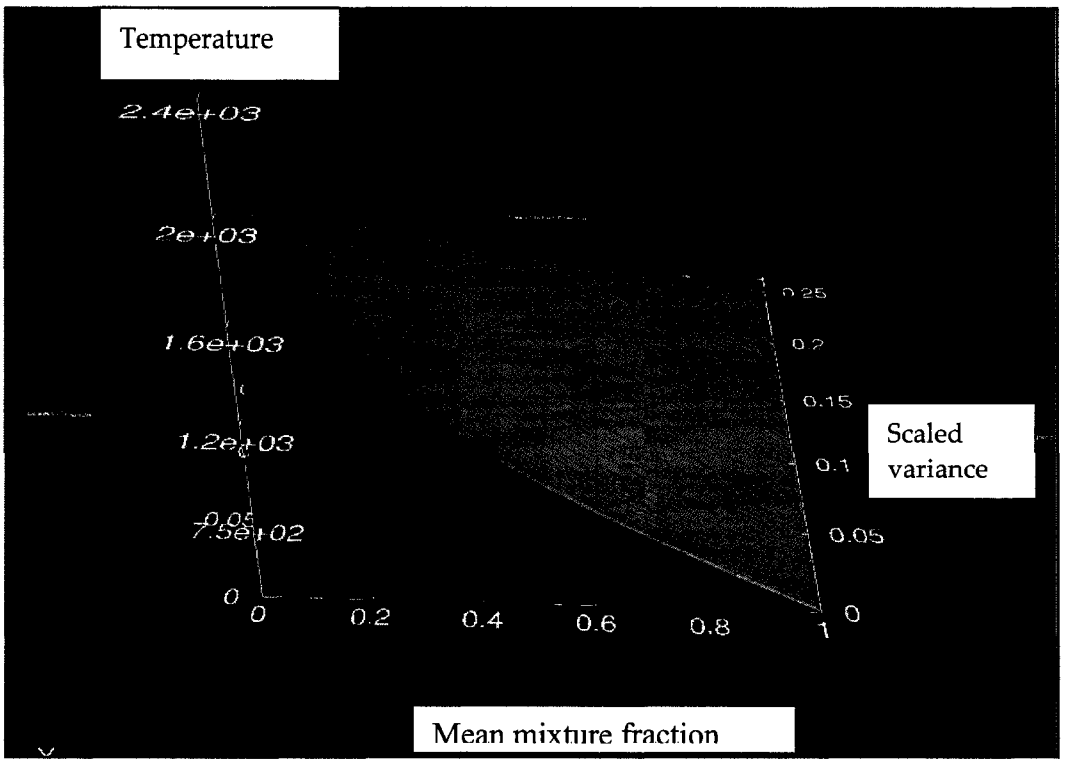

Fig 7.1.9: PDF table generation for non-adiabatic conditions.

The stoichiometric mixture fraction was 0.0597 and the flame-temperature predicted at this value is 2365.1K and the minimum is 350K (fuel temp) at a mixture fraction value of 1. The final results were compared with the 1-D adiabatic flame temperature calculations for different air-fuel ratios at various zones in the combustor. This validates the generation of the pdf table with the assumptions made above. The results can be seen in Fig 7.1.10. Although this step may seem redundant, it is a valuable check, when departing from the default options suggested by Fluent.

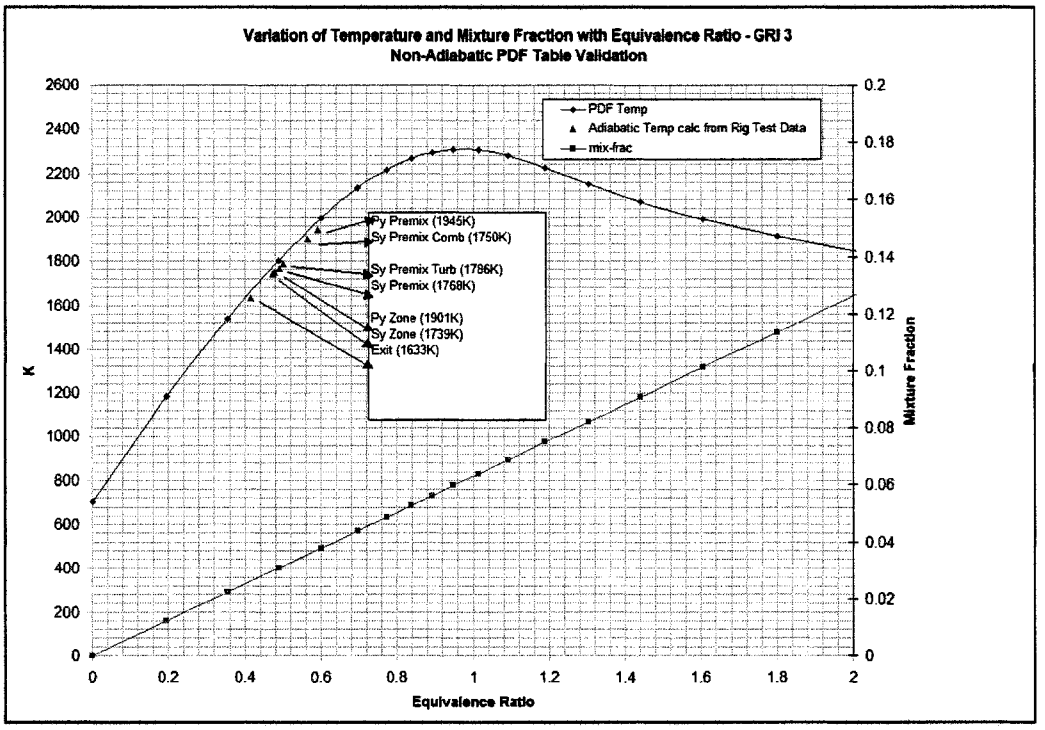

Fig 7.1.10: Temperature predictions across equivalence ratios.

The final step in setting up the model is the calculation of unburnt mixture properties, necessary for the partially premixed model. The laminar flame speed is required at different mixture fraction ratios, since it appears as one of the dominating terms in the model for the turbulent flame speed, incorporated as a source term in the progress variable equation. The result is shown in Fig 7.1.11.

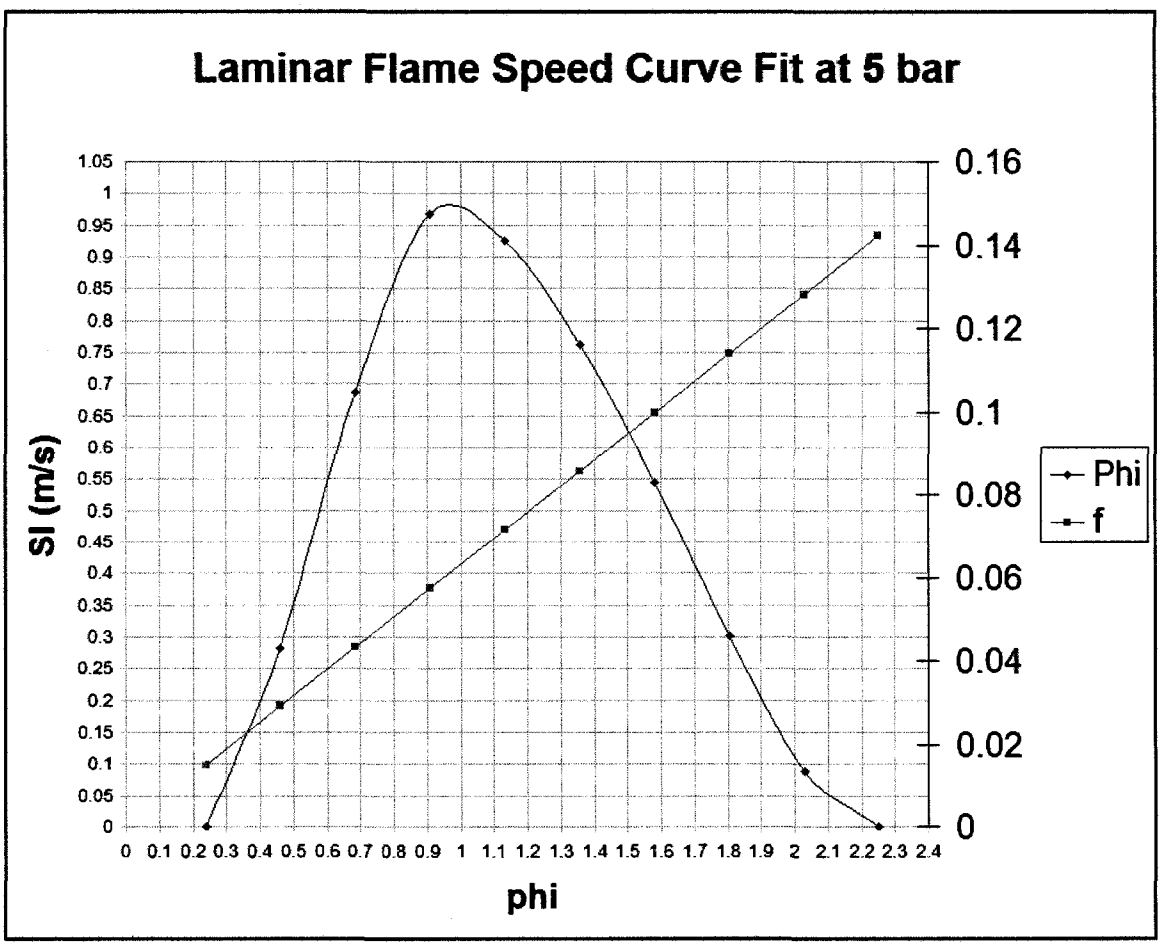

Fig 7.1.11: Laminar Flame Speed Polynomials calculated in Fluent.

7.2 RESULTS

RANS results indicate reasonably accurate predictions of the main temperature field. Due to the complexity of the geometry there was very limited access for traversing and only a centerline continuous traverse of temperature and exit emissions were provided for the purposes of validation. Some previous calculations done using an in-house code are shown with permission for purposes of qualitative comparisons. LES calculations provide very accurate results for CO and NOx when the post-processor is used.

The overall emissions predictions at the exit could not be matched with RANS methods. The experimental data indicates emissions of CO and NOx to be around 10 ppm and 17 ppm respectively when corrected to 15% Oxygen. The RANS results with the steady-flamelet partially premixed model under-predict CO emissions by more than 5 times and NOx by almost two orders of magnitude. Table 7.2.1 below summarizes the key findings in ppm at baseload fuel composition, measured at the exit and corrected to 15% Oxygen.

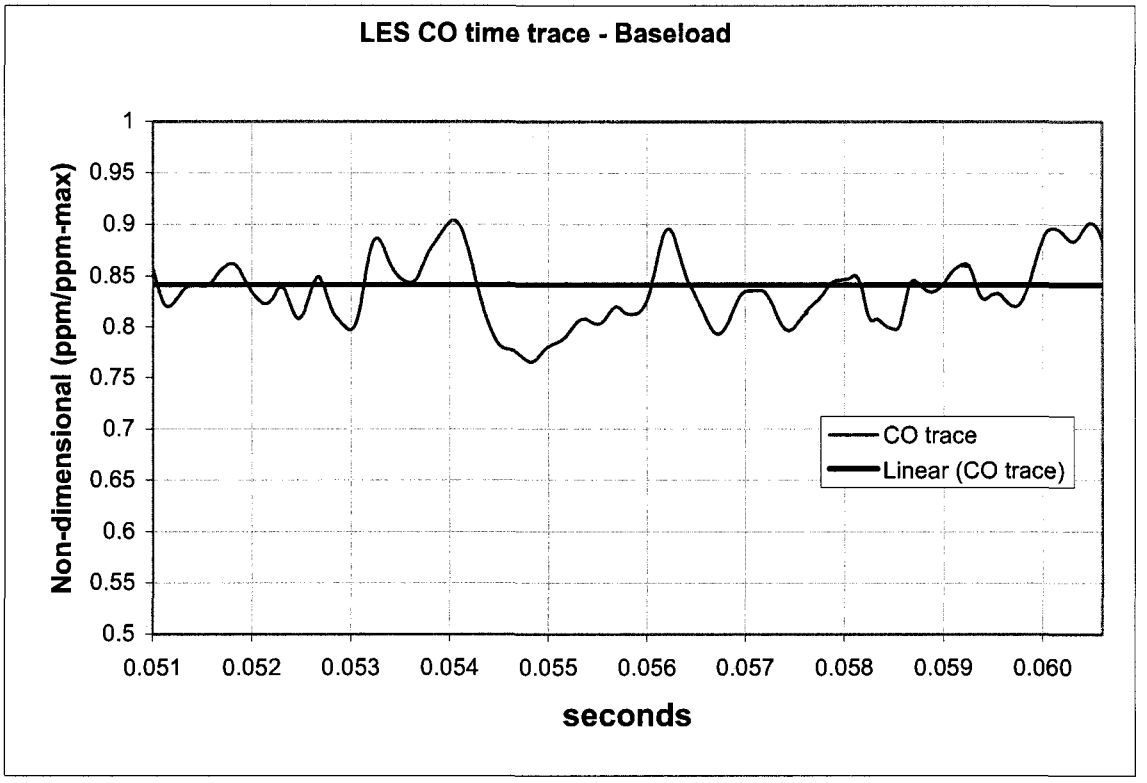

Fig 7.2.1: Time Trace of LES over 9 ms (one flow through time)

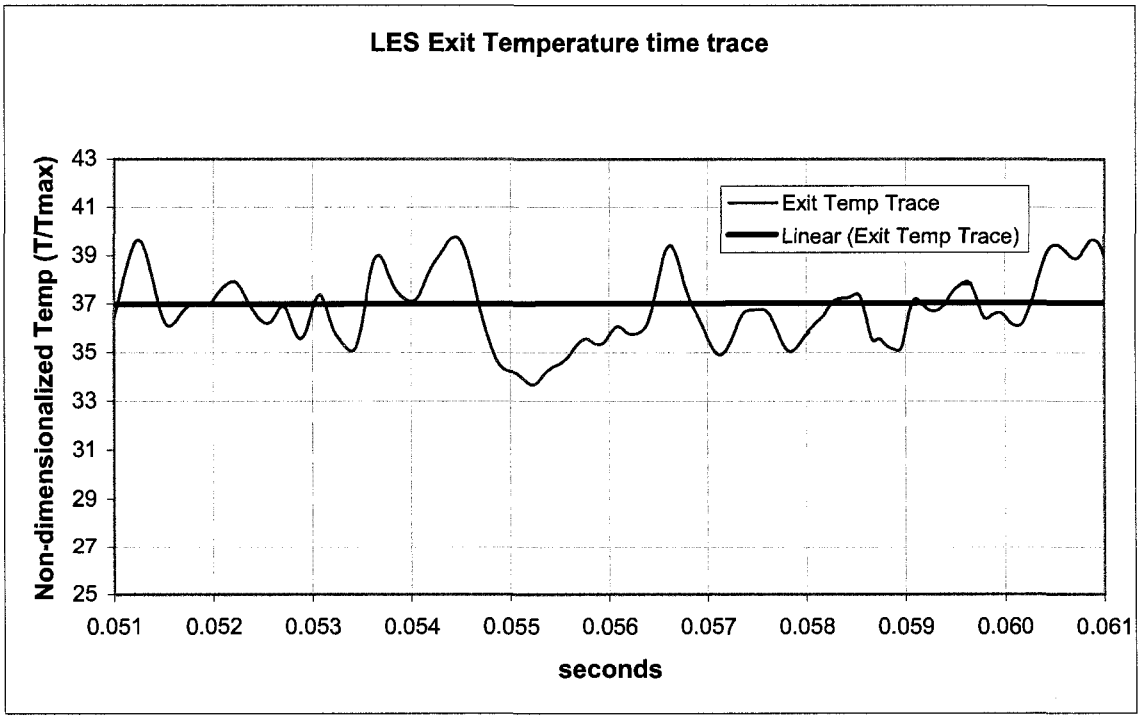

Fig 7.2.2: Time Trace of Average Exit Temp over 9 ms (one flow through time)

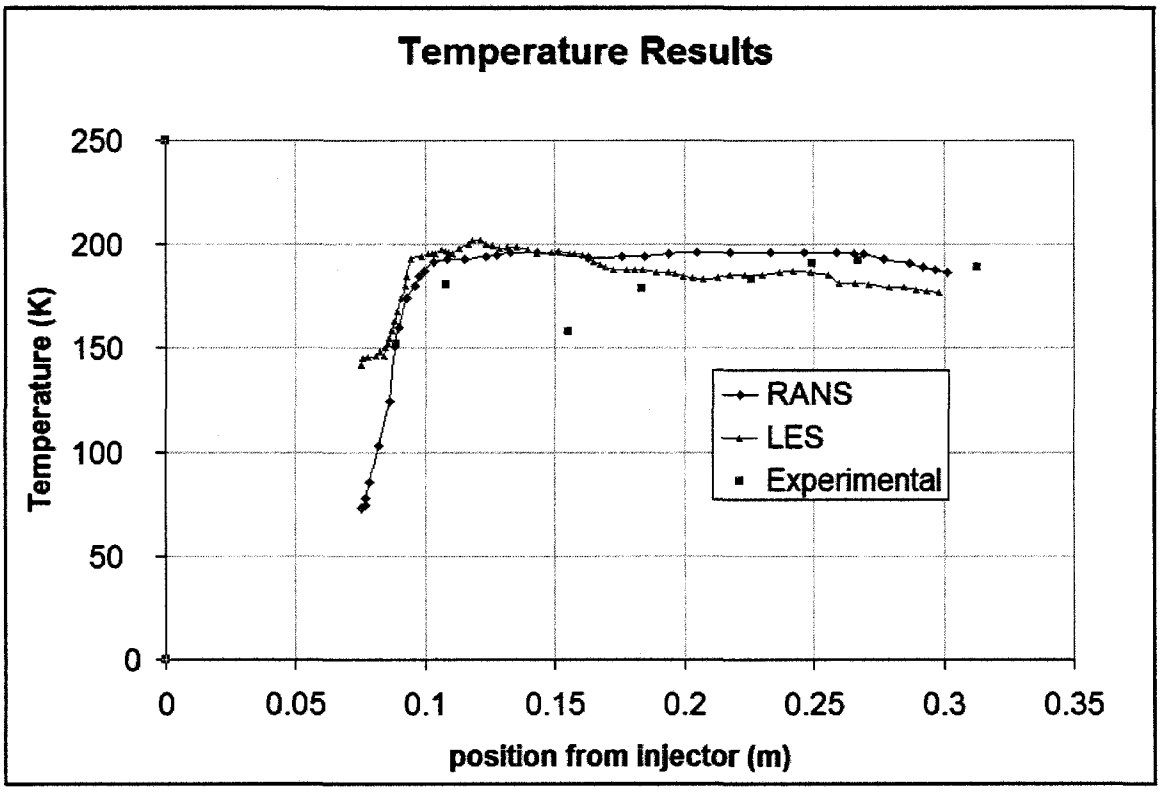

Fig 7.2.3: Temperature predictions along centerline (normalized).

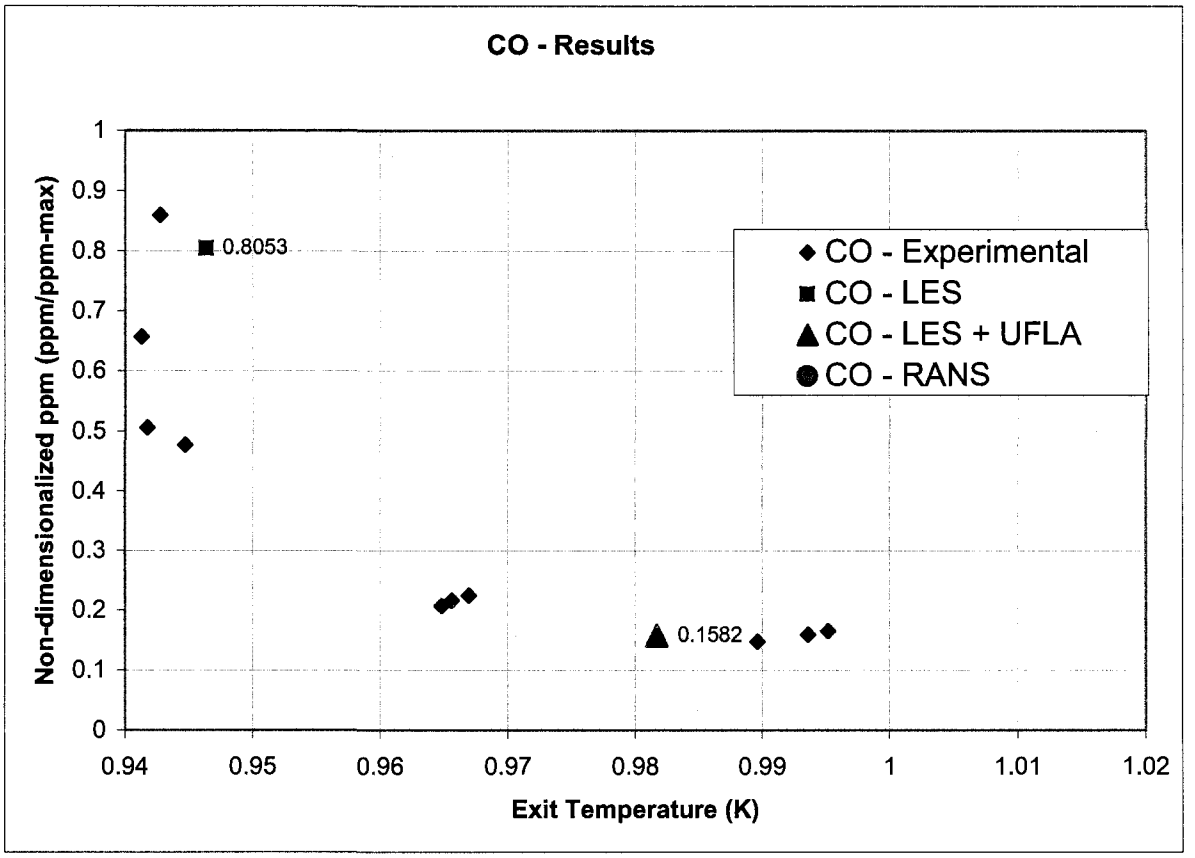

Fig 7.2.4: CO emission Results.

It can be seen from Fig 7.2.4, that both RANS and LES predictions suffer at approximately z= 0.16m into the domain. This happens to be the junction between the primary zone and the secondary zone, where experiments indicate significant uncertainty in the data. It is thus inconclusive at this point to advance a reason for the deviation observed in the graphs above. However, as consistent with the earlier discussion mean temperature fields are relatively insensitive to the turbulence model. Unfortunately, species profiles at various locations were not available for a more thorough comparison. However, the main interest for

the industry was the exit emissions and to obtain trends for different fuels with a comprehensive chemical mechanism. RANS was performed with a reduced order 'skeletal' mechanism by Smooke [93], which does not contain NOx species. It is found that this mechanism is quite adequate to predict reasonably close values of CO as can be seen in Table 7.2.1. The GRI3 mechanism [94] contains NOx species, though the emissions can be seen to be over-predicted. Clearly NOx prediction requires a post-processor that takes into account the residence time effects and history of mixing. The NOx post-processor does this in Fluent and requires a converged field.

The exit emissions were very well predicted with subsequent post-processing using both the unsteady flamelet method as well as NOx post-processing. This can be seen in Figs 7.2.4 where the combustion model is shown to respond well to the changing temperature and is capable of predicting the trend. The unsteady flamelet method has shown to be capable of calculating CO emissions very accurately (especially when the combustion is lean-premixed). The averaged LES field under predicts the exit temperature slightly but unfortunately, this is a range where CO has a highly non-linear dependence on temperature and very small changes can result in drastic changes in CO as seen in the experimental results in Fig 7.2.4. The unsteady flamelet method takes into account the

unsteady effects and usually results in differing mean temperatures and species predictions. This can be seen in the result after running this method. Temperature increases towards the experimental value and the CO correspondingly decreases. The probability marker history through the domain is shown in Fig 7.2.5 below.

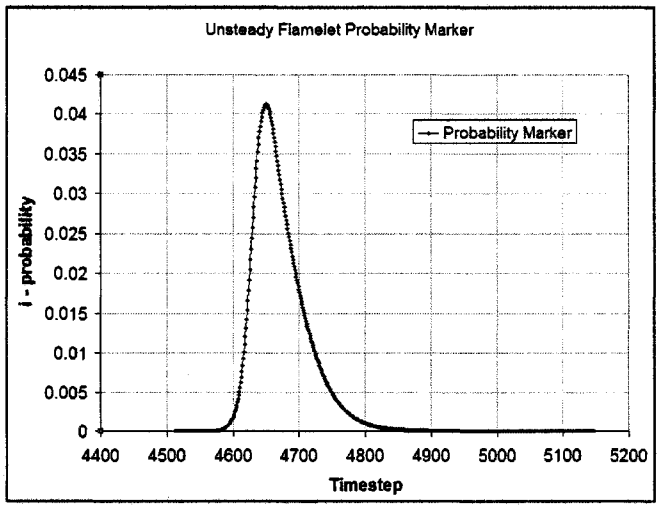

Fig 7.2.5: Unsteady Laminar Flamelet Probability Marker history.

NOx emissions, following the trend of the experimental data, are not as responsive to temperature changes, and are overpredicted before and after running the unsteady flamelet model. This is consistent with the findings of Odedra and Malalasekara [96] who used this model in the RANS context with the GRI3 mechanism for a methane flame in a bluff body combustor. It is also consistent with the observations of Riesmier et. al. [52] of flames in a BMW Rolls-Royce aero combustor, where the NOx was still overpredicted. In the current simulations it was found that though the unsteady flamelet model can predict

CO emissions very accurately, especially with LES, it still over-predicts NOx species. In contrast, it was found that the NOx post processor which solves for the transport equations of NO and N2O on a converged flow field, either steady or unsteady can help with this. The final result can be seen in the NOx charts shown below. Thus, in this case, it was found helpful to use a two-pronged approach for CO and NOx emissions predicting. Although it is a little cumbersome, the best method seems to be to calculate the averaged LES, run the unsteady flamelet model and then use a UDF (fluent subroutine) to update the mean temperature values with the values obtained from the unsteady flamelet predictions as input for the NOx postprocessor and then run the NOx processor to obtain final NOx predictions. The result can be seen in Fig 7.2.6. The prediction without the post-processor reports the NO emissions value of 189 ppm. Solving explicitly for NO and N2O shows a much closer result. The Y-axis is logarithmic to highlight the trends.

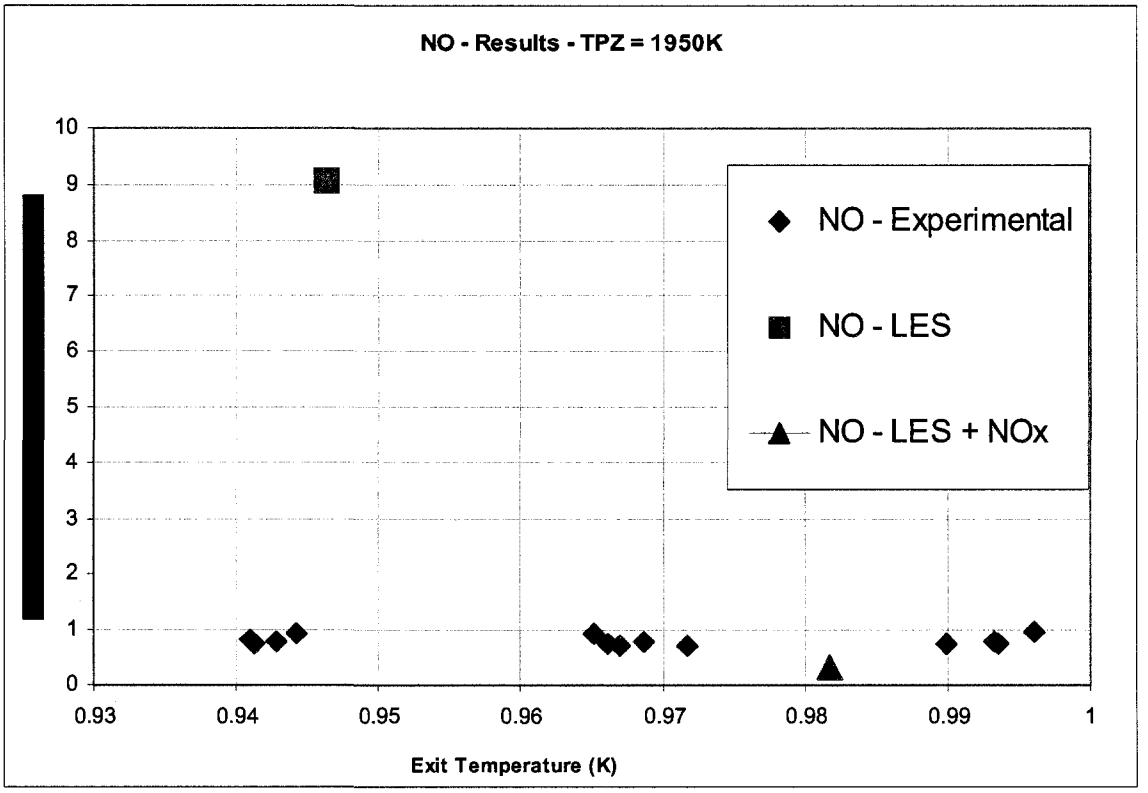

Fig 7.2.6: NO predictions before and after running the post-processor.

The main contribution to NO formation in this combustor was due to the intermediate N2O reactions which are important in lean premixed combustion since thermal NOx is designed to be as low as possible – a consequence of the design temperature to remain at or below 1800-1900K. Given this, it was decided to solve a transport equation for N2O along with NO. Thermal NOx becomes important only above these temperatures and doubles for every 90K rise above 2000K. Prompt NOx was observed to remain low consistent with the fact that there is no fuel-rich combustion in this environment. The main reason for NOx formation is the reaction of oxygen radicals with Nitrogen. The prediction of the

concentration of this radical as well as the OH radical becomes important when thermal NOx is considered in the reaction rate equation used by Fluent in predicting thermal NOx. The steady flamelet/LES approach is the best in obtaining high quality predictions of these 'fast' chemistry species and the NOx processor was given the option of directly using these calculated mass fractions for its calculations. Significant errors can result if equilibrium of these species is assumed. Re-burn – the reduction of CHx species with NO, was also considered due to the secondary addition of air and fuel since the effect is important between 1600K and 2100K.

7.3 Some critical modeling considerations

A few issues that were key to setting up the model for realistic predictions are discussed below.

1. Effect of Modeling Cooling Air

Modeling the cooling air as a uniform flux through the walls is standard practice with combustion models such as the eddy dissipation model and the equilibrium models. However, the model quenched the zones adjacent to the walls to a degree that was clearly unphysical. The reason for this is still unclear. One possible explanation could be that the perpendicular angle of entry (normal to the boundary) is incorrect and too much cooling air is drawn into the main flow, diluting and thus causing quenching. Attempts were then made to angle the entry of the flow to the real angle of 45 degrees. This very mildly alleviated the situation. The effect of removing the cooling air completely, caused the model to burn all the way up to the wall, which is also unphysical. Finally, the effect of cooling air was included as mass and energy source terms in the continuity and enthalpy equations respectively. This produced a more realistic flow-field than the other two and this method was used henceforth to include cooling air effects.

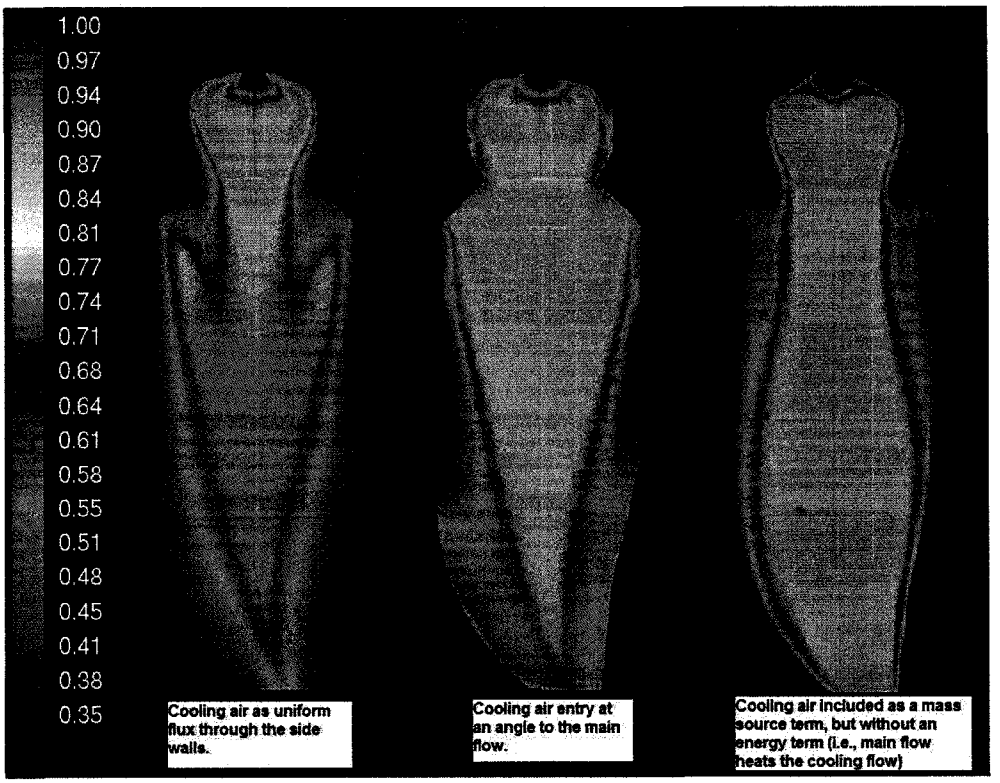

Fig 7.3.1: Temperature contours with cooling air modeling.

2. Modeling the Constant A of the TFC model and the critical strain rate g_{cr}.

A survey of the turbulent flame speed closure model (TFC model) indicates an ambiguity in the description of the 'critical strain rate' which is a parameter which needs to be modeled correctly in order to accurately represent realistic quenching. The turbulent flame speed constant 'A' is also 'tuned' to experimental data due to the empiricism that was involved in formulating this model. Biagioli [7] indicates some reasons for doing this in context of trying to arrive at the right location for flame stabilization in an Alstom EV burner:

1. Adjustment due change in geometry (A was obtained as a model constant based on idealized reactors.) and flow state (RANS with the k-epsilon model).

2. Possibility of flamelet models losing validity at lower Damköhler numbers such as found in industrial burners.

3. Not enough cells used for flame-front resolution in LES, so that the flame-front thickness is overestimated.

4. Neglecting contribution of the laminar flame speed S_L at subgrid scales in LES.

Polifke et. al. [49], on the other hand, investigated for the right value of g_{cr} and concluded that Zimont's extrapolation model worked best for atmospheric pressures but greatly under predicted the value at high pressures. The authors then had no choice but to determine the values based on the simulations. It was encouraging however to see that once the right value was obtained it was fairly consistent. Some of these reasons were investigated in context of the geometry and flow regime of the current simulations in RANS and LES.

In the current simulations, it was found that these issues were not trivial and mean the difference between a properly combusting flow-field and a quenched one. Recall from Chapter 2, that these two parameters occur in context of determining the progress variable source term for the partially premixed model. This implies that unless they are properly modeled, the prediction of the flame-front can be affected. Before any tuning was done, the model was run with its default values (A=0.52, g_{cr}=1e+8) and it was found that the flow-field was mostly quenched. Working on a premise that the geometry and ambient conditions justified an increase of the constant A, the best value for RANS was found to be between 0.8 and 1.3. Also, following Polifke's [49] reasoning that at high pressures, the critical strain rate could take on much higher values than Zimont's extrapolation model for g_{cr} would predict, it was found that in the RANS context, a value between 53000 /s to 58000 /s with constant A=1.3 provided the most realistic flow-field. The difference can be seen below in Fig 7.3.2,

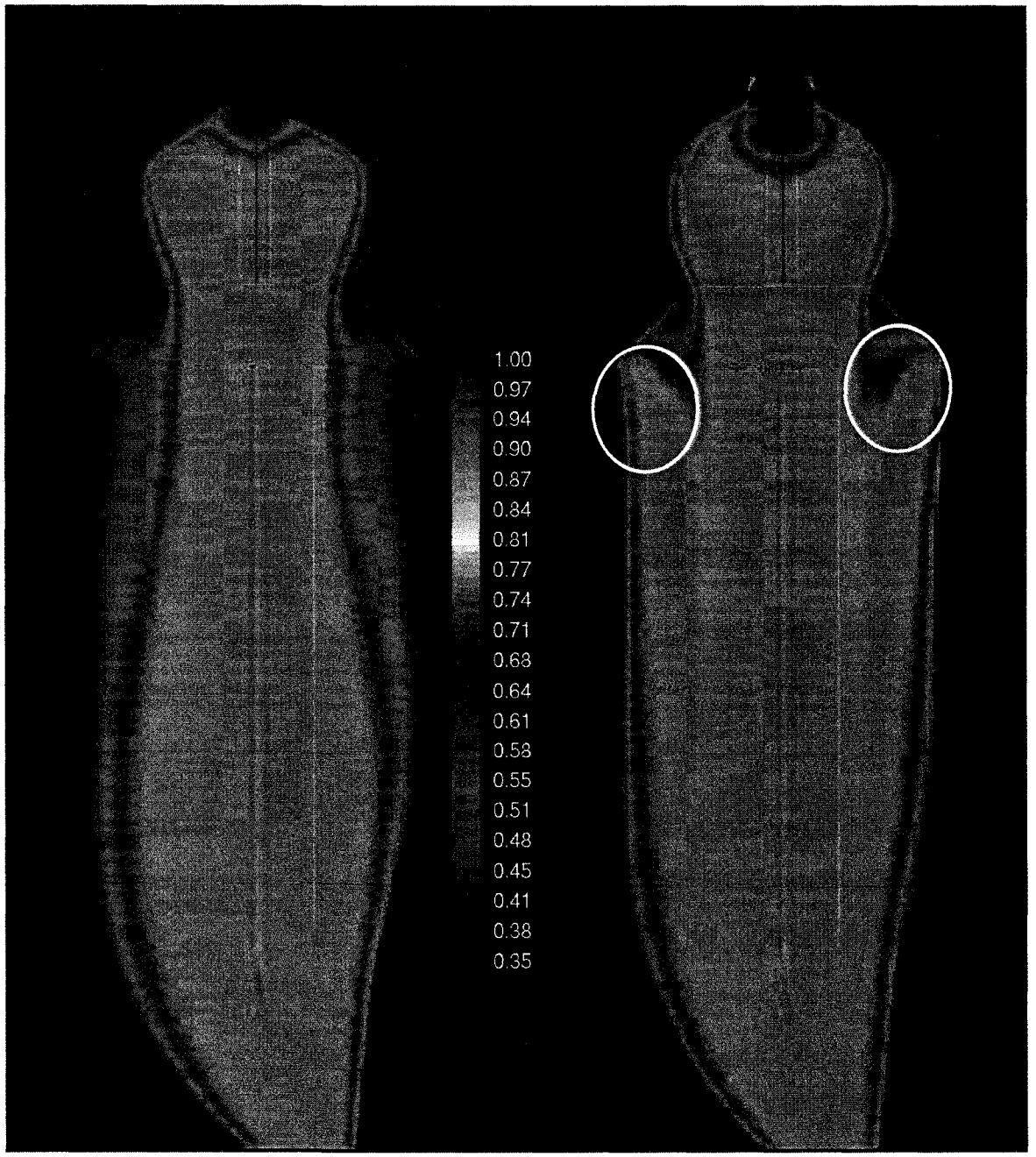

Fig 7.3.2: Effect of constant A: *(left)* A=0.8, gcr=58000/s *(right)* A=1.3, gcr=58000/s

It can be seen in the Fig 6.2.6 that the increase in constant A, gave rise to secondary flames, which can be seen at the exit of the secondary premixer arms (marked in white circles). This is consistent with the design intentions of this

combustor. Experimental data also shows high temperature areas in this region though for confidentiality reasons, this data cannot be reproduced here.

At default values, the model failed to light at all. Keeping the default value of A, but with gcr=40,000, the model severely under-predicted the temperature field as seen below in Fig 7.20:

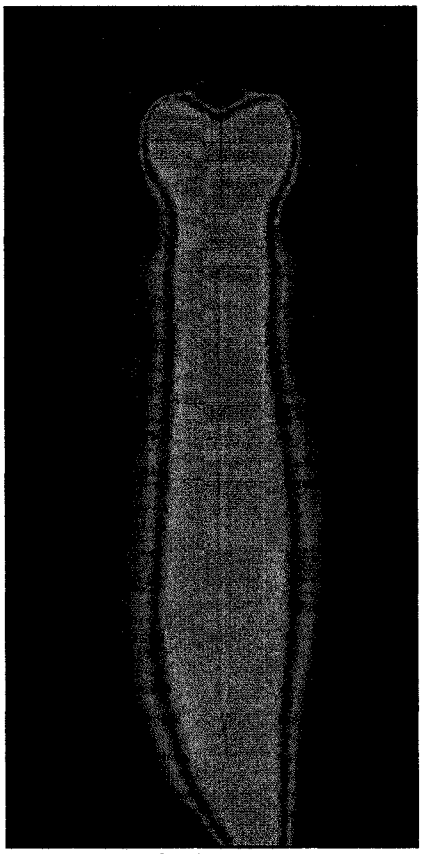

Fig 7.3.3: Default A=0.52

This was surprising since the default value of g_{cr} is 1e+8 i.e., zero quenching according to:

$$G = \frac{1}{2}\mathrm{erfc}\left\{-\sqrt{\frac{1}{2\sigma}}\left(\ln\left(\frac{\varepsilon_{cr}}{\varepsilon}\right)+\frac{\sigma}{2}\right)\right\} \text{ where } \sigma = \mu_{str}\ln\left(\frac{L}{\eta}\right) \text{ and } \varepsilon_{cr} = 15\upsilon g_{cr}^2$$

Apparently the model lit up at a higher probability of quenching. The reasons for this anomaly are not fully clear and indicate the need for further investigation. However, it is clear that with the right values, it is possible to obtain results that are able to describe the physics at much less computational expense than the species transport models. Also this anomaly did not affect the flow in the LES context where g_{cr} was left at its default and only the constant A was increased to 2, consistent with Biagioli's argument for very low subgrid burning velocity. RANS studies were qualitative at best and quantitative accuracy was found mostly in the mean temperature field. There was no opportunity to check velocity profiles at different stations, as these data were not available. However, the use of this model in the literature ([18], [7], [49]) has shown it to be fairly accurate – as long as the mixing was properly predicted. Infact, some unsteady phenomena – bistable flame behaviour - experienced by Biagioli [7], could not be captured with RANS methods and had to be abandoned in favor of LES, which was able to reproduce the correct flame anchoring.

In the studies done in this thesis the effect of increasing the constant A increased the turbulent burning velocity as seen in:

$$U_t = AG(u')^{3/4} U_l^{1/2} \alpha^{-1/4} l_t^{1/4}$$

This had a direct impact on flame anchoring. Overly increasing this constant (>2 in RANS) had the effect of numerical flashback into the premixers, where the flame traveled upstream to anchor at the fuel injectors – a certain impossibility, given that the turbulent intensities and strain rates in this region are so high as to quench any flame initiated here. Flame also anchored to the walls (corner recirculation zones) , which was also not a design condition nor was ever observed in thermal paint studies of this combustor.

Thus clearly, there is a definite range and limit to the 'tuning' that needs to be done with this constant, unlike the constants for the eddy-break up model which are often tuned between orders of magnitude!

The practice may be summed up best by Polifke et. al.

'It is important, however, that the model parameters are not simply "tuned" to give best agreement with validation experiments. Instead, prescriptions based on physico-chemical reasoning are provided to derive model parameters from first principles or at least from chemical-kinetic model systems with detailed chemical mechanisms.' – Polifke et. al.(2002) [49].

3. Premixer Anomaly

A slight anomaly was noticed with both RANS and LES studies in the primary premixer. The partially premixed model seemed to predict an unphysical ignition in the vicinity of the high-velocity fuel injectors, a fact which has been noticed by Caracciolo et. al[18], in their validation of this model for a DLR burner (Fig 7.3.4). In their case, the authors advanced the explanation that modeling of the critical strain rate could be the cause for this unphysical light-up. Modeling with a finite g_{cr} alleviated the problem in their case, but this procedure did not work in the simulations performed in this thesis.

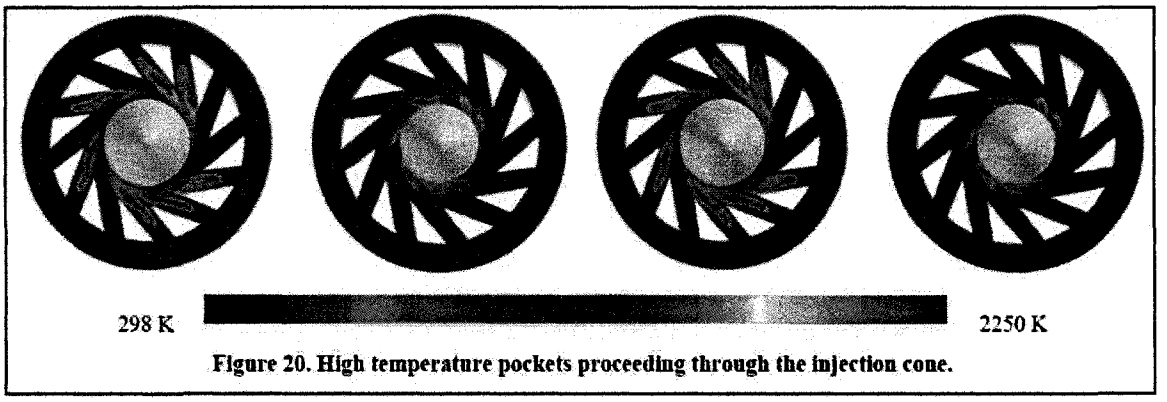

Fig 7.3.4: High Temperatures in the Premixer Ducts - from [18]

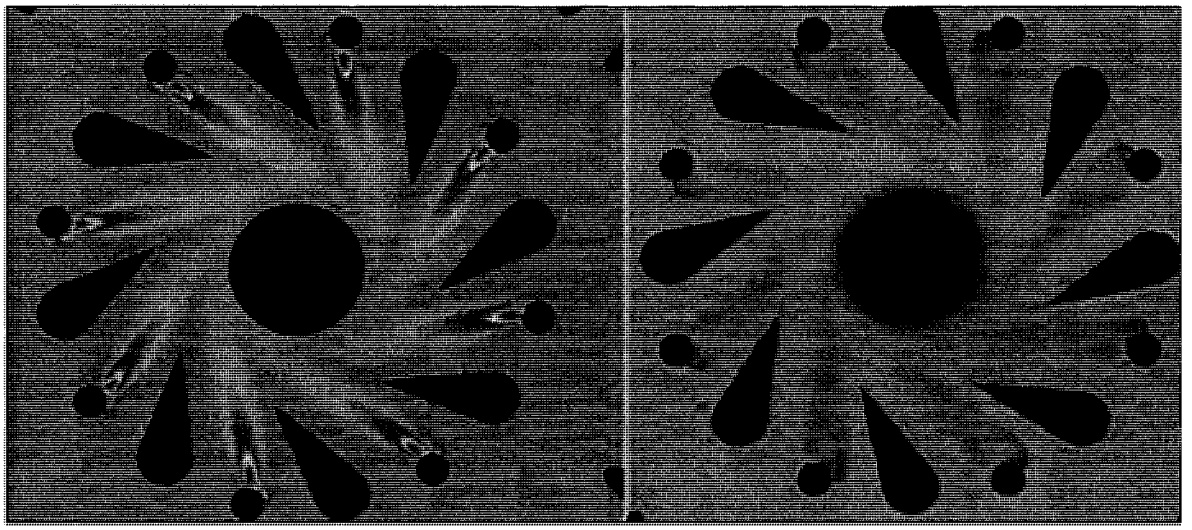

Fig 7.3.5: *(left)* High temperature pockets in the current simulation's primary premixer. *(right)* resolved by considering non-adiabatic effects.

The work-around was to consider the walls as non-adiabatic and apply a real wall temperature to the injector walls and vane blades (Fig 7.3.5). The problem was aggravated in the sense that this combustor operates at high preheat air which is close to self-ignition when mixed with the fuel. It may be that the partially premixed model predicts a premature heat release given these conditions (cold fuel issuing into hot air), which indicate the need for further validation of this model at high ambient pressures and temperatures. Contours of the progress variable indicated, however that the flame was not located in this region. Another reason why these high temperature regions occurred was when Fluent's recommended method of changing the discretization schemes in a step-by-step manner was followed. Basically, the accepted practice is to solve for a first order solution and then switch each equation to second order, one after the

other due to the complexity of achieving convergence in combustion simulations. However, this resulted in unphysical temperatures and non-convergence when the energy equation was switched to second order. In the final analysis, the reasons for the premature light up are not clear, the resolution seems to be to switch everything to second order at once and model the walls in the primary premixer as non-adiabatic when the preheat temperatures are high. This resulted in rather slow convergence, but did not cause unphysical temperatures in the premixer with resulting incorrect profiles of mixture fraction into the primary premixer – a critical factor in determining the entry equivalence ratio to the primary zone and subsequent heat release. It must be mentioned that none of the RANS simulations reached the convergence criteria of 1e-6 for energy. It was then that the focus was switched to the LES simulations and due to the small time step that was involved with its unsteady nature, sharp gradients did not evolve and the compressible fuel jets were correctly modeled. This may be one reason why the mean temperature in the RANS simulations in the primary zone was lower than the corresponding LES predictions.

4. Compressibility Effects in the PDF

Fluent, by default calculates the pdf look up table assuming incompressibility. This has the undesirable result of increasing the velocity of fuel jets in the primary premixer by almost 40 to 50 m/s above the right value of approximately 230 m/s. An animation of the mixing at the exit of premixing ducts, during the LES run, showed that the higher velocities caused the jets to mix incorrectly and produce stoichiometric pockets of air and fuel and has a direct impact on the emissions. By turning on this option in Fluent, the jet velocities are calculated using the ideal gas law and the resulting decrease in stoichiometric pockets was immediately evident. This effect is more apparent in the swirl injector passage (inner passage) than the swirl combustor passage (outer) due to the difference in the number and diameter of the fuel jets. Red regions represent rich zones which are at or above stoichiometric levels (Fig 7.23).

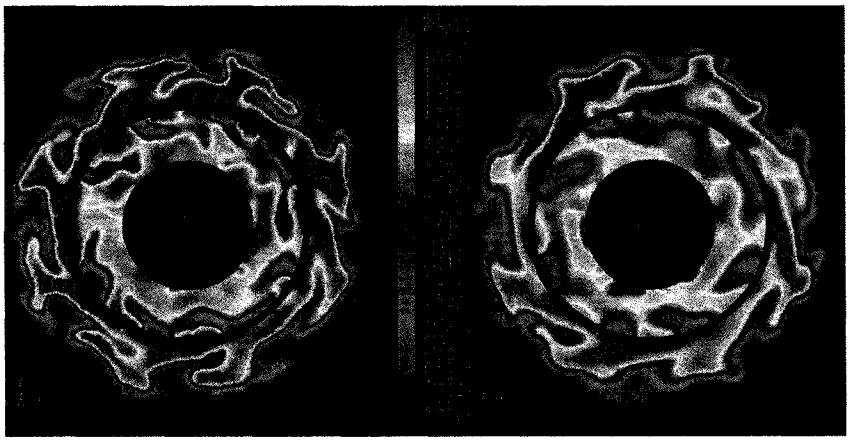

Fig 7.3.6: *(left)* Section of premixer exit without compressibility effects *(right)* with compressibility effects included. (LES simulation)

7.4 Qualitative Comparisons

Some qualitative comparisons are now made with earlier published and unpublished internal data on this combustor, but due to the different boundary conditions (though still at baseload), it is not possible to verify quantitative accuracy. In particular, earlier simulations done on this combustor consistently predicted a region of cold flow, downstream of the torch igniter, which was not observed experimentally and flame anchoring to the combustor walls with a flamelet model used by Eggels [74].

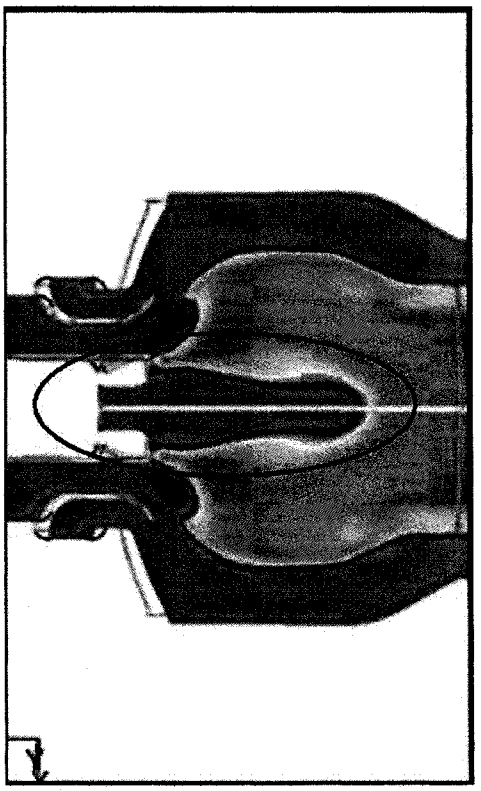

Fig 7.4.1: CFD RANS of primary zone (Internal Data, 2004)

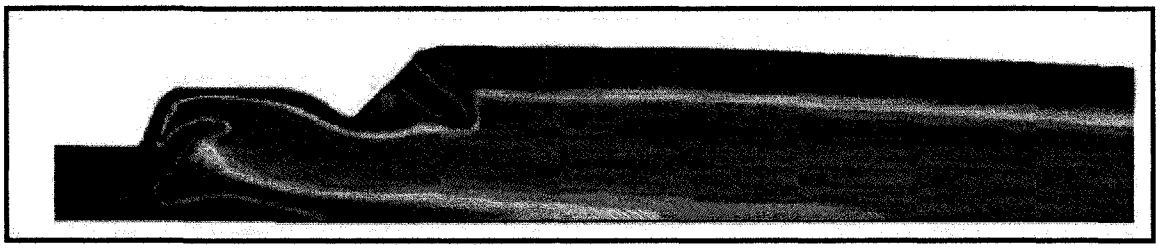

Fig: 7.4.2: FGM Model, Eggels [74].

The pictures show the cold flow, which is not physical. A black circle in Fig 7.4.1 marks this region. Fig 7.4.2, shows flame anchoring close to the wall.

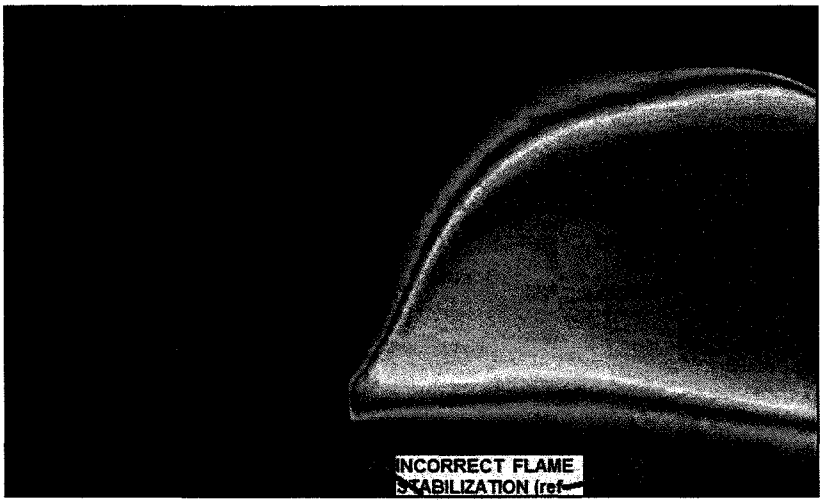

Fig 7.4.3: Current RANS Simulation of Primary (without torch swirl)

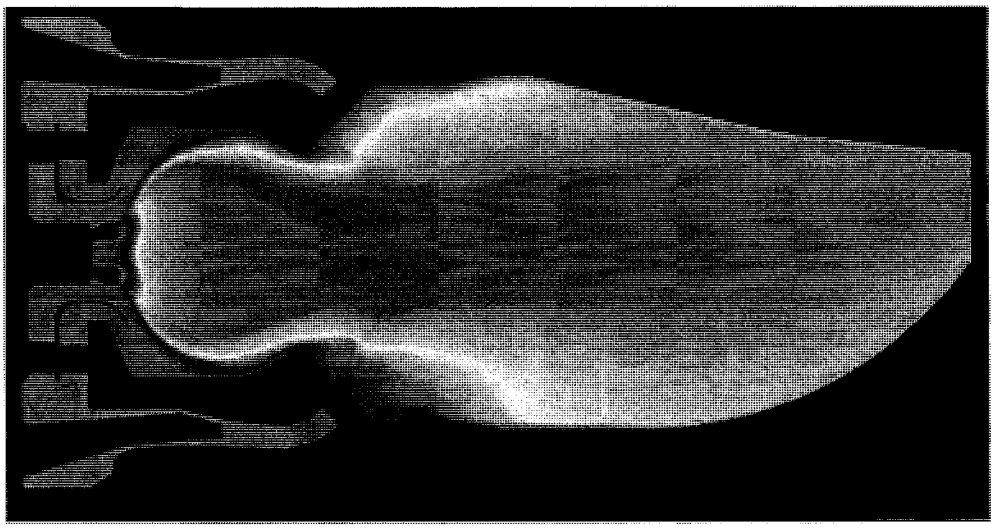

Fig 7.4.4: RANS simulation including torch swirl (short combustor).

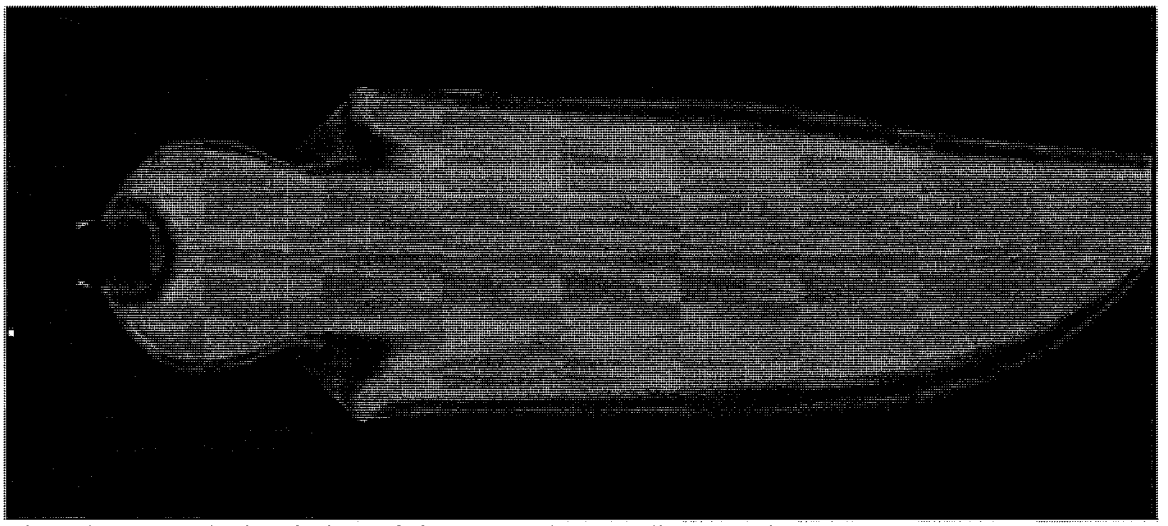

Fig 7.4.5: RANS simulation of 'long' combustor. (leaner mixture than short)

The first issue was primarily due to neglecting to swirl the torch igniter air[4]. It caused the torch flow (which is merely meant for purging the duct) to punch through the recirculation zone in the primary and predict a 'Type 1' flame as seen from Schmittel et. al. [6] and also the type shown in fig (c) of Xin et. al. [98]

[4] After communication with Eggels and others, it was decided to swirl the torch air.

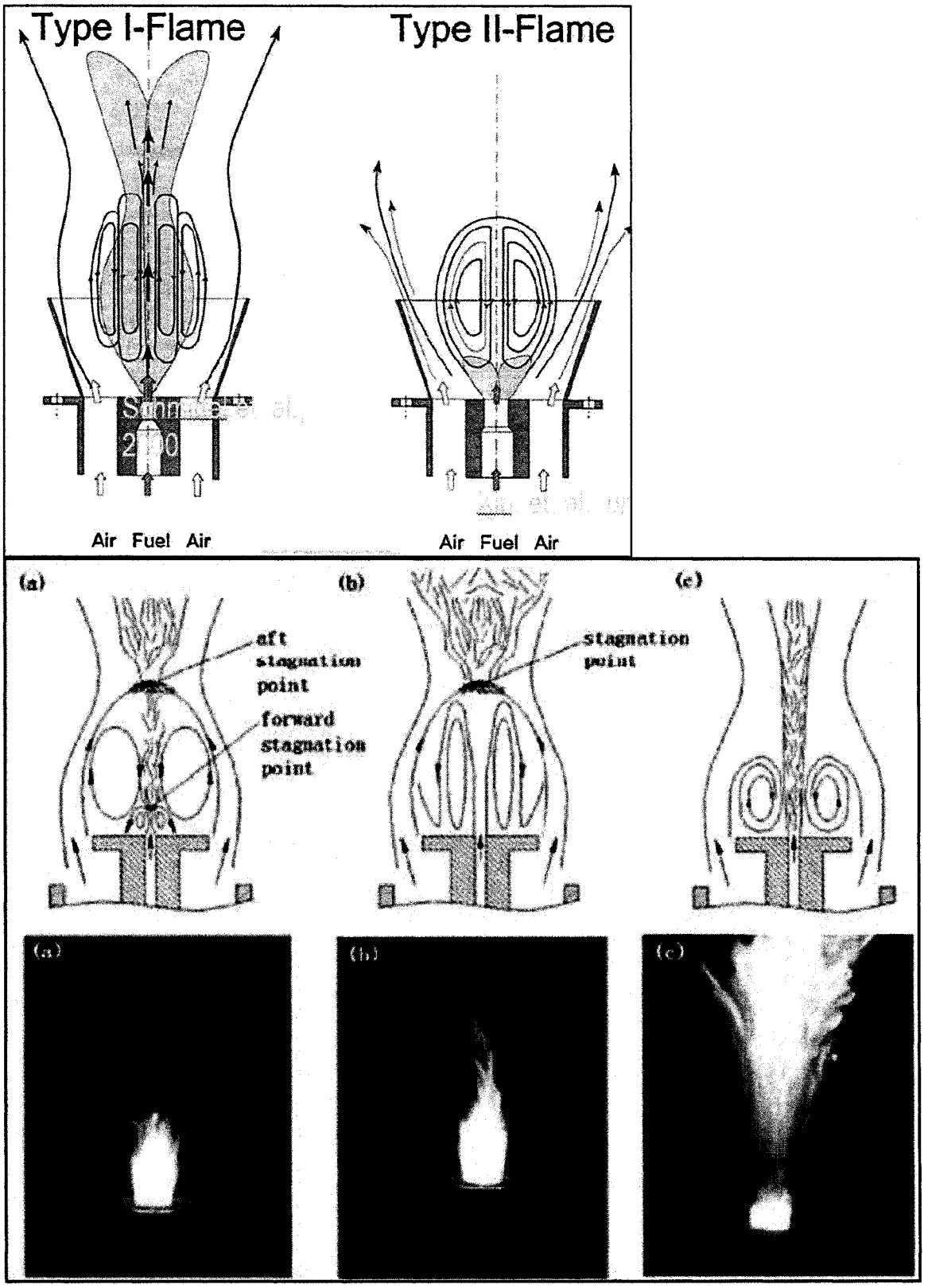

Fig 7.4.6: Effect of central injection *(top)* Schmittel et. al. *(bottom)* Xin et. al. [98]

It was found after consultation with design engineers, that the torch flow was indeed swirled through vanes and could range from a value between 30 to 40 degrees. Accordingly, this was implemented and the final result could be seen in Fig 6.2.12. The following vector plot indicates that the flame in the RB211 is of the Type 2 kind where there is backflow throughout the primary zone as seen in Fig 6.2.14. Thus the torch swirl directly affects the vortex-breakdown in the primary zone. It is well known that the formation of the vortex breakdown is extremely sensitive to perturbations, which is a reason why the inclusion or exclusion of the torch swirl seems to affect the fluid dynamics so much. It is notable that this seems to be due to the density differences between the hot recirculating air in the central vortex and the incoming cold air through the torch (central) injector.

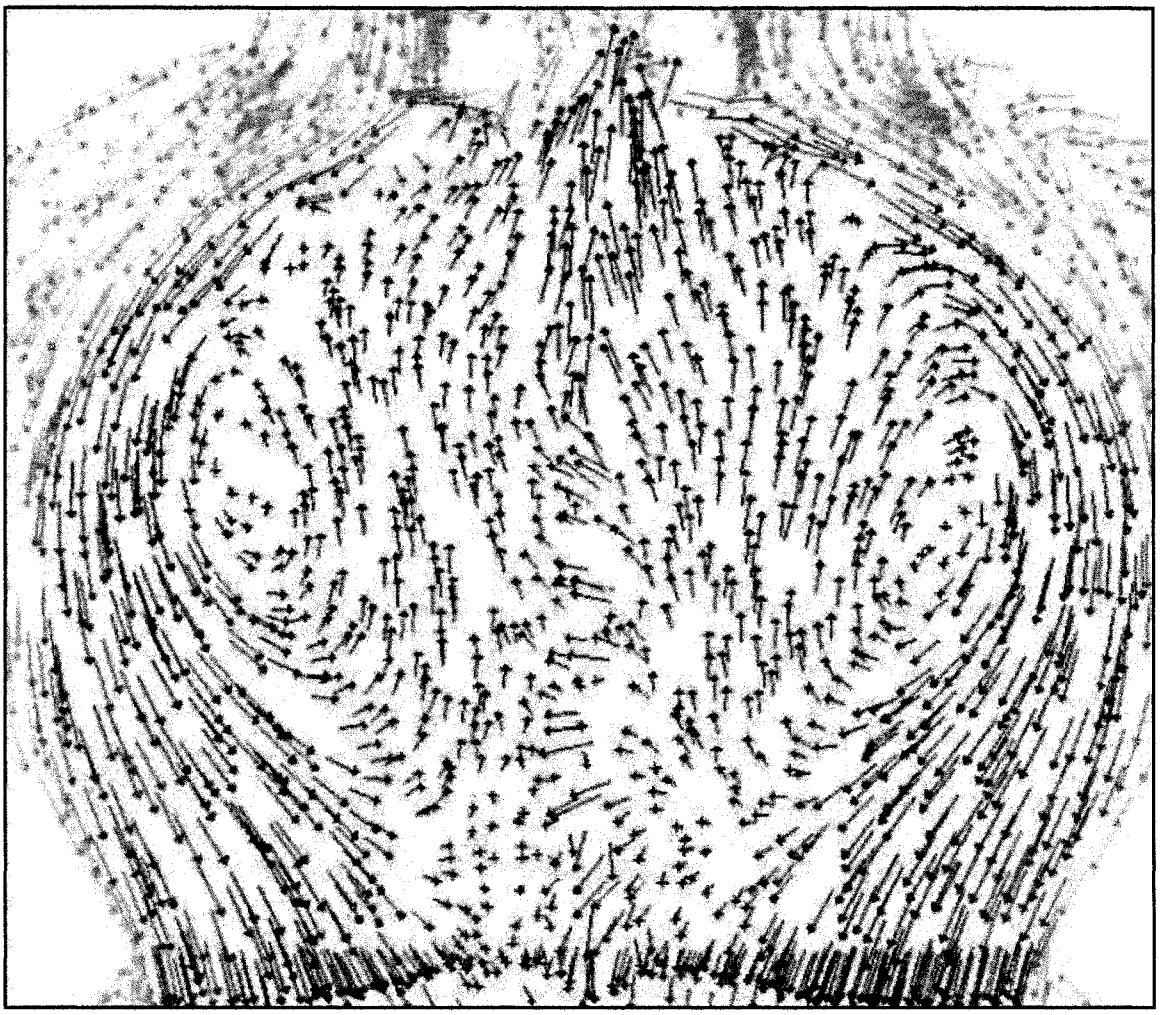

Fig 7.4.7: Vortex Breakdown in the primary zone with torch swirl included.

In summary of this section, it is clear that the flame does not anchor to the walls at any point and also does not experience a cold plug flow region in the center. Taken together with the discussion in the previous sections, with the modeling of cooling air, the critical strain rate, the constant A, as well as including non-adiabatic effects and compressibility in the pdf generation, it is believed that the final model is well representative of the actual flow-field. It is noteworthy that every single one of these factors has a direct impact on the emissions, though for

lack of time and computational resources, it is not possible to test each one's independent contribution. Suffice to say that it is necessary to pack in as much physics as possible in order to avoid unphysical results, especially when 'full' geometries are considered.

Comparison of RANS predictions with LES.

To be consistent with the data gathered from slices in the cold-flow region, it is of interest; to not only compare RANS with LES but also to note the effect of combustion on the flow-field in general. The sequence of pictures coloured by velocity magnitude, below in Fig 7.4.8 (a-e) were taken from the averaged LES and show the flow field is not that different from the cold flow analysis. The 'smoke rings' are better defined and mark the flame boundary. Within this boundary, hot products recirculate to meet the incoming fresh mixtures from the primary premixer. Figs 7.4.9 (a-k) show the comparison between LES (left) and RANS (right).

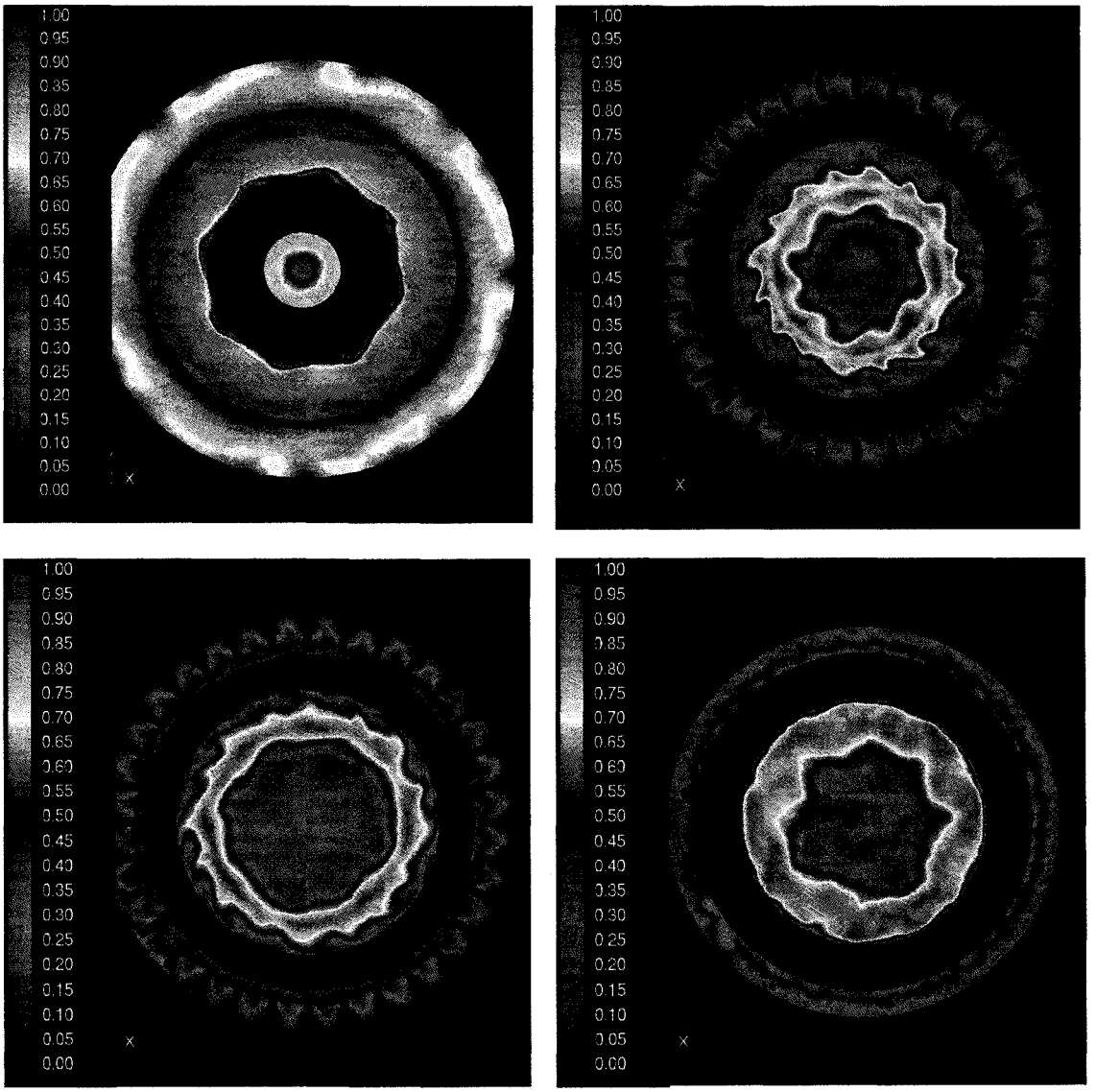

Fig 7.4.8 (a-e in clockwise): Evolution of initially separated counter swirling flows through the combustion chamber. Slices were taken at z= 42.7, 61.4, 73.5, 111.1 mm. Compare with Fig 5.2.5 for cold flow. Sequence is left to right, top to bottom.

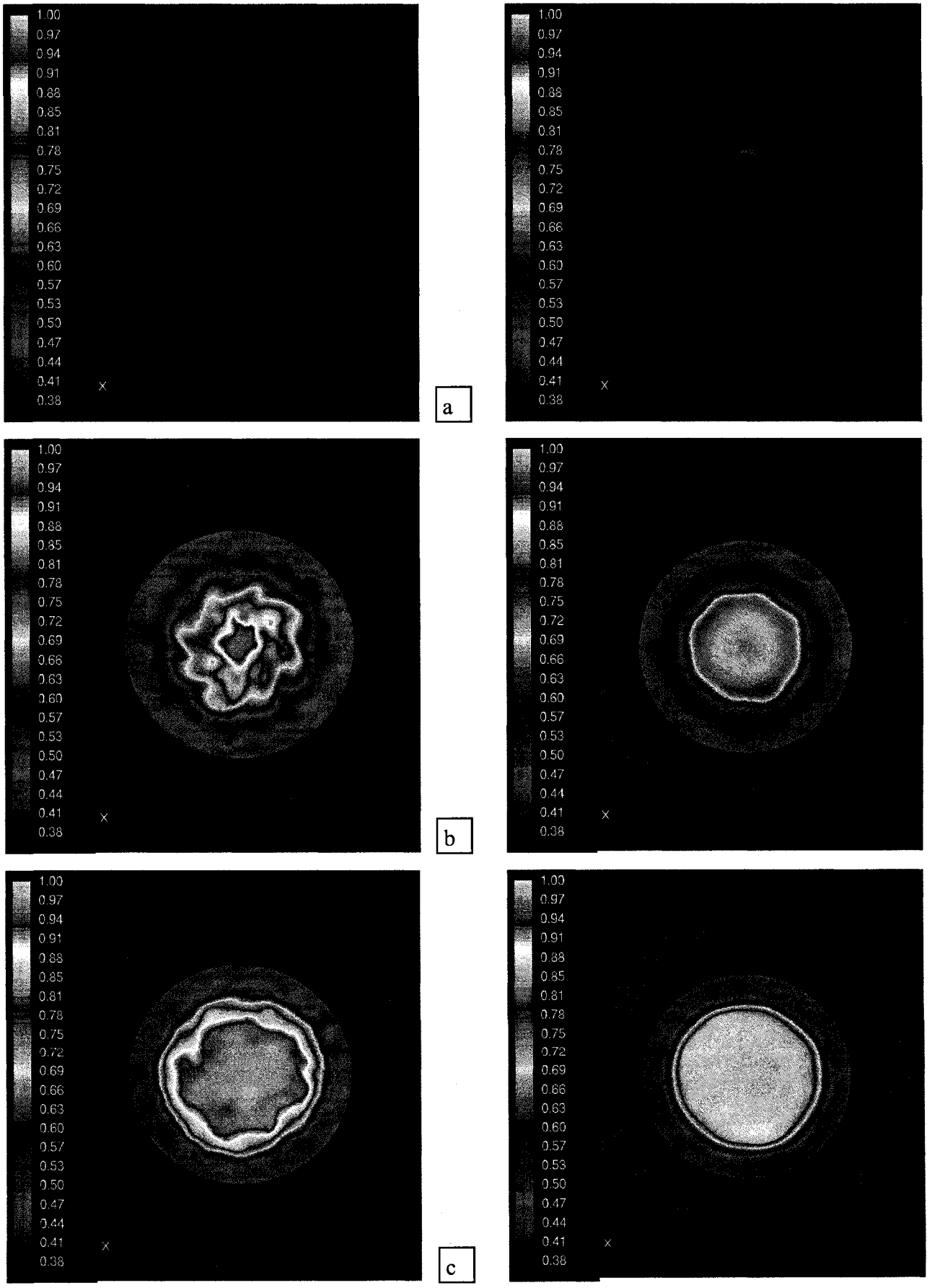
1.00
0.97
0.94
0.91
0.88
0.85
0.81
0.78
0.75
0.72
0.69
0.66
0.63
0.60
0.57
0.53
0.50
0.47
0.44
0.41
0.38
a
b
c

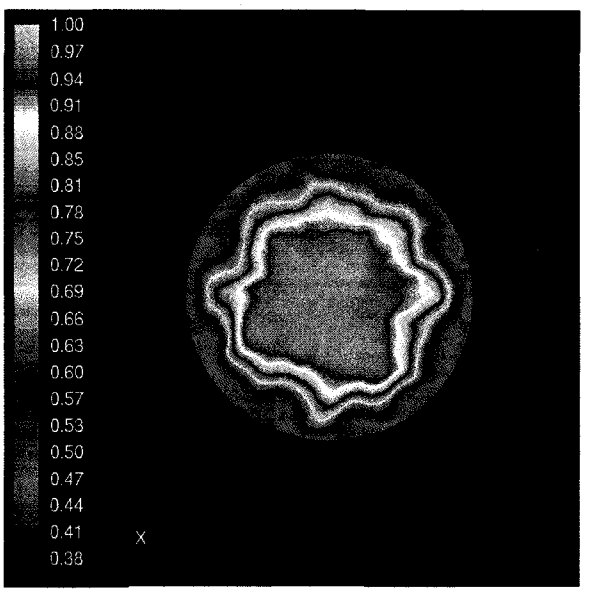
1.00
0.97
0.94
0.91
0.88
0.85
0.81
0.78
0.75
0.72
0.69
0.66
0.63
0.60
0.57
0.53
0.50
0.47
0.44
0.41
0.38
X

d

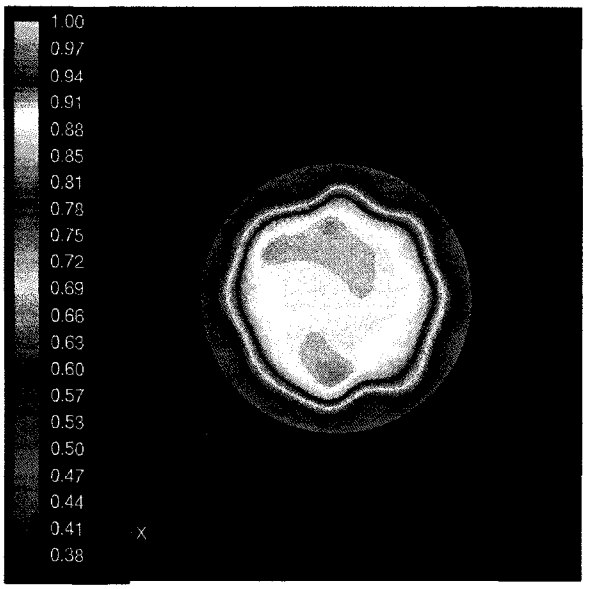
1.00
0.97
0.94
0.91
0.88
0.85
0.81
0.78
0.75
0.72
0.69
0.66
0.63
0.60
0.57
0.53
0.50
0.47
0.44
0.41
0.38
X

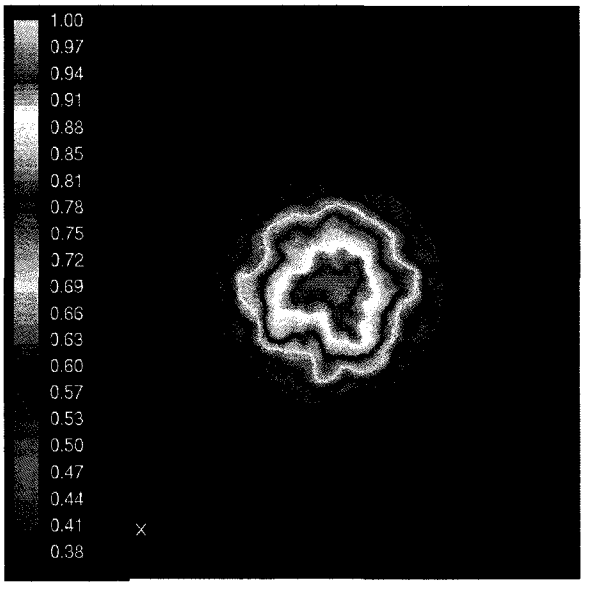
1.00
0.97
0.94
0.91
0.88
0.85
0.81
0.78
0.75
0.72
0.69
0.66
0.63
0.60
0.57
0.53
0.50
0.47
0.44
0.41
0.38
X

e

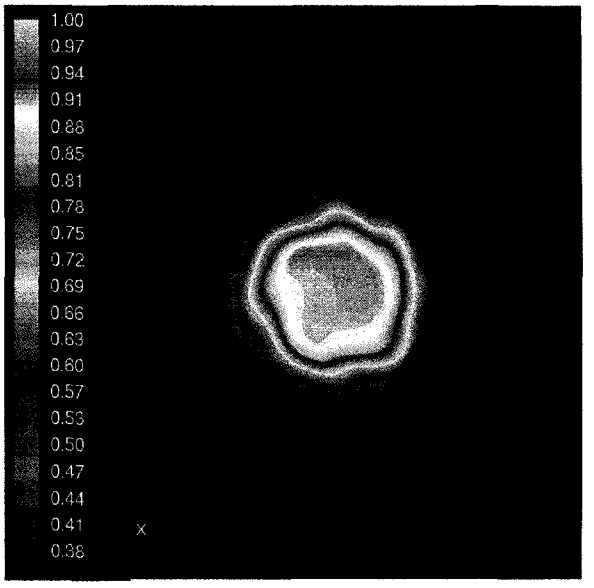
1.00
0.97
0.94
0.91
0.88
0.85
0.81
0.78
0.75
0.72
0.69
0.66
0.63
0.60
0.57
0.53
0.50
0.47
0.44
0.41
0.38
X

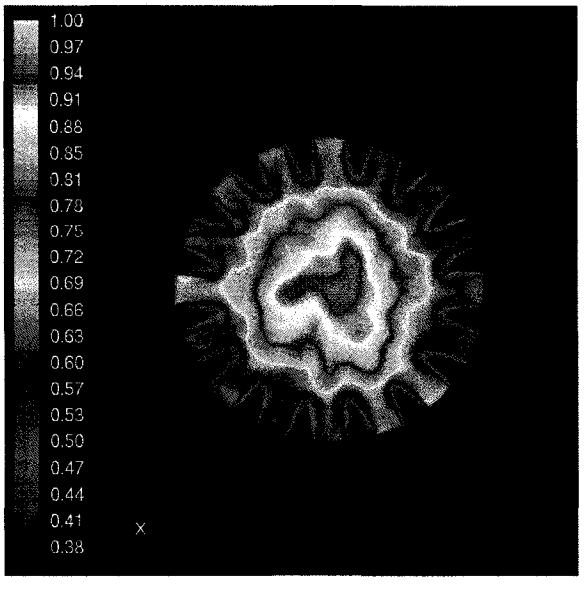
1.00
0.97
0.94
0.91
0.88
0.85
0.81
0.78
0.75
0.72
0.69
0.66
0.63
0.60
0.57
0.53
0.50
0.47
0.44
0.41
0.38
X

f

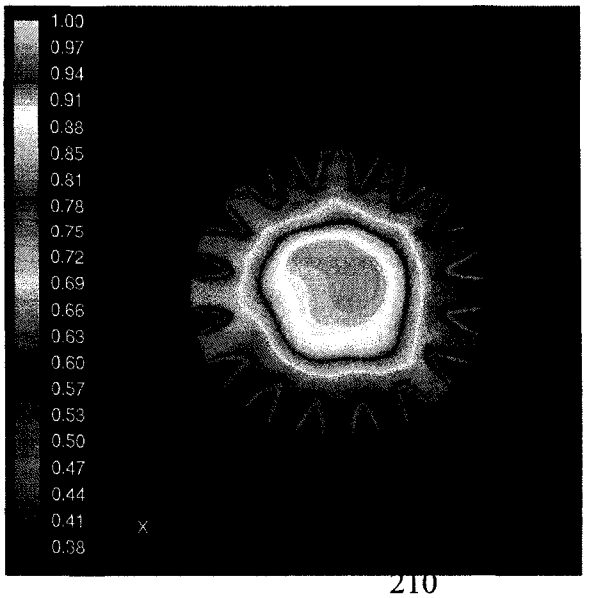
1.00
0.97
0.94
0.91
0.88
0.85
0.81
0.78
0.75
0.72
0.69
0.66
0.63
0.60
0.57
0.53
0.50
0.47
0.44
0.41
0.38
X

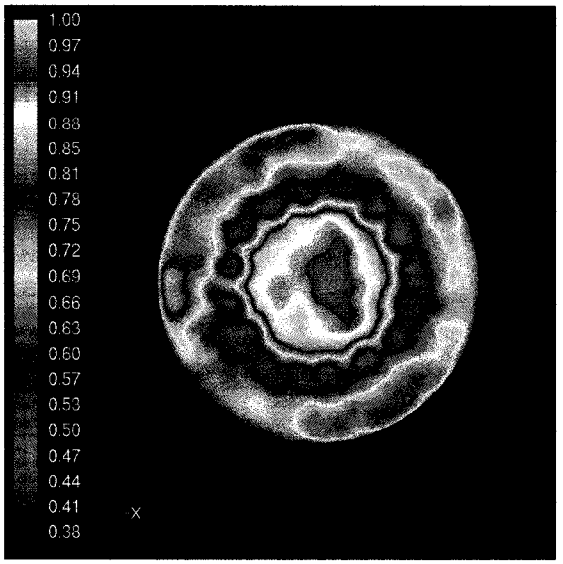
1.00
0.97
0.94
0.91
0.88
0.85
0.81
0.78
0.75
0.72
0.69
0.66
0.63
0.60
0.57
0.53
0.50
0.47
0.44
0.41
0.38
X

g

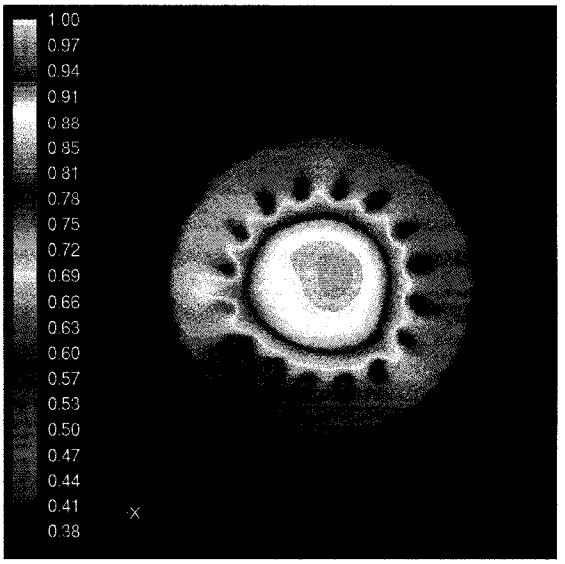
1.00
0.97
0.94
0.91
0.88
0.85
0.81
0.78
0.75
0.72
0.69
0.66
0.63
0.60
0.57
0.53
0.50
0.47
0.44
0.41
0.38
X

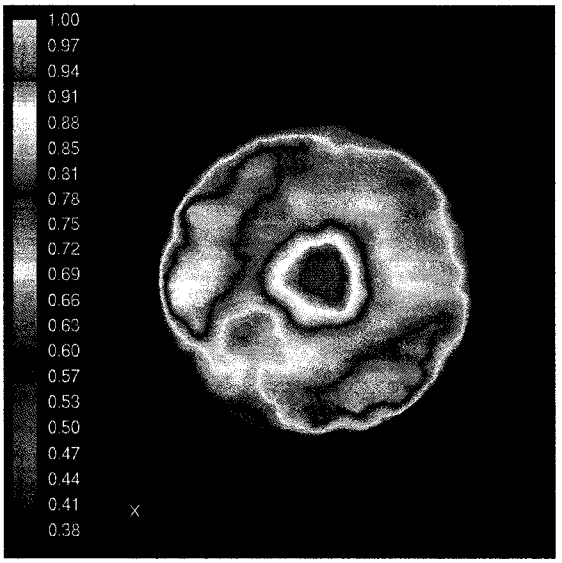
1.00
0.97
0.94
0.91
0.88
0.85
0.81
0.78
0.75
0.72
0.69
0.66
0.63
0.60
0.57
0.53
0.50
0.47
0.44
0.41
0.38
X

h

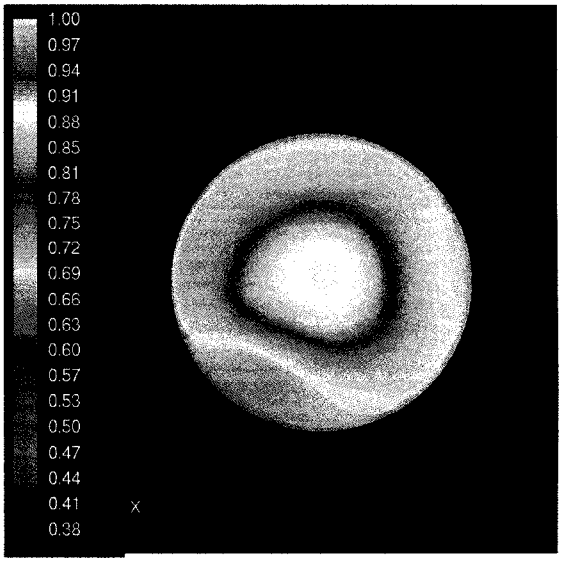
1.00
0.97
0.94
0.91
0.88
0.85
0.81
0.78
0.75
0.72
0.69
0.66
0.63
0.60
0.57
0.53
0.50
0.47
0.44
0.41
0.38
X

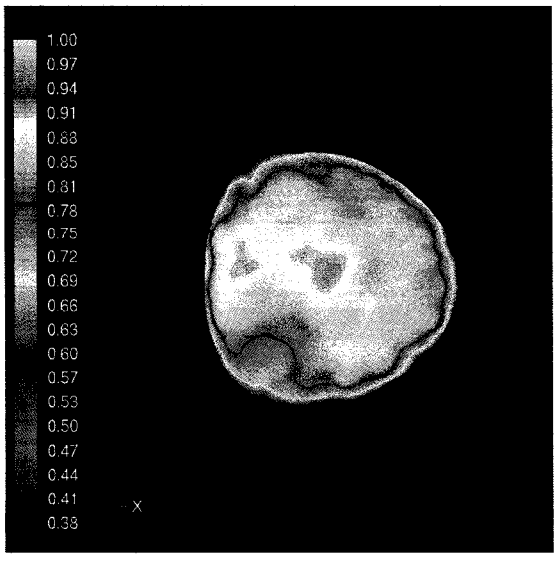
1.00
0.97
0.94
0.91
0.88
0.85
0.81
0.78
0.75
0.72
0.69
0.66
0.63
0.60
0.57
0.53
0.50
0.47
0.44
0.41
0.38
X

i

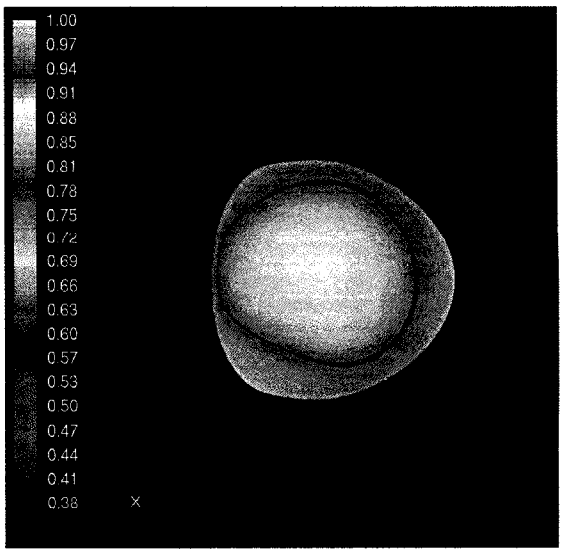
1.00
0.97
0.94
0.91
0.88
0.85
0.81
0.78
0.75
0.72
0.69
0.66
0.63
0.60
0.57
0.53
0.50
0.47
0.44
0.41
0.38
X

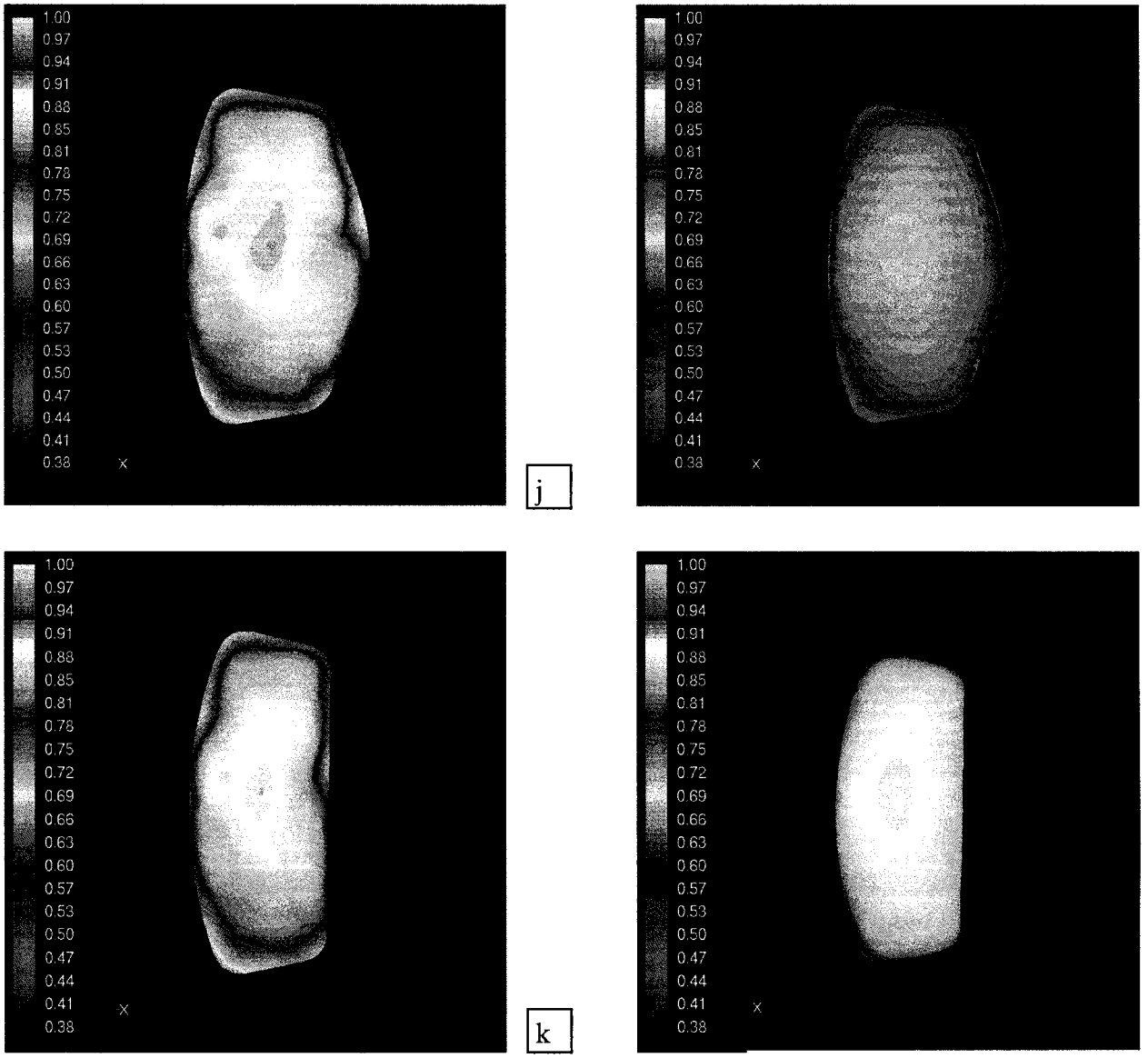

Fig 7.4.9 (a-k): Temperature contours at z (mm) = 42.7, 61.4, 73.5, 111.1, 150, 172, 200, 243, 333, 472, Outlet. ***Left Column: LES, Right Column: RANS***

It is clear that RANS calculations produce temperature fields that are lower than LES predictions. Some noteworthy features are the progress of the secondary jets in Fig 7.4.9 (f), (g) and (h). The RANS predictions do not show the flame to develop immediately on entrance but merge with the central flow. This can be seen in Fig 7.4.9(g) where the RANS picture shows the 'just-igniting' secondary

jet, where as the LES shows it to have ignited already no doubt ignited by the recirculation zones found between the secondary windows, which ingest high temperature products from the primary. This has been observed in an animation and provides a great deal of insight into the highly complex events that happen in the interface between the primary and secondary zones. Fig 7.4.9 (h) LES shows a clear distinction between the central and secondary flames made clear by the change in the colormap that has been designed to demarcate the main flame zones. No such distinction can be seen in the corresponding RANS prediction. This carries over into the higher temperatures for RANS at the exit in Fig 7.4.9 (j) and finally the outlet in (k) whereas the earlier ignition predicted by the LES shows the temperature to come down earlier. This is perhaps the reason why the RANS predicts lower CO emissions compared to the LES.

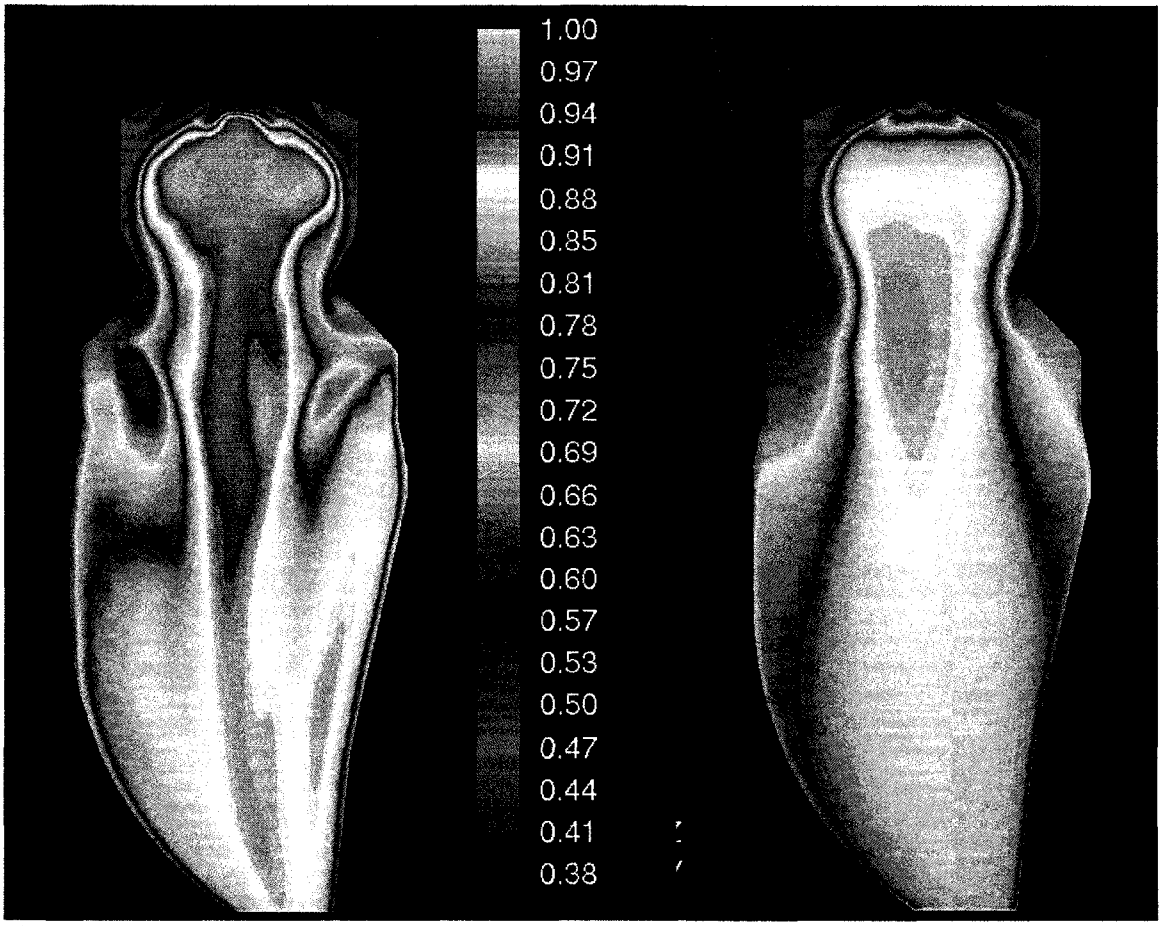

Fig 7.4.10: Temperature Contours on a slice between the secondary windows. (*left:* LES, *right:* RANS)

temperature contours steady/averaged flows in the combustor. It is clear that RANS does not predict a flame immediately downstream of the secondary injectors. This can be explained by the correct mixing predicted by LES at this point. The Vorticity structures seen in Figs 7.4.13 and 7.4.14 explain the existence of a flame near the secondary injectors.

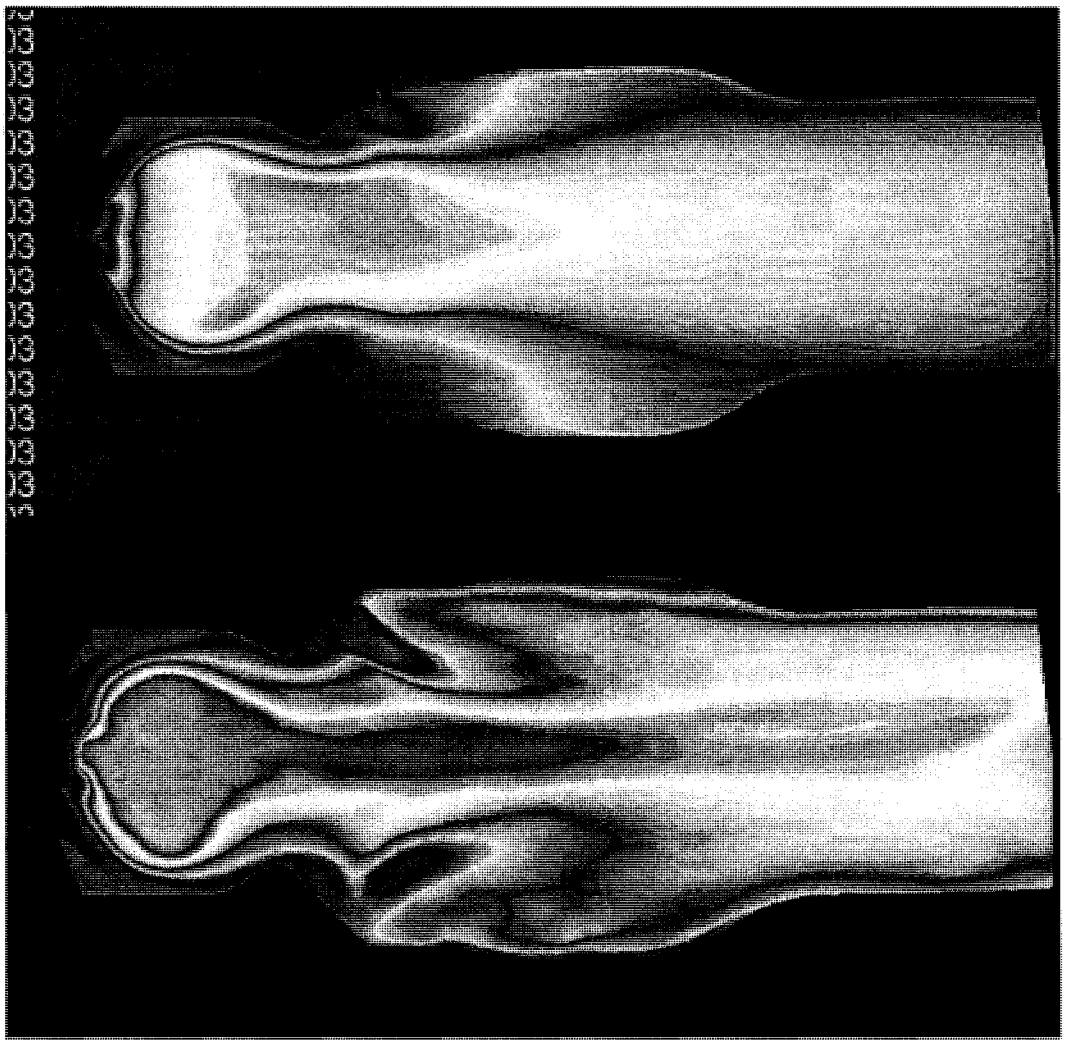

Fig 7.4.11: Slice through the secondary windows (*top* RANS, *bottom* LES)

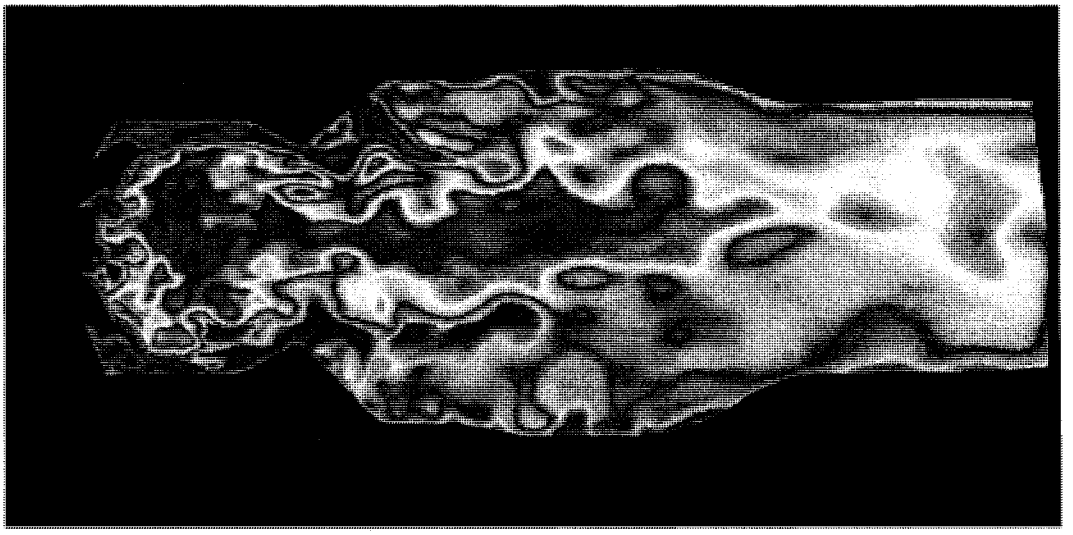

Fig 7.4.12: Instantaneous snapshot of temperature contours – LES.

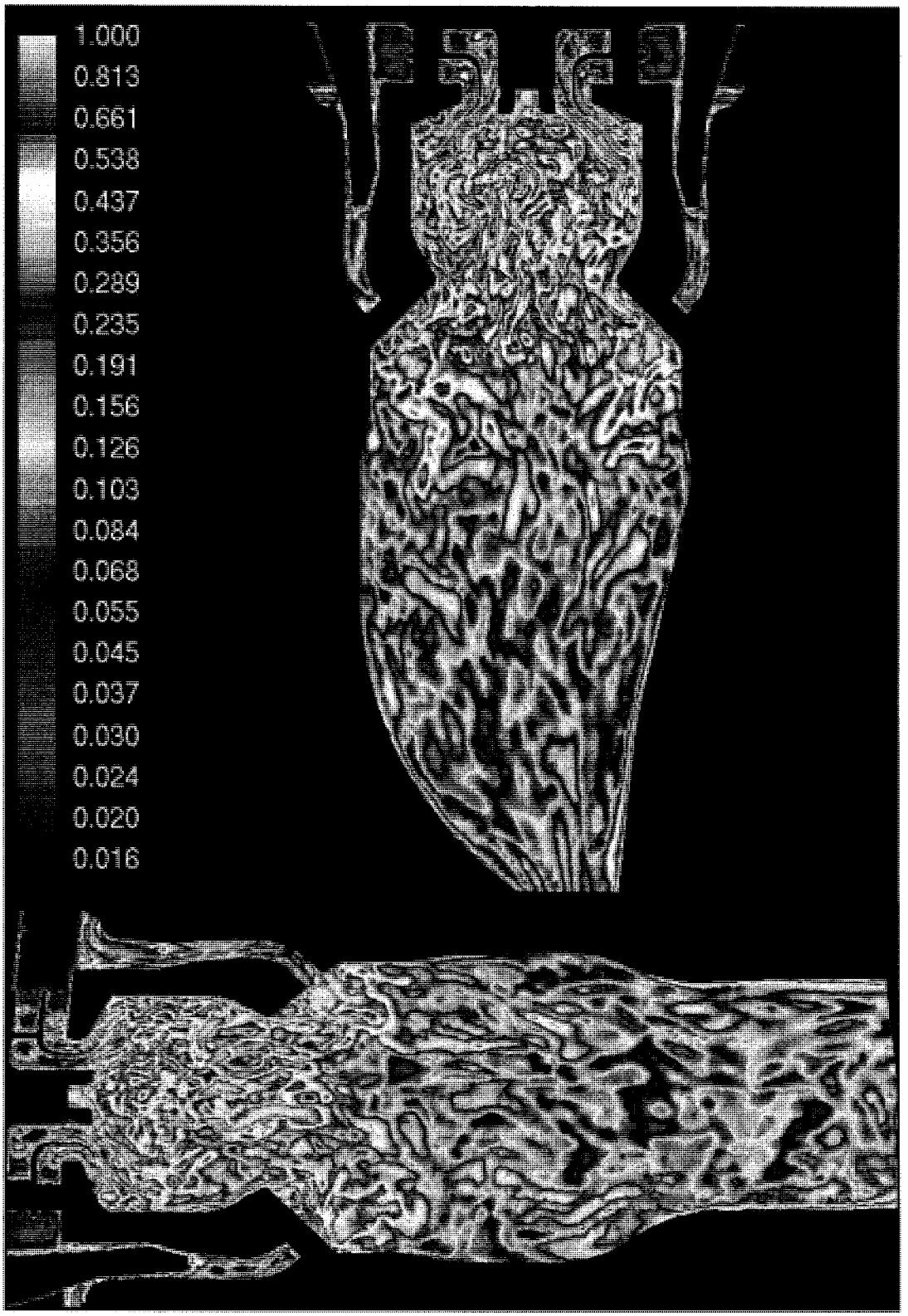

Fig 7.4.13: Vortical structures showing intense mixing in primary and high secondary mixing near secondary feed tubes. (Instantaneous LES, log scale).

As mentioned earlier, the intense mixing between the secondary windows interacts with the flow of products from the primary zone and this interaction can be seen in Fig 7.4.11 (bottom). The much more uniform secondary zone confirms the 'plug-flow' nature of mixing in this region. Fig 7.4.14 shows the vortices that characterize the mixing between the secondary windows.

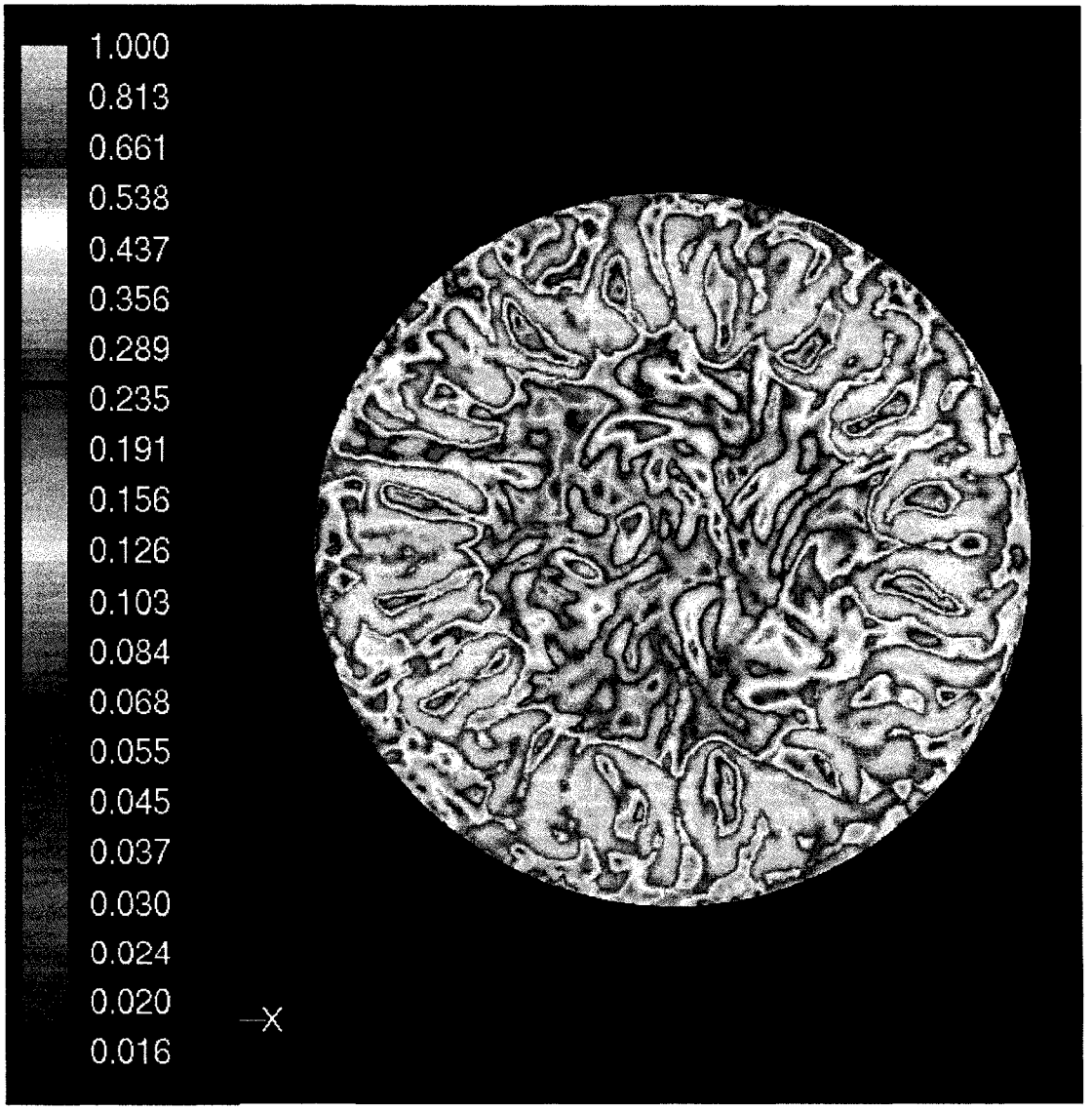

Fig 7.4.14: Vortical structures circumferential, near the walls where the secondary premix ducts eject air-fuel mixture into the secondary zone. This plane is slightly downstream of this position to show the difference between the primary and secondary mixing.

8. CONCLUSIONS

Emissions predictions were carried out using LES and RANS on an industrial gas turbine combustor at its typical operating conditions of high pressure and preheat. Good agreement was achieved in the case of NO and CO predictions and provide basis for establishing quantitative trends. The methodology used has been validated with experimental data and provides insight into the detailed mixing processes involved that directly impact emissions. Recently developed models, as well as greater access to computational resources, has shown that combustion simulations can be carried out with a much higher degree of accuracy than possible until recent years. However, the fundamental complexities remain and combustion modeling is likely to remain a task requiring expert knowledge of the fundamental processes. The study confirms that there isn't a single approach to the task of modeling turbulence-combustion phenomena and is especially difficult when the case of partial premixing is considered. Emissions predictions are especially sensitive to boundary conditions and model constants, the former often difficult to implement when simplified geometries are considered and the latter, a weakness of empirical models and dimensional arguments used in formulating the model. Boundary conditions for full geometries, such as the one considered in this thesis are easier to implement, but the final analysis is not amenable to smaller computers and

require supercomputing access. Fundamental research is required in the case of evaluating scalar dissipation and it is clear that the unsteadiness and fluctuations of this parameter must be considered since NOx emissions depend heavily on the history of mixing. Experimental research is also required in the case of determining turbulent flame speeds, critical stretch rates for flames of different fuels to aid the modeling using Zimont's modified partially premixed model. Other issues that were identified were the partially premixed model's tendency to overly quench the main flame when secondary cooling air is introduced as a cooling mass flux. Considering all this, a step-by-step approach is required to finally arrive at the best predictions possible given the tools available. Post-processing for CO and NOx still remains as a separate step and bears further investigation. The modeling of the NOx source term in the case of the NOx post-processing method is again a result of experimental evidence rather than first principle analysis. The reasons for this are obvious: numerous intermediate mechanisms exist to describe the NOx species production and tradeoffs are made between full and reduced order mechanisms. Such tradeoffs frequently involve a change of combustion regime (premixed, non-premixed, partially premixed), ambient conditions, fuel composition and concentration. It also involves the degree of fidelity required to predict certain combustion events. For example, the prediction of auto-ignition, ignition delay and other highly transient phenomena

as well as simulation of rich mixture combustion involves the consideration of many more (hundreds more) radicals than the prediction of a steady combusting flow. And so, the vast body of experimental evidence has to be correlated in order to arrive at 'global' reactions that dominate the production/destruction of NOx and it is the task of the combustion modeller to carefully select those that are applicable to his model rather than use these mechanisms as a black box.

Industry requirements have been observed to demand more as recent legislation has spurred on the development of combustors operating at 'threshold' levels of autoignition and blowout. Of special importance is the case of lean-extinction and flashback, which is a feature of lean-premixed, low emissions technology and requires very detailed modeling if such events are to be predicted correctly. Full engine rig testing still remains the only way to guarantee fuel acceptability. However, the method used in this thesis provides enough confidence to apply it to a parametric analysis of fuels for emissions predictions and can be considered an important step in guiding the selection of fuels. The same resources were used for LES predictions as little as two years ago for RANS predictions. The use of polyhedral meshes, with least squares interpolation cut down the sizes while retaining a degree of accuracy superior to that of equivalent tetrahedral meshes. LES performed on these meshes validate the use and application of these

timesaving topologies to industrial applications. It is well established that LES is likely to be adopted as a routine tool, in view of its remarkably accurate predictions even with relatively coarse meshes. A natural extension of this work is to introduce the additional complexity of multiphase combustion regimes for example, those that involve liquid fuel sprays. However, this would include the need for variable Schmidt and non-unity Lewis numbers, thus indicating the need for generalizing the flamelet equations, if the flamelet approach is considered. A weakness of the mixture fraction method is that at most, two different fuels can be used as within a joint probability density function framework – at which point the dimensionality of the pdf increases and can no longer be said to be efficient. Finite-rate combustion models like the transported pdf methods which no longer rely on a presumed distribution of the mixture fraction fluctuations, are not viable at this point for practical industry geometries, though excellent results have been obtained for simpler configurations. It is to be expected however, that such methods, with better algorithms can be applied to simplified geometries of real combustors with success, since they can include complex chemical kinetic mechanisms of the scale required for prediction of events like autoignition. Other fields like acoustic instability analysis and chemical reactor network (CRN) developments, which rely on extra-CFD tools, are best served by coupling them to the LES methods described here since the

mixing characteristics are of great importance for CRN flow-splits and the unsteadiness is characteristic of acoustic analysis. RANS methods have clearly shown themselves to be incapable of determining anything beyond the mean fields. While, for the industry, it has usually been enough to obtain these, newer combustion methods have drastically increased the level of detail that must be obtained from CFD simulations as subtler effects of acoustic instabilities, transient events, fuel-flexibility implications play an increasingly important role in determining the trade-off between achieving emissions targets and technological limits. Some of those limits on design considerations may be imposed due to the difficulty faced by instrumentation in obtaining true pictures of what happens in the environmentally harsh heart of the combustor. It is here that the true strength of simulation of turbulent combustion shows itself in providing a level of access that otherwise cannot be obtained.

The main conclusion reached from this work, is that LES, with polyhedral meshing capabilities, is able to reproduce not only qualitative trends, but also quantitative data on emissions predictions. While simulation of more complex events like autoignition, is still some way off, due to combustion model complexities, it is well established that RANS methods carried out on very dense meshes can be increasingly replaced by high quality LES simulations at the same

expense as, say, an RSM simulation. It is especially attractive to the simulations of separated flows as found in gas turbine combustors since wall effects are not of overly great concern, except perhaps when quenching due to wall effects is required. This however is secondary to simulating acoustic instabilities and emissions predictions of flexible fuel gas turbine combustors. The time-dependent nature of LES, is suited to gauging flashback and blowout with unsteady boundary conditions. The notable success achieved overall, ensures the safe adoption of LES, perhaps with more experimental evidence of velocity fields for complex combustors, into standard industry practice.

Academically, the main contribution of this thesis is the validation of the LES/emissions post-processing method for a practical combustor. The limitations of some of the sub-models, are also brought out clearly in this context and provide basis for further fundamental research. For industry, the main contribution of this thesis is the proven justification for adopting higher fidelity models. Based on this work, the scope has been extended to include a fleet of combustors with varying boundary conditions and fuel compositions.

REFERENCES

1. Analysis and Modeling Group, National Climate Change Process, *'Canada's Emissions Outlook: An Update'*, December 1999.
2. Döbbeling et. al., *'25 Years of BBC/ABB/Alstom Lean Premix Combustion Technologies.'* Journal of Engineering for Gas Turbines and Power, January 2007, Volume 129, Issue 1, pp. 2-12.
3. Kim W-W., Syed S., et. al., *'Large Eddy Simulation Needs For Gas Turbine Combustor Design', AIAA-2004-0331.* 42nd AIAA Aerospace Sciences Meeting and Exhibit, 5- 8 January 2004, Reno, Nevada.
4. Sommerer et. al., *'Large eddy simulation and experimental study of flashback and blow-off in a lean partially premixed swirled burner'*, Journal of Turbulence, Volume 5, Number 1, March 2004 , pp. 37-37(1).
5. Lucca-Negro O., O'Doherty T., *'Vortex Breakdown: A Review'*, Progress in Energy and Combustion Science, Volume 27, Number 4, 2001, pp. 431-481(51).
6. Schmittel et. al., *'Turbulent Swirling Flames: Experimental Investigation Of The Flow Field And Formation of Nitrogen Oxide'*, Proceedings of the Combustion Institute, Volume 28, 2000, pp. 303–309.
7. Biagioli, Fernando (2006) *'Stabilization mechanism of turbulent premixed flames in strongly swirled flows'*, Combustion Theory and Modelling, 10:3, pp. 389 – 412.
8. Mahesh et. al., *'Large-Eddy Simulation of Reacting Turbulent Flows in Complex Geometries'*, Journal of Applied Mechanics, May 2006, Volume 73, Issue 3, pp. 374-381.
9. Schmitt et. al., *'Large-eddy simulation and experimental study of heat transfer, nitric oxide emissions and combustion instability in a swirled turbulent high-pressure burner'*, Journal of Fluid Mechanics, 2007, vol. 570, pp. 17-46.
10. Selle et. al., *'Compressible large eddy simulation of turbulent combustion in complex geometry on unstructured meshes'*, Combustion and Flame, Volume 137, Issue 4, June 2004, pp. 489-505.
11. Wang et. al., *'Large-eddy simulations of gas-turbine swirl injector flow dynamics'*, Journal of Fluid Mechanics, 2007, vol. 583, pp. 99–122.
12. Roux et. al., *'Studies of mean and unsteady flow in a swirled combustor using experiments, acoustic analysis, and large eddy simulations'*, Combustion and Flame, Volume 141, Issues 1-2, April 2005, Pages 40-54.
13. Sengissen et. al., *'Large eddy simulation of piloting effects on turbulent swirling flames'*, Proceedings of the Combustion Institute, Volume 31, Issue 2, January 2007, Pages 1729-1736.

14. Magnussen B. F., Hjertager B.H., *'On mathematical models of turbulent combustion with special emphasis on soot formation and combustion'.*, Proceedings of 16th Symposium (International) on Combustion, The Combustion Institute, 1976, pp.719-29.
15. Barths, H., et. al., *'Simulation of Pollutant Formation in a Gas-Turbine Combustor Using Unsteady Flamelets'*, Proceedings of 16th Symposium (International) on Combustion, The Combustion Institute, 1998, pp.1841-1847.
16. Pitsch H. and Ihme M., *'An Unsteady/Flamelet Progress Variable Method for LES of Nonpremixed Turbulent Combustion'* 43rd AIAA Aerospace Sciences Meeting and Exhibit, 10-13 January 2005, Reno, Nevada.
17. Bilger R. W. et. al., *'Paradigms in turbulent combustion research'*, Proceedings of the Combustion Institute, Volume 30, Issue 1, January 2005, pp. 21-42.
18. Caracciolo L., Rubini P. A., *'Validation of a Partially Premixed Combustion Model for Gas Turbine Applications'*, GT2006-90956, Proceedings of GT2006, ASME Turbo Expo 2006: Power for Land, Sea and Air, May 8-11, 2006, Barcelona, Spain.
19. Lumley J.L. and Yaglom A. M., *'A Century of Turbulence'*, Flow, Turbulence and Combustion, August 2001, Volume 66, pp 241-286.
20. Hanjalic K., *'Will RANS Survive LES? A View of Perspectives'*, Journal of Fluids Engineering, September 2005, Volume 127, Issue 5, pp. 831-839.
21. Shih T.-H., et. al., *'A new k-ε eddy viscosity model for high reynolds number turbulent flows*, Computers & Fluids, Volume 24, Issue 3, March 1995, pp. 227-238.
22. Yahkot V. and Orszag S. A., *'Renormalization group analysis of turbulence I. Basic theory'*, Journal of Scientific Computing, Volume 1, Number 1, March 1986, pp 3-51.
23. Fluent User Manual (version 6.3.26).
24. Piomelli U., *'Large-eddy simulation: achievements and challenges'*, Progress in Aerospace Sciences, Volume 35, Number 4, May 1999, pp. 335-362(28).
25. Pitsch H., *'Large-eddy simulation of turbulent combustion'*, Annual Review of Fluid Mechanics, January 2006, Volume 38, pp. 453-482.
26. Smagorinsky, J., *'General circulation experiments with the primitive equations, I, The basic experiment'*, Monthly Weather Review, 91, pp. 99-152, 1963.
27. Lilly D. K., *'The representation of small-scale turbulence in numerical simulation experiments'*, Proceedings of the IBM Scientific Computing Symposium on Environmental Sciences (Yorktown Heights, New York), 1967, editor: H. H. Goldstine, IBM form no. 320-1951, p 195.

28. Deardorff, J.W., *'Three-dimensional numerical study of neutral and unstable planetary boundary layers'*. Boundary-Layer Meteorology, 1974, Volume 7, Number 1, pp. 81-106.
29. Pope S.B., *'Ten questions concerning the large-eddy simulation of turbulent flows'*, March 2004, New Journal of Physics, Volume 6, 35.
30. Schumann U., *'Subgrid scale model for finite difference simulations of turbulent flows in plane channels and annuli'*, Journal of Computational Physics, Volume 18, Issue 4, August 1975, pp. 376-40.
31. Leonard A., *'Energy Cascade in Large-Eddy Simulations of Turbulent Fluid Flows'*, Advances in Geophysics, Volume 18A, 1974, p.237.
32. *Large-Eddy Simulations of Complex Engineering and Geophysical Flows*, Eds. B. Galperin and S. A. Orszag, Cambridge University Press, 1993, pp. 441-454.
33. Germano et. al., *'A dynamic subgrid-scale eddy viscosity model'*, Physics of Fluids A, July 1991, Volume 3, Issue 7, p. 1760-1765.
34. Jiang L-Y and Campbell I., *'Reynolds analogy in combustor modeling'*, International Journal of Heat and Mass Transfer, February 2008, Volume 51, pp. 1251-1263.
35. Lilly, D. K., *'A Proposed Modification of the Germano Subgrid-Scale Closure Method'*, Physics of Fluids A, 1991, Volume 4, No. 3, pp. 633-635.
36. Iaccarino G., *'Predictions of a Turbulent Separated Flow Using Commercial CFD Codes'*, Journal of Fluids Engineering, December 2001, Volume 123, pp. 819-828.
37. Westbrook, C. K. and Dryer, F. L., *'Simplified Reaction Mechanisms for the Oxidation of Hydrocarbon Fuels in Flames'*, Combustion Science and Technology, December 1981, Volume 27, pp. 31–43.
38. Peters, N. and Rogg, B., *'Reduced Kinetic Mechanisms for Applications in Combustion Systems'*, 1993, Springer Verlag, Berlin, pp. 58-75.
39. Nicol D. G., et. al., *'The Importance of the Nitrous Oxide Pathway to NOx in Lean-Premixed Combustion'*, Journal of Engineering for Gas Turbines and Power, January 1995, Volume 117, Issue 1, pp. 100-111.
40. Novosselov I.V. and Malte P. C., *'Development and Application of an Eight-Step Global Mechanism for CFD and CRN Simulations of Lean-Premixed Combustors'*, Journal of Engineering for Gas Turbines and Power, March 2008, Volume 130, Issue 1, pp. 021502-1 to 021502-9.
41. Bissières D. et. al., *'Large Eddy Simulation predictions and validations of a gas turbine combustion chamber'*, CERFACS, Report Number: TR/CFD/05/29.
42. Bell J., et. al., *'Numerical Simulations of Shock-Induced Mixing and Combustion'*, presented at the 19th International Colloquium on the

Dynamics of Explosions and Reactive Systems, July 27-August 1, Hakone, Kanagawa, Japan, 2003.
43. Spalding D. B., *'Mixing and chemical reaction in steady confined turbulent flames'*, Symposium (International) on Combustion, Volume 13, Issue 1, 1971, pp. 649-657.
44. Peters N., *'Turbulent Combustion'*, Cambridge University Press, Aug 15 2000, ISBN 0 521 66082 3.
45. Singer M. A., Pope S.B., *'Exploiting ISAT to solve the reaction–diffusion equation'*, Combustion Theory and Modelling, April 2004, Volume 8, pp 361-383.
46. Le Clercq P., et. al., *'Liquid Fuel Flameless Combustion RANS Simulation'*, GT2008-50552, Proceedings of ASME Turbo Expo 2008: Power for Land, Sea and Air, GT2008, June 9-13, 2008, Berlin, Germany.
47. Sivathanu Y. R., Faeth G. M., *'Generalized State Relationships for Scalar Properties in Non-Premixed Hydrocarbon/Air Flames'*, Combustion and Flame, 1990, Volume 82, pp. 211-230.
48. Kim J. S., Williams F. A., *'Extinction of Diffusion Flames with Non-Unity Lewis Number'*, 1997, Journal of Engineering Mathematics, Volume 31, pp. 101-118.
49. Polifke W., et. al., *'Modeling of Inhomogeneously Premixed Combustion With an Extended TFC Model'*, Journal of Engineering for Gas Turbines and Power, January 2002, Volume 124, pp. 58-65.
50. Biagioli et. al., *'Development and Validation of a Turbulent Combustion Model for Imperfectly Premixed Reactants'*, unpublished data obtained through private communication.
51. Charles D. Pierce, *'Progress Variable Approach for Large Eddy Simulation of Turbulent Combustion'*, PhD Thesis, Stanford University, June 2001.
52. Riesmeier E., et. al., *'Flamelet Modeling of Pollutant Formation in a Gas Turbine Combustion Chamber Using Detailed Chemistry for a Kerosene Model Fuel'*, Journal of Engineering for Gas Turbines and Power, October 2004, Volume 126, pp. 819-905.
53. Wood J. P., *'Lean premixed combustion models at elevated pressure for the gas turbine.'*, Ph.D. thesis, 2004, Cranfield University, UK.
54. Biagioli, private communication, 18/2/2008.
55. Bray K., et. al., *'Role of the progress variable in models for partially premixed turbulent combustion'*, Combustion and Flame, March 2005, Volume 141, pp. 431–437.
56. Zimont V. L., *'Gas Premixed Combustion at High Turbulence. Turbulent Fame Closure Combustion Model'*, Experimental Thermal and Fluid Science, 2000, Volume 21, pp. 179-186.

57. Bourque et. al., *'Effect Of Higher-Order Hydrocarbons on Methane-Based Fuel Chemistry at Gas Turbine Pressures'*, GT2007-28039, Proceedings of GT2007, ASME Turbo Expo 2007: Power for Land, Sea and Air, May 14-17, 2007, Montreal, Canada.
58. J. Gottgens, et. al., *'Analytic Approximations of Burning Velocities and Flame Thicknesses of Lean Hydrogen, Methane, Ethylene, Ethane, Acetylene and Propane Flames'*, Symposium (International) on Combustion, Volume 24, Issue 1, 1992, pp. 129-135.
59. Pope S. B., *'Pdf methods for turbulent reactive flows'*, Progress in Energy and Combustion Science, Volume 11, Issue 2, 1985, pp. 119-192.
60. Pope S. B. and Cao R. R., *'The influence of chemical mechanisms on PDF calculations of nonpremixed piloted jet flames'*, Combustion and Flame, Volume 143, Issue 4, December 2005, pp. 450-470.
61. Pope et. al., *'Turbulent lifted flames in a vitiated coflow investigated using joint PDF calculations'*, Combustion and Flame, Volume 142, Issue 4, September 2005, Pages 438-453.
62. Leeds NOx mechanism can be obtained from Hughes K. J., et. al., http://www.chem.leeds.ac.uk/Combustion/nox.htm
63. Hanson R. K., Salimian S., *'Survey of Rate Constants in H/N/O Systems'*, from, W. C. Gardiner, editor, Combustion Chemistry, page 361, 1984.
64. De Soete G. G., *'Overall reaction rates of NO and N2 formation from fuel nitrogen'*, Symposium (International) on Combustion, Volume 15, Issue 1, 1975, pp. 1093-1102.
65. Briones A. M., et. al., *'Effect of multistage combustion on NOx emissions in methane–air flames'*, Combustion and Flame, Volume 149, Issue 4, June 2007, pp. 448-462.
66. *'Combustion Modeling Strategies in Fluent'*, Fluent Software Training Presentation, April 2005.
67. Price G. R., *'CFD Predictions and Field Measurements of NOx Emissions from LM1600 Gas Turbine During Part Load Operation'*, Journal of Engineering for Gas Turbines and Power, April 2002, Volume 124, pp. 276-283.
68. Samuelsen et. al., Technical Report, UCI Combustion Laboratory, University of California, Irvine. DOE subcontract 94-01-SR020.
69. Polifke W., et. al., *'Impact of the Fuel Time Lag Distribution in Elliptical Premix Nozzles on Combustion Stability'*, Technical Report AIAA 2001-2104, 7th AIAA/CEAS Aeroacoustics Conference, May 28–30, 2001, Maastricht, The Netherlands.
70. Gordon R. L., et. al., *'Transport budgets in turbulent lifted flames of methane autoigniting in a vitiated co-flow'*, Combustion and Flame, Volume 151, Issue 3, November 2007, pp. 495-511.

71. Barth T. J., Jespersen D., *'The design and application of upwind schemes on unstructured meshes'*, Technical Report AIAA-89-0366, AIAA 27th Aerospace Sciences Meeting, Reno, Nevada, 1989.
72. Leonard B. P., Mokhtari S., *'ULTRA-SHARP Nonoscillatory Convection Schemes for High-Speed Steady Multidimensional Flow'*, NASA TM 1-2568 (ICOMP-90-12), NASA Lewis Research Center, 1990.
73. Grinstein F.F., Fureby C., *'LES studies of the flow in a swirl gas combustor'*, Proceedings of the Combustion Institute, Volume 30, Issue 2, January 2005, pp. 1791-1798.
74. Eggels R. L.G.M., *'Modelling of NOx formation of a premixed DLE Gas Turbine Combustor'*, 2001-GT-0069, Proceedings of TURBOEXPO 2001, 46th ASME International Gas Turbine & Aeroengine Technical Congress, June 4-7, 2001, New Orleans, Louisiana, USA.
75. Lefebvere A. H., *'Gas turbine combustion'*, 2nd Edition, 1999, Taylor & Francis.
76. *'Using natural gas in engines'*, IMechE seminar publication, 1357-9193; 1996-2 - Conference proceedings 'Organized by the Combustion Engines Group of the Institution of Mechanical Engineers'.
77. *'New Perspectives in Aeronautics'*, 1998-2002 Project Synopsis, European Commission – Community Research. p 200.
78. Schülter J.U., Schönfeld T., *'LES of Jets in Cross Flow and Its Application to a Gas Turbine Burner'*, Flow, Turbulence and Combustion, 2000, Volume 65, pp. 177–203.
79. Muppidi S., Mahesh K., *'Direct numerical simulation of turbulent jets in crossflow'*, Technical Report AIAA-2005-1115, 43rd AIAA Aerospace Sciences Meeting and Exhibit, Jan 10-13, Reno, Nevada.
80. Brundish K., Miller M., *'RB211 DLE Combustor Internal Traversing'*, QinetiQ Report QINETIQ/FST/CAT/CR012731, October 2001.
81. Lysenko D. A., Solomatnikov A. A., *'Numerical Modeling of Turbulent Heat Exchange in the Combustion Chambers of Gas Turbine Plants with the use of the Fluent Package'*, Journal of Engineering Physics and Thermophysics, 2003, Volume 76, Number 4, pp. 888-891.
82. Spadaccini L. J., et. al., *'Influence of aerodynamic phenomena on pollutant formation in combustion (Phase I. Gaseous fuels)'*. U.S. Environmental Protection Agency Rep. EPA-600/2-76-247a., 1976.
83. Pierce C. D., Moin P., *'Progress-variable approach for large-eddy simulation of non-premixed turbulent combustion'*, Journal of Fluid Mechanics, 2004, Volume 504, pp.73-97.
84. TNF Workshop web site. http://www.ca.sandia.gov/TNF , Sandia National Laboratories,2003.

85. Stårner S.H., Bilger R.W., *'Characteristics of a piloted diffusion flame designed for study of combustion turbulence interactions'*, Combustion and Flame, Volume 61, Issue 1, July 1985, pp. 29-38.
86. Stein O., Kempf A., *'LES of the Sydney swirl flame series: A study of vortex breakdown in isothermal and reacting flows'*, Proceedings of the Combustion Institute, Volume 31, Issue 2, January 2007, pp. 1755-1763.
87. Kempf A., et. al., *'Investigation of lengthscales, scalar dissipation, and flame orientation in a piloted diffusion flame by LES'*, Proceedings of the Combustion Institute, Volume 30, Issue 1, January 2005, pp. 557-565.
88. http://www.ca.sandia.gov/TNF/DataArch/FlameD/SandiaPilotDoc20.pdf
89. Lockwood F.C., et. al., *'An experimental and theoretical investigation of turbulent mixing in a cylindrical furnace'*, Combustion and Flame, Volume 23, Issue 3, December 1974, pp. 283-293.
90. Vanka S. P., *'Calculation of axisymmetric, turbulent, confined diffusion flames'*, AIAA Journal, Volume 24, March 1986, p. 462-469.
91. Kim Y. M., Chung T. J., *'Finite-Element Analysis of Turbulent Diffusion Flames'*, AIAA Journal, Volume , 1989, Volume 27, Number 3, pp. 330-339.
92. Steele, R. C., *'NOx and N2O Formation in Lean-Premixed Jet-Stirred Reactors Operated From 1 to 7 atm.'*, Ph.D. Thesis, University of Washington, Seattle, WA, 1995.
93. Smooke M. D., et. al., *'A comparison between numerical calculations and experimental measurements of the structure of a counterflow diffusion flame burning diluted methane in diluted air'*, Symposium (International) on Combustion, Volume 21, Issue 1, 1988, pp. 1783-1792.
94. *The GRI3 Mechanism by* Gregory P. Smith, David M. Golden, Michael Frenklach, Nigel W. Moriarty, Boris Eiteneer, Mikhail Goldenberg, C. Thomas Bowman, Ronald K. Hanson, Soonho Song, William C. Gardiner, Jr., Vitali V. Lissianski, and Zhiwei Q in http://www.me.berkeley.edu/gri_mech/
95. Pope S. B., *'Advances in pdf methods for reactive flows'*, Paper No: 801, Advances in Turbulence X, Proceedings of the Tenth European Turbulence Conference, H. I. Andersson & P.-°A. Krogstad (Eds.) CIMNE, Barcelona 2004.
96. Odedra , Malalasekara, *'Eulerian particle flamelet modeling of a bluff-body CH4/H2 flame'*, Combustion and Flame, Volume 151, Issue 3, November 2007, pp. 512-531.
97. James S., et. al., *'Large eddy simulations of turbulent flames usingthe filtered density function model'*, Proceedings of the Combustion Institute, Volume 31, Issue 2, January 2007, pp. 1737-1745.
98. Xin et. al., unpublished data.

APPENDIX: CONVERGENCE CHARTS

Some sample convergence charts are shown below:

RANS:

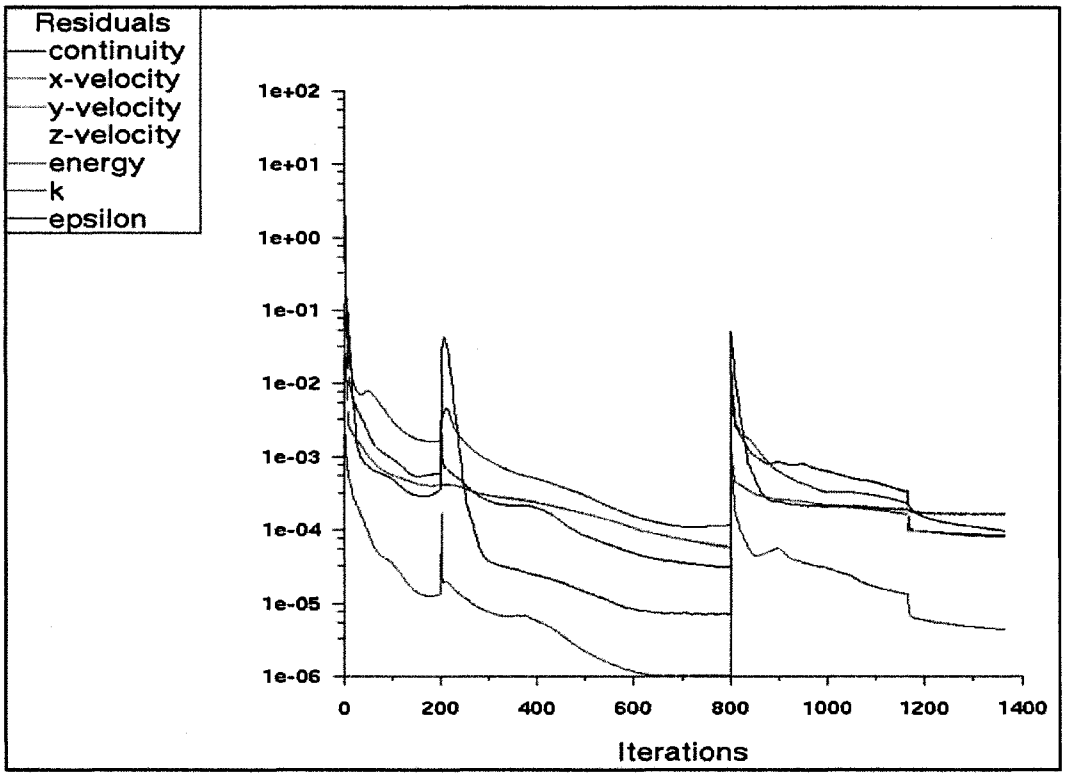

Fig A1: Example of RANS Convergence

The RANS result above is for a 5.7 million-polyhedral cell mesh built from a 23 million high quality tetrahedral mesh. This was done, so that, a coarse grid solution can be interpolated back onto a high-density grid and accelerate convergence. As can be seen, convergence was very fast for this mesh. Various

solution monitors (velocity and temperature) were implemented to check for true convergence. The first peak indicates change of turbulence model from k-epsilon standard to k-epsilon Realizable. The second peak indicates change of discretization for all equations. The bottom picture shows the last 15 iterations.

LES convergence:

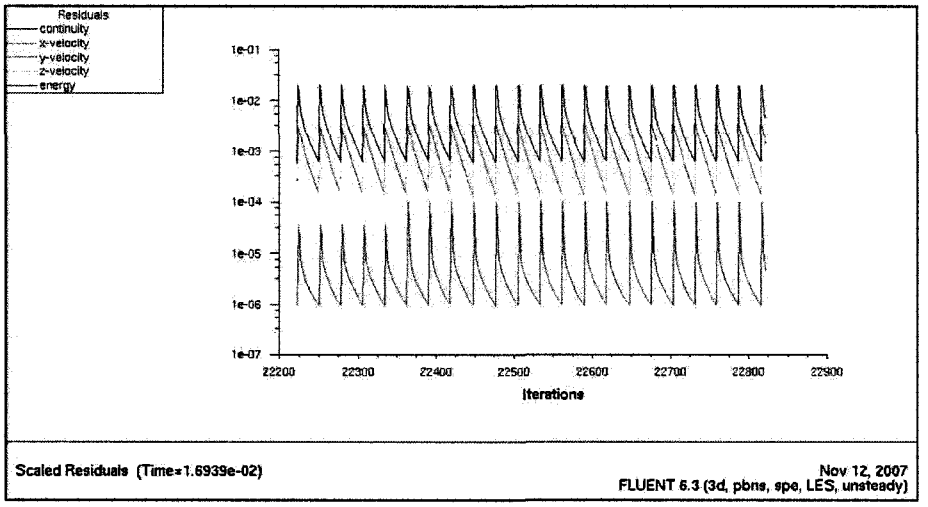

Fig A2: Example of LES Convergence (cold flow).

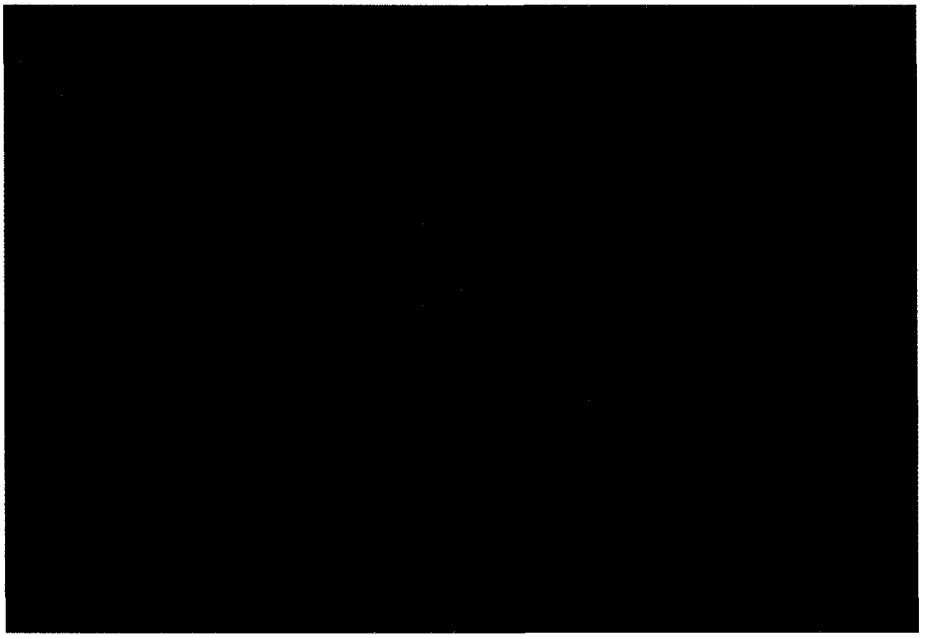

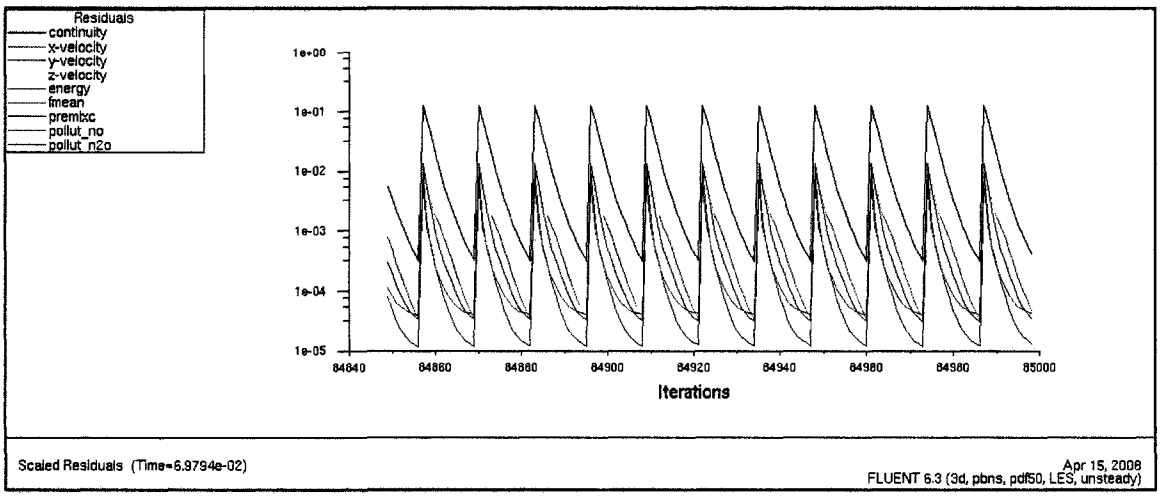

Fig A3: Example of LES Convergence (Reacting).